TRIMERIC PERFLUORO-*ORTHO*-PHENYLENE MERCURY AS A BUILDING BLOCK FOR SUPRAMOLECULAR MATERIALS

A Dissertation

by

MASON REAMES HANELINE

Submitted to the Office of Graduate Studies of
Texas A&M University
in partial fulfillment of the requirements for the degree of

DOCTOR OF PHILOSOPHY

December 2004

Major Subject: Chemistry

TRIMERIC PERFLUORO-*ORTHO*-PHENYLENE MERCURY AS A BUILDING BLOCK FOR SUPRAMOLECULAR MATERIALS

A Dissertation

by

MASON REAMES HANELINE

Submitted to Texas A&M University
in partial fulfillment of the requirements
for the degree of

DOCTOR OF PHILOSOPHY

Approved as to style and content by:

François P. Gabbaï (Chair of Committee)	John P. Fackler, Jr. (Member)
Michael B. Hall (Member)	Donald G. Naugle (Member)
	Emile A. Schweikert (Head of Department)

December 2004

Major Subject: Chemistry

ABSTRACT

Trimeric Perfluoro-*ortho*-phenylene Mercury as a Building Block for Supramolecular Materials. (December 2004)

Mason Reames Haneline, B.S., Virginia Polytechnic Institute and State University

Chair of Advisory Committee: Dr. François P. Gabbaï

Trimeric perfluoro-*ortho*-phenylene mercury (**1**) constitutes one of the simplest trifunctional Lewis acidic hosts. Cooperative effects arising from the proximity of the mercury(II) centers, the electron-withdrawing properties of the backbone and the accessibility of the electrophilic sites leads to the facile complexation of neutral and electron rich substrates. The planarity of the structure as well as its overall polarizability compounded with relativistic effects at mercury also permits the occurrence of non-covalent interactions. The main objective of this dissertation was to explore the potential of **1** as a building block for supramolecular materials.

Compound **1** was investigated using single crystal x-ray diffraction and was found to display a rich polymorphism. The electronic structure, probed by DFT methods, shows that the LUMO of **1** has a large contribution from the mercury 6p orbitals and features a large lobe protruding above and below the center of the trinuclear mercury core. Complexes in which two nitronyl nitroxide radicals (NIT-Ph = 2-(phenyl)-4,4,5,5-tetramethylimidazoline-1-oxyl-3-oxide) coordinate to the trinuclear

core of **1** above and below the Hg_3 plane reveal that **1** does not significantly mediate magnetic interactions.

The ability of **1** to complex π-basic molecules such as tetrathiafulvalene (TTF), toluene, *o*-xylene, *m*-xylene, *p*-xylene, mesitylene, biphenyl, naphthalene, acenaphthalene, anthracene, pyrene, triphenylene, perylene, and coronene was also investigated and show that **1** and arenes form extended binary stacks in which the two components alternate. The photoluminescence observed in some of these supramolecular complexes corresponds to the phosphorescence of the arene indicating a mercury heavy atom effect. Complexation of **1** in solution was observed with hexaalkoxytriphenylenes (HAT*n*, $n = 1, 6$) by fluorescence and NMR spectroscopy.

Finally, compound **1** forms electrophilic double sandwich structures with ferrocene and nickelocene in which a molecule of **1** caps each of the Cp ligands. The nickelocene adduct is stabilized towards oxidation, and the photophysical and magnetic properties indicate the occurrence of a mercury heavy atom effect.

ACKNOWLEDGEMENTS

I would like to thank my research advisor, Dr. François P. Gabbaï, for his tireless efforts throughout the past four years. I would also like to thank my committee members, Dr. Fackler, Dr. Hall, and Dr. Naugle. Other members of the faculty I would like to thank include Dr. Hughbanks, Dr. Dunbar, Dr. Don Darensbourg, Dr. Schaak, and Dr. Miller. The members of the Gabbaï group during my tenure here have also been very helpful. I would like to thank Dr. Julie B. King, Dr. James D. Hoefelmeyer, Samuel Cozzens, Alexandre Picot, Huadong Wang, Thomas J. Taylor, Charlotte N. Burress, Ching-wen Chiu, Dr. Jim Gardinier, Dr. Marcus Schulte, Dr. Mitsukimi Tsunoda, Dr. Stephane Sole, Dr. Mieock Kim, and Dr. Mohand-Ameziane Meliami for their help and advice over the past four years. Jared M. Benedict and Harold C. Huslage were undergraduates that helped me synthesize some compounds and I would like to acknowledge them. Also I would like to thank Procter & Gamble for a graduate fellowship.

I would also like to thank my undergraduate professors at Virginia Polytechnic Institute and State University, especially Dr. Paul A. Deck, for preparing me for graduate school.

I would also like to thank all of the members of my family for all of their years of support.

Additional thanks goes to Skot Jakubiec, Neil Fallon, Jean-Paul Gaster, Dan Maines, Tim Sult, Ted Nugent, Mr. Bungle, and B. C. Rich.

TABLE OF CONTENTS

CHAPTER Page

LIST OF FIGURES

FIGURE Page

FIGURE Page

FIGURE Page

FIGURE Page

FIGURE Page

FIGURE Page

FIGURE Page

FIGURE Page

FIGURE Page

FIGURE Page

LIST OF TABLES

TABLE Page

CHAPTER I

INTRODUCTION*

For several decades, the field of supramolecular chemistry has been dominated by studies dealing with multidentate Lewis bases. More recently, the lack of receptors capable of complexing both neutral and anionic electron-rich substrates led to the emergence of polydentate Lewis acids.[1] Typically, such derivatives are comprised of several electrophilic main-group element moieties linked by organic or inorganic backbones. Polyfunctional organomercurials constitute one of the most developed classes of polydentate Lewis acids. In addition to being air and water stable, the unsaturated mercury(II) centers of these derivatives exhibit appreciable Lewis acidity in a direction perpendicular to the primary bonds. Taking advantage of these properties, several polydentate organomercurial species have been constructed and have now emerged as useful Lewis acidic hosts[2,3,4,5] and catalysts.[6,7,8] Most of the compounds used as anion receptors are macrocyclic species. These include tri- and tetranuclear mercuracarborands developed by Hawthorne as well as a series of fluorinated species investigated by the group of Shur.[3,4] In this collection of species, trimeric perfluoro-*ortho*-phenylene mercury ([(*o*-$C_6F_4Hg)_3$], **1**) stands out as a unique tridentate Lewis acid. The nature of the metal, the planarity of the structure, the electron-withdrawing

---

This dissertation follows the style and format of the *Journal of the American Chemical Society*.

* Reprinted in part with permission from *Chem. Eur. J., 9* Haneline, M. R.; Taylor, R. E.; Gabbaï, F. P., "Trimeric Perfluoro-ortho-phenylene Mercury: A Versatile Lewis Acid Host", 5188, Copyright 2003 Wiley-VCH Verlag GmbH&Co. KGaA.

properties of the backbone, as well as the proximity and accessibility of the mercury(II) centers make for a distinctive set of chemical properties.

The synthesis of compound **1** was reported several decades ago and involves the decarboxylation of the tetrafluorophthalate mercury salt (Figure 1.1).[9] The molecule possesses three mercury(II) centers located at approximately 3.5 Å from one another thus forming an equilateral triangle. The ^{199}Hg and ^{19}F NMR-active nuclei can be used as spectroscopic handles to monitor its chemistry (Figure 1.1).[10]

In addition to cooperative effects arising from the proximity of the mercury(II) centers, the electron-withdrawing properties of the backbone and the accessibility of the mercury centers convey unusual Lewis acidic properties to the molecule.[11] The importance of this electronic effect is nicely illustrated by the relative halophilicity of **1** and that of its non-fluorinated analogue trimeric *ortho*-phenylene mercury ([(*o*-$C_6H_4Hg)_3$]).[12] As shown by Shur, while both molecules interact with halide ions in solution, the lability of the complex formed by [(*o*-$C_6H_4Hg)_3$] impedes their isolation

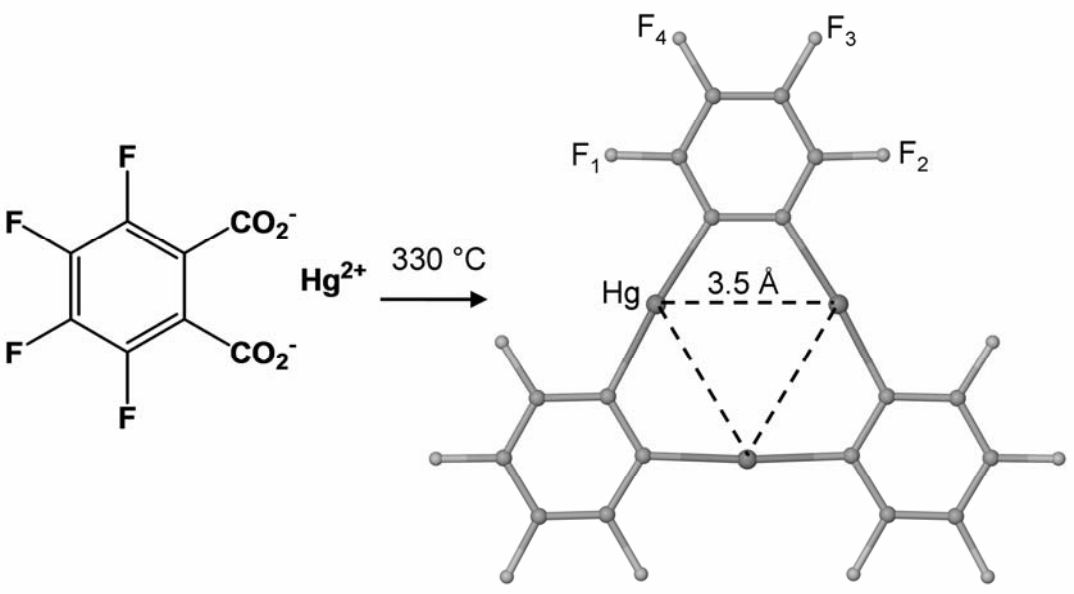

$\delta(^{199}Hg)$ = -1046 ppm
$\delta(^{19}F_1)$ = -121.6 ppm
$\delta(^{19}F_4)$ = -157.7 ppm

NMR Coupling constants in Hz in **1**				
	F_2	F_3	F_4	Hg
F_1	18.5	3.5	27	393
F_2		23	3.5	19
F_3			15	103
F_4				19

Figure 1.1. Synthesis of **1**; ^{19}F and ^{199}Hg NMR spectroscopic features in CH_2Cl_2 ($CFCl_3$ and Me_2Hg external reference).

and structural characterization.[13] With **1**, however, a number of anionic complexes including bromide, iodide, and thiocyanide salts have been isolated.[13,14,15] These anionic complexes adopt multidecker structures with the anions sandwiched between successive molecules of **1** (Figure 1.2). As a result of this structure, the anion interacts with all neighboring mercury centers and is, therefore, hexacoordinate. It is worth noting that ESI mass spectrometric studies carried out in collaboration with Russell suggest the gas-phase formation of stable 2:1 complexes in which the halide, that is, fluoride, chloride, bromide, or iodide, is sandwiched by two molecules of **1** (Figure 1.3).[16] While these 2:1 complexes have not been detected in solution, Chistyakov and co-workers have predicted their existence on the basis of quantum chemical calculations.[4a] We also note that Hawthorne has isolated discrete sandwich species in which a halide anion is octahedrally coordinated to the mercury centers of two mercuracarborand-3 receptors.[17] Related double-decker anionic sandwich complexes involving two molecules of **1** and a *closo*-borane such as $[B_{10}H_{10}]^{2-}$ or $[B_{12}H_{12}]^{2-}$ have been recently isolated and structurally characterized. In this case the dianionic guests form multiple B-H-Hg bridges with the mercury centers of **1**.

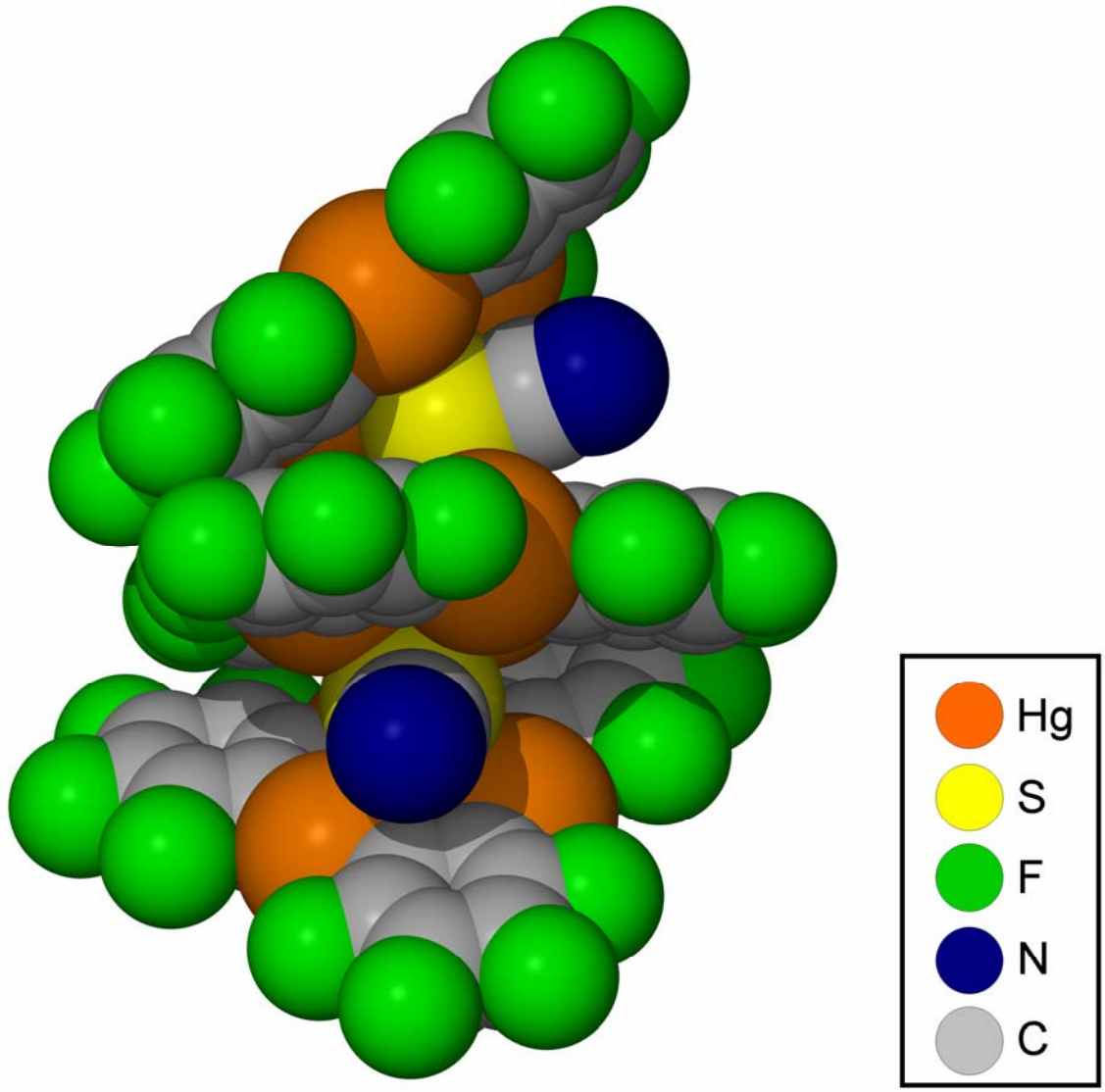

Figure 1.2. Space-filling model of a portion of the polymeric structure of [**1**•SCN]$^{-}$.

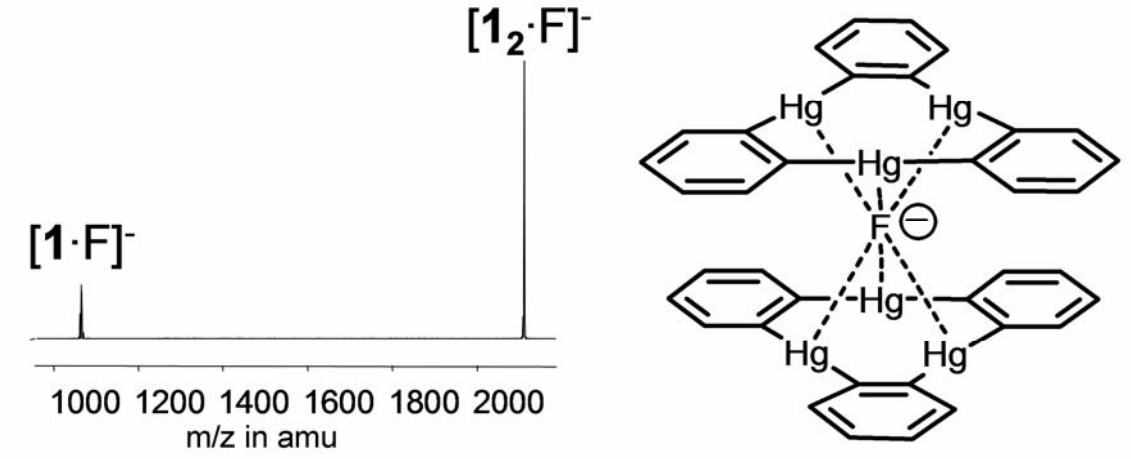

Figure 1.3. Left: ESI MS-MS spectra of the bridged fluoride complex [$\mathbf{1}_2$•F]$^-$ observed at m/z 2118.8. Right: putative structure of the [$\mathbf{1}_2$•F]$^-$; phenylene F atoms omitted.

The Lewis acidic properties of this derivative are also substantiated by its propensity to form adducts with neutral electron-rich substrates. While this chemical trait was brought to light several decades ago by Massey,[18] the structural characterization of some of these adducts has only been recently achieved. As shown by the structures of the HMPA, DMSO, DMF, ethyl acetate, and acetonitrile adducts,[10,19,20] complex **1** is able to coordinate two molecules of the donor above and below the plane formed by the three mercury atoms. In the case of the DMSO and ethyl acetate adducts, a third molecule of the organic substrate binds to one of the mercury centers in a terminal fashion. In all adducts, the three mercury centers of **1** cooperatively interact with the electron-rich terminus of the triply bridging organic substrates. The formation of adducts is not limited to the cases of sulfoxides, formamides, and nitriles; rather it also includes less basic substrates such as ketones and aldehydes.[21] For example, we found that the crystallization of **1** from pure acetaldehyde leads to the formation of the 1:1 complex

[**1**•μ^3-($CH_3C(O)H$)] in which the three mercury centers of **1** cooperatively interact with the oxygen atom of the organic carbonyl (Figure 1.4).[22] The resulting Hg-O distances range from 2.912(13) to 2.965(8) Å and are within the sum of the van der Waals radii for oxygen (r_{vdw} 1.54 Å)[23] and mercury (r_{vdw} 1.73-2.00 Å),[24,25] thus indicating the presence of a donor interaction. A similar conclusion can be reached by inspecting the IR spectrum of this adduct, which reveals a weakened carbonyl stretching vibration (ν_{CO} = 1706 vs 1726 cm^{-1} in pure acetaldehyde). Related structures are also observed with ketones including acetone and benzophenone.[22,26]

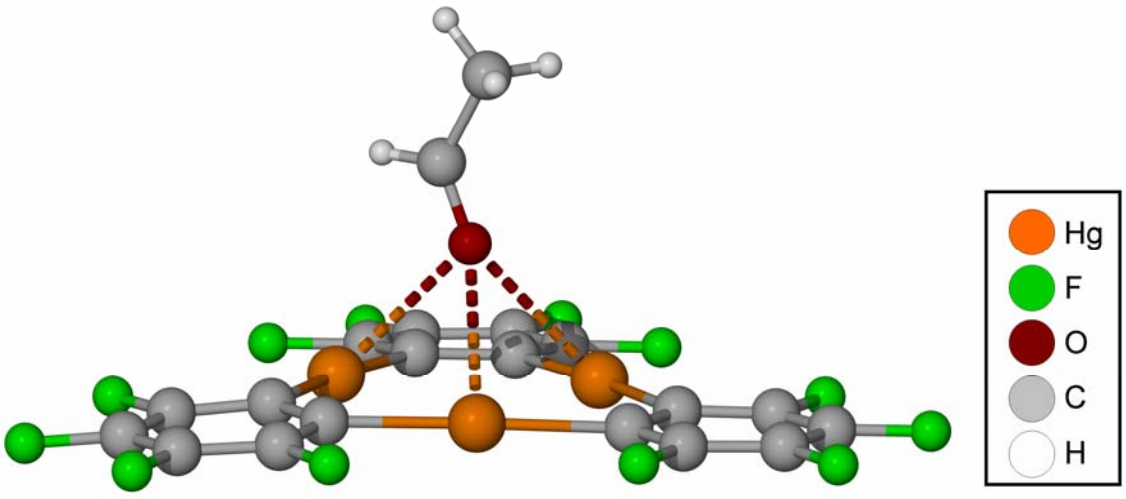

Figure 1.4. Molecular structure of [**1**•μ^3-acetaldehyde] showing the triple coordination of the carbonyl oxygen.

Although it is sometimes difficult to differentiate between the occurrence of covalent and non-covalent interactions, the formation of adducts involving **1** and both neutral and anionic electron-rich substrates apparently results from weak dative bonds.

Such bonds have often been observed in the chemistry of organomercury compounds and are typically referred to as secondary interactions. Yet, in several other instances, the structural chemistry of **1** points to the existence of non-covalent interactions. Evidence for this type of effect has been observed in the structure of the acetone adduct [**1**•μ^3-($(CH_3)_2CO$)], which also forms cofacial dimers (Figure 1.5). This arrangement places the monomeric units in close contact. The parallel trinuclear mercury units are separated by 3.46 Å from one another and adopt an offset arrangement. It appears acceptable to invoke the participation of dispersion forces between the largely aromatic molecules of **1**. Moreover, relativistic effects at mercury cause a contraction of the s and p orbitals followed by an increased shielding of the nuclear charge. As a result, the d electrons and especially the $5d^{10}$ shell experience a greater radial extension accompanied by an increase in polarizability.[27] This effect, which also permits the occurrence of metallophilic interactions,[28] contributes to the general polarizability of **1** thereby adding to its ability to engage in dispersion interactions. Thus in [**1**•μ^3-acetone] both components are held by mercurophilic interactions of 3.51 Å, which is only slightly larger than the mercurophilic interaction distance calculated for the perpendicular $(HgMe_2)_2$ dimer. As demonstrated by Fackler, metallophilic interactions are also responsible for the formation of supramolecules involving **1** and trinuclear gold complexes.[29]

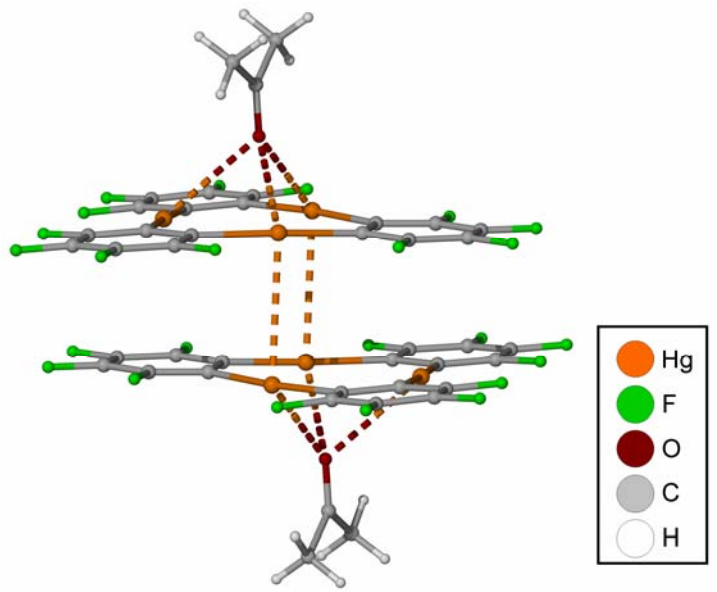

Figure 1.5. View of the cofacial dimers in [**1**•μ^3-acetone].

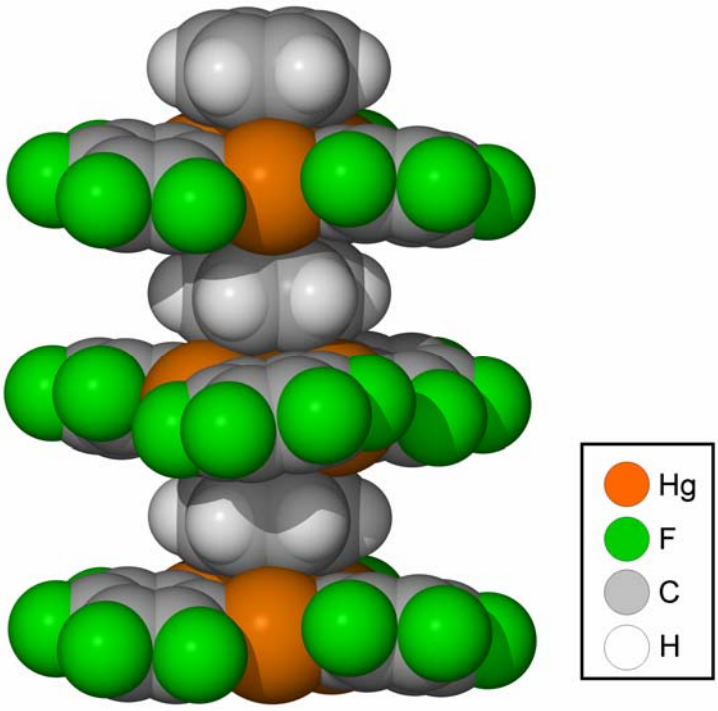

Figure 1.6. Space-filling model of the supramolecular stack of [**1**•C_6H_6].

Arene mercurations constitute a common set of reactions. They follow an electrophilic substitution mechanism and substantiate the strong interactions that can occur between Hg^{II} ions and aromatic substrates. This chemical characteristic is supported by the isolation and structural characterization of arene-mercury π-complexes involving either Hg(I)[30] and Hg(II) ions.[31,32,33,34] In these complexes, the arene is typically η^2-coordinated to the mercury center through Hg-C_{arene} bonds ranging from 2.3 to 2.7 Å. Weaker interactions are observed between aromatic substrates and the mercury center of neutral organomercurial derivatives. With Hg-C_{arene} distances in the range of 3 to 3.4 Å, these interactions are inherently weak[35] and occur mainly in an intramolecular fashion.[36] However, recent reports indicate that unsupported examples of such complexes can be isolated in the case of fluorinated organomercurials.[37] We found that compound **1** crystallizes from benzene to afford [**1**•C_6H_6].[38] This adduct is very stable and can be kept for months at room temperature. It starts losing benzene at 70 ºC as shown by TGA. X-ray analysis reveals the formation of extended stacks that consist of nearly parallel, yet staggered molecules of **1** that sandwich benzene molecules (Figure 1.6). These stacks are rather compact (centroid distance of 3.24 Å) so that secondary π-interactions occur between the benzene molecule and the mercury centers. Each of the six C-C bonds of the benzene molecule interacts with one of the six mercury centers of the two juxtaposed molecules of **1**. The resulting Hg-$C_{benzene}$ distances of 3.408 and 3.457 Å are within the sum of the van der Waals radius of mercury (r_{vdw} 1.73-2.00 Å)[24,25] and that usually accepted for carbon in aromatic system (r_{vdw} 1.7 Å).[39] As a result, the benzene is hexacoordinated in a μ^6-η^2:η^2:η^2:η^2:η^2:η^2 fashion. In an effort to

account for the Lewis acid character of **1**, we have proposed that the cohesion of this supramolecule results from the donation of electrons from the benzene π-orbitals into sets of empty 6p orbitals of the mercury atoms.

In summary, compound **1** constitutes a remarkably versatile derivative that can serve as a tridentate Lewis acid. While the complexation of anions and basic organic substrates has been previously investigated, it has been shown that **1** has an affinity for weakly coordinating organic substrates, such as aldehydes and ketones. This work also points to the propensity of this trinuclear derivative to engage in non-covalent interactions including mercurophilic interactions and dispersion interactions. The following chapters will showcase the ability of compound **1** to engage in the above mentioned mercurophilic interactions and function as a tridentate Lewis acid and supramolecular building block with neutral organic radicals and aromatic substrates.

CHAPTER II

TRIMERIC PERFLUORO-*ORTHO*-PHENYLENE MERCURY, $[Hg(o\text{-}C_6F_4)]_3$: CRYSTAL STRUCTURES, LUMINESCENCE AND MOLECULAR ORBITALS*

2.1 Introduction

Trimeric ortho-phenylene mercury derivatives have been known for over half a century.[9,40-42] These derivatives, which are air and water stable, have been widely used as reagents for the synthesis of organometallic derivatives featuring an *ortho*-phenylene backbone. For example, trimeric *ortho*-phenylene-mercury ($[o\text{-}C_6H_4Hg]_3$) undergoes transmetalation reactions with a variety of main-group elements or low-valent main-group salts. The preparation of *ortho*-dilithiobenzene, tetrameric *ortho*-phenylenemagnesium,[43] dimeric *ortho*-phenylenezinc[44] and 9,10-dibromo-9,10-dihydro-9,10-diindaanthracene[45] are representative examples that demonstrate the importance of this synthetic method. These mercury derivatives can also be used in metathesis reactions; for example trimeric perfluoro-*ortho*-phenylene mercury ($[o\text{-}C_6F_4Hg]_3$, **1**) reacts with BBr_3 to afford 1,2-bis(dibromoboryl)benzene.[46] More recently, the potential of such derivatives to serve as polyfunctional Lewis acid receptors for electron rich species has been uncovered. In particular, trimeric perfluoro-*ortho*-phenylene mercury (**1**) complexes a number of electron rich species[47,48] including halide anions, carborane

---

* Reprinted in part with permission from *J. Am. Chem. Soc., 124*, Haneline, M. R.; Tsunoda, M.; Gabbaï, F. P., "π-Complexation of Biphenyl, Naphthalene, and Triphenylene to Trimeric Perfluoro-*ortho*-phenylene Mercury. Formation of Extended Binary Stacks with Unusual Luminescent Properties", 3737, Copyright 2002 American Chemical Society.

anions, sulfides, organic carbonyls, sulfoxide and nitriles. In the resulting adducts, the halide anion or the electron rich terminus of the polyatomic substrate is typically bound simultaneously to the three mercury centers of **1**. Compound **1** also interacts with arenes including naphthalene, pyrene and triphenylene to afford binary stacks where the arene is π-coordinated to the mercury centers of **1**.[38,47,49]

Based on a molecular weight determination as well as a partial crystal structure,[41,50] $[o\text{-}C_6H_4Hg]_3$ was first proposed to exist in the form of a hexamer of general formula $[o\text{-}C_6H_4Hg]_6$. However, careful crystallographic work by Massey[51,52] demonstrated that it is in fact a trimer which can exist in a monoclinic as well as in an orthorhombic crystal modification. Interestingly, although **1** has been known for almost four decades, its crystal structure in a pure form had not been reported until recently (*vide infra*). In this chapter, four crystal structures of **1**, the luminescent properties of these structures, and ADF calculations of **1** will be described.

2.2 Description of the crystals

Compound **1** is moderately soluble in CS_2 (3 g/L) and CH_2Cl_2 (7 g/L). Upon slow evaporation of a saturated solution in either of these solvents, clear colorless crystals of **1** (modification **A**) as a free acid are readily obtained. These crystals belong to the monoclinic space group $P2_1/n$ (Table 2.1). Interestingly, examination of the cell packing diagram indicates that molecules of **1** associate into compact cofacial dimers with a centroid distance of 3.38 Å (Figure 2.1). As shown by the relatively short distances observed between the mercury centers and the *ipso*-carbon of the juxtaposed molecule (3.443 < Hg-C < 3.650 Å), mercury-arene interactions are likely responsible for the formation of this dimeric unit. As a result of this arrangement, short intermolecular distances are observed between the mercury atoms (3.811 < Hg-Hg < 4.093 Å). These distances are longer than those observed intramolecularly (Hg(1)-Hg(2), 3.647 Å; Hg(2)-Hg(3), 3.622 Å, Hg(1)-Hg(3), 3.622 Å) and slightly exceed the range suggested for mercurophilic interactions.[25,53] The mercury centers are also engaged into mercury-fluorine interactions (3.093 < Hg•••F < 3.295 Å) which are shorter than the sum of the van der Waals radii (r_{vdw}(F) = 1.30-1.38 Å, r_{vdw}(Hg) = 1.73-2.00 Å)[24,25] and link the dimers into extended chains.

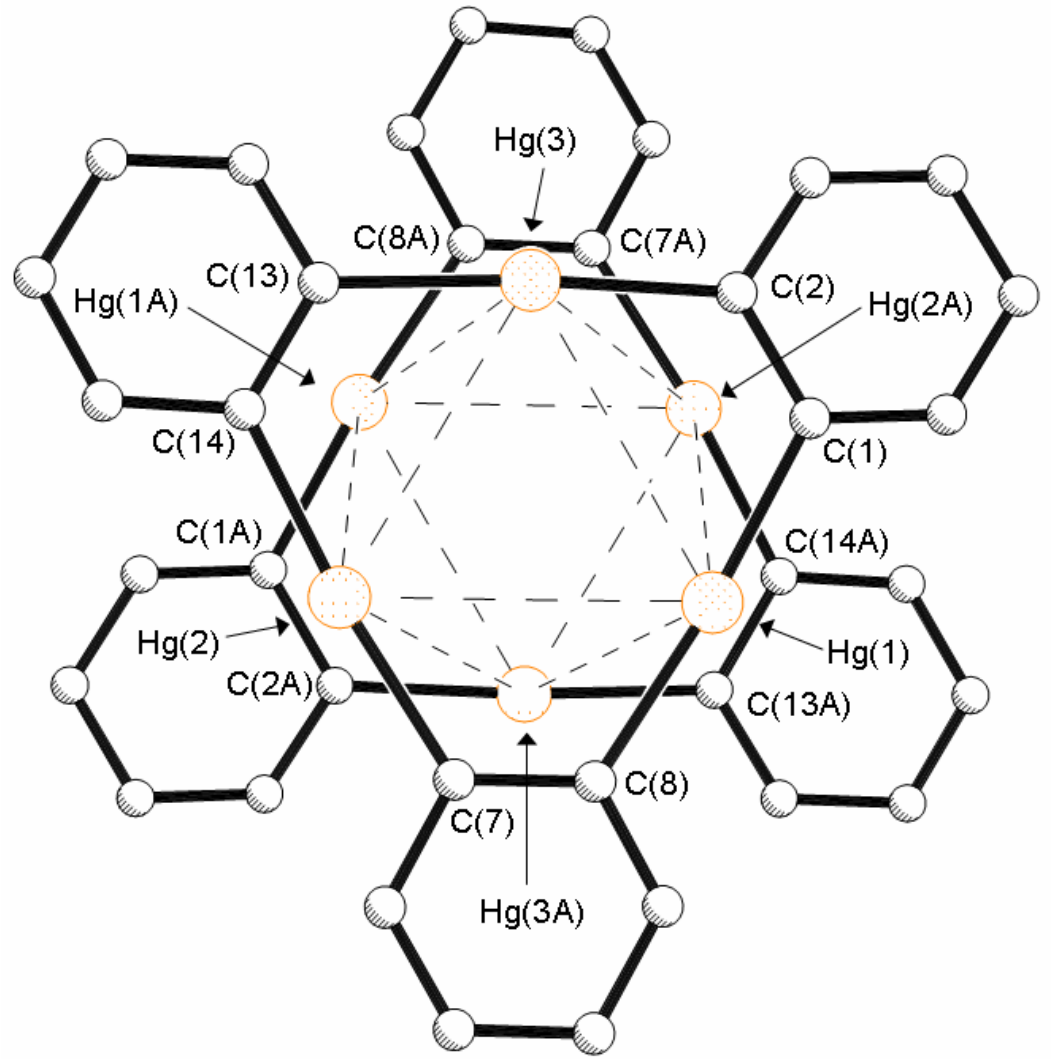

Figure 2.1. Cofacial dimers observed in modification **A.** The fluorine atoms are omitted for clarity. Selected intramolecular bond distances [Å] and angles [deg]. Hg(1)-C(1) 2.060(11), Hg(1)-C(8) 2.092(12), Hg(2)-C(14) 2.051(11), Hg(2)-C(7) 2.079(11), Hg(3)-C(2) 2.046(12), Hg(3)-C(13) 2.067(13), C(1)-Hg(1)-C(8) 174.5(5), C(14)-Hg(2)-C(7) 174.2(5), C(2)-Hg(3)-C(13) 175.6(5). Selected intermolecular bond distances [Å]. Hg(1)-C(13A) 3.479, Hg(1)-C(14A) 3.514, Hg(1)-Hg(2A) 4.018, Hg(2)-C(1A) 3.453, Hg(2)-C(2A) 3.443, Hg(2)-Hg(3A) 4.093, Hg(3)-C(7A) 3.650, Hg(3)-C(8A) 3.502, Hg(3)-Hg(1A) 3.811.

Table 2.1. Crystal data, data collection, and structure refinement for **1** (modification **A-D**).

Crystal data	**B**	**C**	**D**	**A**
Formula	$C_{18}F_{12}Hg_3$	$C_{18}F_{12}Hg_3$	$C_{18}F_{12}Hg_3$	$C_{18}F_{12}Hg_3$
M_r	1045.95	1045.95	1045.95	1045.95
Crystal size (mm^3)	0.29 x 0.20 x 0.20	0.5 x 0.07 x 0.06	0.50 x 0.25 x 0.24	0.26 x 0.15 x 0.17
Crystal system	Monoclinic	Orthorhombic	Monoclinic	Monoclinic
Space group	$P2_1/n$	*P*nma	$P2_1/n$	*C*2/c
a (Å)	10.505(2)	18.070(4)	11.123(2)	16.841(3)
b (Å)	8.6105(17)	21.200(4)	4.6306(9)	13.419(3)
c (Å)	20.489(4)	4.8030(10)	35.509(7)	8.6790(17)
β (°)	97.29(3)		97.29(3)	94.45(3)
V ($Å^3$)	1838.2(6)	1840.0(6)	1814.1(6)	1955.5(7)
Z	4	4	4	4
ρ_{calc} (gcm^{-3})	3.779	3.776	3.830	3.553
μ(Mo K_α)(mm^{-1})	25.116	25.093	25.451	23.611
F(000) (e)	1824	1824	1824	1824
Data Collection				
T/K	293(2)	293(2)	110(2)	293(2)
Scan mode	ω	ω	ω	ω
hkl range	-12→12, -9→9, -23→23	-20→20, -22→23, -5→5	-12→12, -5→5, -40→41	-20→20, -15→15, -10→10
Measured refl.	15685	10141	11948	9213
Unique refl., [R_{int}]	2879 [0.0293]	1381 [0.0284]	3016 [0.0350]	1715 [0.0508]
Refl. used for refinement	2879	1381	3016	1715
Absorption correction	SADABS	SADABS	SADABS	SADABS
T_{min}/T_{max}	0.072358	0.175019	0.143309	0.120405
Refinement				
Refined parameters	298	151	298	150
R1, wR2 [I>2σ (I)]	0.0403, 0.1130	0.0582, 0.1196	0.0504, 0.1020	0.0354, 0.0829
ρ_{fin} (max/min) ($eÅ^{-3}$)	3.959, -2.374	2.703, -1.042	5.651, -2.678	2.870, -1.510
Flack parameter	-	-	-	-

[a] $R1 = (F_o - F_c)/ F_o$.[b] $wR2 = \{[w(F_o^2 - F_c^2)^2]/ [w(F_o^2)^2]\}^{1/2}$; $w = 1/[\sigma^2(F_o^2) + (ap)^2 + bp]$; $p = (F_o^2 + 2F_c^2)/3$; *a* = 0.0850 (**A**), 0.04 (**B**), 0.005 (**C**), 0.04 (**D**); *b* = 5.37 (**A**), 100 (**B**), 200 (**C**), 50 (**D**).

Careful sublimation of **1** leads to the formation of crystals with both block and needle morphologies. The crystals which display a block morphology belong to the monoclinic space group *C*2/c (modification **B**) (Table 2.1). In this modification, the molecules of **1** have a crystallographically imposed C_2 symmetry (Figure 2.2). Examination of the packing diagram reveals the existence of extended stacks that run parallel to one another. Within each stack, the planes defined by the trinuclear mercury cores of the successive molecules are parallel to one another and separated by 3.29 Å. The molecules, which adopt a staggered arrangement, are distinctly offset with respect to one another. As a result, the stacks are tilted and propagate in a direction that makes a 40.7° angle (α = tilt angle) with the vector perpendicular to the plane containing the three mercury atoms. This configuration leads to short distances between the mercury center Hg(1) and two of the carbon atoms of neighboring molecules (Hg(1)-C(1B) 3.385 Å, Hg(1)-C(6B) 3.462 Å) (Figure 2.2). The crystals which display a needle morphology belong to the orthorhombic space group *P*nma (modification **C**) (Table 2.1). The molecules of **1** have a crystallographically imposed mirror symmetry and form extended stacks that retain the mirror symmetry (Figure 2.3). These stacks propagate parallel to one another. The planes defined by the trinuclear mercury cores of the molecules of **1** are once again parallel to one another with an interplane distance of 3.35 Å. Unlike in modification **B**, the successive molecules are eclipsed rather than staggered; however, the molecules are offset so that the resulting stacks are tilted by an angle α = 45.9°. In this modification, one of the phenylene rings of a molecule of **1** sits directly over the center of a neighboring molecule of **1**. This arrangement leads to close

intermolecular Hg-C distances (Hg(2)-C(1B) 3.323 Å, Hg(2)-C(8C) 3.385 Å) (Figure 2.3) and results in Hg-Hg distances of 3.83 Å between Hg(1) and two symmetry equivalent Hg(2) atoms of a neighboring molecule of **1**. A fourth crystalline form (modification **D**) has been obtained by recrystallization of **1** from CH_2Cl_2 solutions containing a small amount of 1,3,5-triisopropylbenzene(Table 2.1). The resulting crystals form thick needles and belong to the monoclinic space group *P*2(1)/n with one molecule of **1** in the asymmetric unit (Figure 2.3). Examination of the packing diagram reveals the existence of stacks that are very similar to those found in form **C** (tilt angle α = 44.6°). However, unlike modification **C**, the stacks do not have mirror symmetry resulting from sideways slippage of the molecules as depicted in Figure 2.3. This arrangement leads to the formation of short intermolecular Hg-C distances (Hg(1)-C(2B) 3.276 Å, Hg(1)-C(3B) 3.449 Å, Hg(1)-C(9A) 3.332 Å, Hg(2)-C(12A) 3.385 Å, Hg(2)-C(13B) 3.343 Å) (Figure 2.2). In addition Hg(3) and Hg(2A) are separated by only 3.56 Å. In all four modifications, the molecules of **1** display essentially the same structure. Each mercury atom has an approximately linear geometry with an average C-Hg-C angle of 175.4° and there no unusual Hg-C distances (av 2.075 Å).

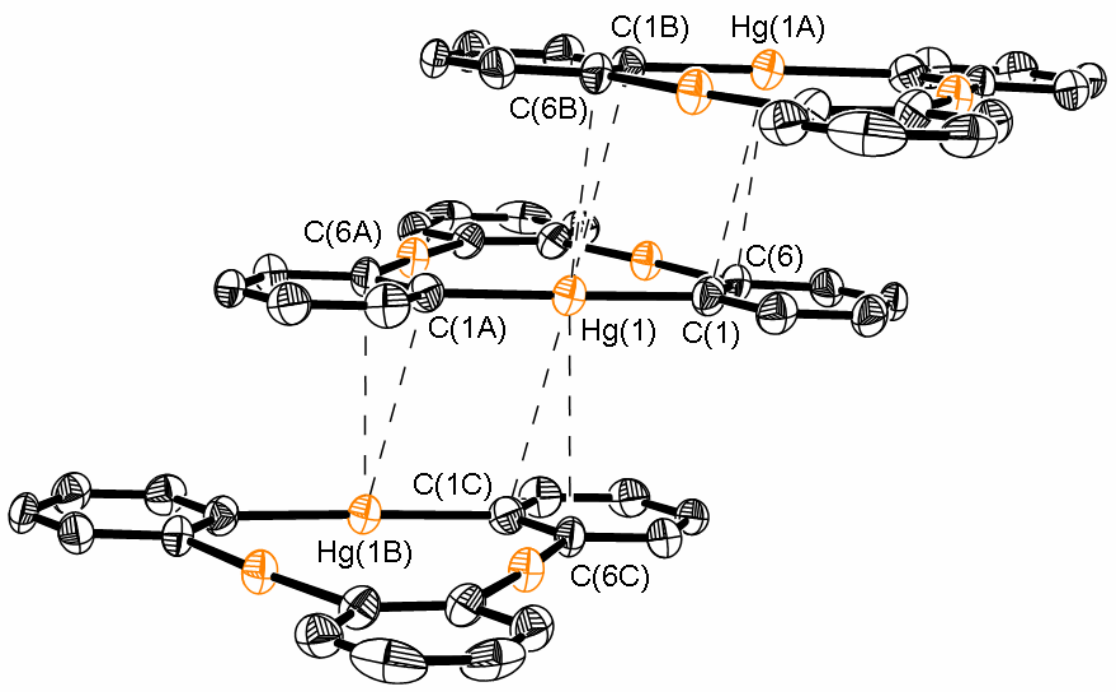

Figure 2.2. Portion of a stack present in modification **B**. The fluorine atoms are omitted for clarity. Selected intramolecular distances (Å) and angles (º): Hg(1)-C(1) 2.085(11), Hg(2)-C(7) 2.085(11), Hg(2)-C(6) 2.087(11), C(1)-Hg(1)-C(1A) 176.1(6), C(7)-Hg(2)-C(6) 174.9(4). Selected intermolecular distances: Hg(1)-C(1B) 3.385 Å, Hg(1)-C(6B) 3.462 Å, Hg(1)-C(1C) 3.385 Å, and Hg(1)-C(6C) 3.462 Å.

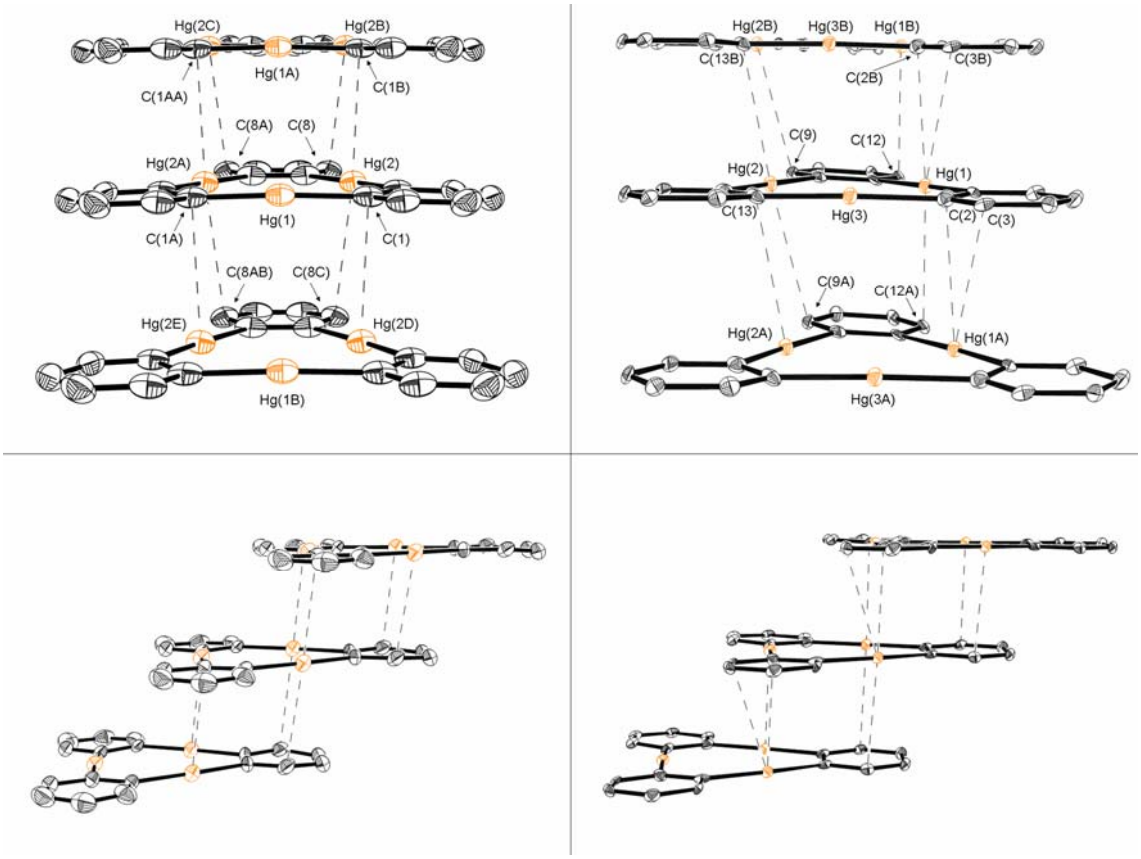

Figure 2.3. Portion of the stacks present in modification **C** (left) and **D** (right). Views along two perpendicular directions are provided for each stack. The Hg-Hg contacts and the fluorine atoms are omitted for clarity. Selected intramolecular distances (Å) and angles (º): morphology **C**: Hg(1)-C(1) 2.03(2), Hg(2)-C(6) 2.06(2), Hg(2)-C(7) 2.084(19), C(1A)-Hg(1)-C(1) 176.0(11), C(6)-Hg(2)-C(7) 175.1(9); morphology **D**: Hg(1)-C(1) 2.089(18), Hg(1)-C(8) 2.084(17), Hg(2)-C(7) 2.100(18), Hg(2)-C(14) 2.091(18), Hg(3)-C(2) 2.075(18), Hg(3)-C(13) 2.039(18), C(8)-Hg(1)-C(1) 174.3(7), C(14)-Hg(2)-C(7) 174.6(7), C(13)-Hg(3)-C(2) 177.2(7). Selected intermolecular distances (Å): morphology **C**: Hg(2)-C(1B) 3.323, Hg(2)-C(8C) 3.385; morphology **D**: Hg(1)-C(2B) 3.276, Hg(1)-C(3B) 3.449, Hg(1)-C(9A) 3.332, Hg(2)-C(12A) 3.385, Hg(2)-C(13B) 3.343.

All four modifications contain short contacts between the mercury centers of **1** and the carbon atoms of a neighboring molecule of **1**. These contacts range from 3.276 to 3.462 Å and are within the sum of the van der Waals radii of mercury (1.7-2.0 Å)[24,25]

and $C_{aromatic}$ (1.7 Å), indicating the presence of secondary Hg-π interactions occurring between the phenylene ring and the acidic mercury centers. Similar distances have been previously observed in adducts involving **1** and various arenes including benzene and naphthalene.[47,49] Within each stack, the mean plane of the molecules are separated by 3.3-3.4 Å. This separation is essentially identical to that found in any π-stacked assemblies and gives evidence for van der Waals interactions. In addition, a short intermolecular Hg-Hg contact of 3.56 Å is found in form **D**. This Hg-Hg distance is similar to that observed in the structure of [**1**-μ_3-acetone] which forms dimers held by mercuriophilic interactions of 3.512 Å.[26,54] Also, it only slightly exceeds the Hg-Hg distance calculated by Pyykkö for the dimer of dimethyl mercury (3.41 Å). The Hg-Hg distances found in form **A** and **C** range from 3.811-4.093 Å and are therefore at the upper limit for the involvement of strong metallophilic interactions. Out of the four modifications thus far characterized, modification **B**-**D** displays stacks in which the successive molecules are offset. Since the electrostatic potential map of **1** shows that the center of the molecule is positively charged with an accumulation of negative charge at the periphery, it appears reasonable to invoke the participation of electrostatic interactions which would be maximized in these offset geometries.

2.3 Luminescent properties of **1**

Solutions of **1** in CH_2Cl_2 do not luminesce and feature an absorption band at 275 nm in agreement with the excitation of the tetrafluorophenylene backbone of the complex.[55] By contrast, when irradiated with UV light from a hand-held UV lamp,

modifications **A**-**D** display photoluminescence; however, this phenomenon has only been studied in detail for modification **A**.

When irradiated with UV light in the crystalline state, modification **A** of compound **1** displays an intense orange photoluminescence. Measurement of the emission spectrum at 77 K (λ_{ex} = 355 nm) reveals the existence of an extremely broad band featuring a maximum at 440 nm and a broad shoulder at 530 nm that expands far in the visible part of the spectrum (Figure 2.4). While a rationalization of the luminescent properties of modification **A** can only be tentatively provided, it is noted that the presence of metallophilic interactions is often associated with unusual luminescent properties.[56] While this phenomenon is especially well characterized in the chemistry of gold(I),[57] a recent report by Burini and Fackler demonstrates that increased metallophilic interactions in stacks involving **1** and trinuclear gold complexes result in low energy emissions. Hence, the aggregation of molecules of **1** into tight dimers could be held responsible for some features of the visible emission observed in crystals of modification **A**.

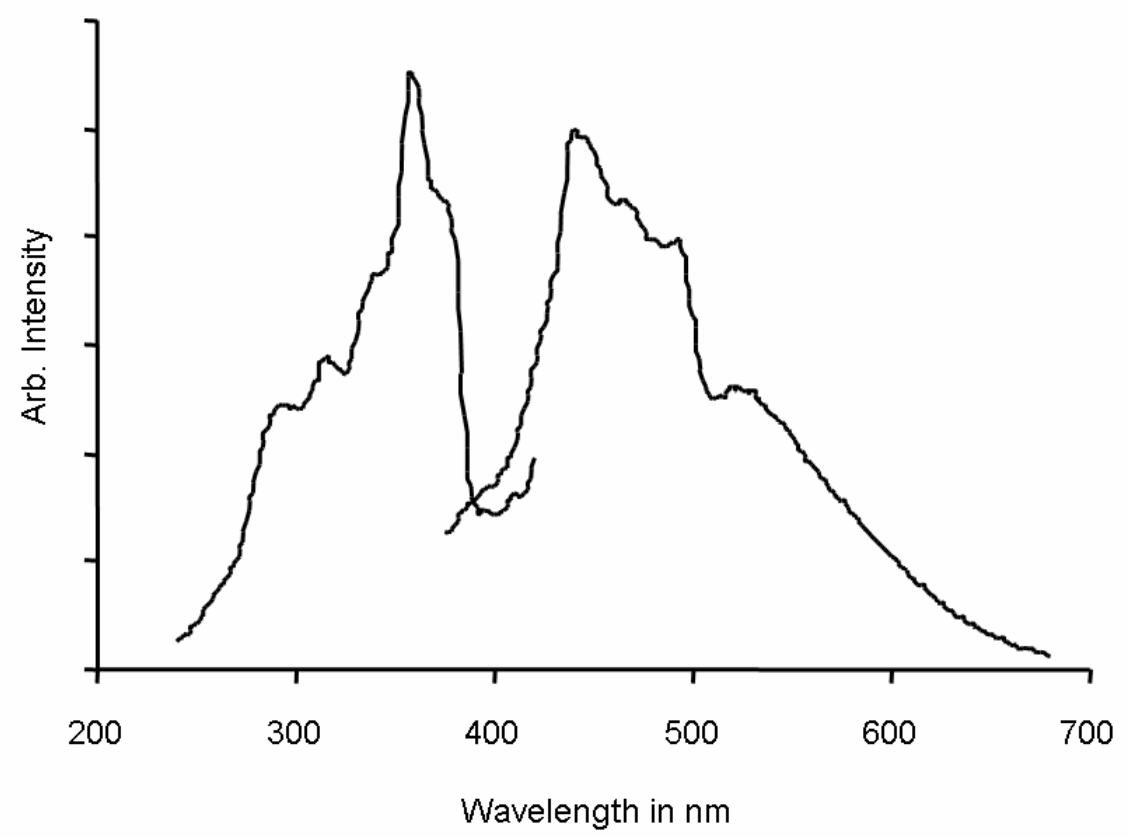

Figure 2.4. Excitation ($\lambda_{emission}$ = 440 nm) and emission ($\lambda_{excitation}$ = 355 nm) spectra of modification **A** of **1** crystallized from CS_2.

2.4 ADF calculations on **1**

Examination of the literature indicates that few theoretical studies have been carried out on compound **1**. Most studies available to date have been carried out using AM1,[4a,58] MNDO[59] or molecular mechanics[60] calculations and some of the results obtained in these studies do not always agree with experimental data. The group of Fackler performed single-point energy density functional theory (DFT) calculations on **1**. These calculations revealed that the electrostatic potential surface at the center of the ring is positive while the periphery is negative. The author's knowledge, however, no

optimization of the geometry of **1** at a high level of theory has been carried out. For these reasons, such calculations have now been undertaken.

Geometry optimization and single-point energy calculations were performed using density functional theory (DFT) in the Amsterdam density functional package (ADF).[61,62,63] The Becke exchange functional and the Lee-Yang-Parr correlation functional (BLYP) were utilized in the calculation.[64,65] The triple-z, double-polarization (TZ2P) basis function was used. The cores of atoms were frozen, C and F up to the 1s level, and Hg up to the 4d level. The scalar zero-order-regular-approximation (ZORA) was applied to account for relativistic effects. All quoted electronic structure data from optimized structures and single-point energy data use an integration of 6.0. The geometry was constrained to be D_3.

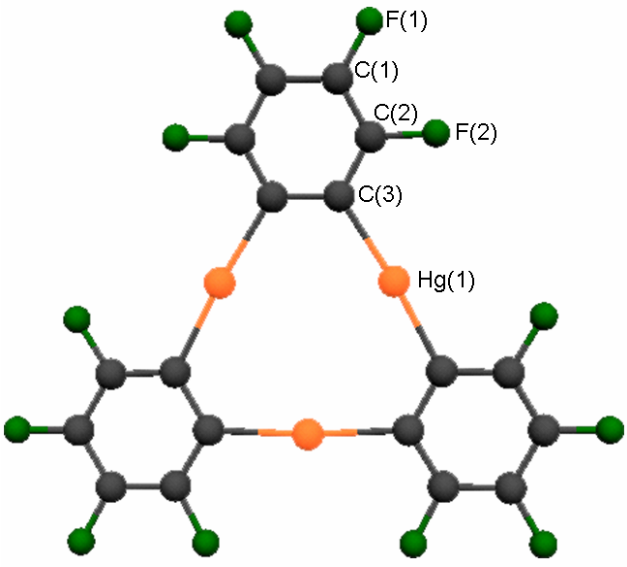

Figure 2.5. Optimized geometry of **1**.

In an effort to better understand the Lewis acidic properties of compound **1**, DFT calculations were performed using the ADF package. The resulting geometry of **1** is D_{3h} (Figure 2.5). The atom coordinates are listed in table 2.2. Examination of the bond distances and angles (Table 2.3) reveals the optimized geometry is comparable to distances and angles measured by X-ray diffraction. The HOMO (Figure 2.6) is largely based on the perfluorophenylene rings of **1**. In contrast the LUMO (Figure 2.6) exhibits a large lobe in the center of **1** that is mainly (44%) composed of mercury 6p orbitals. The HOMO-LUMO gap is 3.357 eV. These results lend support to the claim that the Lewis acidic character of **1** is dominated by the empty 6p orbitals on the mercury. The existence of a large lobe of the LUMO in the middle of the three mercury centers suggests that this particular region of the molecule corresponds to region of maximum Lewis acidity. In agreement with this view this large lobe appears directly aligned with the direction along which nucleophilic substrates such as acetone or iodide anions bind to the molecule.

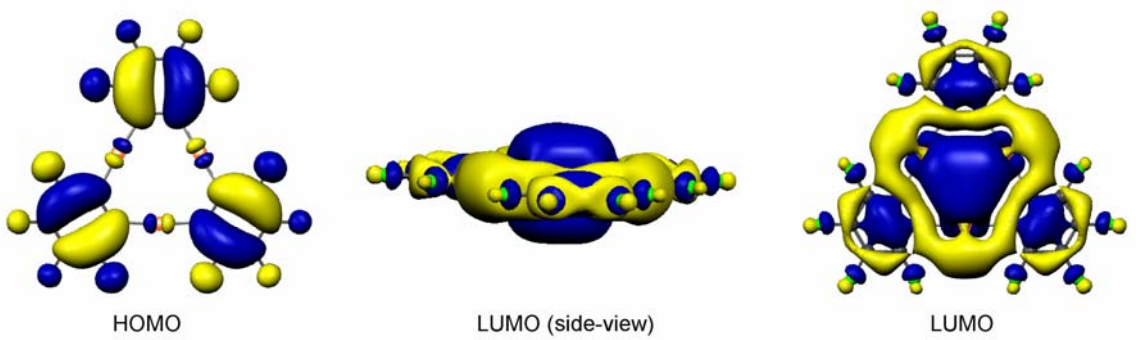

Figure 2.6. Views of the calculated HOMO and LUMO of compound **1**.

Table 2.2. Atomic coordinates in Å for geometry optimized structure of **1**.

	x	y	z
Hg	-1.066479	1.847196	0.000000
C	0.815080	2.829822	0.007289
C	2.043158	2.120791	-0.007289
Hg	2.132959	0.000000	0.000000
C	2.043158	-2.120791	0.007289
C	0.815080	-2.829822	-0.007289
Hg	-1.066479	-1.847196	0.000000
C	-2.858238	-0.709031	0.007289
C	-2.858238	0.709031	-0.007289
C	-4.079501	1.375082	-0.019861
F	-4.127327	2.743087	-0.034519
C	-5.300189	0.697923	-0.009545
F	-6.469262	1.378000	-0.021206
C	-5.300189	-0.697923	0.009545
F	-6.469262	-1.378000	0.021206
C	-4.079501	-1.375082	0.019861
F	-4.127327	-2.743087	0.034519
C	0.848895	-4.220493	-0.019861
F	-0.311920	-4.945914	-0.034519
C	2.045676	-4.939060	-0.009545
F	2.041248	-6.291545	-0.021206
C	3.254514	-4.241137	0.009545
F	4.428014	-4.913545	0.021206
C	3.230606	-2.845411	0.019861
F	4.439247	-2.202826	0.034519
C	3.230606	2.845411	-0.019861
F	4.439247	2.202826	-0.034519
C	3.254514	4.241137	-0.009545
F	4.428014	4.913545	-0.021206
C	2.045676	4.939060	0.009545
F	2.041248	6.291545	0.021206
C	0.848895	4.220493	0.019861
F	-0.311920	4.945914	0.034519

Table 2.3. Intramolecular distances (Å) and angles (º) for geometry optimized structure of **1**.

	Calculated	Average Measured
Hg(1)-C(3)	2.132	2.072
C(1)-C(1A)	1.396	1.389
C(1)-C(2)	1.396	1.381
C(1)-F(1)	1.353	1.342
C(2)-C(3)	1.391	1.376
C(2)-F(2)	1.369	1.357
C(3)-C(3A)	1.418	1.416
Hg(1)-Hg(1A)	3.694	3.610
C(3)-Hg(1)-C(3B)	175.2	175.3

2.5 Summary

Compound **1** displays a rich crystal polymorphism. While more modifications may still be discovered, the existence of these four forms suggests that there is little preference for a given type of interaction. Instead, the molecules of **1** appear to be able to glide somewhat freely with respect to one another. This feature indicates the preponderance of non-directional interactions such as van der Waals interactions between these molecules which are largely aromatic and whose overall polarizability is magnified by relativistic effects at the mercury(II) centers. ADF calculations on **1** reveal the HOMO is largely located on the perfluorophenylene ring while the LUMO is mainly composed of Hg 6p orbitals and has a large lobe located at the center of **1**. These calculations may help elucidate the nature of the interactions occurring between **1** and Lewis basic substrates.

2.6 Experimental details

Compound **1** was prepared by following the published procedure. All solvents used were purchased from Aldrich and used as received. The modifications **B** and **C** were obtained by sublimation of **1** at 280°C under vacuum (10^{-1} torr). Modification D was obtained upon slow evaporation of a solution containing **1** (20 mg), triisopropylbenzene (0.5 mL), in CH_2Cl_2 (5 mL). X-ray data were collected on a Bruker SMART-CCD diffractometer using graphite-monochromated Mo-Kα radiation (λ = 0.71073 Å). Specimens of suitable size and quality were selected and glued onto a glass fiber with freshly prepared epoxy resin. The structure was solved by direct methods,

which successfully located the mercury atoms. Subsequent refinement on F^2 using the SHELXTL/PC package (version 5.1) allowed location of the remaining carbon and fluorine atoms. Further crystallographic details can be found in Table 2.1.

CHAPTER III

COORDINATION OF $[Hg(o\text{-}C_6F_4)]_3$ AND NITRONYL NITROXIDE RADICALS

3.1 Introduction

Polyfunctional organomercurial featuring proximal metal centers have been extensively studied as polydentate Lewis acids. Typical examples of such complexes include 1,8-bis(mercurio)naphathalenes,[66] 1,2-bis(mercurio)benzenes[67] and various macrocyclic species such as mercuracarborands.[2,68] Such derivatives have been investigated for the multiple electrophilic complexation of both anionic and neutral electron-rich substrates. Perfluoro-*ortho*-phenylene mercury (**1**) is a prototypical example of such a polyfunctional Lewis acid. It exhibits fascinating coordination chemistry with anions and has been employed for the observation and isolation of hexacoordinated halide complexes.[4,13,14,16] This derivative also interacts with neutral electron rich substrates[69] including organic carbonyls,[22,26,70] nitriles[19,20,71] and sulfoxides to form discrete 1:1 and 2:1 complexes in which the electron rich terminus of the substrates interacts simultaneously with the three mercury atoms of **1** (Scheme 1). In the 2:1 complexes, two molecules of the donor are coordinated to the mercury centers of **1** on either side of the molecular plane. Work carried out in our laboratory also demonstrates that **1** is a remarkable building block for the construction of supramolecular materials. In particular, **1** readily interacts with various arenes to form extended binary stacks in which the arene is weakly π-coordinated to the mercury centers of **1**.[38,49,72] These supramolecules feature distinct physical properties and display

intense room temperature phosphorescence of the arene in the solid state as a result of a mercury heavy atom effect.[49,72] As part of our continuing interest in the chemistry of this molecule, we are actively exploring its potential for the elaboration of novel materials.

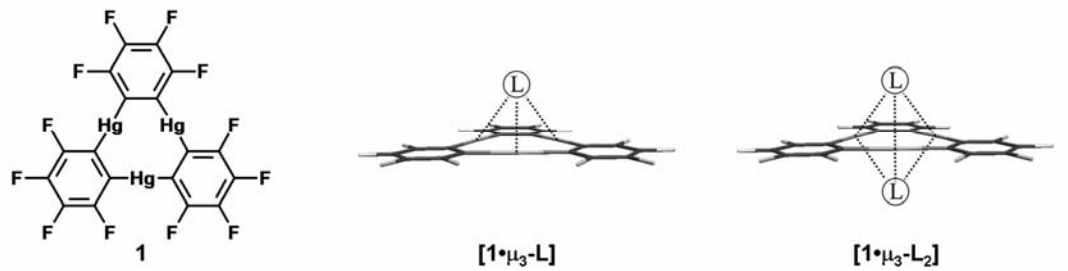

Scheme 3.1: Schematic structures of **1**, the 1:1 and 2:1 complexes formed by **1** and electron rich substrates

Nitroxide and nitronyl nitroxide constitute some of the most stable organic radicals.[73] Like organic carbonyls, these molecules feature an electron rich terminal oxygen atom that should readily coordinate to the mercury centers of **1**. If 2:1 complexes are accessible, three distinct magnetic situations (**A**-**C**) can be envisioned. If **1** is able to mediate magnetic interactions, the organic radicals could couple in either a ferromagnetic (**A**) or antiferromagnetic fashion (**B**). Also, it can be envisaged that **1** does not mediate magnetic interactions leading to a situation in which the organic radicals are uncoupled (**C**). In this chapter, a series of results on adducts of **1** with 1,1,5,5-tetramethylpentamethylene nitroxide (TEMPO) and 2-(phenyl)-4,4,5,5-tetramethylimidazoline-1-oxyl-3-oxide (NIT-Ph) nitronyl radicals which suggest that **1**

does not effectively mediate magnetic interaction between spin carrier coordinated to either side of its molecular plane is described.

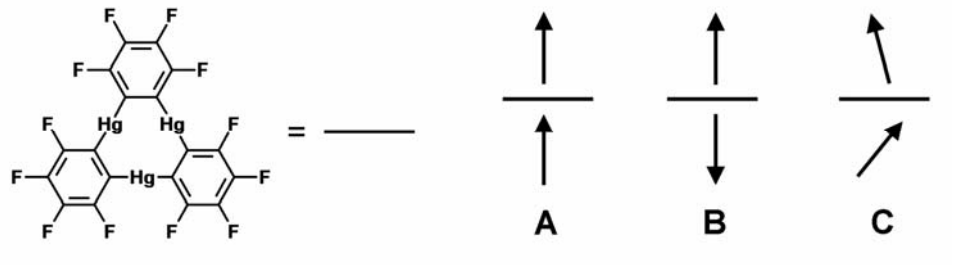

Scheme 3.2

3.2 Synthesis of [**1**•μ_3-TEMPO] (**2**), [(**1**)$_2$•μ_3-μ_3-NIT-Ph] (**3**), and [**1**•μ_3-NIT-Ph] (**4**)

Combining equimolar CH_2Cl_2 solutions of **1** and TEMPO affords pale yellow crystals of [**1**•μ_3-TEMPO] (**2**) upon slow evaporation. When **1** and NIT-Ph are combined in an equimolar ratio in CH_2Cl_2, slow evaporation of the solvent leads to the formation of pink crystals of the 2:1 adduct [(**1**)$_2$•μ_3-μ_3-NIT-Ph] (**3**). Interestingly, a similar experiment carried out with a 5 fold excess of NIT-Ph affords purple needles of the 1:1 adduct [**1**•μ_3-NIT-Ph] (**4**). The stoichiometry of **2-4** was confirmed by elemental analysis. Each was found to be air stable and decomposed at temperatures above 190 ºC. The EPR spectra of these compounds in CH_2Cl_2 correspond to those of the free radical.

3.3 Crystal structures of **2**-**4**

Compound **2** crystallizes in the triclinic space group *P*-1 with one molecule of [**1**•μ_3-TEMPO] in the asymmetric unit (Table 3.1 and Figure 3.1). The resulting Hg-O distances range from 2.889(11)-3.141(12) Å and are well within the sum of the van der Waals radii for mercury (r_{vdw} = 1.75 Å)[24,25] and oxygen (r_{vdw} = 1.54 Å). As a result of these interactions, the oxygen atom is essentially equidistant from the three Lewis acidic sites and sits at a distance *d* of 2.170 Å from the plane defined by the three mercury atoms. The linear nitroxide functionality is nearly perpendicular to this plane and forms an angle α of 86.9º. The metrical and angular parameters observed in **2** resemble those encountered in [**1**•μ_3-acetone] (α = 85.6º ,*d* = 1.945 Å, Hg-O = 2.810(12)-2.983(12) Å),[22,26] [**1**•μ_3-acetaldehyde] (α = 66.3º ,*d* = 2.086 Å, Hg-O = 2.912(13)-2.965(8) Å), [**1**•μ_3-DMF] (α = 88.3º ,*d* = 2.062 Å, Hg-O = 2.799(5)-3.042(5) Å),[19,20,71] and [**1**•μ_3-DMSO] (α = 76.3º ,*d* = 1.879 Å, Hg-O = 2.759(5)-3.120(5) Å).

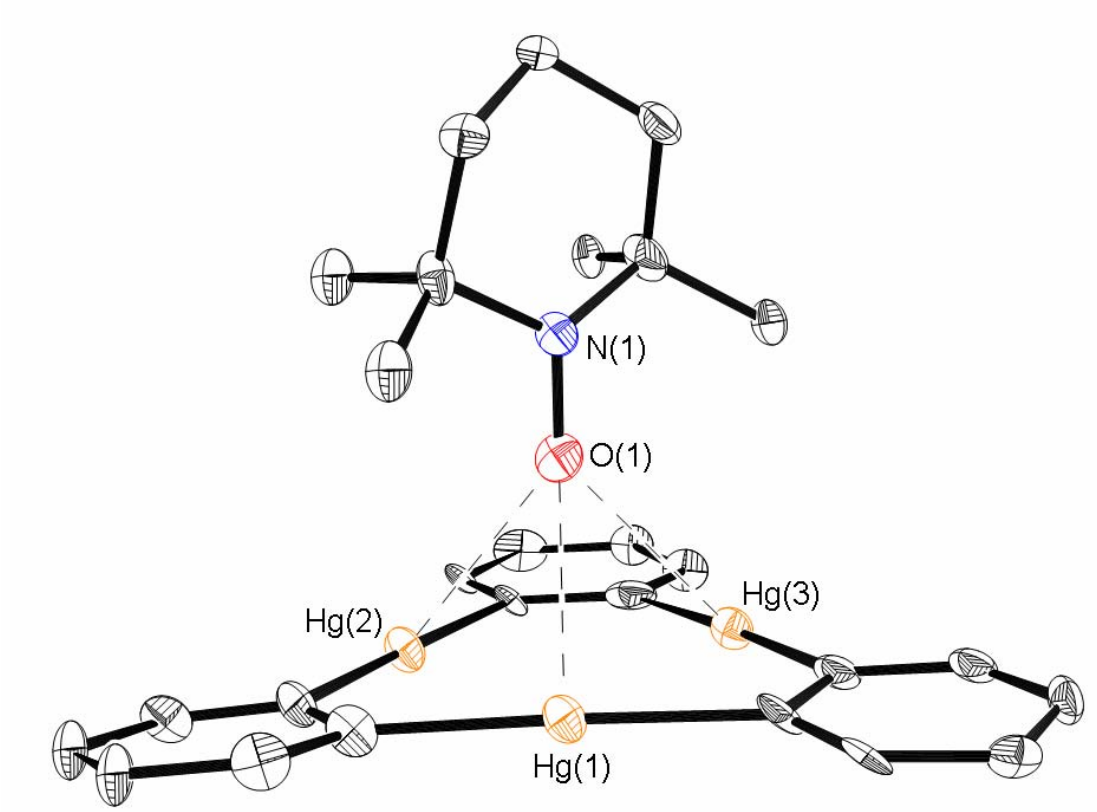

Figure 3.1. Compound **2** with 50% thermal ellipsoids (fluorine and hydrogen atoms omitted for clarity). Intramolecular distances in Å include Hg(1)-O(1) 3.141(12), Hg(2)-O(1) 2.989(12), and Hg(3)-O(1) 2.889(11). Intermolecular bond distances(Å) and angles(º) include Hg(1)-C(1) 2.109(16), Hg(1)-C(8) 2.096(18), Hg(2)-C(7) 2.096(18), Hg(2)-C(14) 2.115(16), Hg(3)-C(2) 2.034(19), Hg(3)-C(13) 2.06(2), O(1)-N(1) 1.306(18), C(8)-Hg(1)-C(1) 175.3(7), C(7)-Hg(2)-C(14) 176.5(7), C(2)-Hg(3)-C(13) 177.1(7).

Table 3.1. Crystal data, data collection, and structure refinement for **2**, **3**, and **4**.

Crystal data	**2**	**3**	**4**
Formula	$C_{27}H_{18}F_{12}Hg_3NO$	$C_{49}H_{17}F_{24}Hg_6N_2O_2$	$C_{31}H_{17}F_{12}Hg_3N_2O_2$
M_r	1202.19	2325.19	1279.24
Crystal size (mm^3)	0.36 x 0.18 x 0.06	0.44 x 0.41 x 0.32	0.34 x 0.28 x 0.22
Crystal system	Triclinic	Monoclinic	Hexagonal
Space group	*P*-1	*C*2/c	$P6_1$
a (Å)	10.263(2)	17.963(4)	11.559(3)
b (Å)	12.009(2)	15.835(3)	11.559(3)
c (Å)	12.669(3)	20.652(4)	44.627(14)
α (°)	87.16(3)		
β (°)	70.83(3)	115.67(3)	
γ (°)	74.77(3)		
V ($Å^3$)	1421.9(5)	5294.8(18)	5164(2)
Z	2	4	6
ρ_{calc} (gcm^{-3})	2.808	2.917	2.468
μ(Mo K_α)(mm^{-1})	16.259	17.460	13.441
F(000) (e)	1086	4148	3486
Data Collection			
T/K	110(2)	110(2)	110(2)
Scan mode	ω	ω	ω
hkl range	-11→11, -13→13, -14→14	-21→21, -18→16, -24→24	-12→12, -12→12, -49→47
Measured refl.	8204	19319	32596
Unique refl., [R_{int}]	3989 [0.0404]	4659 [0.0386]	4893 [0.0737]
Refl. used for refinement	3989	4659	4893
Absorption correction	SADABS	SADABS	Psiscan
T_{min}/T_{max}	0.266545	0.313625	0.827 and 0.352
Refinement			
Refined parameters	361	376	397
R1, wR2 [I>2σ(I)]	0.0596, 0.1329	0.0272, 0.0643	0.0478, 0.1215
ρ_{fin} (max/min) ($eÅ^{-3}$)	3.906, -3.468	1.001, -0.988	2.348, -1.302

[a] $R1 = \Sigma (F_o - F_c)/ \Sigma F_o$. [b] $wR2 = \{[\Sigma w(F_o^2 - F_c^2)^2]/[\Sigma w(F_o^2)^2]\}^{1/2}$; $w = 1/[\sigma^2(F_o^2) + (ap)^2 + bp]$; $p = (F_o^2 + 2F_c^2)/3$; a = 0.02 (**2**), 0.0485 (**3**), 0.07 (**4**); b = 100 (**2**), 0 (**3**), 80 (**4**).

Compound **3** crystallizes in the monoclinic space group *C*2/c. The crystal structure of this derivative consists of isolated C_2 symmetrical molecules of [(**1**)$_2$•μ_3-μ_3-(NIT-Ph)] in which a NIT-Ph molecule is sandwiched by two molecules of **1** (Table 3.1 and Figure 3.2). The two oxygen atoms of the NIT-Ph are triply coordinated to the mercury centers provided by the juxtaposed molecules of **1**. The Hg-O distances (Hg-O = 2.846(6)-2.975(6) Å) as well as the orientation of the linear N-O functionality with respect to the plane of the trinuclear mercury complex (α = 85.1º, d = 2.025 Å) are similar to those found in **2**. Additional interactions between **1** and NIT-Ph include two Hg-$C_{aromatic}$ interactions which occurs between Hg(2) and C(23) with a distance of 3.328(10) Å and another between Hg(2A) and C(23A) with the same distance. Compound **4** crystallizes in the hexagonal space group $P6_1$ (Table 3.1, Figure 3.2, Figure 3.3, and Figure 3.4). Examination of the crystal structure reveals extended helical binary polymeric chains with alternating molecules of **1** and NIT-Ph that propagate parallel to one another. Each oxygen in NIT-Ph is triply coordinated to the three mercury centers of **1** and each molecule of **1** has an oxygen atom of NIT-Ph triply coordinated on either side of it. Thus, the coordination about the molecules of **1** is similar to that encountered in [**1**•(μ_3-L)$_2$] complexes. As a result, the environment of the NIT-Ph molecule as well as the coordination geometry about the NO functionalities is virtually identical to that found in **3** (α = 87.3º, d = 2.123 Å, Hg-O = 2.90(2)-3.020(17) Å). The dihedral angle between the phenyl ring and the five member ring of the NIT-Ph are 79.3° for compound **3** and 75.2° for compound **4**, which are very different from that of pristine NIT-Ph(26.6°).[74]

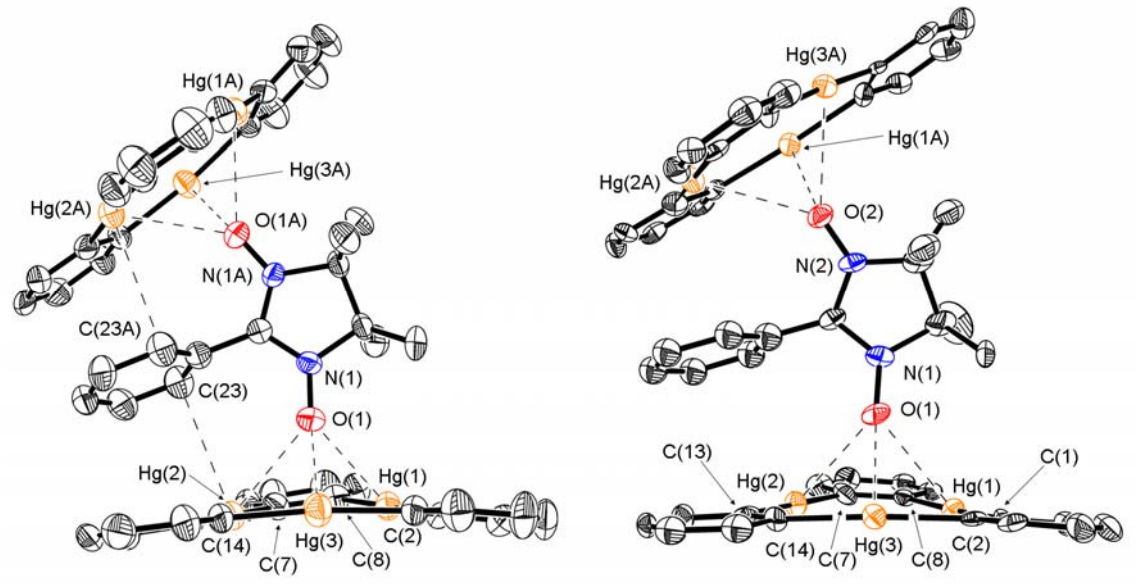

Figure 3.2. Left: Compound **3** with 50% thermal ellipsoids (fluorine and hydrogen atoms omitted for clarity). Intramolecular distances in Å include Hg(1)-O(1) 2.877(6), Hg(2)-O(1) 2.975(6), Hg(3)-O(1) 2.846(6), and Hg(2)-C(23) 3.328(10). Intermolecular bond distances(Å) and angles(º) include Hg(1)-C(1) 2.071(9), Hg(1)-C(8) 2.066(9), Hg(2)-C(7) 2.071(9), Hg(2)-C(14) 2.088(9), Hg(3)-C(2) 2.065(9), Hg(3)-C(13) 2.066(8), O(1)-N(1) 1.277(9), C(8)-Hg(1)-C(1) 176.1(4), C(7)-Hg(2)-C(14) 176.4(4), C(2)-Hg(3)-C(13) 173.8(4). Right: Compound **4** with 30% thermal ellipsoids (fluorine and hydrogen atoms omitted for clarity).Intramolecular distances in Å include Hg(1)-O(1) 3.020(17), Hg(2)-O(1) 2.974(19), Hg(3)-O(1) 2.90(2), Hg(1A)-O(2) 2.91(2), Hg(2A)-O(2) 2.97(2), Hg(3A)-O(2) 2.99(2). Intermolecular bond distances(Å) and angles(º) include Hg(1)-C(1) 2.11(3), Hg(1)-C(8) 2.08(2), Hg(2)-C(7) 2.09(3), Hg(2)-C(14) 2.12(3), Hg(3)-C(2) 2.10(2), Hg(3)-C(13) 2.09(2), O(1)-N(1) 1.28(3), O(2)-N(2) 1.27(3), C(1)-Hg(1)-C(8) 176.4(10), C(7)-Hg(2)-C(14) 177.1(9), C(2)-Hg(3)-C(13) 176.3(9).

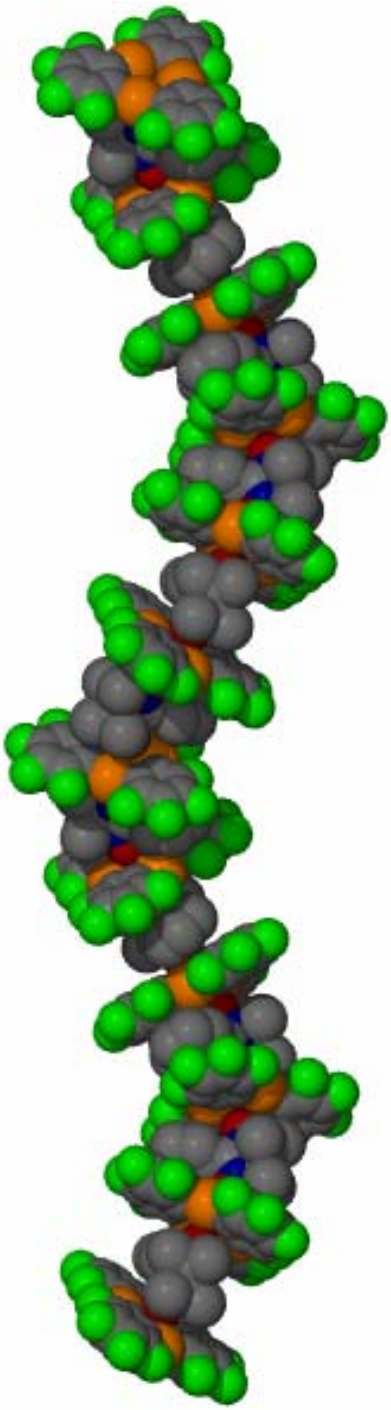

Figure 3.3. Space filling model of the extend structure of compound **4** showing the helical binary supramolecular chains. Color code: Mercury (orange), Fluorine (green), Carbon (grey), Nitrogen (blue), and Oxygen (red).

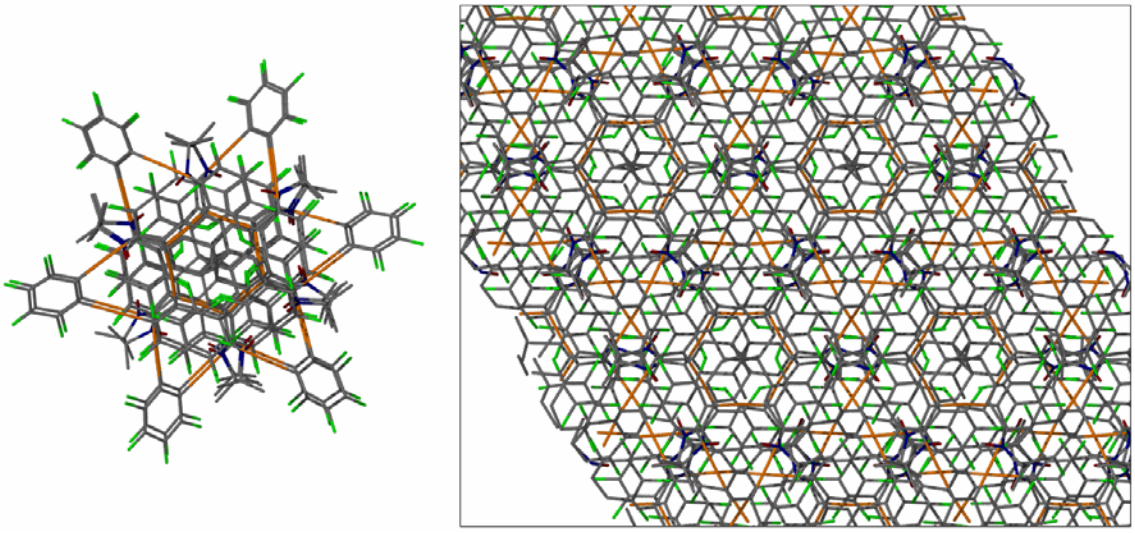

Figure 3.4. Left: Stack of **4** viewed down the c-axis. Right: Packing of **4** viewed down the c-axis.

3.4 Diffuse reflectance absorption spectra of **3** and **4**

Diffuse reflectance spectra were recorded on crushed crystals of pristine TEMPO, compound **2**, pristine NIT-Ph, compound **3** and compound **4** and are shown in Figure 3.5. Pristine TEMPO features an absorption band that corresponds well with free tempo in solution with an absorption maximum at 457 nm. In contrast compound **2** appears to be blue shifted. Pristine NIT-Ph features absorption maxima at 587 and 637 nm with an intense shoulder at 677 nm which agree well with the free NIT-Ph in solution. These transitions are thought to be n→π transitions.[75] Compounds **3** and **4** feature absorption bands that are blue-shifted compared to pristine NIT-Ph and occur at 530 and 577 nm with compound **4** also featuring a shoulder at 677 nm which is less intense.

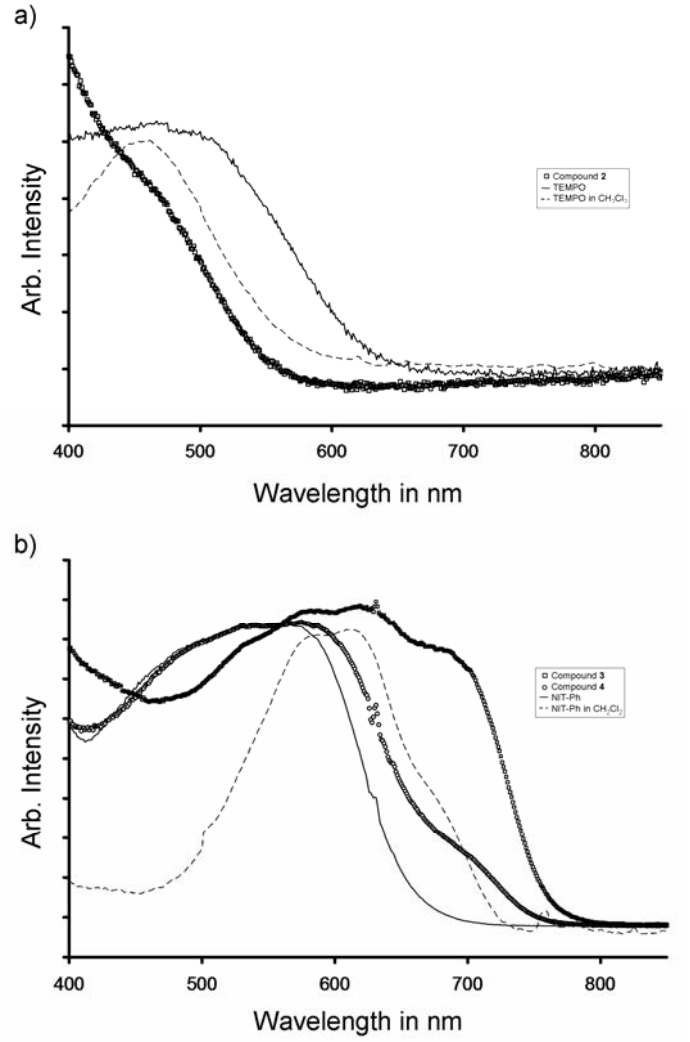

Figure 3.5. Diffuse reflectance absorbance spectra of a) Compound **2**, TEMPO, and TEMPO in CH_2Cl_2 b) Compound **3**, Compound **4**, NIT-Ph, and NIT-Ph in CH_2Cl_2.

3.5 EPR spectra

An EPR spectrum was recorded on a CH_2Cl_2 solution of NIT-Ph and a CH_2Cl_2 solution containing NIT-Ph and an excess of **1** (Figure 3.6). Each spectrum features a five line pattern with g = 2.015 which is consistent with the known spectrum of pristine NIT-Ph (five line pattern, g = 2.0065).[76] EPR spectra were also recorded on crushed single crystals of compounds **3** and **4** (Figure 3.7). Each spectrum features a broad = singlet with g = 2.012 for **3** and g = 2.013 for **4**. These values compare well with the values measured in solution.

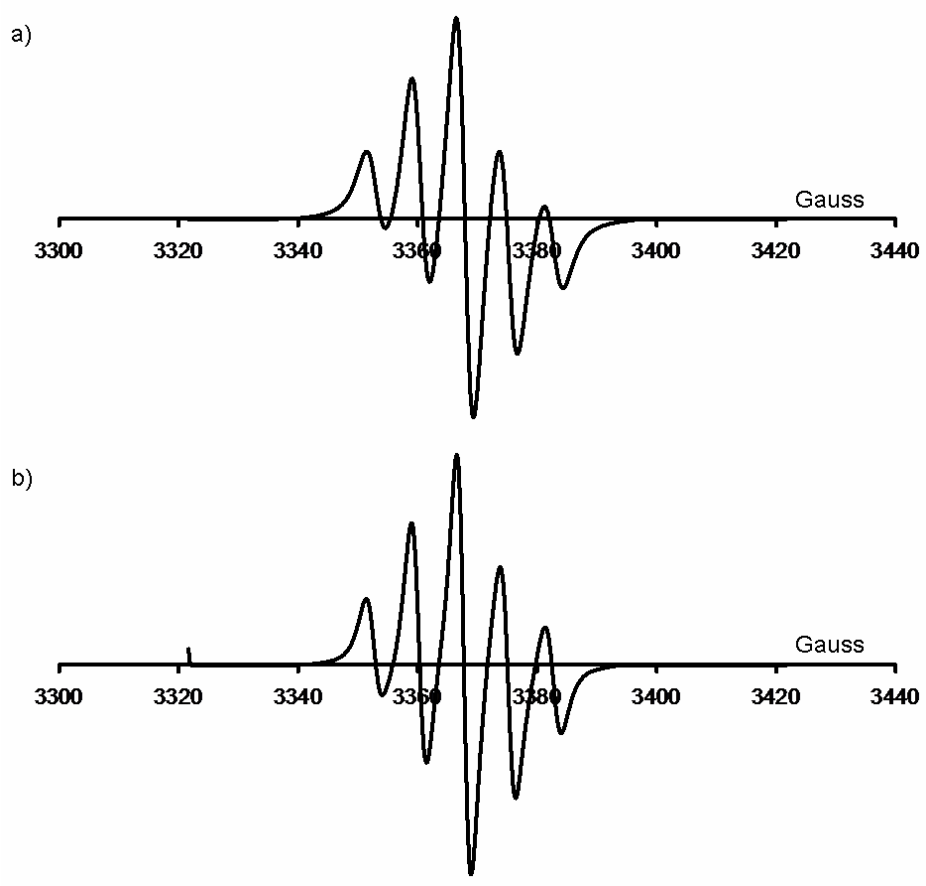

Figure 3.6. EPR spectra of a) NIT-Ph and b) NIT-Ph and **1** in CH_2Cl_2.

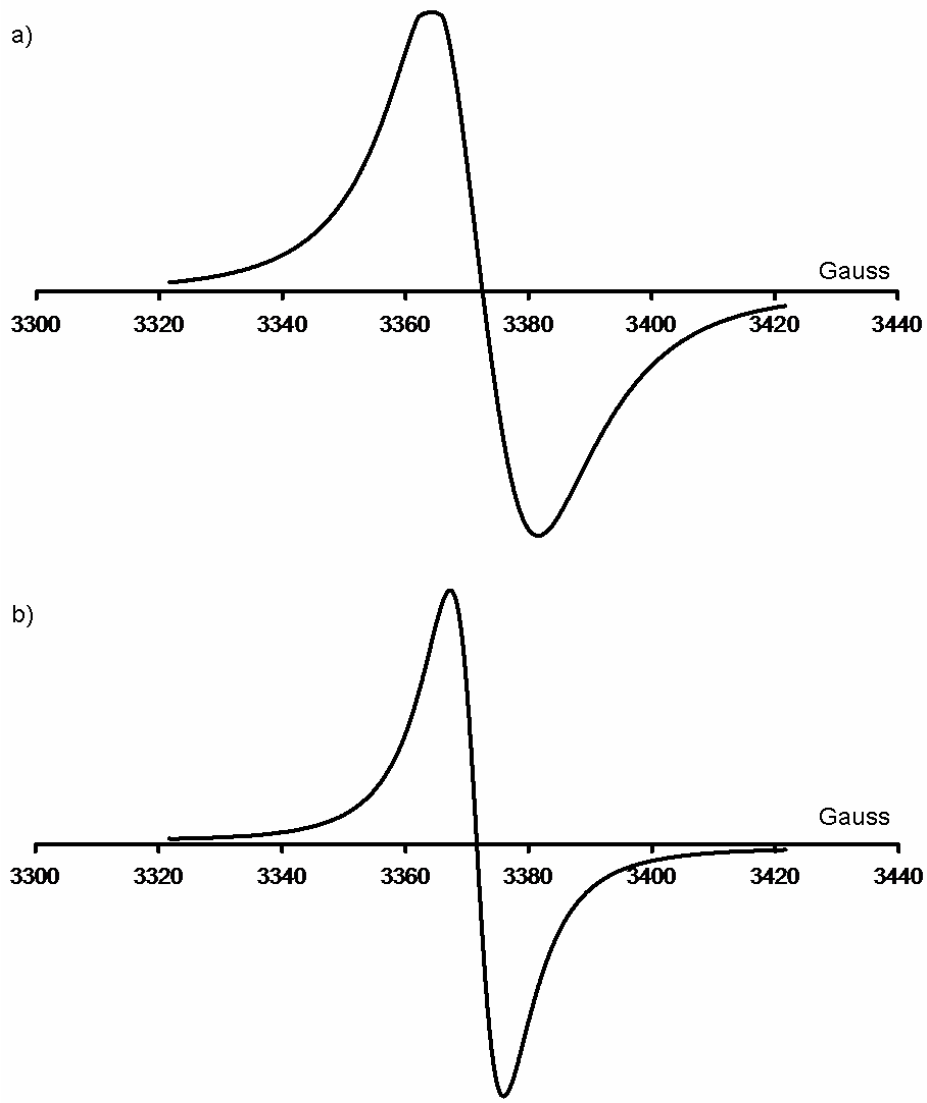

Figure 3.7. Solid-state EPR spectrum of compound a) **3** and b) **4**.

3.6 Magnetic susceptibility measurements

Variable-temperature (2-300 K) magnetic susceptibility data were collected on crushed single crystals of compounds **2-4** (Figure 3.8). The room temperature values of X_mT vs. T for compound **2** is in good agreement with the expected value for an isolated molecule with one unpaired electron (S = 1/2) and remains independent of temperature until approximately 10 K at which point a sharp decrease is observed, indicating probable long-range anti-ferromagnetic coupling.

Compound **3** exhibits simple paramagnetic behavior with a X_mT vs. T value of 0.4 emu K mol^{-1} over the entire temperature range and is in good agreement with the expected value for an isolated molecule with one unpaired electron (S = 1/2). This is expected due to the molecules of NIT-Ph being nearly 13 Å apart, and the absence of interactions between neighboring molecules of **1** that would allow for communication between the unpaired spins.

The room temperature values of X_mT vs. T for compound **4** is in good agreement with the expected value for an isolated molecule with one unpaired electron (S = 1/2) and remains independent of temperature until approximately 10 K at which point a sharp decrease is observed, indicating probable long-range anti-ferromagnetic coupling. This behavior was reproduced using the Heisenberg model for a 1D-chain with the Hamiltonian $\hat{H} = -2J\Sigma\hat{S}_i\Sigma\hat{S}_{i-1}$,[77] which is appropriate given the extended chain structure

of compound **4**. A least squares analysis was performed based on these models, and the best agreement with the data was obtained for J = -0.5694 cm^{-1} and g = 2.0631. This set of parameters accurately reproduces all the features of the X_mT vs. T plot over the entire temperature range. The small magnitude of the coupling constants makes the assignment of the pathways for magnetic communication difficult. Because **2** does not form 1D chains and the X_mT vs. T plots for **2** and **4** are similar. For this reason, it is difficult to assess the role of **1** in the mediation of magnetic interactions. These results also indicate that, if **1** mediates magnetic interactions in the radical chain found in **4**, it does so very weakly.

While many complexes of nitronyl nitroxide derivatives have been synthesized with open-shell metals, few have contained closed-shell metals such as zinc. These few have exhibited behavior consistent with situation **B** where the closed-shell metal is mediating an antiferromagnetic interaction between two nitronyl nitroxides.[78-81]

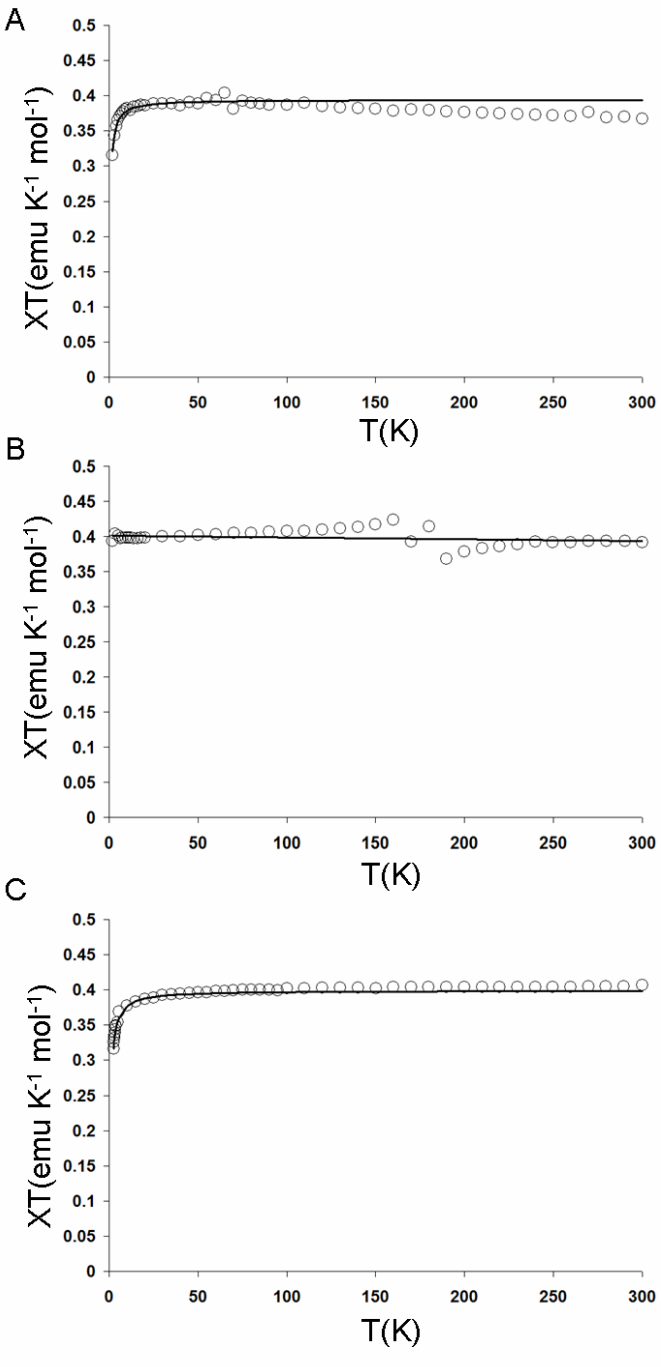

Figure 3.8. Thermal variation of the X_mT product for compound **2** (A), compound **3** (B), and compound **4** (C) in the 2-300 K range. The solid line shows the best fitting yielding g = 2.0631 and J = -0.5694 cm^{-1} for compound **4**.

3.7 Summary

We have demonstrated that **1** forms adducts with organic nitronyl radicals where the electron rich terminus of the N-O moiety coordinates to all three mercury centers of **1**. Absorption spectra of **2-4** feature absorptions that occur at shorter wavelengths than that of the free radical. EPR spectra of **3** and **4** show there is very little change in the g parameter. Magnetic measurements reveal that if **1** mediates magnetic interactions, it does so very weakly.

3.8 Experimental details

General. Due to the toxicity of the mercury compounds discussed in these studies extra care was taken at all times to avoid contact with solid, solution, and air-borne particulate mercury compounds. The studies herein were carried out in well-aerated fume hood. Atlantic Microlab, Inc., Norcross, GA, performed the elemental analyses. NIT-Ph was synthesized in our lab according to the published procedure. The remainder of commercially available starting materials and solvents were purchased from Aldrich Chemical and were used as provided. Compound **1** was prepared according to the published procedure outlined by Sartori and Golloch. Magnetic susceptibility and magnetization measurements were carried out with a Quantum Design SQUID magnetometer MPMS-XL. DC magnetic measurements were performed with an applied field of 1000 G in the 2-300 K temperature range. Data were corrected for the diamagnetic contributions calculated from the Pascal constants.[82]

Synthesis of [1•TEMPO] (2). A solution of compound **1** (100 mg, 96 μmol) in

CH_2Cl_2 was mixed with a solution of TEMPO (15 mg, 98 μmol) in CH_2Cl_2. Upon slow evaporation of the solvent yellow crystals of compound **2** were observed (109 mg, Yield: 95%). mp 239 ºC decomposition. Anal. Calc. For $C_{27}H_{18}F_{12}Hg_3NO$: C, 27.01; H, 1.51. Found: C, 27.03; H, 1.42.

Synthesis of [(1)$_2$•NIT-Ph] (3). A solution of compound **1** (100 mg, 96 μmol) in CH_2Cl_2 was mixed with a solution of NIT-Ph (22.4 mg, 96 μmol) in CH_2Cl_2. Upon evaporation of the solvent the crystals were washed with hexanes to remove excess NIT-Ph. The remaining pink crystals were then washed quickly with 0.5 ml of CH_2Cl_2 to insure purity and found to be 40 mg (Yield: 18%) of compound **3**. mp 220 ºC decomposition. Anal. Calc. For $C_{49}H_{17}F_{24}Hg_6N_2O_2$: C, 25.35; H, 0.74. Found: C, 25.57; H, 0.72.

Synthesis of [1•NIT-Ph] (4). A solution of compound **1** (100 mg, 96 μmol) in CH_2Cl_2 was mixed with a solution of NIT-Ph (100 mg, 0.529 mmol) in CH_2Cl_2. Upon evaporation of the solvent the crystals were washed with hexanes to remove excess NIT-Ph. The remaining purple crystals were then washed quickly with 0.5 ml of CH_2Cl_2 to insure purity and found to be 90 mg (Yield: 73%) of compound **4**. mp 190 ºC decomposition. Anal. Calc. For $C_{31}H_{17}F_{12}Hg_3N_2O_2$: C, 29.10; H, 1.34. Found: C, 28.99; H, 1.32.

Single-Crystal X-ray Analysis. X-ray data for **2-4** were collected on a Bruker Smart-CCD diffractometer using graphite-monochromated Mo-Kα radiation (λ = 0.71073 Å). Specimens of suitable size and quality were selected and mounted onto a glass fiber with Apezion grease and run at 110 K. The structures were solved by direct

methods, which successfully located most of the non-hydrogen atoms. Subsequent refinement on F^2 using the SHELXTL/PC package (version 6.1) allowed location of the remaining non-hydrogen atoms.

Magnetic Analysis. Magnetic susceptibility and magnetization measurements were carried out with a Quantum Design SQUID magnetometer MPMS-XL. DC magnetic measurements were performed with an applied field of 1000 G in the 2-300 K temperature range. Data were corrected for the diamagnetic contributions calculated from the Pascal constants. The data was sufficiently modeled based on the equations outlined by Carlin. The Hamiltonian is $\hat{H} = \text{-}2\text{J}\Sigma\hat{S}_i\Sigma\hat{S}_{i-1}$ where J is the intrachain exchange coupling constant. Thus the equation for XT is $XT = \frac{Ng^2\mu_B^2 S(S+1)}{3k}\frac{(1-u)}{(1+u)}$ where $u = (T/T_0) - \coth(T_0/T)$ and $T_0 = 2JS(S+1)/k$. Using these equations values of J = -0.4092 cm^{-1} and g = 2.0509 (compound **2**) and J = -0.5694 cm^{-1} and g = 2.0631 (compound **4**) were obtained.

CHAPTER IV

COORDINATION OF TTF AND TCNQ TO $[Hg(o\text{-}C_6F_4)]_3$*

4.1 Introduction

Trimeric perfluoro-*ortho*-phenylene mercury (**1**) is a simple trifunctional Lewis acid which has been used for the complexation of both anionic and neutral Lewis basic substrates.[3,13,15,20,47,59,71] In a series of studies, we also demonstrated that this trinuclear mercury derivative readily complexes with aromatic substrates including benzene, naphthalene, biphenyl, pyrene and triphenylene.[38,49,72] The resulting adducts consists of supramolecular stacks in which the arene interacts with the mercury centers of **1** through secondary mercury-π interactions. It occurred to us that similar structures might result by interaction of **1** with more π–basic molecules. As a result, we have investigated its interaction with tetrathiafulvalene (TTF). As part of this work and in order to shed further light on the chemical affinity of **1**, we have also studied its interaction with the typical π-acidic 7,7,8,8-tetracyanoquinodimethane (TCNQ). These efforts were further motivated by a series of recent investigations in which it has been demonstrated π–basic trinuclear gold(I) derivatives interact with various π-acidic molecules including C_6F_6, TCNQ [83] and nitrofluorenones.[84]

---

* Reprinted with permission from, *C. R. Chimie, 7* Haneline, M. R.; Gabbaï, F. P., "TTF and TCNQ adducts of trimeric perfluoro-*ortho*-phenylene mercury", 871, Copyright 2004 Elsevier. DOI:10.1016/j.crci.2003.12.018

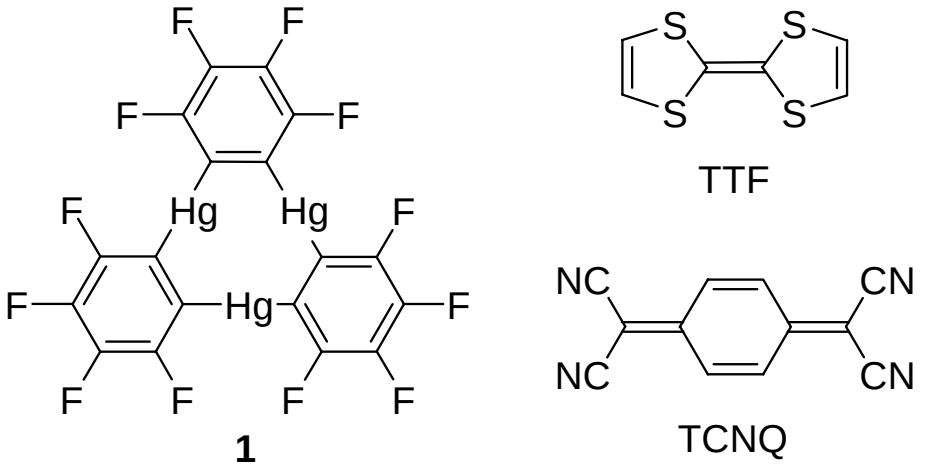

Scheme 4.1

4.2 Synthesis of [(**1**)$_2$•TTF] (**5**) and [(**1**)$_2$•TCNQ] (**6**)

When **1** and TTF are combined in a 1:1 mixture of CH_2Cl_2 and CS_2, slow evaporation of the solvent leads to the formation of orange needles of the 2:1 adduct [(**1**)$_2$•TTF] (**5**). Interestingly, a similar experiment carried out with TCNQ affords light yellow needles of an adduct of identical stoichiometry, namely [(**1**)$_2$•TCNQ] (**6**). In both cases, the color of these complexes corresponds to that of the organic molecule which rules out the presence of intense charge transfer bands. The ^{199}Hg, ^{19}F, and ^{1}H NMR spectra of these compounds in CD_2Cl_2 as well as their UV absorption spectra correspond to those of the free molecular components which indicates complete dissociation of the adducts upon dissolution.

4.3 Crystal structures of **5** and **6**

Compound **5** crystallizes in the triclinic space group *P*-1 with one centrosymmetrical [(**1**)$_2$•TTF] adduct per unit cell (Table 4.1, Figure 4.1). Examination

of the structure indicates that each molecule of TTF is sandwiched by two molecules of **1** and engages in multiple Hg-S secondary interactions that are shorter than the sum of the van der Waals radii of the two elements (sulfur (r_{vdw} = 2.03 Å) and mercury (r_{vdw} = 1.73-2.00 Å)[24,25]). As shown in Figure 4.1, the S(1) and S(2) atoms coordinate to the Hg(1) mercury center in a bidentate fashion (Hg(1)-S(1) 3.529(5) Å, Hg(1)-S(2) 3.533(5) Å). The sulfur atom S(1) forms an additional interaction with the mercury center Hg(3) (Hg(3)-S(1A) 3.467(5) Å). These secondary interactions are comparable to those found in $[\mathbf{1}\bullet SCN]^-$ and $[\mathbf{1}\bullet\mu_6\text{-}SMe_2]_n$. They are also respectively longer and shorter than the primary Hg-S bond (2.40 Å) and the secondary Hg-S interactions (3.89 Å) observed in the structure of $[tht\bullet HgCl_2]$[85]. It is interesting to point to the structural resemblance that exist between **2** and a series of gold-containing supramolecules reported by Balch as well as Burini and Fackler. As mentioned earlier, these supramolecules consist of stacks in whichtrinuclear gold(I) complexes alternate with organic derivatives such as fluorenones, hexafluorobenzene, and TCNQ. At the difference of **5**, the trinuclear gold(I) complexes are electron-rich while the organic substrates are electron-poor. Compound **5**, which contains electron-poor mercury centers and electron-rich TTF molecules, can therefore be regarded as the charge-reverse analogue of the gold assemblies.

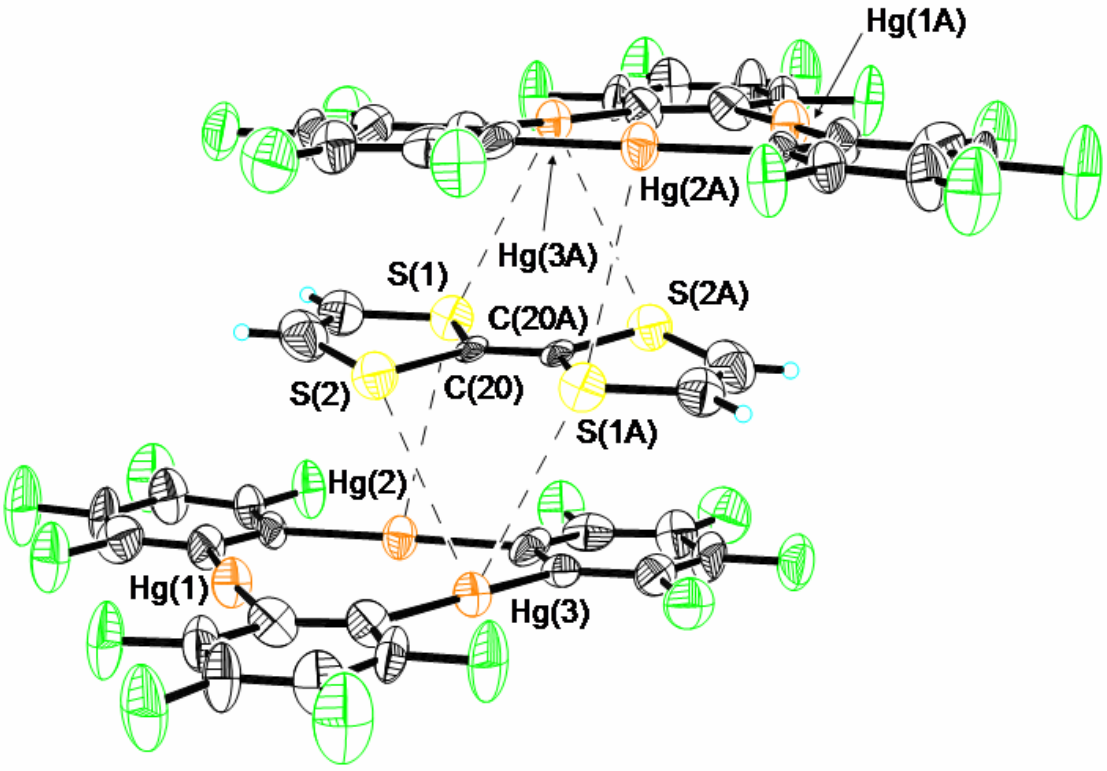

Figure 4.1. Crystal structure of **5**. Mercury (orange), Sulfur (yellow), Fluorine (green), and Carbon (black). Intramolecular distances(Å): Hg(2)-S(1) 3.529(5), Hg(3)-S(2) 3.533(5), Hg(3)-S(1A) 3.467(5). Intermolecular bond distances(Å) and angles(degrees): Hg(1)-C(8) 2.111(14), Hg(1)-C(1) 2.122(14), Hg(2)-C(7) 2.051(13), Hg(2)-C(14) 2.086(15), Hg(3)-C(2) 2.041(16), Hg(3)-C(13) 2.069(15), C(20)-C(20A) 1.37(2), S(1)-C(20) 1.779(13), S(2)-C(20) 1.729(13), C(8)-Hg(1)-C(1) 174.8(6), C(7)-Hg(2)-C(14) 176.4(7), C(2)-Hg(3)-C(13) 174.4(6), S(2)-C(20)-S(1) 114.4(7).

Table 4.1. Crystal data, data collection, and structure refinement for **5** and **6**-$(CS_2)_3$.

Crystal data	**5**	**6**-$(CS_2)_3$
Formula	$C_{42}H_4F_{24}Hg_6S_4$	$C_{51}H_4F_{24}Hg_6N_4S_6$
M_r	2296.23	2524.48
Crystal size (mm^3)	0.29 x 0.055 x 0.055	0.31 x 0.15 x 0.080
Crystal system	Triclinic	Triclinic
Space group	*P-1*	*P-1*
a (Å)	8.9347(18)	8.9533(18)
b (Å)	10.017(2)	12.038(2)
c (Å)	13.669(3)	14.641(3)
α (°)	87.57(3)	96.47(3)
β (°)	75.12(3)	96.35(3)
γ (°)	78.75(3)	109.82(3)
V ($Å^3$)	1159.5(4)	1456.3(5)
Z	1	1
ρ_{calc} (gcm^{-3})	3.288	2.878
μ(Mo K_α)(mm^{-1})	20.098	16.088
F(000) (e)	1016	1130
Data Collection		
T/K	293(2)	293(2)
Scan mode	ω	ω
hkl range	-10→9, -11→11, -16→16	-10→10, -14→14, -17→16
Measured refl.	11377	13915
Unique refl., [R_{int}]	4068 [0.0486]	5088 [0.0286]
Refl. used for refinement	4068	5088
Absorption correction	SADABS	SADABS
T_{min}/T_{max}	0.122867	0.315385
Refinement		
Refined parameters	343	412
R1, wR2 [I>2σ(I)]	0.0443, 0.1168	0.0460, 0.1091
ρ_{fin} (max/min) ($eÅ^{-3}$)	2.319, -1.982	4.332, -1.558
Flack parameter	-	-

[a] R1 = $(F_o - F_c)/ F_o$. [b] wR2 = $\{ [w(F_o^2 - F_c^2)^2]/ [w(F_o^2)^2]\}^{1/2}$; $w = 1/ [\sigma^2(F_o^2) + (ap)^2 + bp]$; $p = (F_o^2 + 2F_c^2)/3$; a = 0.0851 (**5**), 0.0808 (**6**); b = 0 (**5**), 15.0890 (**6**).

As in the case of **5**, compound **6** crystallizes in the triclinic *P*-1 space group with one centrosymmetrical [(**1**)$_2$•TCNQ] adduct per unit cell which also contains three molecule of CS_2 (Table 4.1, Figures 4.2-4.4). Examination of the atomic connectivity reveals the simultaneous coordination of one of the nitrile nitrogen atoms to the three mercury centers of **1**, Figure 4.2. The resulting Hg-N distances range from 3.102(11) to 3.134(11) Å and are well within the sum of the van der Waals radii for mercury (r_{vdw} = 1.73-2.00 Å)[24,25] and nitrogen (r_{vdw} = 1.60 Å). As a result of these interactions, the nitrogen atom is essentially equidistant from the three Lewis acidic sites and sits at 2.32 Å from the plane defined by the three mercury atoms. The linear nitrile functionality is almost perpendicular to the plane of the trinuclear complex with which it forms an angle of 88.7°. The metrical and angular parameters observed in **6** resemble those encountered in [**1**•(μ_3-acetonitrile)$_2$], [**1**•μ_3-acrylonitrile], [**1**•(μ_3-benzonitrile)·(μ_1-benzonitrile)$_2$], and [**1**•μ_3-n-butyronitrile] (Avg. Hg-N = 2.97 Å). The *trans* nitrile group of the TCNQ molecules coordinates to another molecule of **1** thus completing the [(**1**)$_2$•TCNQ] unit. The remaining two nitrile groups of the TCNQ molecule do not engage in any donor interactions. Three molecules of CS_2 are trapped between neighboring [(**1**)$_2$•TCNQ] units and interact with the mercury centers of the juxtaposed molecules of **1**. Two of these molecules are symmetrically equivalent and are terminally ligated to the mercury center Hg(2) (Hg(2)-S(2) 3.532(6) Å). The third molecule of CS_2 is centrosymmetrical and interacts via each of its two sulfur atoms with four mercury centers provided by the two molecules of **1** (Hg(2)-S(3) 3.640(7) Å, Hg(3)-S(3) 3.485(6) Å). These Hg-S distances are comparable to those observed in the structure of **5** and are once again

shorter than the sum of the van der Waals radii of the two elements. As a result of these interactions the solid state structure of **6**-$(CS_2)_3$ consist of extended one dimensional chain as depicted in figure 4.4.

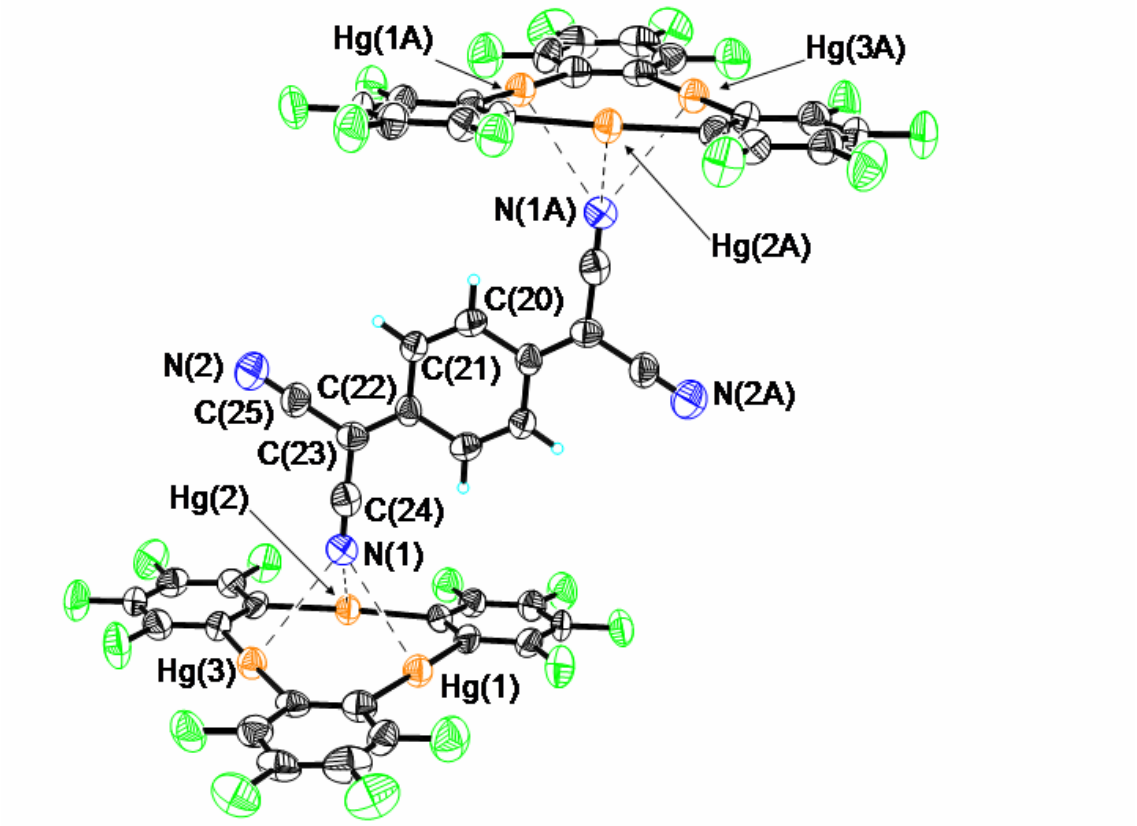

Figure 4.2. Crystal structure of **6** illustrating the Hg-N interactions. Mercury (orange), Fluorine (green), Nitrogen (blue), and Carbon (black). Intramolecular distances(Å): Hg(1)-N(1) 3.102(11), Hg(2)-N(1) 3.128(12), Hg(3)-N(1) 3.134(11). Intermolecular bond distances(Å) and angles(degrees): Hg(1)-C(1) 2.089(14), Hg(1)-C(8) 2.099(12), Hg(2)-C(14) 2.104(12), Hg(2)-C(7) 2.109(12), Hg(3)-C(13) 2.079(14), Hg(3)-C(2) 2.079(13), N(1)-C(24) 1.157(17), N(2)-C(25) 1.130(18), C(20)-C(21) 1.335(18), C(21)-C(22) 1.438(17), C(22)-C(23) 1.366(17), C(23)-C(24) 1.424(18), C(23)-C(25) 1.449(18), C(1)-Hg(1)-C(8) 175.3(5), C(14)-Hg(2)-C(7) 176.0(5), C(13)-Hg(3)-C(2) 176.2(5), C(24)-C(23)-C(25) 116.1(11), N(1)-C(24)-C(23) 178.6(15), N(2)-C(25)-C(23) 177.8(17).

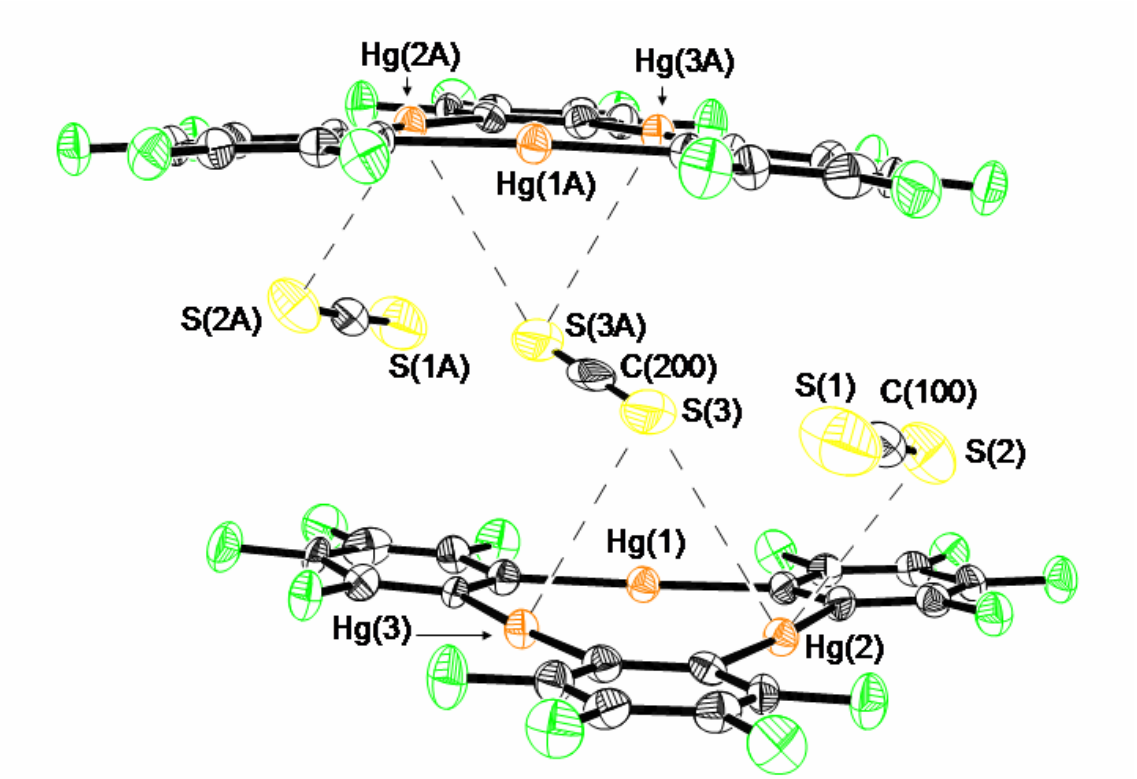

Figure 4.3. Crystal structure of **6** illustrating the Hg-S interactions. Mercury (orange), Fluorine (green), Sulfur (yellow), and Carbon (grey). Intramolecular distances(Å): Hg(2)-S(2) 3.532(6), Hg(2)-S(3) 3.640(7), Hg(3)-S(3) 3.485(6). Intermolecular bond distances(Å) and angles(degrees): S(1)-C(100) 1.57(3), S(2)-C(100) 1.51(2), S(3)-C(200) 1.553(11), S(2)-C(100)-S(1) 174.6(18), S(3)-C(200)-S(3A) 180.0(16).

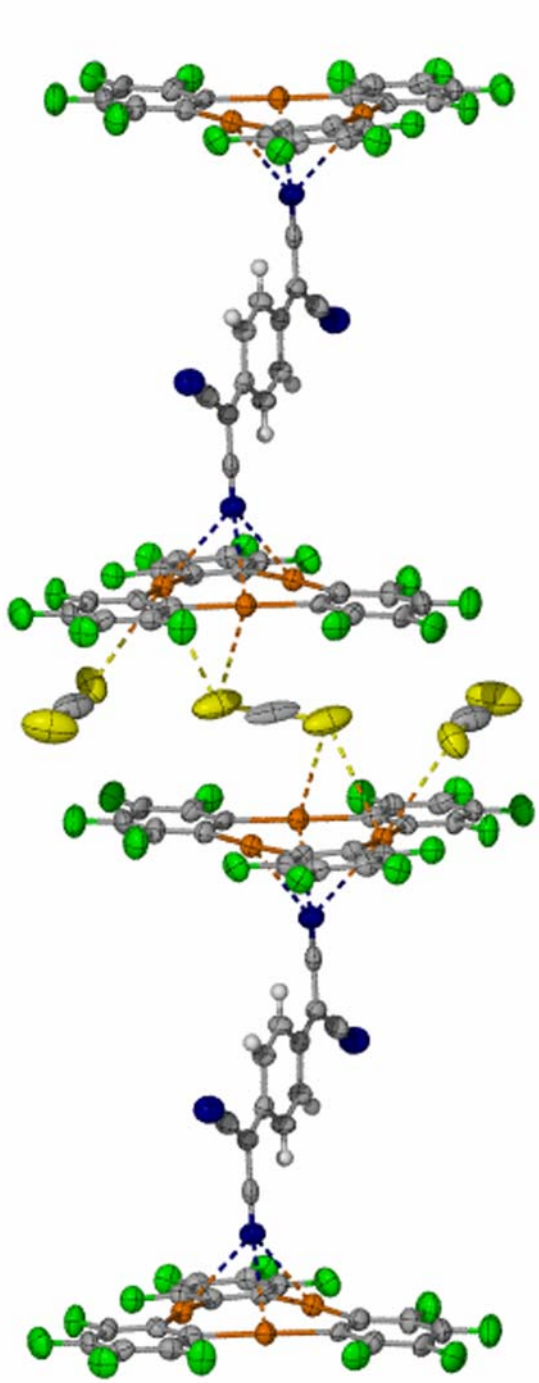

Figure 4.4. Extended structure of **6**. Mercury (orange), Fluorine (green), Nitrogen (blue), Sulfur (yellow), and Carbon (grey).

4.4 Summary

The results reported herein further document the acceptor ability of **1**. While known π donors such as TTF coordinate to **1** in a stacking fashion, known π acceptors such as TCNQ interact with **1** through the electron rich terminus of the nitrile groups. These results clearly indicate that compound **1** is a Lewis acid. It is also important to note that the spectroscopic and structural results presented herein do not support oxidation of the TTF molecules. As a result, compound **5** cannot be described as a charge transfer salt. Rather, its cohesion apparently results from the presence of secondary donor interaction occurring between the sulfur atoms of TTF and the mercury centers of **1**.

4.5 Experimental details

General. Due to the toxicity of the mercury compounds discussed in these studies extra care was taken at all times to avoid contact with solid, solution, and air-borne particulate mercury compounds. The studies herein were carried out in well-aerated fume hood. The infrared spectra were recorded as KBr pellets on a Mattson Genesis Series FTIR. Atlantic Microlab, Inc., Norcross, GA, performed the elemental analyses. TTF was purchased from TCI America and used as provided. Other commercially available starting materials and solvents were purchased from Aldrich Chemical and were used as provided. Compound **1** was prepared according to the published procedure outlined by Sartori and Golloch.

Synthesis of 1_2•TTF (5). Compound **1** (100 mg, 9.6 μmol) was dissolved in a 1:1 mixture of CS_2 and CH_2Cl_2 (30 ml). In a separate vial TTF (10 mg, 5.1 μmol) was dissolved in a 1:1 mixture of CS_2 and CH_2Cl_2 (3 ml). The two solutions were mixed thoroughly. Partial evaporation of the solvent resulted in the crystallization of **5**, which was isolated in a 70% yield (153 mg, 6.7 μmol). mp decomposition 285 °C. Anal. Calc. (Found) for $(C_{18}F_{12}Hg_3)_2$•$(C_6S_4H_4)$: C, 21.96 (22.16); H, 0.18 (0.16).

Synthesis of 1_2•TCNQ•3CS_2 (6-$(CS_2)_3$). Compound **1** (100 mg, 9.6 μmol) was dissolved in a 1:1 mixture of CS_2 and CH_2Cl_2 (30 ml). In a separate vial TCNQ (10 mg, 5.2 μmol) was dissolved in a 1:1 mixture of CS_2 and CH_2Cl_2 (3 ml). The two solutions were mixed thoroughly. Partial evaporation of the solvent resulted in the crystallization of **6**, which was isolated in a 22.7% yield (30 mg, 1.2 μmol). mp decomposition 275 °C. Anal. Calc. (Found) for $(C_{18}F_{12}Hg_3)_2$•$(C_{12}N_4H_4)$•$(CS_2)_3$: C, 24.26 (23.78); H, 0.16 (0.15).

Crystal Structures. X-ray data for **5** and **6** were collected on a Bruker SMART-CCD diffractometer using graphite monochromated Mo-Kα radiation (λ = 0.71073 Å). Specimens of suitable size and quality were selected and glued onto a glass fiber with superglue. The structure was solved by direct methods, which successfully located most of the non-hydrogen atoms. Subsequent refinement on F^2 using the SHELXTL/PC package (version 5.1) allowed location of the remaining non-hydrogen atoms. Further crystallographic details can be found in Table 4.1.

CHAPTER V

COORDINATION OF SUBSTITUTED BENZENES TO $[Hg(o\text{-}C_6F_4)]_3$*

5.1 Introduction

The complexation of arenes to mercury(II) cations constitutes a well established phenomenon.[30-34,86] While original efforts focused on the spectroscopic characterization of the resulting arene-mercury complexes, structural studies have also been performed and indicate that the arene ligand shows a propensity for both η^1/η^2-coordination to the mercury centers as shown by the work of the groups of Olah, Dean,[32] Kochi,[33] and Barron.[34,86] The formation of such complexes results in the activation of the arene substrates toward electrophilic mercuration reactions. Further support for electrophilic aromatic substitution reaction has been provided by Barron and co-workers who showed that arene mercury(II) cationic complexes catalyze H/D exchange reactions of C_6D_6 with arenes.[87] While such reactivity is apparently limited to the case of arene complexes of mercury(II) salts, the mercury centers of organomercurials can also bind arenes in a π-fashion. Typically, however, the -coordination of arenes observed in organomercurials is relatively weak and results in Hg-$C_{aromatic}$ distances in the range 3–3.4. While in most cases, arene coordination occurs intramolecularly,[88] a growing number of investigations indicate that intermolecular -arene complexation constitutes a viable motif.[37,38,49] Nevertheless, the observation of such complexes necessitates the use of

---

* Reprinted with permission from, *J. Chem. Soc., Dalton Trans., 13*, Haneline, M. R.; King, J. B.; Gabbaï, F. P., "Methyl Substituted Benzene Adducts of Trimeric Perfluoro-ortho-phenylene Mercury", 2686, Copyright 2003 The Royal Society of Chemistry.

organomercurials in which the Lewis acidity of the mercury center is enhanced through the use of fluorinated and therefore electron withdrawing ligands.[37,38,49] We first observed such a phenomenon in the isolation of π-complexes involving *ortho*-bis(chloromercurio)tetrafluorophenylene and benzene. Taking advantage of favorable cooperative effects, we turned our attention to the case of trimeric perfluoro-*ortho*-phenylene mercury (**1**), a tridentate Lewis acid[1,2,5,89] which readily complexes neutral[10,18,19,20,22,26] and anionic substrates.[3,4,13,15] Compound **1** crystallizes from benzene solutions to afford the complex [**1**•benzene]. The resulting complex [**1**•benzene] adopts a stacked structure in which the benzene molecules are sandwiched between nearly parallel, yet staggered molecules of **1**. As a result of this arrangement, the benzene molecule interacts with the six mercury centers of the two juxtaposed molecules of **1** in a μ_6-η^2:η^2:η^2:η^2:η^2:η^2 fashion. Formation of binary stacks is also observed with larger arenes such as biphenyl, naphthalene and triphenylene. In an effort to determine how steric effects might affect complex formation, we have now turned our attention to the case of methylated benzenes and wish to report on the complexation of toluene, *ortho*-xylene, *meta*-xylene, *para*-xylene and mesitylene by **1**.

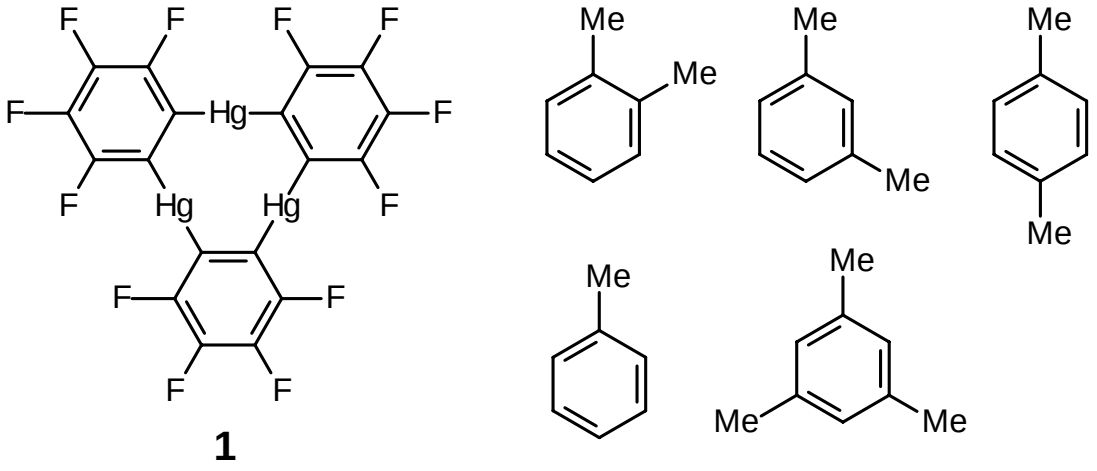

1

Scheme 5.1

5.2 Synthesis and thermal stability of [**1**•toluene] (**7**), [**1**•*ortho*-xylene] (**8**), [**1**•*meta*-xylene] (**9**), [**1**•*para*-xylene] (**10**) and [**1**•mesitylene] (**11**)

Compound **1** is only sparingly soluble in benzene (<0.2 mg ml^{-1}) and mesitylene (0.34 mg ml^{-1}), but dissolves in toluene (6.5 mg ml^{-1}), *ortho*-xylene (4.5 mg ml^{-1}), *meta*-xylene (2.5 mg ml^{-1}), and *para*-xylene (4.0 mg ml^{-1}). The ^{199}Hg NMR resonance of **1** in toluene, *ortho*-xylene, *meta*-xylene, and *para*-xylene appears at –1051.8, –1053.5, –1051.4 and –1059.1 ppm, respectively. Despite extended acquisition time, the ^{199}Hg NMR resonance of **1** in benzene or mesitylene could not be obtained due to the poor solubility of **1** in those solvents. We also note that the detection of the ^{199}Hg NMR resonance of **1** is complicated by its high multiplicity which results from Hg–F coupling. Slow evaporation of solutions of **1** in toluene, *ortho*-xylene, *meta*-xylene, *para*-xylene and mesitylene affords [**1**•toluene] (**7**), [**1**•*ortho*-xylene] (**8**), [**1**•*meta*-xylene] (**9**), [**1**•*para*-xylene] (**10**) and [**1**•mesitylene] (**11**), respectively, as crystalline complexes.

These colorless complexes are stable for months at room temperature. Upon elevation of the temperature, however, loss of the arene is readily observed. These adducts have been characterized by elemental analysis and thermogravimetric analysis. Compounds **7–10** feature a similar behavior with loss of arene occurring in the temperature range of 35–125 °C. For compound **11**, however, higher temperatures (90–160 °C) are required. In all cases, heating to temperatures higher than 160 °C leads to further weight loss which results from the sublimation of the trimercury derivative **1**.

The ^{199}Hg NMR resonance of **1** in toluene, *ortho*-xylene, *meta*-xylene and *para*-xylene resonance is slightly upfield from the resonance observed for **1** in CH_2Cl_2 (–1045.2 ppm). This phenomenon possibly reflects the solvation of the mercury centers by molecules of arenes. The facile crystallization of these binary solids and their thermal stability at ambient temperature points to the affinity of **1** for aromatic substrates. These results are in agreement with previous studies dealing with the complexation of benzene, biphenyl, naphthalene and triphenylene by **1**.[38,49]

5.3 Crystal structures of **7-11**

The crystal structures of compound **7–11** have been determined and the pertinent crystallographic data have been assembled in Tables 5.1–5.4 and in the captions of Figures 5.1, 5.4 and 5.5. In all cases, there is one molecule of **1**·arene in the asymmetric unit. The structures of **7**, **9** and **10** reveal the existence of binary stacks. The dihedral angles formed between the planar trinuclear core of **1** and the aromatic ring (3.5, 5.0 and 7.1° for **7**, **9** and **10**, respectively) indicate that the alternating molecules are almost

parallel to one another. The distances separating the centroid of the substituted benzene ring from the centroid of the two proximal molecules of **1** (3.63 and 3.81 for **7**, 3.40 and 3.89, for **9**, 3.60 and 3.61 for **10**) are relatively close; hence the stacks are regular and do not feature any discontinuity. In each stack, the successive molecules of **1** adopt an eclipsed rather than a staggered arrangement. It is also worth noting that the stacks are tilted with respect to the normal of the plane containing the three mercury centers of **1** (Fig. 5.2). This tilt (29.3, 23.2 and 21.0° for **7**, **9** and **10**, respectively) results from a moderate slippage of the sandwiched aromatic with respect to the centroid of the Hg_3 core of two closest molecules of **1**. Despite this slippage which is best measured by the offset distances defined in Fig. 5.3 (1.61 and 2.04 for **7**, 0.90 and 1.95, for **9**, 1.38 and 1.38 for **10**) we note that the aromatic ring of the substituted benzene remains situated above and below the core of the trinuclear complexes. In each case, the substituted benzene derivatives exhibit Hg-$C_{aromatic}$ interactions with distances ranging from 3.189(15) to 3.506(8) with the mercury centers of the neighboring molecules of **1**. While in **7**, **9** and **10**, the arene is almost equidistant from the two neighboring molecules of **1**, the molecule of *ortho*-xylene in **8** appears preferentially bound to one of the two proximal molecules of **1** with which it forms four short Hg-$C_{aromatic}$ contacts with distances ranging from 3.265(11) to 3.474(11) (Fig. 5.4). By contrast, the *ortho*-xylene molecule forms a single dihapto contact between the C(01)–C(06) atom pair and the Hg(2) center of the most distant neighboring molecule of **1** ((Hg(2)–C(01) 3.324(12), Hg(2)–C(06) 3.217(12)). The disparity found in the distances formed between the centroid of the substituted benzene ring and those of the closest two molecules of **1** (3.28

and 4.00) corroborate this general observation. This situation is even more acute in **11** which features very disparate inter-centroid distances of 3.41 and 4.52. As a result, **11** can be described as a 1 to 1 complex (Fig. 5.5). In this 1 to 1 complex, the mesitylene molecule is located directly above of the trinuclear core of **1** and interacts with the mercury centers *via* three contacts of 3.506(8), 3.445(8) and 3.443(8) which involve the non-substituted carbon atoms of the aromatic ring. Inspection of the cell packing diagram indicate that the 1 to 1 complexes interact with one another *via* an additional Hg-$C_{aromatic}$ interaction with a distance of 3.443(8) involving C(02) and the Hg(1) center of a neighboring molecule.

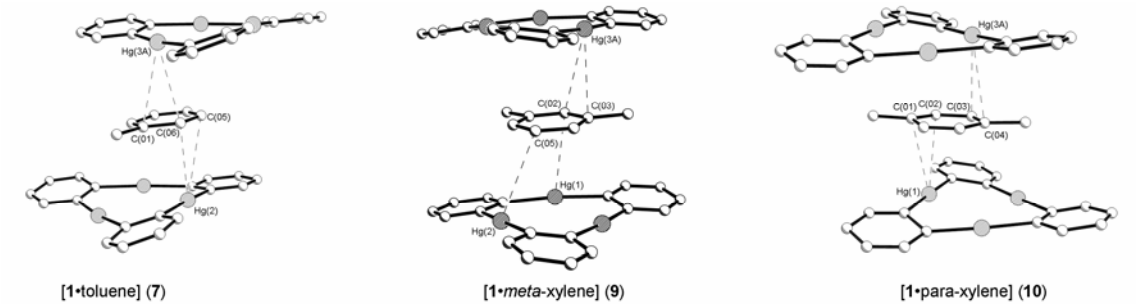

Figure 5.1. Molecular structures of compounds **7**, **9**, and **10**. Intermolecular bond distances [Å] for each compound. Compound **7**: Hg(3)-C(06) 3.189(15), Hg(3)-C(01) 3.323(15), Hg(2A)-C(05) 3.403(15), Hg(2A)-C(06) 3.387(15). Compound **9**: Hg(1)-C(02) 3.359(9), Hg(2)-C(05) 3.462(11), Hg(3A)-C(02) 3.383(11), Hg(3A)-C(03) 3.243(11). Compound **10**: Hg(1)-C(02) 3.20(2), Hg(1)-C(01) 3.43(3), Hg(3A)-C(03) 3.47(3), Hg(3A)-C(04) 3.32(3).

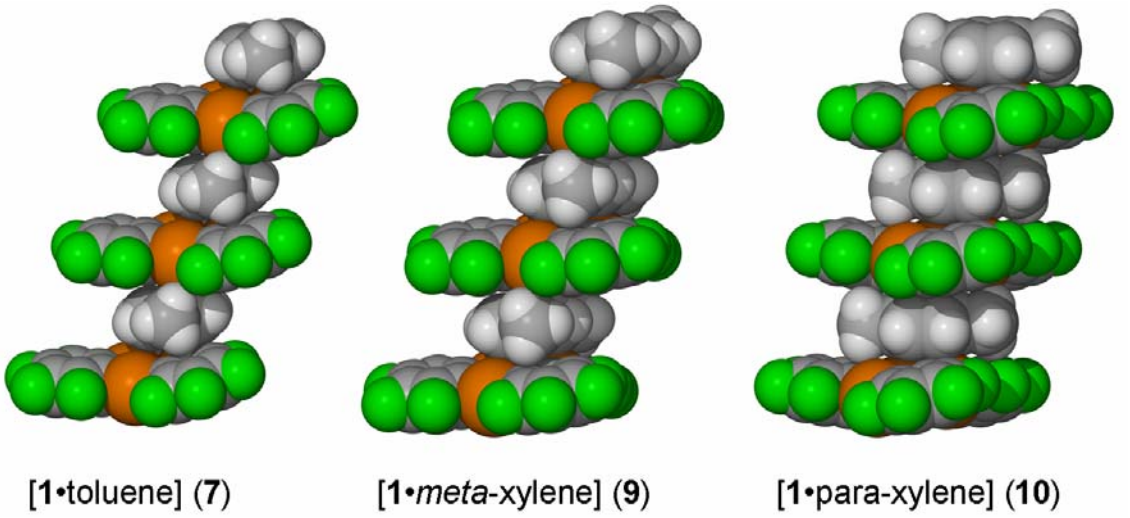

Figure 5.2. Space-filling models of compounds **7**, **9**, and **10**.

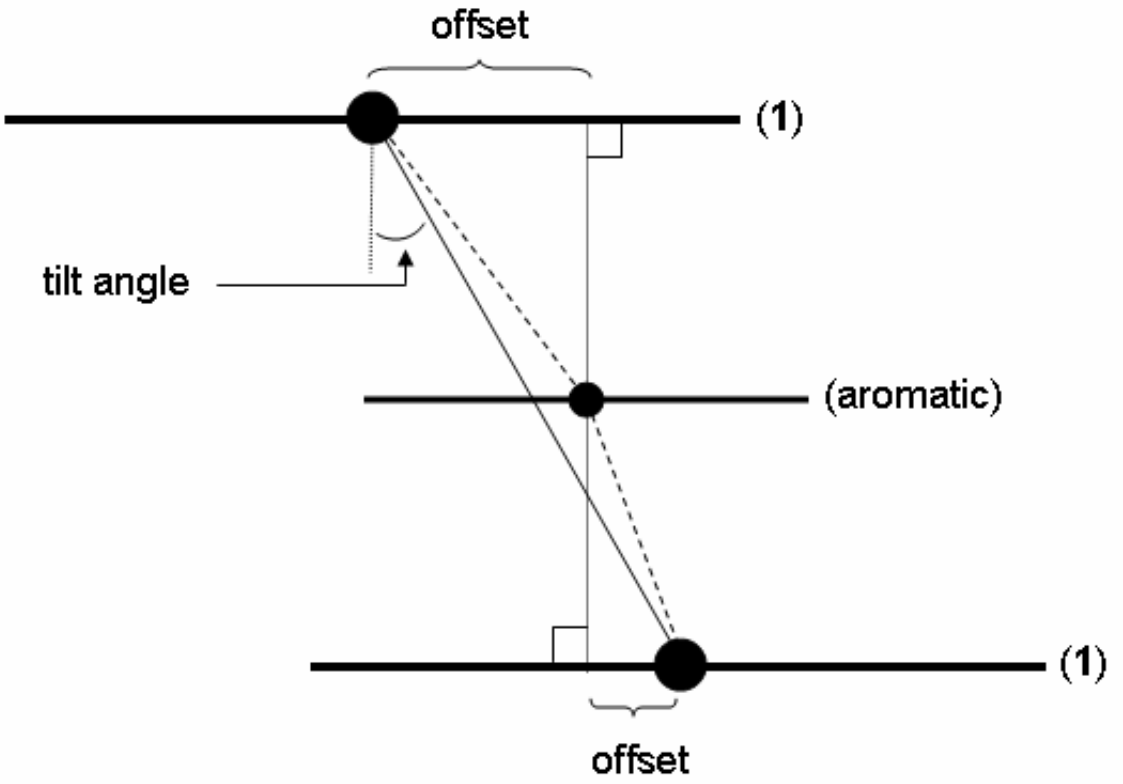

Figure 5.3. Diagram defining tilt angle and offset.

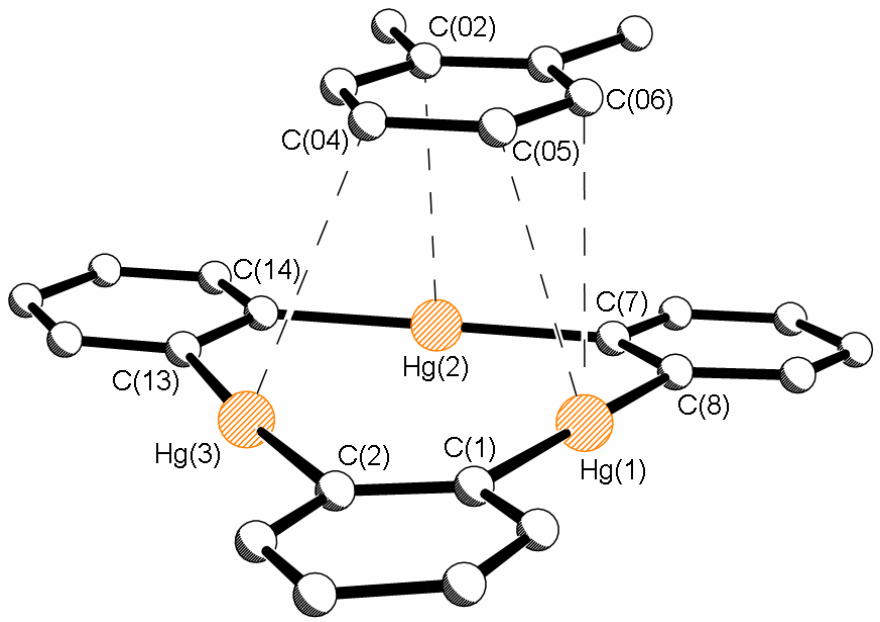

Figure 5.4. Molecular structure of compound **8** showing the ortho-xylene derivative and the closest neighboring molecule of 1. Intermolecular bond distances [Å]: Hg(1)-C(05) 3.321(12), Hg(1)-C(06) 3.451(11), Hg(2)-C(02) 3.265(11), Hg(3)-C(04) 3.474(11).

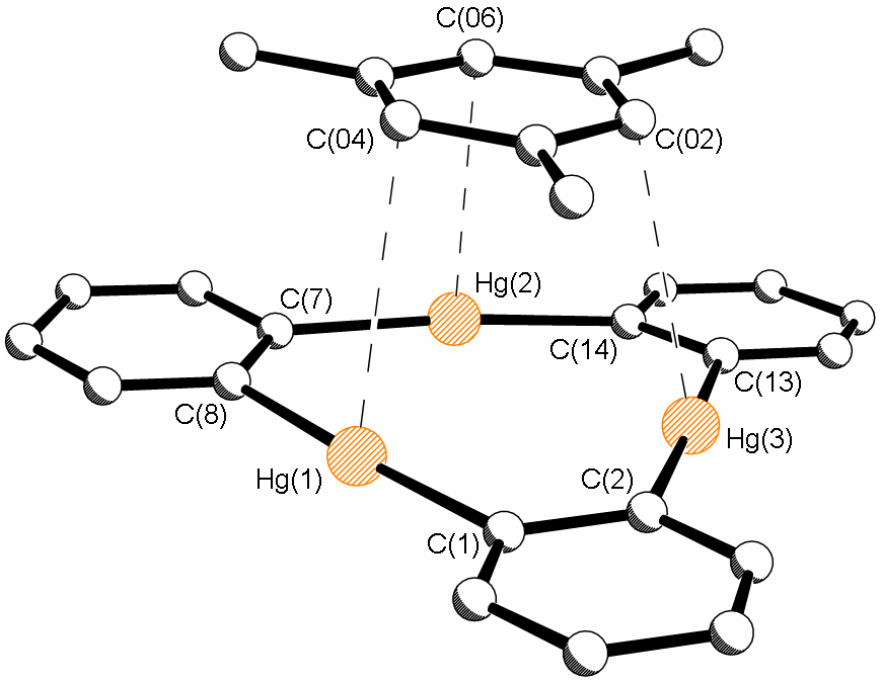

Figure 5.5. Molecular structure of compound **11**. Intermolecular bond distances [Å]: Hg(1)-C(04) 3.506(8), Hg(2)-C(06) 3.445(8), Hg(3)-C(02) 3.443(8).

Table 5.1. Crystal data, data collection, and structure refinement for **7-9**.

Crystal data	**7**	**8**	**9**
Formula	$C_{25}H_8F_{12}Hg_3$	$C_{26}H_{10}F_{12}Hg_3$	$C_{26}H_{10}F_{12}Hg_3$
M_r	1138.08	1152.11	1152.11
Crystal size (mm^3)	0.44 x 0.21 x 0.16	0.33 x 0.17 x 0.14	0.54 x 0.06 x 0.06
Crystal system	Monoclinic	Monoclinic	Orthorombic
Space group	$P2_1/c$	$P2_1/n$	$Pna2_1$
a [Å]	9.514(2)	20.050(4)	15.923(3)
b [Å]	7.4205(19)	6.8569(14)	21.678(4)
c [Å]	35.267(9)	20.158(4)	7.2192(14)
β (°)	93.550(4)	115.23(3)	
V ($Å^3$)	2485.1(11)	2507.0(9)	2491.9(9)
Z	4	4	4
ρ_{calc} (gcm^{-3})	3.042	3.052	3.071
μ(Mo K_α)(mm^{-1})	18.592	18.432	18.544
F(000) (e)	2024	2056	2056
Data Collection			
T/K	110(2)	110(2)	200(2)
Scan mode	ω	ω	ω
hkl range	-10→10, -8→8, -40→40	-23→21, -8→6, -23→23	-17→17, -24→23, -8→8
Measured refl.	21172	16191	19871
Unique refl., [R_{int}]	3906 [0.1125]	4385 [0.0440]	3573 [0.0368]
Refl. used for refinement	3906	4385	3573
Absorption correction	Empirical	SADABS	SADABS
T_{min}/T_{max}	0.2620/0.9655	0.4031	0.326298
Refinement			
Refined parameters	361	370	370
R1, wR2 [I>2σ(I)]	0.0433, 0.1046	0.0439, 0.1033	0.0217, 0.0498
ρ_{fin} (max/min) ($eÅ^{-3}$)	1.681, -2.237	4.019, -2.832	1.249, -0.562
Flack parameter	-	-	

[a] $R1 = \Sigma (F_o - F_c)/ \Sigma F_o$. [b] $wR2 = \{[\Sigma w(F_o^2 - F_c^2)^2]/ [\Sigma w(F_o^2)^2]\}^{1/2}$; $w = 1/[\sigma^2(F_o^2) + (ap)^2 + bp]$; $p = (F_o^2 + 2F_c^2)/3$; a = 0.0747 (**7**), 0.0700 (**8**), 0.0690 (**9**); b = 0 (**7**), 0 (**8**), 70 (**9**).

Table 5.2. Crystal data, data collection, and structure refinement for **10** and **11**.

Crystal data	**10**	**11**
Formula	$C_{26}H_{10}F_{12}Hg_3$	$C_{27}H_{12}F_{12}Hg_3$
M_r	1152.11	1166.14
Crystal size (mm^3)	0.30 x 0.15 x 0.13	0.25 x 0.24 x 0.40
Crystal system	Orthorhombic	Monoclinic
Space group	$Pna2_1$	$P2_1/c$
a [Å]	16.854(3)	16.453(3)
b [Å]	20.891(4)	7.3780(15)
c [Å]	7.1384(14)	22.030(4)
β (°)		96.43(3)
V ($Å^3$)	2513.4(9)	2657.4(9)
Z	4	4
ρ_{calc} (gcm^{-3})	3.045	2.915
μ(Mo K_α)(mm^{-1})	18.385	17.391
F(000) (e)	2056	2088
Data Collection		
T/K	293(2)	293(2)
Scan mode	ω	ω
hkl range	-19→18, -23→23, -7→8	-22→19, -9→9, -29→29
Measured refl.	15314	29640
Unique refl., [R_{int}]	3779 [0.0452]	6307 [0.0508]
Refl. used for refinement	3779	6307
Absorption correction	SADABS	SADABS
T_{min}/T_{max}	0.624366	0.252773
Refinement		
Refined parameters	370	379
R1, wR2 [I>2σ(I)]	0.0488, 0.1140	0.0420, 0.1035
ρ_{fin} (max/min) ($eÅ^{-3}$)	4.333, -1.446	3.708, -1.449
Flack parameter	-	-

[a] $R1 = \Sigma (F_o - F_c)/ \Sigma F_o$. [b] $wR2 = \{[\Sigma w(F_o^2 - F_c^2)^2]/ [\Sigma w(F_o^2)^2]\}^{1/2}$; $w = 1/[\sigma^2(F_o^2) + (ap)^2 + bp]$; $p = (F_o^2 + 2F_c^2)/3$; a = 0.0272 (**10**), 0.0800 (**11**); b = 0 (**10**) , 40 (**11**).

Table 5.3. Metrical parameters for the respective orientation of the molecular component in **7**-**11**.

Complex	**7**	**8**	**9**	**10**	**11**
Interplanar angle (°)	3.5	1.9	5.0	6.9	2.3
Intercentroid distances [Å]	3.63, 3.81	3.28 3.99	3.40, 3.89	3.61, 3.60	3.39, 4.54
Interplanar separations/Å	3.28, 3.26	3.23, 3.21	3.41, 3.33	3.34, 3.27	3.39, 3.39
Intercomponent offset/ Å	1.61 2.04	0.59 2.39	0.90 1.95	1.37 1.38	0.10 3.02
Tilt (°)	29.3	20.4	23.2	21.0	23.2

Table 5.4. Selected intramolecular distances and angles.

	7	**8**	**9**	**10**	**11**
Distance [Å]					
Hg(1)-C(8)	2.063(13)	2.065(10)	2.051(9)	2.087(18)	2.074(8)
Hg(1)-C(1)	2.069(14)	2.072(10)	2.054(8)	2.103(19)	2.071(8)
Hg(2)-C(7)	2.046(13)	2.070(11)	2.076(8)	2.031(18)	2.078(9)
Hg(2)-C(14)	2.067(13)	2.062(10)	2.076(9)	2.076(19)	2.065(8)
Hg(3)-C(2)	2.049(13)	2.086(10)	2.075(9)	2.05(2)	2.053(8)
Hg(3)-C(13)	2.084(13)	2.075(10)	2.066(8)	2.098(17)	2.066(8)
Angles [º]					
C(8)-Hg(1)-C(1)	174.6(5)	176.6(4)	174.7(4)	177.5(8)	176.4(3)
C(7)-Hg(2)-C(14)	173.5(6)	175.1(4)	173.6(3)	174.4(8)	174.6(3)
C(2)-Hg(3)-C(13)	173.2(5)	174.6(4)	175.9(4)	177.6(10)	176.3(3)

Atom numbering scheme for **1**

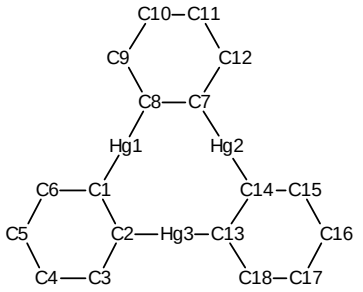

Although electrostatic forces likely contribute to the stability of these assemblies, it is important to note that in all cases, there are short contacts between the mercury centers of **1** and the substituted benzene molecules. These distances are in the 3.2–3.5 range and exceed the Hg–C bonds observed in arene mercury(II) cation complexes by approximately 0.8. Nevertheless, they remain within the sum of the van der Waals radius of mercury (r_{vdw}(Hg) = 1.73–2.00)[24,25] and that of carbon in aromatic systems ($r_{vdw}(C_{aromatic})$ = 1.7). They are similar to those observed in [**1**•benzene], [**1**•biphenyl], [**1**•naphthalene] and [**1**•triphenylene] (3.25–3.55) and indicate the presence of weak secondary interactions. Similar contacts are present in the structure of [**1**·4-phenylpyridine]. While **1**·benzene features stacks whose propagation direction is perpendicular to the plane of **1**, the stacks observed in **7**, **9** and **10** are tilted with respect to the normal of the plane containing the three mercury centers of **1**. This structural difference likely arises from the increased steric requirements of the substituted benzene derivatives which apparently interfere with the regularity of the stacking motif. Further increase of the steric bulk as in **11**, prevents efficient stacking and leads to the formation of 1 1 complexes. In a final note, although arene–fluoroarene interactions are not evident in **7–11**, these supramolecules are reminiscent of those involving methyl substituted benzenes and electron deficient molecules.[90,91]

5.4 Summary

The results presented herein further document the affinity of **1** for aromatic derivatives. While previous studies focused on unsubstituted arenes, the present findings

indicate that **1** tolerates increased steric bulk and readily complexes methyl substituted benzenes. In compounds **7–11** the supramolecular stacks are held by the presence of secondary -interactions between the mercury centers of **1** and the aromatic molecule. We have previously proposed that the formation of such species results from donor interactions involving the filled orbitals of the aromatic substrate and the empty 6p orbitals of the mercury centers. While such interactions are likely to be at play in the structure of **7–11**, we note that in several cases, the aromatic molecule appears randomly oriented above and below the trinuclear core of **1**. This feature might be taken as an evidence for the weakness of the donor interactions and probably reflects the participation of less directional electrostatic and dispersion forces. DFT calculations undertaken on **1** show a positively charged electrostatic potential surface in the center of the complex. With a negatively charged electrostatic potential surface at their locus,[92] the observed arrangement of the aromatic molecules might also result from favorable electrostatic interactions. Finally, we note that dispersion forces between the soft mercury atoms of **1** and the polarizable aromatic derivatives may also be present.[93]

5.5 Experimental details

General. Due to the toxicity of the mercury compounds discussed in these studies extra care was taken at all times to avoid contact with solid, solution, and air-borne particulate mercury compounds. The studies herein were carried out in a well-aerated fume hood. Atlantic Microlab, Inc., Norcross, GA, performed the elemental analyses. All commercially available starting materials and solvents were purchased

from Aldrich Chemical and were used as provided. Compound **1** was prepared according to the published procedure outlined by Sartori and Golloch. All NMR measurements were acquired at ambient temperature on an INOVA 400 MHz spectrometer.

General Synthetic Procedure. Compound **1** was dissolved by boiling in the selected solvents: toluene, *o*-xylene, *m*-xylene, *p*-xylene, and mesitylene. Upon cooling, followed by slow evaporation of the solvent in a well-aerated fume hood, crystallization occurs to afford quantitative yields of [**1**·toluene] (**7**), [**1**·*ortho*-xylene] (**8**), [**1**·*meta*-xylene] (**9**), [**1**·*para*-xylene] (**10**) and [**1**·mesitylene] (**11**). Compound **7**. Found: C, 26.42; H, 0.76. $C_{25}H_8F_{12}Hg_3$ requires C, 26.38; H, 0.71. Compound **8**. Found C, 27.55; H, 0.86. $C_{26}H_{10}F_{12}Hg_3$ requires C, 27.10; H, 0.88. Compound **9**. Found: C, 27.11; H, 0.84. $C_{26}H_{10}F_{12}Hg_3$ requires C, 27.10; H, 0.88. Compound **10**. Found: C, 27.40; H, 0.93. $C_{26}H_{10}F_{12}Hg_3$ requires C, 27.10; H, 0.88. Compound **11**. Found: C, 27.71; H, 1.01. $C_{27}H_{12}F_{12}Hg_3$ requires C, 27.81; H, 1.04%.

Single-Crystal X-ray Analysis. X-Ray data for **7**, **8**, **9**, **10** and **11** were collected on a Bruker Smart-CCD diffractometer using graphite-monochromated Mo-Kα radiation (λ = 0.71073). Specimens of suitable size and quality were selected and mounted onto a glass fiber with either Apiezon grease (for low-temperature data collections) or epoxy (for room-temperature data collections). The structures were solved by direct methods, which successfully located most of the non-hydrogen atoms. Subsequent refinement on F^2 using the SHELXTL/PC package (version 6.1) allowed location of the remaining non-hydrogen atoms.

Solubility Measurements. A weighed vial and stir bar were charged with a known amount of **1** (approximately 20 mg for toluene, *o*-xylene, *m*-xylene, and *p*-xylene and approximately 2 mg for benzene and mesitylene). The solvent was then added incrementally to the vial while stirring until the presence of solid **1** was no longer observed. The vial was then reweighed to determine the amount of solvent added.

Thermal Gravimetric Analyses. These analyses were carried out on a TA Instruments TGA Q500 using an argon flow (rate 60 ml min^{-1}), a heating rate of 2 °C min^{-1} and a sample size between 6 and 45 mg. The temperature range in which the weight loss occurs is given for each compound, along with the calculated and observed weight loss (WL_{calc} and WL_{obs}, respectively). **7**, 37 °C –114 °C (WL_{calc}, 8.10%; WL_{obs}, 8.09%); **8**, 47 °C –115 °C (WL_{calc}, 9.22%; WL_{obs}, 8.65%); **9**, 42 °C –124 °C (WL_{calc}, 9.22%; WL_{obs}, 8.97%); **10**, 43 °C –117 °C (WL_{calc}, 9.22%; WL_{obs}, 9.52%); **11**, 91 °C – 154 °C (WL_{calc}, 10.31%; WL_{obs}, 10.56%).

CHAPTER VI

COORDINATION OF POLYCYCLIC AROMATIC HYDROCARBONS TO [Hg(*o*-C_6F_4)]$_3$ AND LUMINESCENT PROPERTIES*

6.1 Introduction

The supramolecular chemistry of polyfunctional Lewis acids[1,2,5,89,94] is a vibrant area of research with applications in the field of catalysis[7,8,95] and molecular recognition.[4,7,8,13,14,16,17,20,37,48,66,67,96,97,98,99,100] While different Lewis acidic elements have been employed, those containing mercury in combination with electron-withdrawing backbones constitute a unique class. These derivatives exhibit fascinating host-guest chemistry with anions.[1,2,4,5,8,13,14,16,17,48,89,94] Depending on the structure of the guest, highly unusual complexes containing hypercoordinated anions can be isolated. In the case of organic substrates such as ethers,[7,37] ketones, formamides, sulfoxides, and nitriles,[20,100] polydentate mercury Lewis acids form chelate complexes in which the electron-rich terminus of the substrate interacts concomitantly with two, three, and sometimes four of the Lewis acidic mercury centers. In parallel to those studies, there

---

* Reprinted in part from *J. Am. Chem. Soc., 124*, Haneline, M. R.; Tsunoda, M.; Gabbaï, F. P., "π-Complexation of Biphenyl, Naphthalene, and Triphenylene to Trimeric Perfluoro-*ortho*-phenylene Mercury. Formation of Extended Binary Stacks with Unusual Luminescent Properties", 3737, Copyright 2002 American Chemical Society, *Chem. Eur. J., 9*, Haneline, M. R.; Taylor, R. E.; Gabbaï, F. P., "Trimeric Perfluoro-ortho-phenylene Mercury: A Versatile Lewis Acid Host", 5188, Copyright 2003 Wiley-VCH Verlag GmbH&Co. KGaA, and *Inorg. Chem., 42*, Omary, M. A.; Kassab, R. M.; Haneline, M. R.; Elbjeirami, O.; Gabbaï, F. P., "Enhancement of the Phosphorescence of Organic Luminophores upon Interaction with a Mercury Trifunctional Lewis Acid", 2176, Copyright 2003 American Chemical Society.

has been a recent focus on the interaction of polyfunctional organomercurials with arenes.

The affinity of mercury for unsaturated substrates is well documented. In addition to the mercuration of alkenes, alkynes, and aromatic derivatives which reflect this chemical trait, different types of arene-mercury -complexes have been isolated. While Crabtree has collected solid evidence for the formation of the [Hg(η^2-arene)] exciplexes,[101] Hg(I) and Hg(II) complexes have been structurally characterized. In this domain, the contributions of Olah, Dean, Kochi, and more recently Barron are especially noteworthy. Interestingly, related, yet weaker, arene π-complexes have been observed in the chemistry of organomercurials. In most cases, π-coordination occurs intramolecularly,[36,88] although unsupported complexes have been isolated recently. With Hg-C_{arene} distances in the range of 3-3.4 Å, these interactions are inherently weak. Nevertheless, solution NMR measurements have been performed and suggest an energy range of 1-2 kcal/mol. Following the isolation of π-complexes involving *ortho*-bis(chloromercurio)tetrafluorophenylene and benzene, we investigated the interaction of benzene with trimeric perfluoro-*ortho*-phenylene mercury (**1**) and observed the formation of compact stacks in which **1** and hexacoordinated benzene molecules alternate. In an extension of these studies, the interaction of **1** with biphenyl, naphthalene, acenaphthalene, anthracene, pyrene, triphenylene, perylene, and coronene has now been examined and will be presented in this chapter. In addition to the structures and luminescent properties of the various adducts, this chapter will also

include the results of an investigation of [**1**•benzene] by static solid-state wide line deuterium NMR spectroscopy.

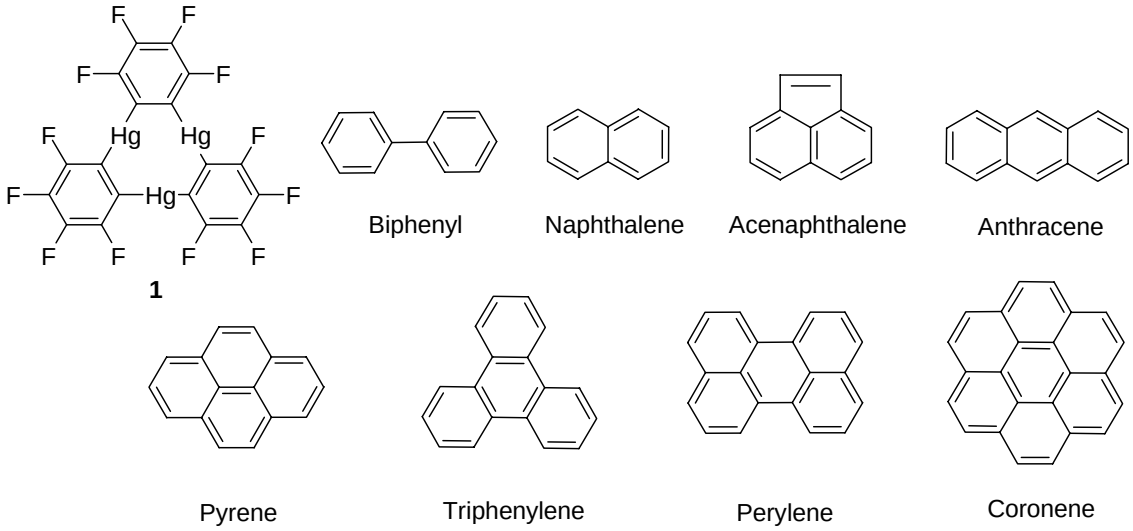

Scheme 6.1

6.2 Reinvestigation of [**1**•Benzene]

In order to better understand the cohesive interactions present in [**1**•benzene], their manifestation was searched for in the dynamic behavior of the sandwiched benzene molecules. Static solid-state wide line deuterium NMR spectroscopy is an adequate technique for studying such phenomena.[102,103] As shown by the spectra of [**1**•C_6D_6] (Figure 6.1), the line shape already features some distortion arising from molecular reorientation at –120 ºC. Line narrowing occurs at higher temperature indicating that the guest molecule enters the intermediate motional regime. These spectra could be satisfactorily simulated on the basis of a 6-fold jump reorientation of the benzene guest. Generation of an Arrhenius plot with the jump rates obtained from the simulations

affords an activation energy of 50 ± 1 kJ/mol (Figure 6.2). To the author's knowledge, this is the highest activation energy ever measured for an enclathrated or complexed benzene molecule,[102-104] suggesting the presence of strong interactions between the mercury atoms of **1** and the benzene molecules.

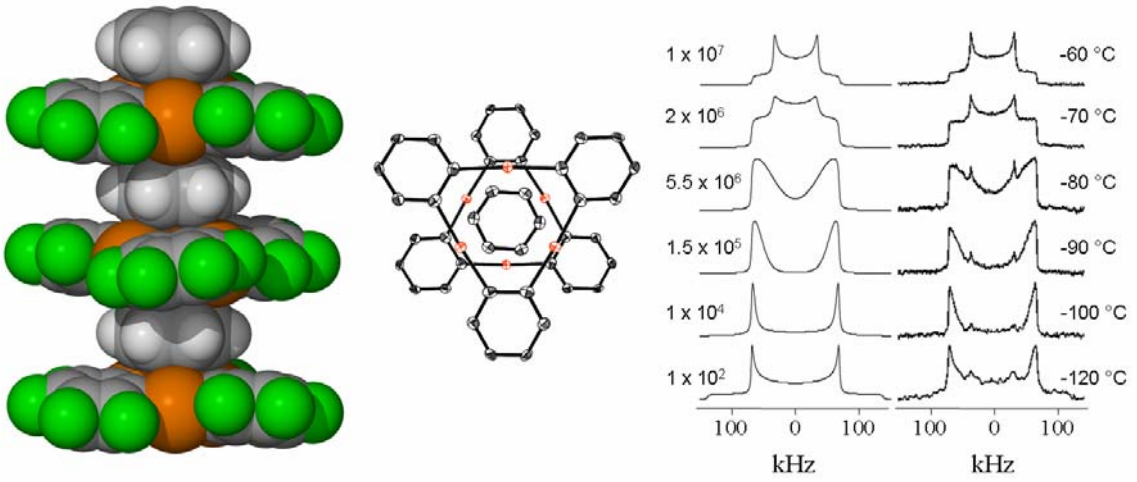

Figure 6.1. Left: Space filling model of [**1**•benzene] stacks. Middle: Top view of the thermal ellipsoid plot of [**1**•benzene•**1**]. Right: Static solid-state wide line deuterium NMR spectra of [**1**•benzene] at various temperatures and simulated spectra with rates of the benzene 6-fold jump.

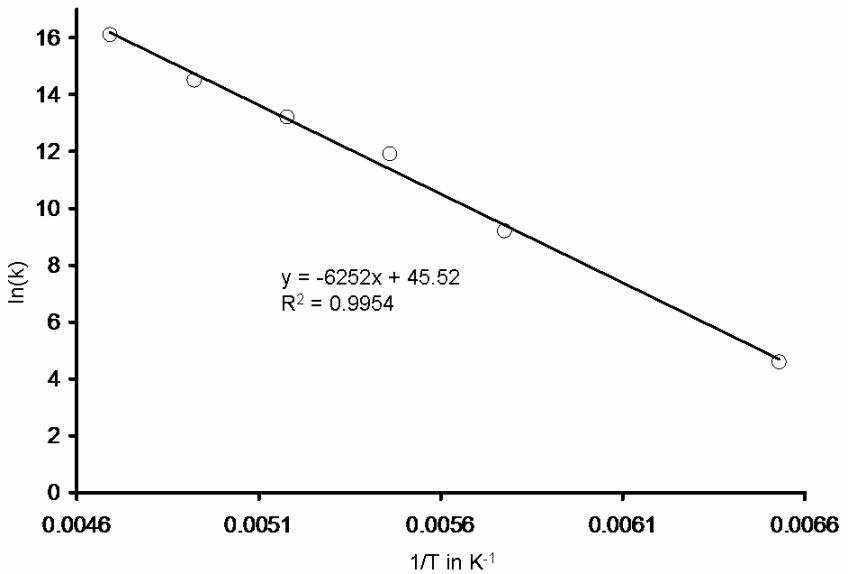

Figure 6.2. Arrhenius plot for [**1**•benzene] yielding an activation energy of 50 ± 1 kJ/mol.

6.3 Synthesis of [**1**•biphenyl] (**12**), [**1**•naphthalene] (**13**), [**1**•acenaphthalene] (**14**), [**1**•anthracene] (**15**), [**1**•pyrene] (**16**), [**1**•triphenylene] (**17**), [**1**•perylene] (**18**), and [**1**•coronene] (**19**)

Following our discovery that **1** complexes benzene, we decided to expand our studies to the case of larger arenes. When a CS_2 or CH_2Cl_2 solution of **1** is mixed with a solution of biphenyl in the same solvent, slow evaporation of the solvent leads to crystallization of a 1:1 adduct [**1**•biphenyl] (**12**) which is isolated in a pure form. A similar observation is made in the case of naphthalene, which also forms a 1:1 adduct with **1** [**1**•naphthalene] (**13**). Interestingly, when a CS_2 or CH_2Cl_2 of **1** is mixed with a solution of acenaphthalene, pyrene, triphenylene, perylene, or coronene in the same solvent, precipitation of a 1:1 adduct [**1**•acenaphthalene] (**14**), [**1**•anthracene] (**15**), [**1**•pyrene] (**16**), [**1**•triphenylene] (**17**), [**1**•perylene] (**18**), and [**1**•coronene] (**19**) occurs

spontaneously. Single crystals of **16** and **17** can be obtained by slow diffusion of a CH_2Cl_2 solution of **1** into a CH_2Cl_2 solution of triphenylene. Single crystals of **14**, **15**, **18**, and **19** can be obtained by mixing THF solutions of **1** and the corresponding arene. The stoichiometry of **12-19** was confirmed by elemental analysis as well as X-ray structural studies (vide infra). Compounds **12**, **13**, and **17** are colorless but luminesce when irradiated with UV light. Compounds **14**, **16**, **18**, and **19** possess the color of the corresponding arene and compound **15** is colorless.

6.4 Crystal structures of **12-19**

Compound **12** crystallizes in the monoclinic space group *C*2/*c* with one-half of a molecule of **1** and one-half of a molecule of biphenyl in the asymmetric unit (Table 6.1). The sandwiched biphenyl molecule is nonplanar and has a dihedral angle of 30.4. With Hg-$C_{biphenyl}$ distances ranging from 3.351 to 3.511 Å, the biphenyl molecule is weakly π-coordinated to four mercury centers of the neighboring molecules of **1** (Tables 6.1 and 6.2, Figure 6.3). The carbon atoms C(03) and C(04) engage in a η^2-interaction with the mercury center Hg(2), while the C(01)-C(01A)-C(06A) portion of the biphenyl is involved in an η^3-interaction with Hg(2A) (Table 6.2). The cohesion of the stacks is further cemented by symmetry-related interactions that involve C(03A)-C(04A) and Hg(2B) as well as C(01A)-C(01)-C(06) and Hg(2C).

Table 6.1. Crystal data, data collection, and structure refinement for **12**, **13**, **14** and **15**.

Crystal data	**12**	**13**	**14**	**15**
Formula	$C_{30}H_{10}F_{12}Hg_3$	$C_{28}H_8F_{12}Hg_3$	$C_{30}H_8F_{12}Hg_3$	$C_{36}H_{18}F_{12}Hg_3O$
M_r	1200.15	1194.11	1198.13	1296.27
Crystal size (mm^3)	0.14 x 0.10 x 0.70	0.15 x 0.23 x 0.35	0.35 x 0.31 x 0.25	0.39 x 0.24 x 0.21
Crystal system	Monoclinic	Monoclinic	Monoclinic	Monoclinic
Space group	*C*2/c	$P2_1/n$	*P*2(1)/n	*P*2(1)/n
a (Å)	7.3093(15)	19.632(4)	20.992(4)	10.656(2)
b (Å)	19.747(4)	7.0170(14)	6.8769(14)	27.528(6)
c (Å)	19.450(4)	21.212(4)	21.144(4)	11.074(2)
β (°)	97.17(3)	116.41(3)	119.22(3)	101.25(3)
V ($Å^3$)	2785.3(10)	2617.2(9)	2663.8(9)	3186.2(11)
Z	4	4	4	4
ρ_{calc} (gcm^{-3})	2.862	2.980	2.987	2.702
μ(Mo K_α)(mm^{-1})	16.597	17.659	17.354	14.522
F(000) (e)	2152	2096	2144	2360
Data Collection				
T/K	293(2)	293(2)	293(2)	110(2)
Scan mode	ω	ω	ω	ω
hkl range	-8→8, -22→23, -23→20	-21→22, -8→8, -24→24	-21→23, -7→7, -23→23	-11→11, -30→30, -12→12
Measured refl.	8736	15732	15638	20079
Unique refl., [R_{int}]	2451 [0.0966]	3965 [0.0472]	3827 [0.0371]	4569 [0.0263]
Refl. used for refinement	2451	3965	3827	4569
Absorption correction	SADABS	SADABS	SADABS	SADABS
T_{min}/T_{max}	0.070697	0.266223	0.242088	0.303555
Refinement				
Refined parameters	205	388	406	469
R1, wR2 [I>2σ(I)]	0.0677, 0.1603	0.0607, 0.1611	0.0551, 0.1194	0.0491, 0.1019
ρ_{fin} (max/min) ($eÅ^{-3}$)	2.327, -3.969	6.045, -2.476	7.472, -1.860	4.633, -1.756
Flack parameter	-	-	-	-

[a] $R1 = \Sigma (F_o - F_c)/ \Sigma F_o$. [b] $wR2 = \{[\Sigma w(F_o^2 - F_c^2)^2]/ [\Sigma w(F_o^2)^2]\}^{1/2}$; $w = 1/[\sigma^2(F_o^2) + (ap)^2 + bp]$; $p = (F_o^2 + 2F_c^2)/3$; a = 0.1178 (**12**), 0.1392 (**13**); 0.04 (**14**), 0.04 (**15**); b = 0 (**12**), 0 (**13**), 150 (**14**), 150 (**15**).

Table 6.2. Intermolecular Distances (Å) in the Structures of **12**-19.[a]

		Compound **12**			
Hg(2)···C(04)	3.462	Hg(2)···C(01)[b]	3.511		
Hg(2)···C(03)	3.360	Hg(2)···C(01)[c]	3.351		
		Hg(2)···C(06)[c]	3.424		
		Compound **13**			
Hg(1)···C(21)[d]	3.438	Hg(2)···C(25)[d]	3.246	Hg(3)···C(22)	3.534
Hg(1)···C(22)[d]	3.386	Hg(2)···C(30)[d]	3.301	Hg(3)···C(23)[d]	3.544
		Hg(2)···C(21)	3.407	Hg(3)···F(4)[e]	3.292
		Hg(2)···C(28)	3.478	Hg(3)···F(10)[f]	3.012
		Hg(2)···C(29)	3.296		
		Compound **14**			
Hg(1)···C(28)	3.276(17)	Hg(2)···C(21)	3.376(19)	Hg(3)···C(22A)	3.313(18)
Hg(1)···C(28A)	3.403(17)	Hg(2)···F(5)[h]	3.033	Hg(3)···C(23)	3.466(19)
Hg(1)···C(27)[g]	3.39(2)			Hg(3)···C(22B)[g]	3.417(17)
				Hg(3)···C(25A)[g]	3.426(18)
		Compound **15**			
Hg(1)···C(27)	3.326(13)	Hg(2)···O(1)	2.881(10)	Hg(3)···C(30)	3.297(13)
Hg(1)···C(26)	3.445(14)			Hg(3)···C(34)	3.357(13)
Hg(1)···C(25)[i]	3.213(13)			Hg(3)···C(29)	3.516(13)
Hg(1)···C(32)[i]	3.373(13)			Hg(3)···C(21)[i]	3.341(14)
				Hg(3)···C(22)[i]	3.434(14)
		Compound **16**			
Hg(1)···C(38)	3.353(16)	Hg(2)···C(39)	3.487(16)	Hg(3)···C(33B)	3.424(14)
Hg(1)···C(38A)	3.460(14)	Hg(2)···C(40)	3.553(17)	Hg(3)···C(40A)	3.408(15)
Hg(1)···C(36)[j]	3.536(17)	Hg(2)···F(5)[k]	3.266		
		Compound **17**			
Hg(2)···C(13)	3.511	Hg(2)···C(17)[l]	3.541		
Hg(2)···C(14)	3.460	Hg(2)···C(18)[l]	3.465		
Hg(1)···F(3)[m]	3.270				
Hg(1)···F(3C)[n]	3.270				
		Compound **18**			
Hg(1)···C(22)	3.499(17)	Hg(2)···C(26A)	3.302(13)	Hg(3)···C(32)	3.306(15)
Hg(1)···C(32A)[o]	3.374(17)	Hg(2)···C(23B)	3.536(13)	Hg(3)···C(32A)	3.509(13)
Hg(1)···C(32B)[o]	3.438(17)	Hg(2)···C(28)[o]	3.508(17)	Hg(3)···C(30)[o]	3.507(17)
				Hg(3)···C(31)[o]	3.533(17)
		Compound **19**			
Hg(1)···C(22B)	3.404(9)	Hg(2)···C(25)	3.326(9)	Hg(3)···C(23)	3.512(10)
Hg(1)···C(32B)	3.517(9)	Hg(2)···C(24A)	3.344(10)	Hg(3)···C(22b)[p]	3.379(10)
Hg(1)···C(26b)[p]	3.53(10)			Hg(3)···C(24b)[p]	3.439(10)
Hg(1)···C(28b)[p]	3.49(10)			Hg(3)···F(10)[q]	3.274(10)

[a] The symmetry operations used to generate the atoms of neighboring units are indicated in the following footnotes. [b] -x, y, 0.5-z. [c] x+1, y, z. [d] x, y+1, z. [e] -x+0.5, y-0.5, z+1.5. [f] - x+0.5, -y+0.5, z+0.5. [g] x, y+1, z. [h] -0.5+x, 1.5-y, -0.5+z. [i] 0.5+x, 0.5-y, 0.5+z. [j] x, y-1, z. [k] x, -0.5-y, 0.5+z. [l] x-1, y, z. [m] -x+0.5, -y+0.5, z-0.5. [n] x-0.5, -y+0.5, -z+2. [o] x+1, y, z. [p] -0.5+x, 0.5-y, -0.5+z. [q] 0.5+x, 0.5-y, -0.5+z.

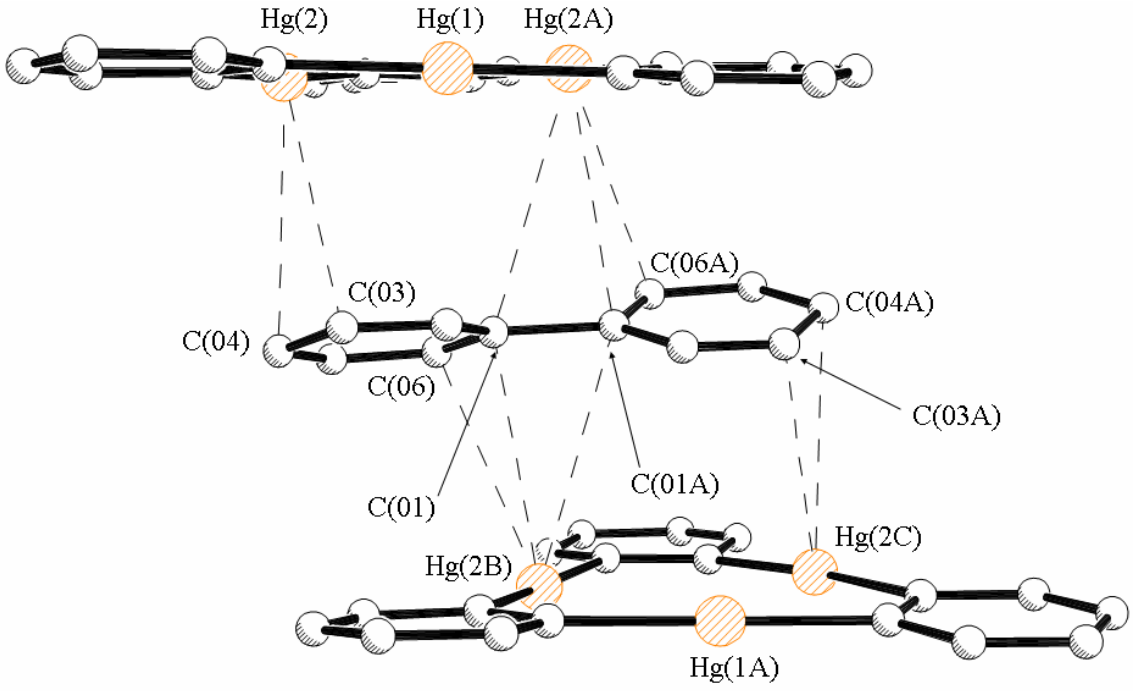

Figure 6.3. Molecular structure of **12**. Fluorine and hydrogen atoms are omitted for clarity. Short contacts and distances are shown. Selected intramolecular bond distances [Å] and angles [deg]. Hg(1)-C(1) 2.070(18), Hg(2)-C(6) 2.075(17), Hg(2)-C(7) 2.063(19), C(1A)-Hg(1)-C(1) 177.4(10), C(7)-Hg(2)-C(6) 174.0(8).

Compound **13** crystallizes in the monoclinic space group $P2_1/n$ with one molecule of compound **1** and one molecule of naphthalene in the asymmetric unit (Tables 6.1 and 6.2, Figure 6.4). The stacks consist of alternating molecules of **1** and naphthalene. Inspection of the packing diagram reveals that the molecules of **1** and naphthalene are not strictly parallel and form an interplane angle of 3.9. The sandwiched naphthalene molecule engages in a double η^2-coordination involving C(21)-C(22) and Hg(1A) as well as C(25)-C(30) and Hg(2A) (Table 6.2). Short distances are also observed between the C(21)-C(29)-C(28) portion of the naphthalene molecule which is η^3-coordinated to the mercury atom Hg(2). Further contacts involve C(22) and

Hg(3) as well as C(23) and Hg(3A). The resulting Hg-$C_{naphthalene}$ distances, ranging from 3.246 to 3.544 Å, are comparable to the Hg-$C_{biphenyl}$ distances in compound **12**. In compound **13**, one mercury atom (Hg(3)) does not interact with the arene but forms contacts with fluorine atoms of other stacks. These distances (Table 6.2) are within the sum of the van der Waals radii (r_{vdw}(F) = 1.30-1.38 Å, r_{vdw}(Hg) = 1.73-2.00 Å)[24,25] and substantiate the presence of secondary interactions.

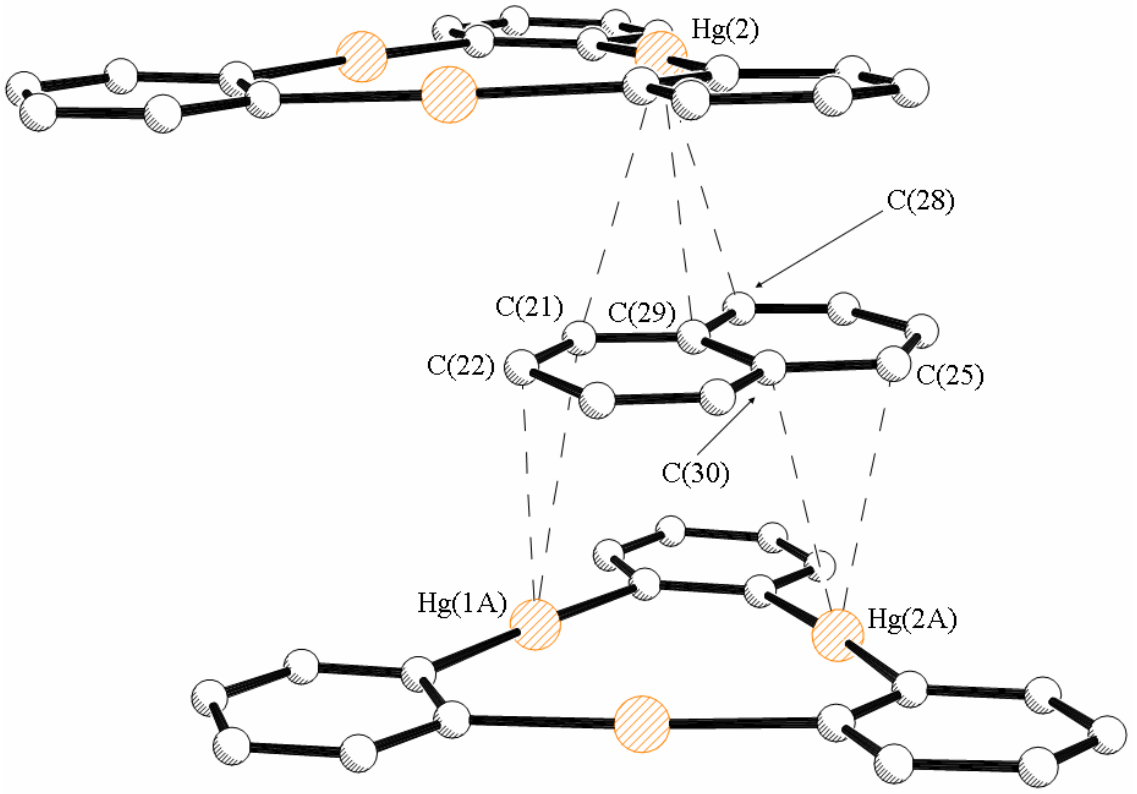

Figure 6.4. Molecular structure of **13**. Fluorine and hydrogen atoms are omitted for clarity. Short contacts and distances are shown. Selected intramolecular bond distances [Å] and angles [deg]. Hg(1)-C(1) 2.053(12), Hg(1)-C(8) 2.060(12), Hg(2)-C(14) 2.100(12), Hg(2)-C(7) 2.078(12), Hg(3)-C(13) 2.062(12), Hg(3)-C(2) 2.089(13), C(1)-Hg(1)-C(8) 178.1(5), C(14)-Hg(2)-C(7) 174.6(5), C(13)-Hg(3)-C(2) 175.9(5).

Compound **14** crystallizes in the monoclinic space group $P2_1/n$ with one molecule of **1**, one molecule of acenaphthalene in the asymmetric unit (Tables 6.1 and 6.2, Figure 6.5). The infinite stacks consist of alternating molecules of **1** and acenaphthalene. Inspection of the crystal structure shows that molecules of **1** and acenaphthalene are essentially parallel to one another. The sandwiched acenaphthalene molecule engages in three dihapto interactions that involve C(23)-C(22A) and Hg(3), C(28)-C(28A) and Hg(1), and C(22B)-C(25A) and Hg(3A). Short distances are also observed between C(21) and Hg(2) as well as C(27) and Hg(1A) (Table 6.2). The Hg-$C_{acenaphthalene}$ distances have values ranging from 3.276 to 3.466 Å. As in the case of **13**, one of the mercury atoms (Hg(2)) does not interact with the arene but forms a contact with fluorine atoms of neighboring molecules. This distance (Table 6.2) is within the sum of the van der Waals radii (r_{vdw}(F) = 1.30-1.38 Å, r_{vdw}(Hg) = 1.73-2.00 Å)[24,25] and substantiate the presence of secondary interactions.

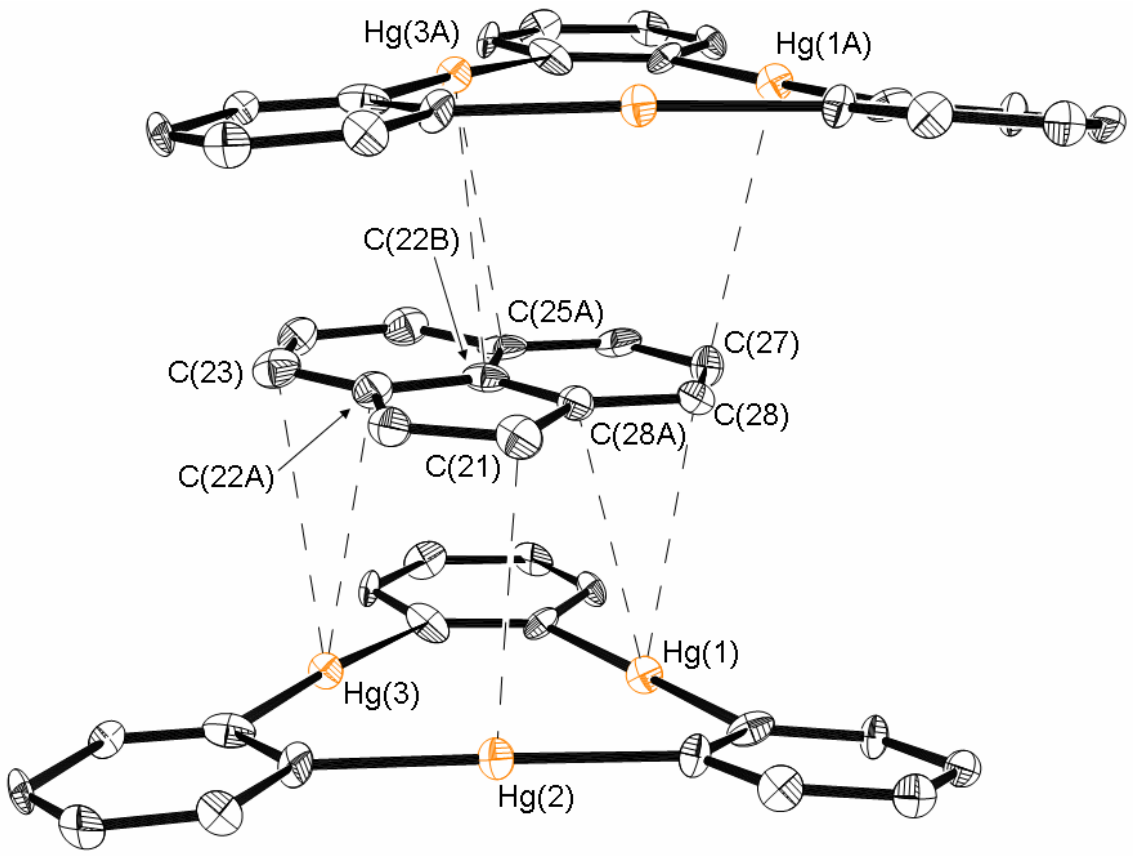

Figure 6.5. Molecular structure of **14**. Fluorine and hydrogen atoms are omitted for clarity. Short contacts and distances are shown. Selected intramolecular bond distances [Å] and angles [deg]. Hg(1)-C(1) 2.063(16),Hg(1)-C(8) 2.085(17), Hg(2)-C(7) 2.067(16), Hg(2)-C(14) 2.071(17), Hg(3)-C(13) 2.084(17), Hg(3)-C(2) 2.105(16), C(1)-Hg(1)-C(8) 176.3(6), C(7)-Hg(2)-C(14) 176.4(7), C(13)-Hg(3)-C(2) 174.6(8).

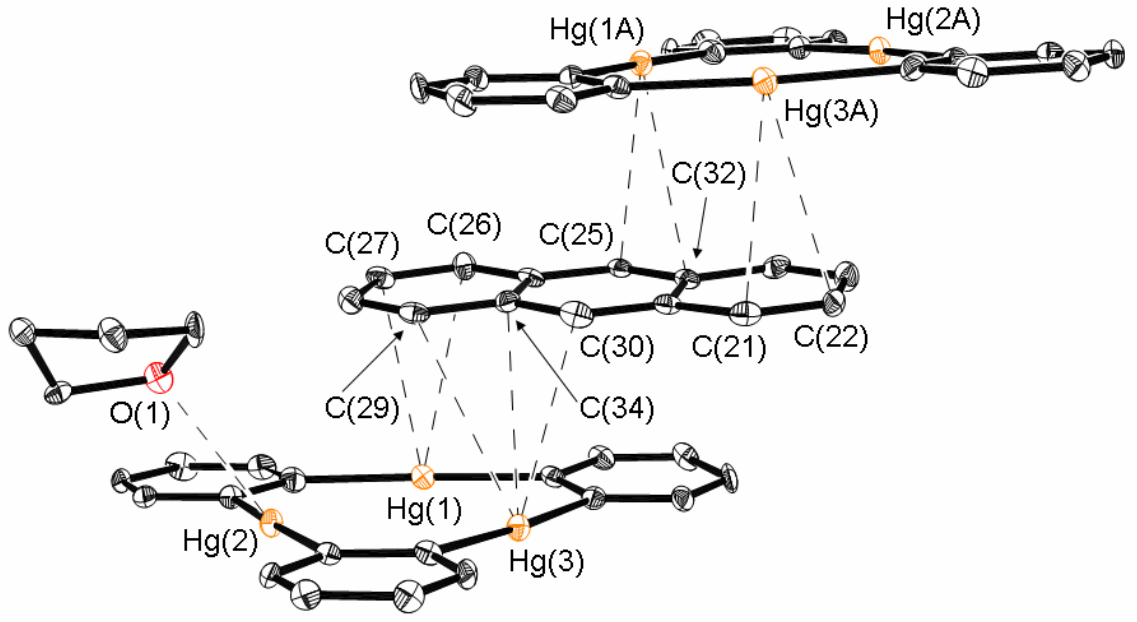

Figure 6.6. Molecular structure of **15**. Fluorine and hydrogen atoms are omitted for clarity. Short contacts and distances are shown. Selected intramolecular bond distances [Å] and angles [deg]: Hg(1)-C(1) 2.079(14), Hg(1)-C(8) 2.077(14), Hg(2)-C(14) 2.068(13), Hg(2)-C(7) 2.103(13), Hg(3)-C(13) 2.097(14), Hg(3)-C(2) 2.087(14), C(1)-Hg(1)-C(8) 176.7(5), C(14)-Hg(2)-C(7) 174.3(5), C(13)-Hg(3)-C(2) 175.9(5).

Compound **15** crystallizes in the monoclinic space group $P2_1/n$ with one molecule of **1**, one molecule of anthracene and one molecule of THF in the asymmetric unit (Tables 6.1 and 6.2, Figure 6.6). The infinite stacks consist of alternating molecules of **1** and anthracene. Inspection of the crystal structure shows that molecules of **1** and anthracene are essentially parallel to one another. The sandwiched anthracene molecule engages in one trihapto interaction that involves C(29)-C(30)-C(34) and Hg(3) and three dihapto interactions that involve C(26)-C(27) and Hg(1), C(25)-C(32) and Hg(1A), and C(21)-C(22) and Hg(3A) (Table 6.2). The Hg-$C_{anthracene}$ distances have values ranging from 3.213 to 3.516 Å. The oxygen of the THF molecule interacts with

Hg(2) at a distance of 2.881(10) Å. This distance is within the sum of the van der Waals radii of mercury (r_{vdw} = 1.75 Å)[24,25] and oxygen (r_{vdw} = 1.54 Å).[23] It is also similar to the mercury-oxygen distances observed in [**1**•μ_3-acetone] (Hg-O = 2.810(12)-2.983(12) Å),[22,70] [**1**•μ_3-acetaldehyde] (Hg-O = 2.912(13)-2.965(8) Å), [**1**•μ_3-DMF] (Hg-O = 2.799(5)-3.042(5) Å),[19,71] and [**1**•μ_3-DMSO] (Hg-O = 2.759(5)-3.120(5) Å).

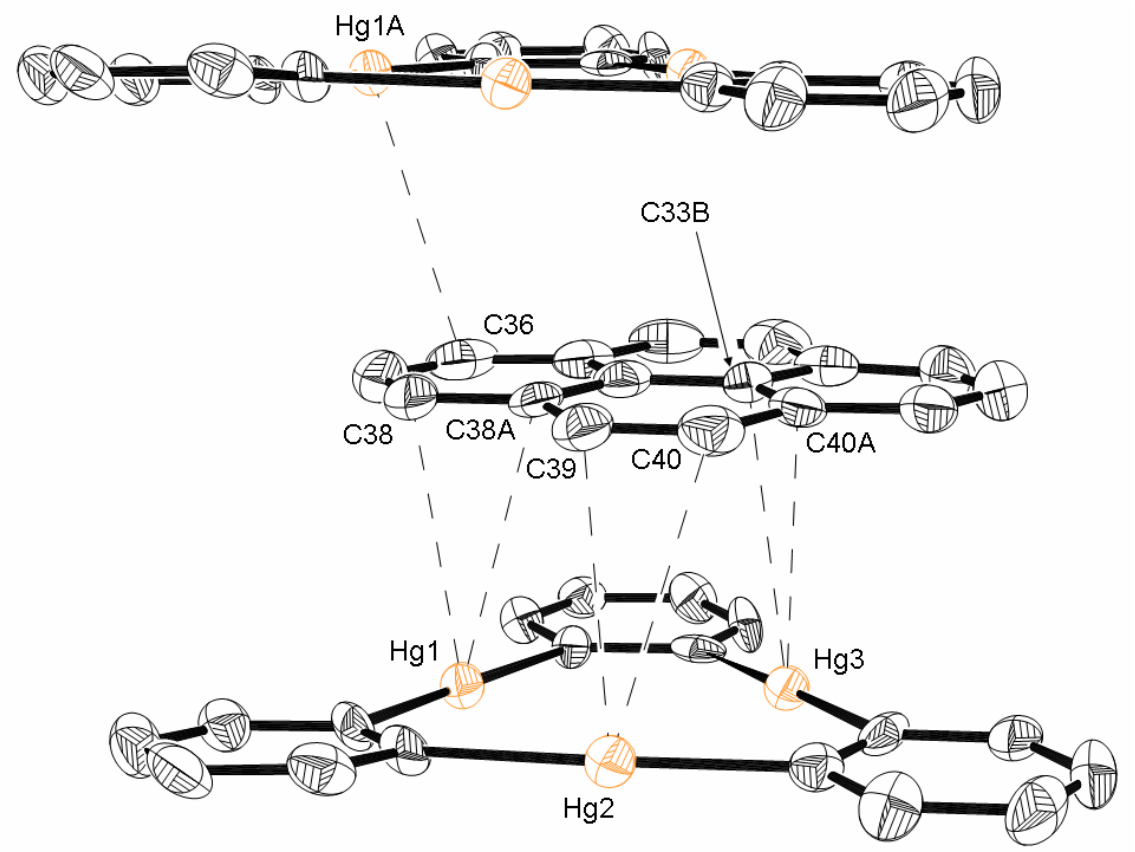

Figure 6.7. Molecular structure of **16**. Thermal ellipsoids are at 30%. Fluorine and hydrogen atoms are omitted for clarity. Selected intramolecular bond distances [Å] and angles [deg]: Hg(1)-C(1) 2.101(13), Hg(1)-C(8) 2.077(14), Hg(2)-C(7) 2.098(15), Hg(2)-C(14) 2.082(15), Hg(3)-C(2) 2.011(16), Hg(3)-C(13) 2.056(15), C(8)-Hg(1)-C(1) 175.9(5), C(14)-Hg(2)-C(7) 177.1(6), C(2)-Hg(3)-C(13) 178.6(7).

Compound **16** crystallizes in the monoclinic space group $P2_1/c$ with one molecule of **1** and one molecule of pyrene in the asymmetric unit (Tables 6.2 and 6.3, Figure 6.7). The infinite stacks consist of alternating molecules of **1** and pyrene. Inspection of the crystal structure shows that molecules of **1** and pyrene are essentially parallel to one another. The sandwiched pyrene molecule engages in three dihapto interactions that involve C(38)-C(38A) and Hg(1), C(39)-C(40) and Hg(2), and C(33B)-C(40A) and Hg(3). A short distance is also observed between C(36) and Hg(1A) (Table 6.2). The Hg-C_{pyrene} distances have values ranging from 3.353 to 3.553 Å. As in the case of **13**, one of the mercury atoms (Hg(2)) does not interact with the arene but forms contacts with fluorine atoms of neighboring molecules. These distances (Table 6.2) are within the sum of the van der Waals radii (r_{vdw}(F) = 1.30-1.38 Å, r_{vdw}(Hg) = 1.73-2.00 Å)[24,25] and substantiate the presence of secondary interactions.

Table 6.3. Crystal data, data collection, and structure refinement for **16**, **17**, **18** and **19**.

Crystal data	**16**	**17**	**18**	**19**
Formula	$C_{34}H_{10}F_{12}Hg_3$	$C_{36}H_{12}F_{12}Hg_3$	$C_{38}H_{12}F_{12}Hg_3$	$C_{42}H_{12}F_{12}Hg_3$
M_r	1248.19	1274.23	1298.25	1346.29
Crystal size (mm^3)	0.118 x 0.643 x 0.036	0.07 x 0.08 x 0.40	0.51 x 0.21 x 0.20	0.45 x 0.32 x 0.22
Crystal system	Monoclinic	Orthorhombic	Triclinic	Monoclinic
Space group	*P*2(1)/c	*P*bcn	*P*-1	*P*2(1)/n
a (Å)	21.908(4)	7.2103(14)	7.2355(14)	11.987(2)
b (Å)	7.0456(14)	35.982(7)	11.375(2)	21.312(4)
c (Å)	21.918(4)	11.670(2)	18.819(4)	13.980(3)
α (°)			91.22(3)	
β (°)	117.61(3)	-	96.05(3)	113.22(3)
γ (°)			93.05(3)	
V ($Å^3$)	2998.0(10)	3027.7(10)	1537.4(5)	3282.3(11)
Z	4	4	2	4
ρ_{calc} (gcm^{-3})	2.765	2.795	2.804	2.724
μ(Mo K_α)(mm^{-1})	15.426	15.278	15.046	14.101
F(000) (e)	2248	2304	1176	2448
Data Collection				
T/K	293(2)	180(2)	293(2)	110(2)
Scan mode	ω	ω	ω	ω
hkl range	-23→24, -7→7, -24→24	-9→9, -48→47, -13→15	-8→8, -12→12, -20→20	-13→13, -23→23, -15→15
Measured refl.	20577	33533	12787	20577
Unique refl., [R_{int}]	4335 [0.1123]	3765 [0.0584]	4406 [0.0334]	4731 [0.0281]
Refl. used for refinement	4335	3765	4406	4731
Absorption correction	None	SADABS	SADABS	SADABS
T_{min}/T_{max}		0.316523	0.188068	0.254042
Refinement				
Refined parameters	442	231	478	514
R1, wR2 [I>2σ(I)]	0.0572, 0.1396	0.0384, 0.0710	0.0564, 0.1304	0.0392, 0.0948
ρ_{fin} (max/min) ($eÅ^{-3}$)	2.170, -2.336	1.022, -2.056	6.265, -1.786	4.544, -2.372
Flack parameter	-		-	-

[a] R1 = Σ (F_o - F_c)/ Σ F_o.[b] wR2 = {[Σw(F_o^2 - F_c^2)^2]/ [Σw(F_o^2)^2]}$^{1/2}$; w = 1/[σ^2(F_o^2) + (ap)^2 + bp]; p = (F_o^2 + 2F_c^2)/3; a = 0.0874 (**16**), 0.0203 (**17**), 0.07 (**18**), 0.055300 (**19**); b = 0 (**16**), 42.07 (**17**), 50 (**18**), 23.0532 (**19**).

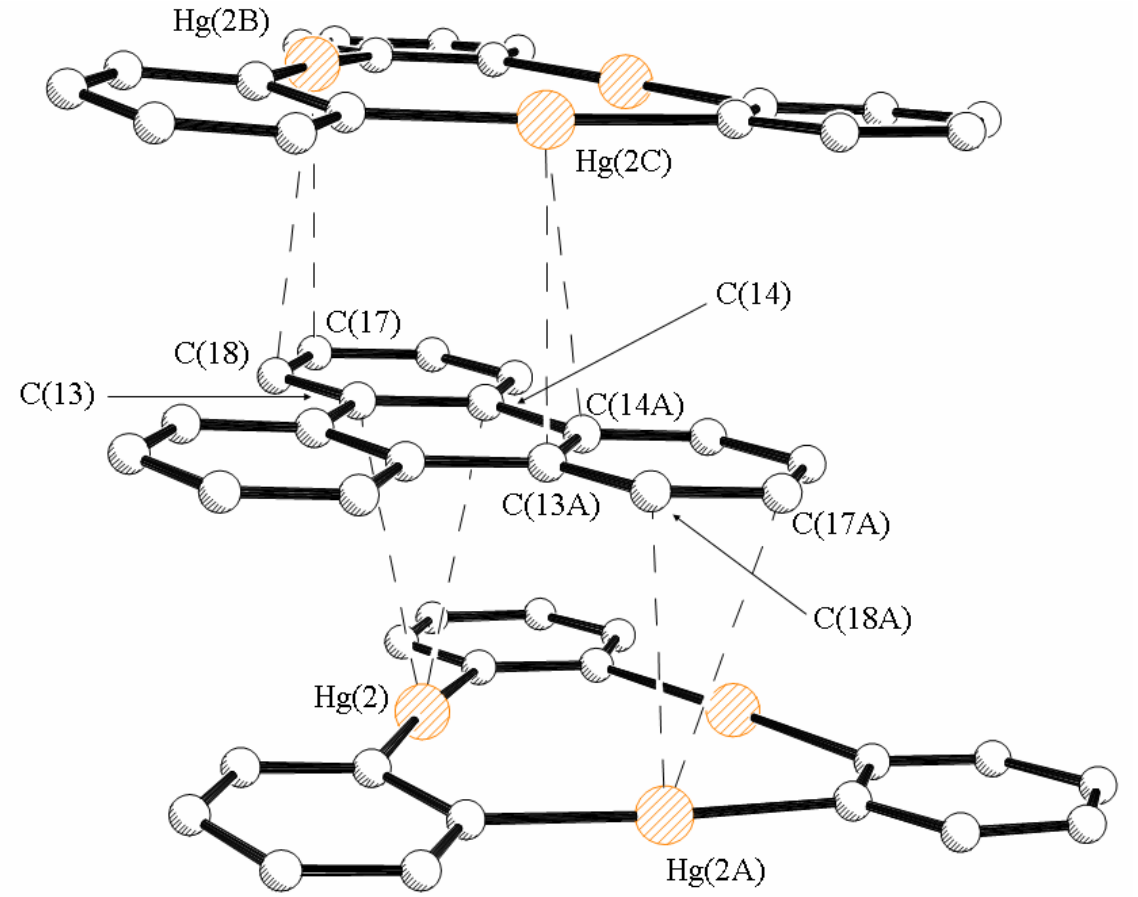

Figure 6.8. Molecular structure of **17**. Fluorine and hydrogen atoms are omitted for clarity. Short contacts and distances are shown. Selected intramolecular bond distances [Å] and angles [deg]: Hg(1)-C(1) 2.070(8), Hg(2)-C(6) 2.071(7), Hg(2)-C(7) 2.069(7), C(1A)-Hg(1)-C(1) 175.9(5), C(7)-Hg(2)-C(6) 175.7(3).

Compound **17** crystallizes in the orthorhombic space group *Pbcn* with one-half of a molecule of **1** and one-half of a molecule of triphenylene in the asymmetric unit(Tables 6.2 and 6.3, Figure 6.8). The molecules are essentially planar and parallel to one another. The C(13)-C(14) as well as C(17A)-C(18A) portions of the triphenylene are η^2-coordinated to Hg(2) and Hg(2A) (Table 6.2). Symmetry-related interactions occur between C(13A)-C(14A) and Hg(2C) as well as between C(17)-C(18) and Hg(2B). The Hg-$C_{triphenylene}$ distances have values ranging from 3.460 to 3.541 Å. Interestingly, at the difference of compound **12** and **13**, arene-fluoroarene interactions occur in the structure of **17**. These interactions involve a tetrafluorophenylene and a phenylene ring which result in a centroid distance of 3.605 Å. As in the case of **13**, one of the mercury atoms (Hg(1)) does not interact with the arene but forms contacts with fluorine atoms of neighboring molecules. These distances (Table 6.2) are within the sum of the van der Waals radii (r_{vdw}(F) = 1.30-1.38 Å, r_{vdw}(Hg) = 1.73-2.00 Å)[24,25] and substantiate the presence of secondary interactions.

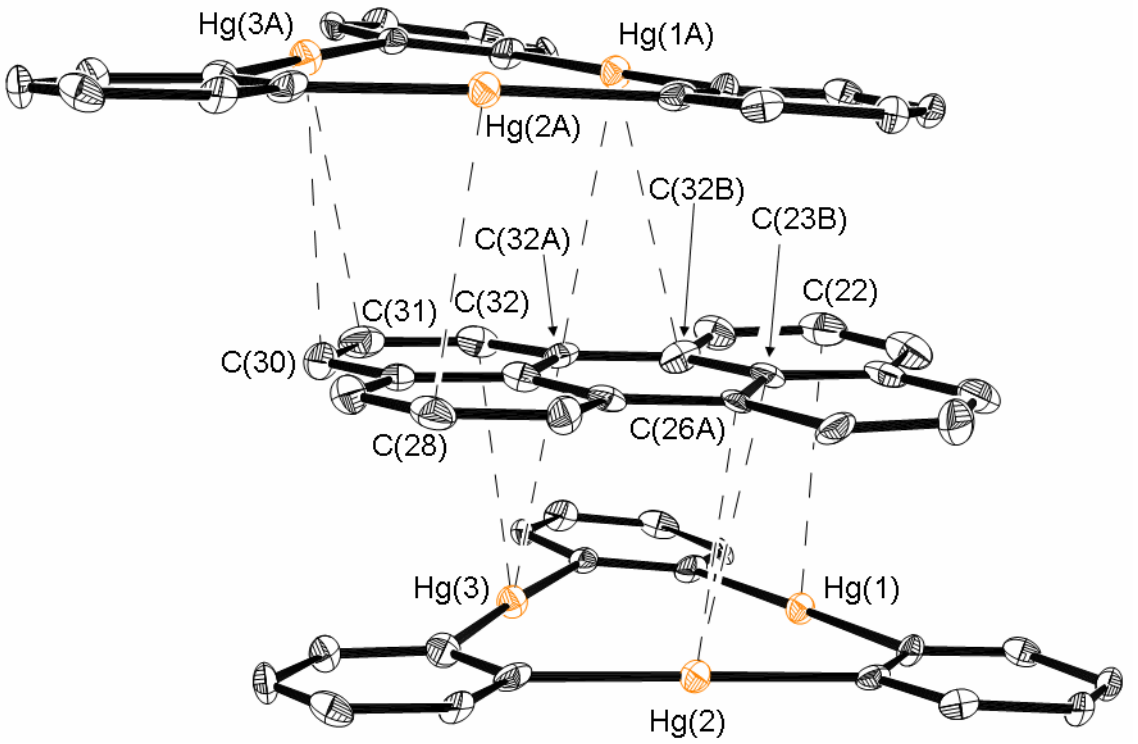

Figure 6.9. Molecular structure of **18**. Fluorine and hydrogen atoms are omitted for clarity. Short contacts and distances are shown. Selected intramolecular bond distances [Å] and angles [deg]: Hg(1)-C(1) 2.090(13), Hg(1)-C(8) 2.095(13), Hg(2)-C(7) 2.074(15), Hg(2)-C(14) 2.081(15), Hg(3)-C(2) 2.072(14), Hg(3)-C(13) 2.075(15), C(1)-Hg(1)-C(8) 175.7(6), C(7)-Hg(2)-C(14) 175.8(5), C(2)-Hg(3)-C(13) 176.3(6).

Compound **18** crystallizes in the triclinic space group *P-1* with one molecule of **1** and one molecule of perylene in the asymmetric unit (Tables 6.2 and 6.3, Figure 6.9). The infinite stacks consist of alternating molecules of **1** and perylene. Inspection of the crystal structure shows that molecules of **1** and perylene are essentially parallel to one another. The sandwiched perylene molecule engages in four dihapto interactions that involve C(23B)-C(26A) and Hg(2), C(32)-C(32A) and Hg(2A), C(32A)-C(32B) and

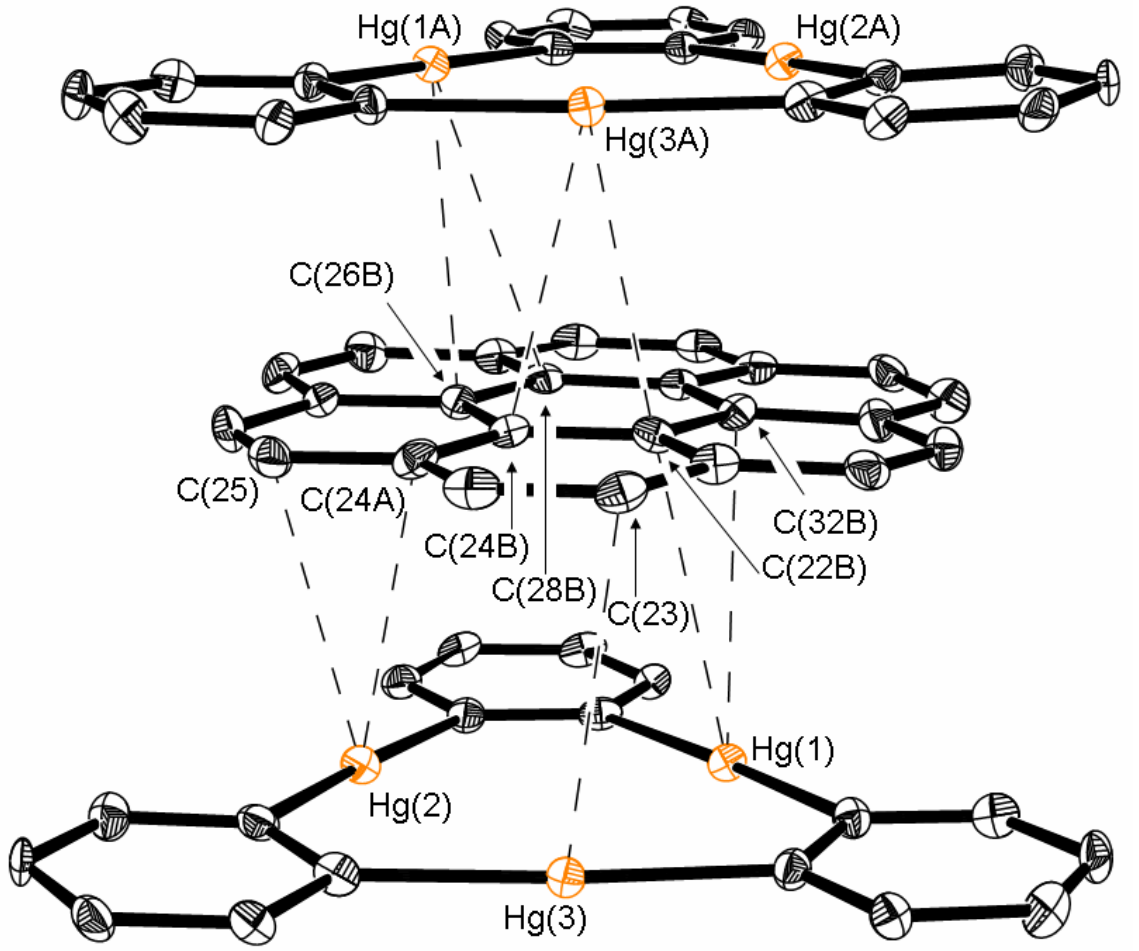

Figure 6.10. Molecular structure of **19**. Fluorine and hydrogen atoms are omitted for clarity. Short contacts and distances are shown. Selected intramolecular bond distances [Å] and angles [deg]: Hg(1)-C(1) 2.071(9), Hg(1)-C(8) 2.094(9), Hg(2)-C(7) 2.071(10), Hg(2)-C(14) 2.082(9), Hg(3)-C(2) 2.071(9), Hg(3)-C(13) 2.062(9), C(1)-Hg(1)-C(8) 175.6(4), C(7)-Hg(2)-C(14) 175.6(4), C(13)-Hg(3)-C(2) 175.8(4).

Hg(1A), and C(30)-C(31) and Hg(3A). Short distances are also observed between C(22) and Hg(1) as well as C(28) and Hg(2A). The Hg-$C_{perylene}$ distances have values ranging from 3.302 to 3.536 Å (Table 6.2).

Compound **19** crystallizes in the monoclinic space group $P2_1/c$ with one molecule of **1** and one molecule of coronene in the asymmetric unit (Tables 6.2 and 6.3, Figure 6.10). The infinite stacks consist of alternating molecules of **1** and coronene. Inspection of the crystal structure shows that molecules of **1** and coronene are essentially parallel to one another. The sandwiched pyrene molecule engages in four dihapto interactions that involve C(22B)-C(32B) and Hg(1), C(24A)-C(25) and Hg(2), C(26B)-C(28B) and Hg(1A), and C(22B)-C(24B) and Hg(3A). A short distance is also observed between C(23) and Hg(3) (Table 6.2). The Hg-$C_{coronene}$ distances have values ranging from 3.326 to 3.557 Å. As in the case of **13**, one of the mercury atoms (Hg(3)) does not interact with the arene but forms contacts with fluorine atoms of neighboring molecules.

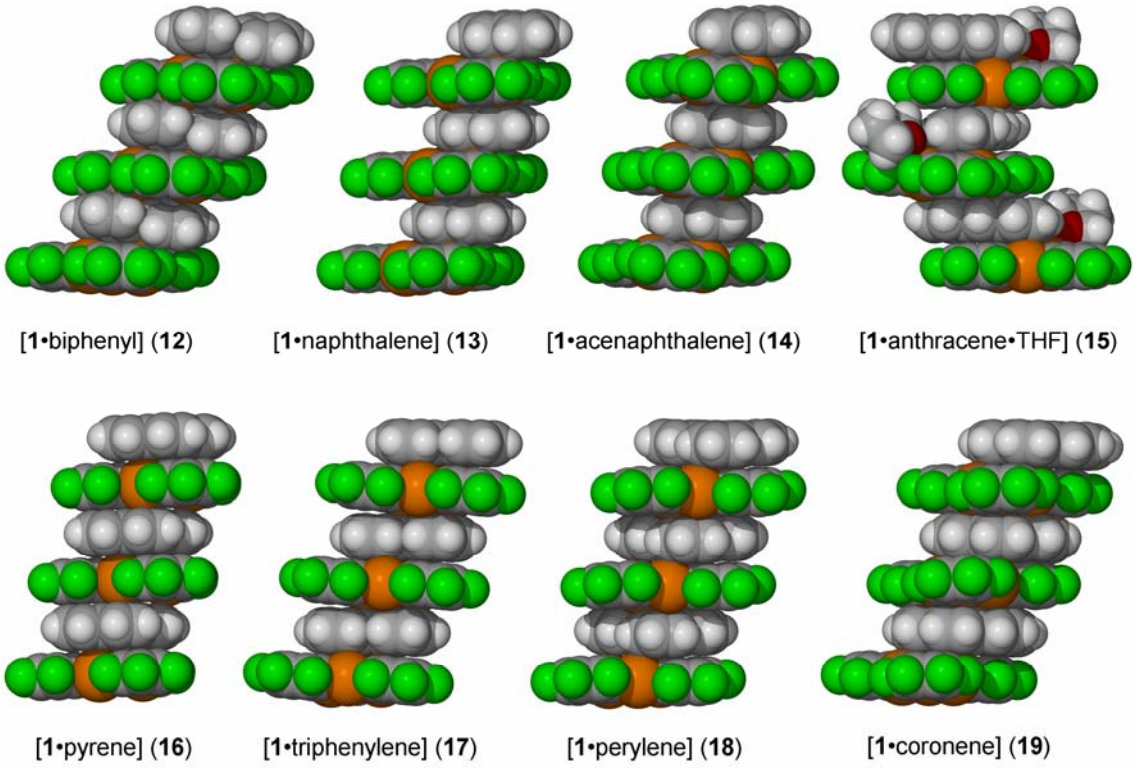

Figure 6.11. Space filling models of the stacks of **12-19**.

While electrostatic forces likely contribute to the stability of these assemblies, it is important to note that in all eight cases (Figure 6.11), there are short contacts between the mercury centers of **1** and the aromatic molecules. These contacts range from 3.25 to 3.55 Å and are within the sum of the van der Waals radius of mercury (r_{vdw}(Hg) = 1.73-2.00 Å)[24,25] and that usually accepted for carbon in aromatic systems ($r_{vdw}(C_{aromatic})$ = 1.7 Å). They reflect the presence of secondary polyhapto-π interactions occurring between the electron-rich aromatic molecules and the acidic mercury centers.[35,36,88] Similar distances have been previously observed in [**1**•benzene] (3.408 and 3.457 Å). Despite the weakness of the individual interactions,[35] each aromatic molecule establishes

multiple links to neighboring mercury centers thus strengthening the cohesion of each stack. In the case of the triphenylene adduct **17**, an arene-fluoroarene interaction is observed. With a centroid distance of 3.605 Å, this interaction resembles that encountered in several purely organic arene-fluoroarene assemblies.[91,105,106,107,108] Such interactions have been proposed to result, at least in part, from electrostatic interactions[109,110] and have been observed in related complexes.[37,100b,111] In **12-19**, the coordinated aromatic derivatives do not appear to be affected by their participation in the stacks. While no lengthening of the C-C bonds could be confirmed within the error of the crystallographic measurements, the Ph-Ph twist angle of 30.4 in the structure of the biphenyl molecule in **12** is between that observed for free biphenyl in the molten state (25)[112] and in solution (32).[113] As a final structural remark, the structural resemblance that exists between compounds **12-19** and a series of gold-containing supramolecules reported by Balch as well as Burini and Fackler. These supramolecules consist of stacks in which trinuclear gold(I) complexes alternate with organic derivatives such as fluorenones, hexafluorobenzene, and TCNQ. At the difference of **12-19**, the trinuclear gold(I) complexes are electron-rich while the organic substrates are electron-poor. Compounds **12-19**, which contain electron-poor mercury centers and unsubstituted arenes, can therefore be regarded as the charge-reverse analogues of the gold assemblies.

6.5 Luminescence studies on **12**, **13**, **16** and **17**

Under a hand-held UV lamp, compounds **12**, **13**, **16** and **17** display luminescence in the visible region of the spectrum. The emission spectra and excited state lifetimes of compounds **12**, **13**, and **16** were measure by the Omary group at University of North Texas and the spectra are shown in Figure 6.12. The emission spectrum of compound **17** is shown in Figure 6.13. In all four cases, the selected excitation wavelength falls within the $S_0 \rightarrow S_1$ absorption band of the pure arene.[114-115,116,117,118] For **12**, **13**, and **16** the resulting emission spectra exhibit well-defined vibrational features and correspond very closely to that expected for the $T_1 \rightarrow S_0$ phosphorescence of biphenyl,[119] naphthalene,[120] and pyrene,[121] respectively, which have been the object of detailed spectral analyses in the literature.[119,121,122] Excitation spectra of **12**, **13**, and **16** show only weak signals due to direct $S_0 \rightarrow T_1$ arene absorption, suggesting that other photophysical processes lead to the observed $T_1 \rightarrow S_0$ phosphorescence. Excited-state lifetime measurements at (ambient temperature, 77 K) yielded τ = (454 ± 5 μs, 337 ± 5 μs), (712 ± 12 μs, 985 ± 11 μs), and (568 ± 8 μs, 423 ± 8 μs) for **12**, **13**, and **16**, respectively. These microsecond-level lifetimes clearly represent phosphorescence, in contrast to the monomer fluorescence bands exhibited by free biphenyl, naphthalene, and pyrene at much higher energies and with nanosecond-level lifetimes. The excited-state lifetimes measured in microseconds for **12**, **13**, and **16** are much shorter than those reported for the monomer phosphorescence bands of the free arenes (4.4, 2.3, and 0.7 *seconds* for biphenyl, naphthalene, and pyrene in frozen glasses, respectively).[122,123] The strong spin-orbit coupling effect due to the presence of mercury atoms[124] in **12**, **13**, and **16** makes the

phosphorescence transition from the triplet excited state of the organic component a more allowed transition, hence leading to shorter lifetimes than those exhibited by the pure organic compounds in which phosphorescence is strongly forbidden. Similar effects have been reported for aromatic substrates sequestered in Tl^{+} exchanged zeolites.

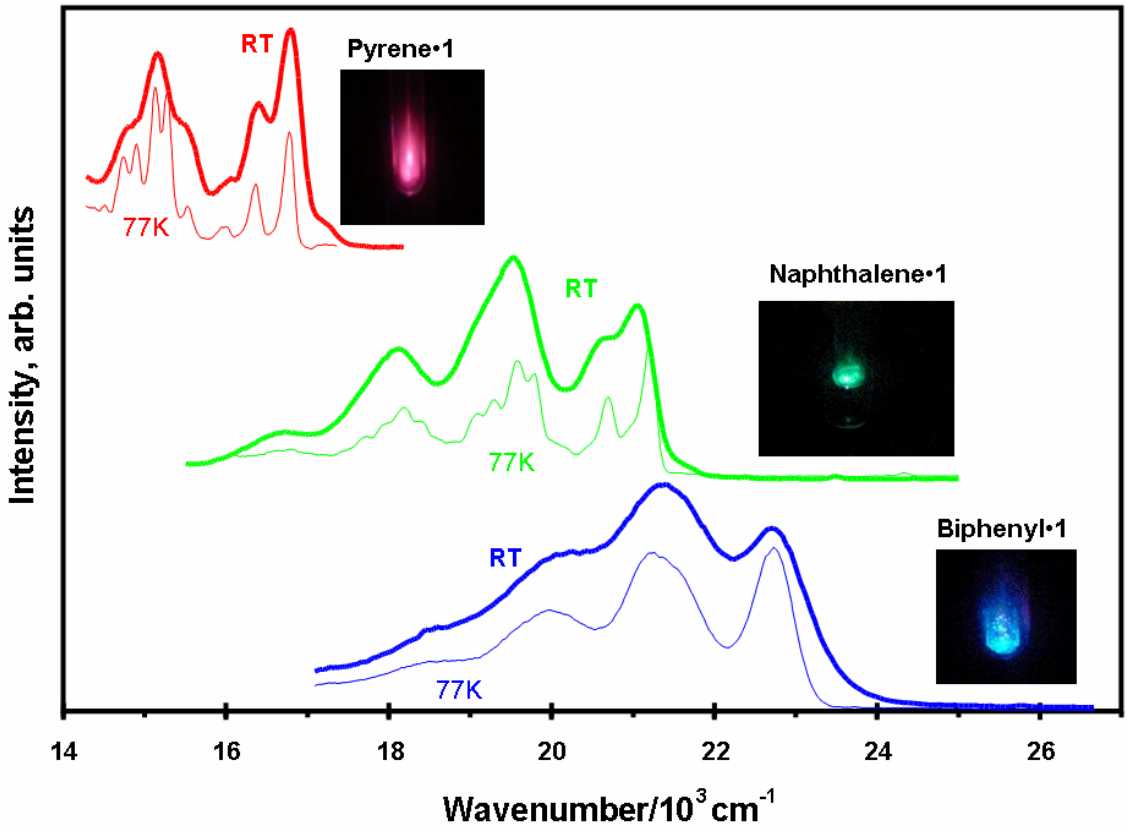

Figure 6.12. Photoluminescence spectra for crystalline solids of **12**, **13**, and **16**. Intensities of different spectra were adjusted arbitrarily for clarity. Photographs are shown for the emissions of crystalline solids at ambient temperature.

In the case of **17**, the emission appears at longer wavelengths than those typically observed for the room-temperature phosphorescence of triphenylene.[125] While the

photophysics of arene-fluoroarene assemblies have not been unraveled, the presence of arene-fluoroarene interactions in the structure of **17** can be tentatively correlated to this red-shifted emission.

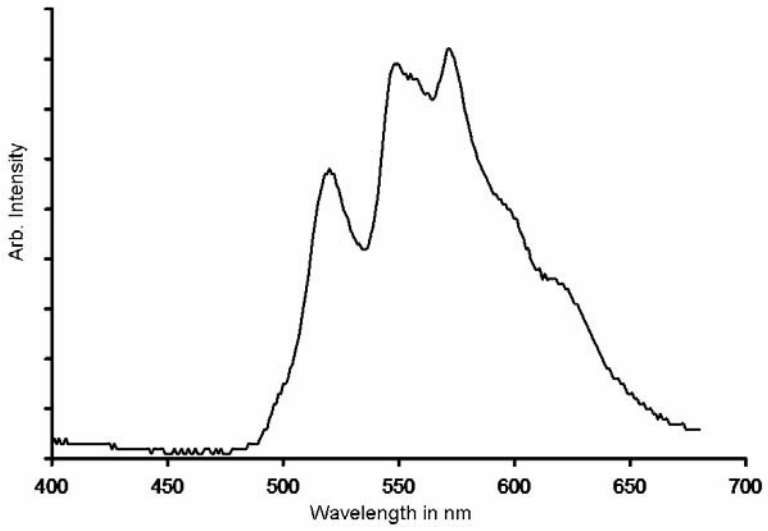

Figure 6.13. Emission spectra for solid **17** recorded at room temperature.

6.6 Summary

The results reported herein further document the affinity of **1** for aromatic substrates. While the biphenyl and naphthalene adducts **12** and **13** can be isolated upon concentration of the mother liquor, spontaneous precipitation occurs in the cases of the larger arenes. The structures of adducts **12-19** reveal the existence of stacks in which molecules of **1** and molecules of arenes alternate. In each stack, secondary π-interactions occur between the arene and the mercury centers of **1**, thus providing cohesion to the stacks. It is important to note that DFT calculations carried out on **1** show the existence

of a positively charged electrostatic potential surface in the center of the macrocycle. Hence, it is probable that electrostatic forces also play a role in the formation of the observed structures. Finally, compounds **12**, **13**, **16**, and **17** show luminescence in the solid state. While more work is needed to clarify the origin of the photoluminescence in the case of **17**, the emission observed for **12**, **13** and **16** corresponds to the phosphorescence of the aromatic substrate. This observation indicates the occurrence of a heavy atom effect that promotes intersystem spin crossing from the S_1 to the T_1 state. Hence, compound **1** could be used as a luminescence-based sensor for arenes or incorporated into electroluminescent devices such as OLEDs.

6.7 Experimental details

General. Atlantic Microlab, Inc., Norcross, GA, performed the elemental analyses. All commercially available starting materials and solvents were purchased from Aldrich Chemical and used as provided. Compound **1** was prepared according to the published procedure. The luminescence spectra were recorded with a SLM/AMINCO, Model 8100 spectrofluorometer equipped with a xenon lamp. Low-temperature measurements were made in a cryogenic device of local design. Collodion was used to attach the powder samples to the holder. The collodion was scanned for a baseline subtraction. Liquid nitrogen was used to obtain the 77 K measurements.

Crystallization of 1•Biphenyl (12). Compound **1** (0.26 g, 0.25 mmol) was dissolved in CH_2Cl_2 (50 mL). In a separate vial, biphenyl (0.075 g, 0.52 mmol) was dissolved in CH_2Cl_2 (20 mL). The two solutions were mixed. Upon concentration by

partial evaporation of the solvent, crystals of **12** formed in a 68% yield (0.20 g, 0.17 mmol). mp 290-293 ºC. Anal. Calcd for $C_{30}H_{10}F_{12}Hg_3$: C, 30.0; H, 0.8. Found: C, 29.76; H, 0.82.

Synthesis of 1•Naphthalene (13). Compound **1** (0.27 g, 0.26 mmol) was dissolved in CH_2Cl_2 (50 mL). In a separate vial, naphthalene (0.080 g, 0.62 mmol) was dissolved in CH_2Cl_2 (20 mL). The two solutions were mixed. Upon concentration by partial evaporation of the solvent, crystals of **13** formed in a 73% yield (0.22 g, 0.19 mmol). mp 305-307 ºC. Anal. Calcd for $C_{28}H_8F_{12}Hg_3$: C, 28.63; H, 0.69. Found: C, 28.77; H, 0.64.

Synthesis of 1•Acenaphthalene (14). Compound **1** (0.24 g, 0.23 mmol) was dissolved in THF (50 mL). In a separate vial, acenaphthalene (0.036 g, 0.24 mmol) was dissolved in THF (20 mL). Upon concentration by partial evaporation of the solvent, crystals of **14** formed in a quantitative yield. mp 345 ºC (decomp.). Anal. Calcd for $C_{30}H_8F_{12}Hg_3$: C, 30.07; H, 0.67. Found: C, 30.78; H, 0.67.

Synthesis of 1•Anthracene•THF (15). Compound **1** (0.24 g, 0.23 mmol) was dissolved in THF (50 mL). In a separate vial, anthracene (0.043 g, 0.24 mmol) was dissolved in THF (20 mL). Upon concentration by partial evaporation of the solvent, crystals of **15** formed in a quantitative yield. mp 417-420 ºC. Anal. Calcd for $C_{36}H_{18}F_{12}Hg_3O$: C, 33.35; H, 1.40. Found: C, 32.98; H, 1.18.

Synthesis of 1•Pyrene (16). Compound **1** (0.24 g, 0.23 mmol) was dissolved in CH_2Cl_2 (50 mL). In a separate vial, pyrene (0.049 g, 0.24 mmol) was dissolved in CH_2Cl_2 (20 mL). Upon mixing of the two solutions, a yellow precipitate formed. The

precipitate was washed with a small amount of CH_2Cl_2 to afford pure **16** in a 68% yield (0.20 g, 0.16 mmol). Single crystals of **16** were obtained by allowing slow diffusion of a CH_2Cl_2 solution of **1** into a CH_2Cl_2 solution of pyrene through an intermediate layer of pristine CH_2Cl_2. mp 525 ºC (decomp.). Anal. Calcd for $C_{34}H_{10}F_{12}Hg_3$: C, 32.76; H, 0.81. Found C, 32.98; H, 0.70.

Synthesis of 1•Triphenylene (17). Compound **1** (0.24 g, 0.23 mmol) was dissolved in CH_2Cl_2 (50 mL). In a separate vial, triphenylene (0.11 g, 0.47 mmol) was dissolved in CH_2Cl_2 (20 mL). Upon mixing of the two solutions, a white precipitate formed. The precipitate was washed with a small amount of CH_2Cl_2 to afford pure **17** in a 67% yield (0.20 g, 0.15 mmol). Single crystals of **17** were obtained by allowing slow diffusion of a CH_2Cl_2 solution of **1** into a CH_2Cl_2 solution of triphenylene through an intermediate layer of pristine CH_2Cl_2. mp 337 ºC (sub.). Anal. Calcd for $C_{36}H_{12}F_{12}Hg_3$: C, 33.93; H, 0.95. Found: C, 33.82; H, 0.94.

Synthesis of 1•Perylene (18). Compound **1** (0.24 g, 0.23 mmol) was dissolved in THF (50 mL). In a separate vial, perylene (0.060 g, 0.24 mmol) was dissolved in THF (20 mL). Upon concentration by partial evaporation of the solvent, crystals of **18** formed in a quantitative yield. mp 425 ºC (decomp.). Anal. Calcd for $C_{38}H_{12}F_{12}Hg_3$: C, 35.15; H, 0.93. Found: C, 35.31; H, 0.86.

Synthesis of 1•Coronene (19). Compound **1** (0.24 g, 0.23 mmol) was dissolved in THF (50 mL). In a separate vial, coronene (0.072 g, 0.24 mmol) was dissolved in THF (20 mL). Upon concentration by partial evaporation of the solvent, crystals of **19**

formed in a quantitative yield. mp 450 ºC (decomp.). Anal. Calcd for $C_{42}H_{12}F_{12}Hg_3$: C, 37.47; H, 0.90. Found: C, 37.51; H, 0.75.

Crystal Structure Determinations. X-ray data for **12-19** were collected on a Bruker SMART-CCD diffractometer using graphite-monochromated Mo-Kα radiation (λ = 0.71073 Å). Specimens of suitable size and quality were selected and glued onto a glass fiber with freshly prepared epoxy resin. The structure was solved by direct methods, which successfully located most of the non-hydrogen atoms. Subsequent refinement on F^2 using the SHELXTL/PC package (version 5.1) allowed location of the remaining non-hydrogen atoms. Further crystallographic details can be found in Table 6.1, 6.2, and 6.3.

CHAPTER VII

INTERACTION OF HEXAALKOXYTRIPHENYLENES (HAT*n*) WITH [Hg(*o*-C_6F_4)]$_3$ IN SOLUTION

7.1 Introduction

Trimeric perfluoro-ortho-phenylene mercury (**1**) constitutes a simple mercury Lewis acid which forms supramolecular binary stacks with arenes as documented in previous chapters. These supramolecular stacks are formed based on mercury π-interactions which are likely complimented by electrostatic forces and van der Waals interactions. Although numerous examples of these have been reported recently, their existence in solution has never been confirmed. Since most arenes, which strongly interact with **1**, form insoluble adducts, strategies allowing to increase the solubility of the adducts had to be considered. One such strategy consists in appending long aliphatic chains to the aromatic substrate in order to increase their solubility in organic solvents as well as that of the resulting adducts. In a pursuit of these goals, hexaalkoxytriphenylenes (HAT*n*, *n* = number of carbon atoms in the alkyl chain) were chosen as aromatic substrates. This chapter will describe the interaction of **1** with various HAT*n* both in the solid-state and in solution.

7.2 Synthesis of [**1**•HAT0•6THF] (**20**), [**1**•HAT1] (**21**), [**1**•HAT2] (**22**), [**1**•HAT3] (**23**), [**1**•HAT4] (**24**), [**1**•HAT5] (**25**), and [**1**•HAT6] (**26**)

Upon slow evaporation of a THF solution containing **1** and hexahydroxytriphenylene (HAT0) colorless needles of [**1**•HAT0•6THF] (**20**) formed. Elemental analysis of this compound is consistent with [**1**•HAT0•2THF] indicating the loss of four equivalents of THF. When equimolar CH_2Cl_2 solutions containing **1** and hexamethoxytriphenylene (HAT1) were mixed, [**1**•HAT1] (**21**) spontaneously precipitated as a white solid. Using the same reaction conditions, a similar observation was made with hexaethoxytriphenylene (HAT2) and hexa-n-propoxytriphenylene (HAT3) which afforded [**1**•HAT2] (**22**) and [**1**•HAT3] (**23**), respectively. Solutions of hexa-n-butoxytriphenylene (HAT4) and **1** formed a precipitate of [**1**•HAT4] (**24**) upon concentration. Upon slow evaporation of the solvent, solutions of hexa-n-pentoxytriphenylene (HAT5) and **1** formed large brittle crystals of [**1**•HAT5] (**25**) that were not suitable for x-ray diffraction. Solutions of hexa-n-hexoxytriphenylene (HAT6) and **1** yielded [**1**•HAT6] (**26**) as a waxy solid that formed only upon total evaporation of the solvent. Compound **26** also precipitates from dichloroethane solutions of **1** and HAT6 upon concentration. The 1:1 stoichiometry of these adducts was confirmed by elemental analysis. Interestingly, the stoichiometry of these assemblies can be somewhat controlled. In the case of HAT1, with propylene oxide rather than CH_2Cl_2 as a solvent, crystals of [HAT1•**1**•HAT1•1.5C_3H_6O] (**21a)** formed upon slow concentration of the solutions. Differential scanning calorimetry (DSC) on **26** does not reveal a liquid crystalline phase (Figure 7.1).

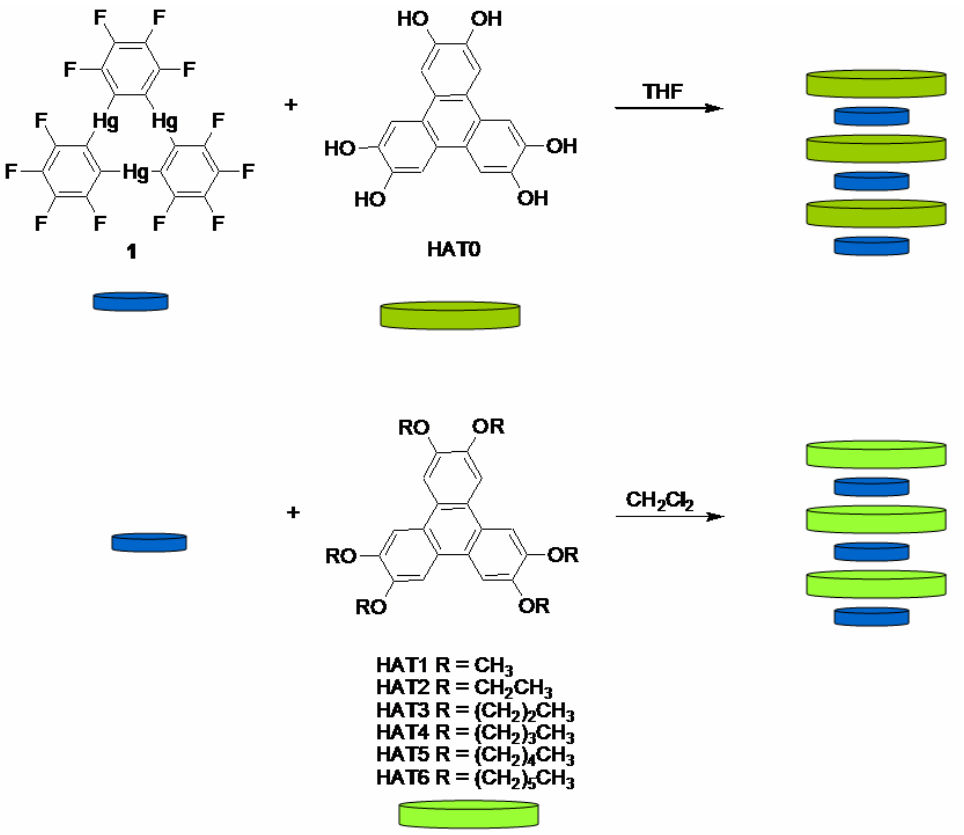
F
F
F
F
F
Hg
Hg
F
F
Hg
F
F
F
F
F
1
+
HO
OH
HO
OH
HO
OH
HAT0
THF
RO
OR
RO
OR
RO
OR
+
CH_2Cl_2
HAT1 R = CH_3
HAT2 R = CH_2CH_3
HAT3 R = $(CH_2)_2CH_3$
HAT4 R = $(CH_2)_3CH_3$
HAT5 R = $(CH_2)_4CH_3$
HAT6 R = $(CH_2)_5CH_3$

Scheme 7.1

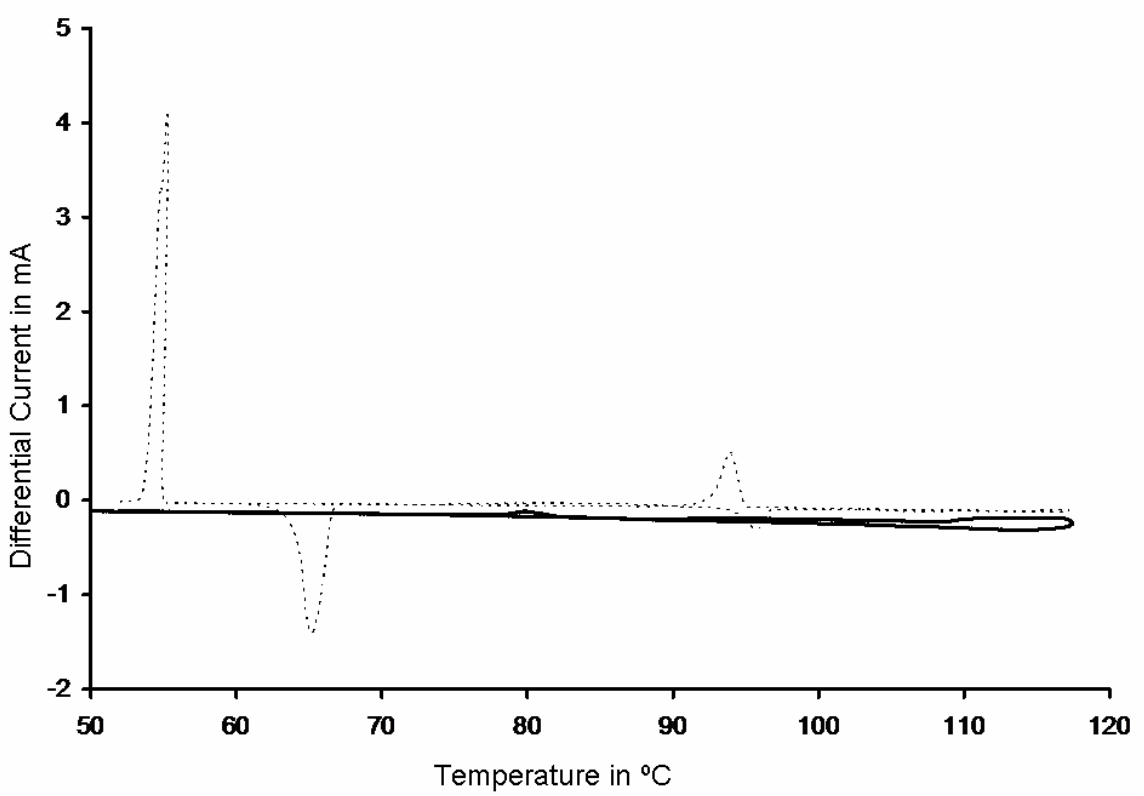

Figure 7.1. DSC of pristine HAT6 (dashed line) and **26** (solid line).

7.3 Crystal structure of [**1**•HAT0•6THF] (**20**)

Compound **20** crystallizes in the monoclinic space group *P*2(1)/n with one molecule of **1**, one molecule of HAT0, and 6 molecules of THF in the asymmetric unit (Table 7.1 and Figure 7.2). Examination of the cell packing diagram indicates that the structure consists of extended binary stacks in which staggered molecules of **1** alternate with the aromatic substrate. The stacks are parallel to the b axis. The THF molecules lie

between the stacks and are hydrogen bonded to the hydroxide functionalities of the HAT0 molecules, thus solvating the supramolecular stacks. These stacks which are distinctly cylindrical can be viewed as columns spaced by 15.584 Å. Figure 7.3 gives a top view of these columns that is reminiscent of a close-packed hexagonal array. It is interesting to note that the proposed arrangement of HAT*n* in the mesophase is also a close-packed hexagonal array of columns consisting of HAT*n* molecules held together by π-stacking interactions.[126] Based on this similarity the structures of **21-26** are predicted to be binary supramolecular stacks with alternating **1** and HAT*n* that form a close-packed hexagonal array of columns. There are no unusual intramolecular bond distances and angles in the structure of the individual components. Several carbons of the HAT0 are in close contact with the mercury atoms of **1** with distance ranging from 3.287-3.550 Å which are within the sum of the van der Waals radii for mercury (1.7-2.0 Å)[24,25] and that accepted for carbon in an aromatic ring (1.7 Å).

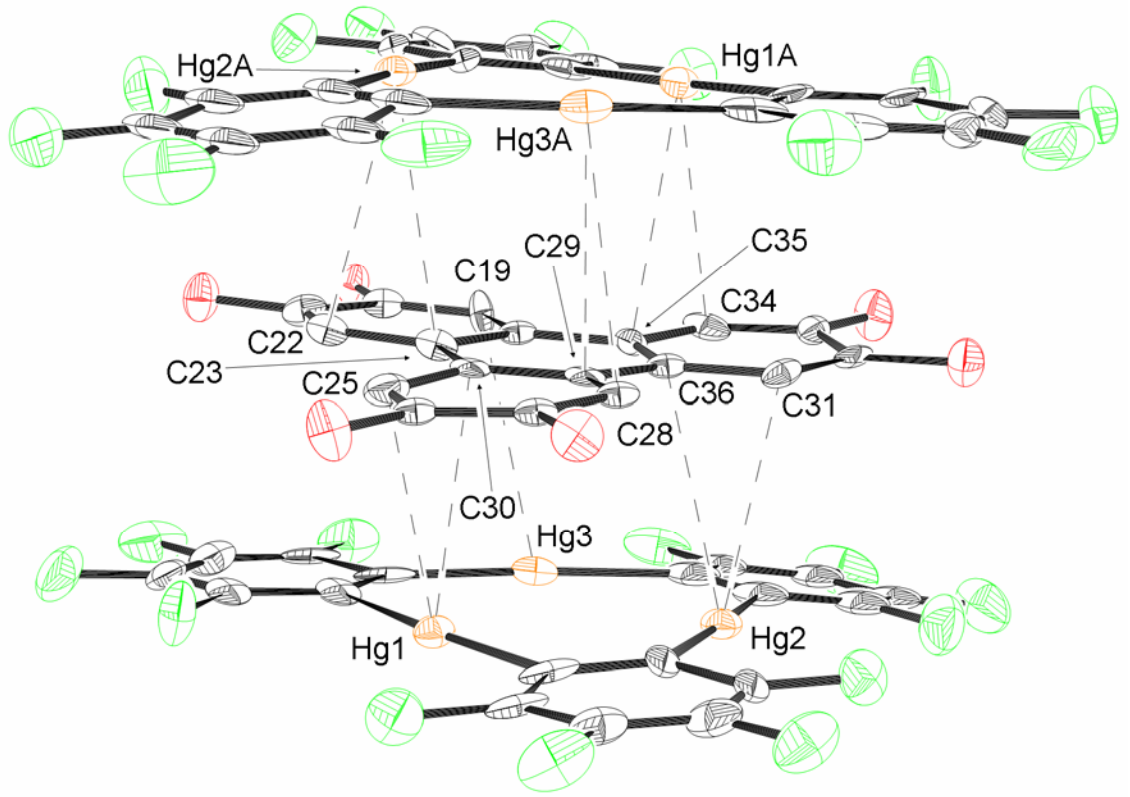

Figure 7.2. Crystal structure of **20**. Hydrogen and THF molecules omitted for clarity. Selected intramolecular distances (Å) and angles (º): Hg(1)-C(1) 2.047(15), Hg(1)-C(8) 2.101(14), Hg(2)-C(7) 2.068(17), Hg(2)-C(14) 2.092(16), Hg(3)-C(2) 2.042(16), Hg(3)-C(13) 2.113(17), C(1)-Hg(1)-C(8) 175.7(6), C(7)-Hg(2)-C(14) 174.1(6), C(2)-Hg(3)-C(13) 172.1(6). Selected intermolecular distances (Å): (Hg(1)-C(30) 3.334(15), Hg(1)-C(25) 3.471(16), Hg(1)-C(23) 3.550(16), Hg(1A)-C(34) 3.287(16), Hg(1A)-C(35) 3.310(16), Hg(2)-C(31) 3.315(15), Hg(2)-C(36) 3.349(15), Hg(2A)-C(22) 3.333(16), Hg(2A)-C(23) 3.411(16), Hg(3A)-C(28) 3.324(16), Hg(3A)-C(29) 3.312(16))

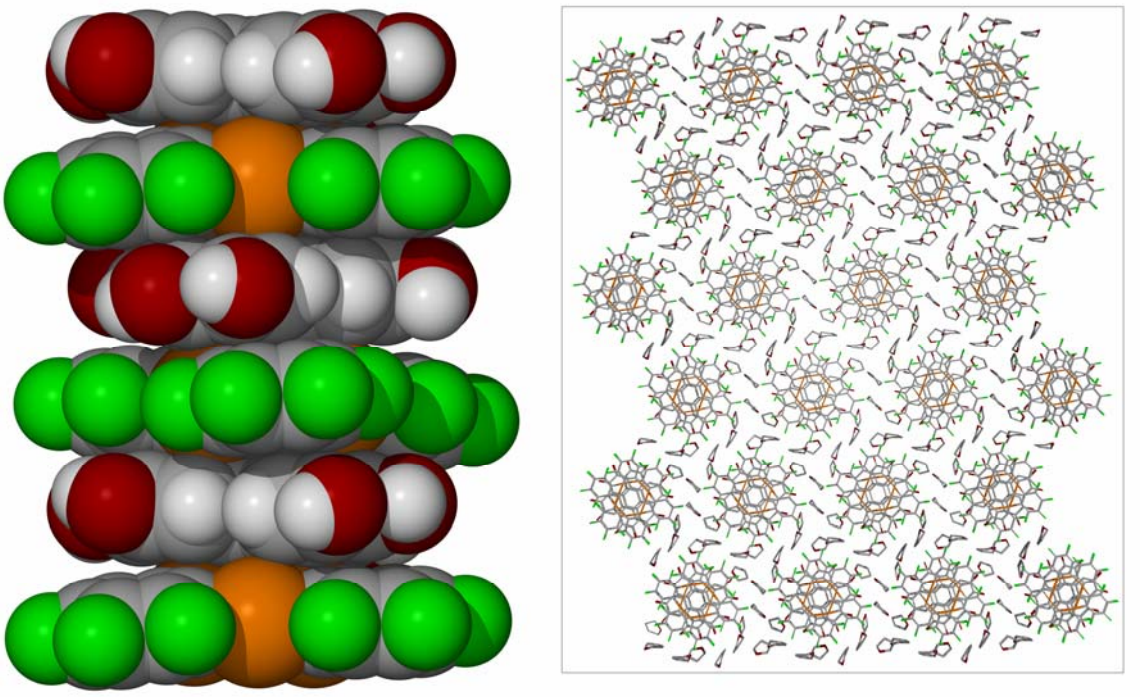

Figure 7.3. Left: Space-filling model of a portion of the stack in **20**. THF molecules are omitted for clarity. Right: View along the b-axis in **20**.

Table 7.1. Crystal data, data collection, and structure refinement for **20** and **21a**.

Crystal data	**20**	**21a**
Formula	$C_{60}H_{60}F_{12}Hg_3O_{12}$	$C_{141}H_{114}F_{24}Hg_6O_{27}$
M_r	1802.85	3899.86
Crystal size (mm^3)	0.41 x 0.23 x 0.22	0.50 x 0.45 x 0.41
Crystal system	Monoclinic	Trigonal
Space group	$P2_1/n$	$P3_2$
a (Å)	16.233(3)	23.297(10)
b (Å)	13.204(3)	23.297(10)
c (Å)	27.192(5)	20.144(12)
β (°)	90.83(3)	
V ($Å^3$)	5828(2)	9468(8)
Z	4	3
ρ_{calc} (gcm^{-3})	2.055	2.052
μ(Mo K_α)(mm^{-1})	7.985	7.383
F(000) (e)	3456	5616
Data Collection		
T/K	153(2)	293(2)
Scan mode	ω	ω
hkl range	-18→17, -14→14, -30→30	-25→25, -25→25, -22→22
Measured refl.	35125	81128
Unique refl., [R_{int}]	8396 [0.0819]	18115 [0.1386]
Refl. used for refinement	8396	18115
Absorption correction	SADABS	None
T_{min}/T_{max}	0.474114	
Refinement		
Refined parameters	682	1572
R1, wR2 [I>2σ(I)]	0.0599, 0.1189	0.0604, 0.1414
ρ_{fin} (max/min) ($eÅ^{-3}$)	3.133, -2.513	4.885, -2.310
Flack parameter	-	-

[a] $R1 = (F_o - F_c)/ F_o$. [b] $wR2 = \{ [w(F_o^2 - F_c^2)^2]/ [w(F_o^2)^2]\}^{1/2}$; $w = 1/ [\sigma^2(F_o^2) + (ap)^2 + bp]$; $p = (F_o^2 + 2F_c^2)/3$; $a = 0.03$ (**5**), 0.1044 (**6**); $b = 150$ (**5**), 0 (**6**).

7.4 Crystal structure of [HAT1•**1**•HAT1•1.5C_3H_6O] (**21a)**

All attempts to crystallize compound **21** resulted in crystals unsuitable for x-ray diffraction. However one attempt yielded a few crystals of a 2:1 HAT1 adduct of **1**, compound **21a**. This compound was prepared by mixing equimolar propylene oxide solutions of **1** and HAT1 and allowing the solvent to evaporate slowly. Compound **21a** crystallizes in the trigonal space group *P*3(2) with two molecules of **1**, four molecules of HAT1, and 3 molecules of propylene oxide in the asymmetric unit (Table 7.1 and Figures 7.4-7.7). Examination of the cell packing reveals the formation of columnar stacks (Figure 7.7) containing two molecules of HAT1 per 1 molecule of **1** in the form [HAT1•**1**•HAT1]. The 3 molecules of propylene oxide are found between the stacks and are disordered. Several carbons of the HAT1 are in close contact with the mercury atoms of **1** with distance ranging from 3.268-3.516 Å which is within the sum of the van der Waals radii for mercury (1.7-2.0 Å)[24,25] and that accepted for carbon in an aromatic ring (1.7 Å). The distance between neighboring columnar stacks is 13.437 Å. Although this structure is not a 1:1 adduct, it demonstrates the stacking nature of these types of compounds and the affinity of **1** for the aromatic core of the HAT*n* molecules.

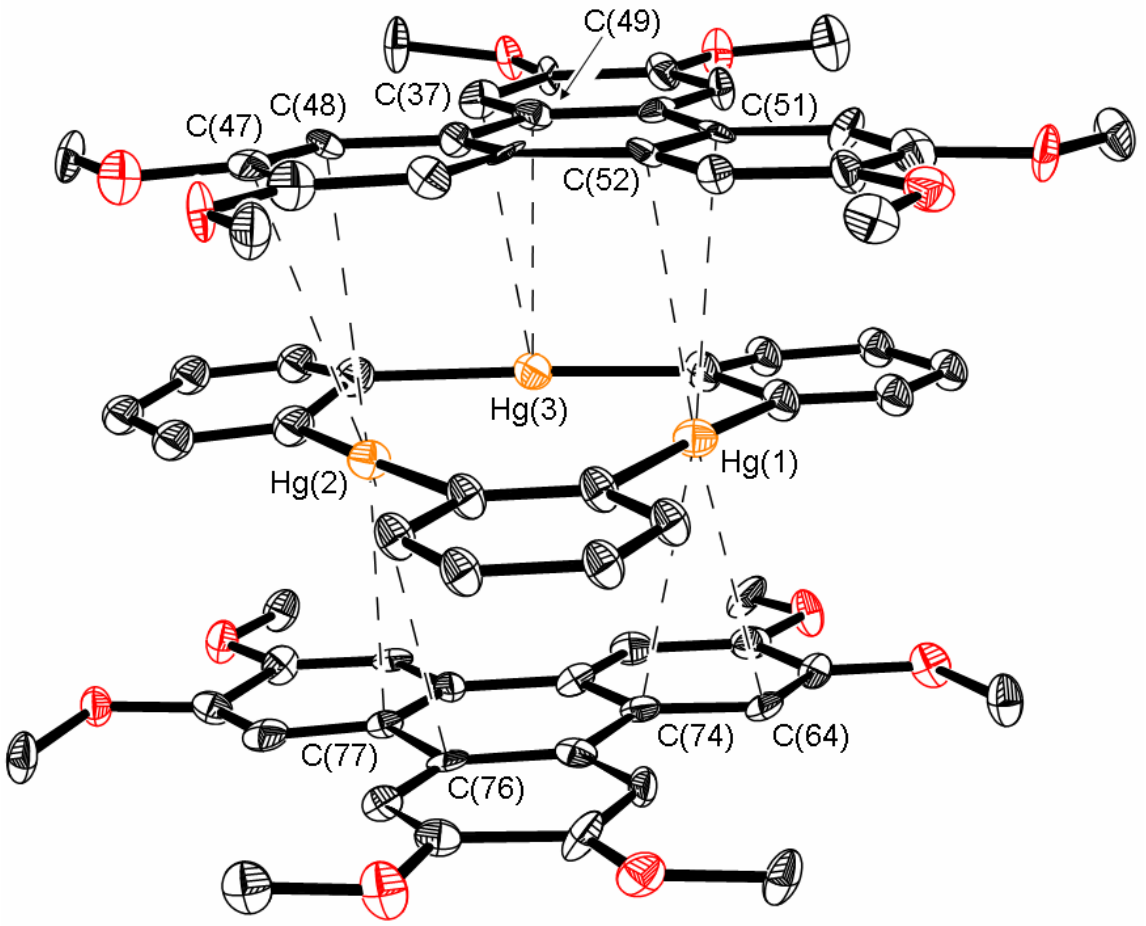

Figure 7.4. Half of the asymmetric unit of **21a**. Fluorine, hydrogen, and propylene oxide omitted for clarity. Selected intramolecular distances (Å) and angles (º): Hg(1)-C(1) 2.094(8), Hg(1)-C(8) 2.074(3), Hg(2)-C(7) 2.105(3), Hg(2)-C(14) 2.131(7), Hg(3)-C(2) 2.020(5), Hg(3)-C(13) 2.119(6), C(8)-Hg(1)-C(1) 176.7(2), C(7)-Hg(2)-C(14) 175.4(2), C(2)-Hg(3)-C(13) 177.9(3). Selected intermolecular distances (Å): Hg(1)-C(52) 3.303(6), Hg(1)-C(51) 3.356(5), Hg(1)-C(74) 3.454(6), Hg(1)-C(64) 3.508(6), Hg(2)-C(77) 3.332(6), Hg(2)-C(76) 3.428(6), Hg(2)-C(47) 3.494(6), Hg(2)-C(48) 3.516(6), Hg(3)-C(37) 3.268(6), Hg(3)-C(49) 3.335(6)

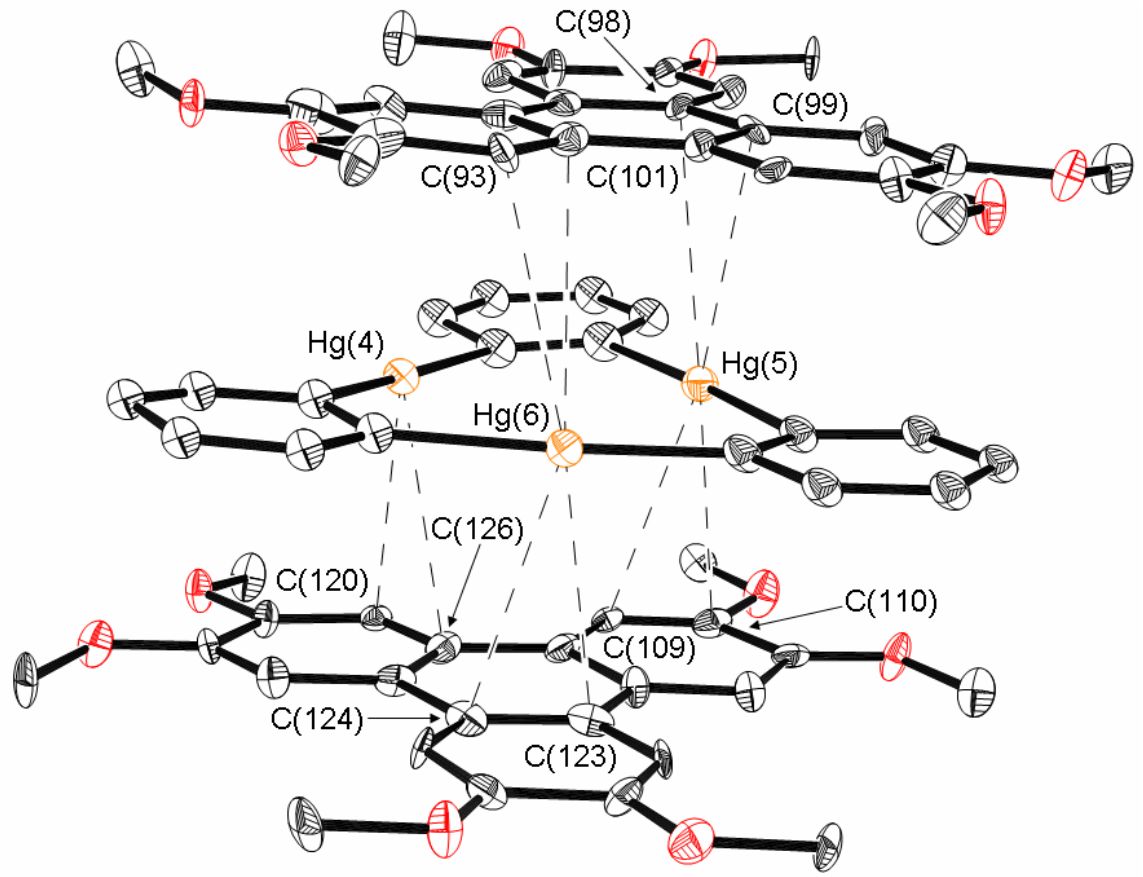

Figure 7.5. Half of the asymmetric unit of **21a**. Fluorine, hydrogen, and propylene oxide omitted for clarity. Selected intramolecular distances (Å) and angles (º): Hg(4)-C(19) 2.077(8), Hg(4)-C(26) 2.213(8), Hg(5)-C(25) 2.076(5), Hg(5)-C(32) 2.033(5), Hg(6)-C(20) 2.119(7), Hg(6)-C(31) 1.988(7), C(19)-Hg(4)-C(26) 174.7(2), C(32)-Hg(5)-C(25) 177.5(3), C(31)-Hg(6)-C(20) 177.1(2). Selected intermolecular distances (Å): Hg(4)-C(120) 3.281(6), Hg(4)-C(126) 3.330(6), Hg(5)-C(98) 3.357(6), Hg(5)-C(99) 3.442(6), Hg(5)-C(110) 3.490(6), Hg(5)-C(109) 3.516(5), Hg(6)-C(123) 3.301(6), Hg(6)-C(124) 3.377(6), Hg(6)-C(101) 3.442(6), Hg(6)-C(93) 3.458(6))

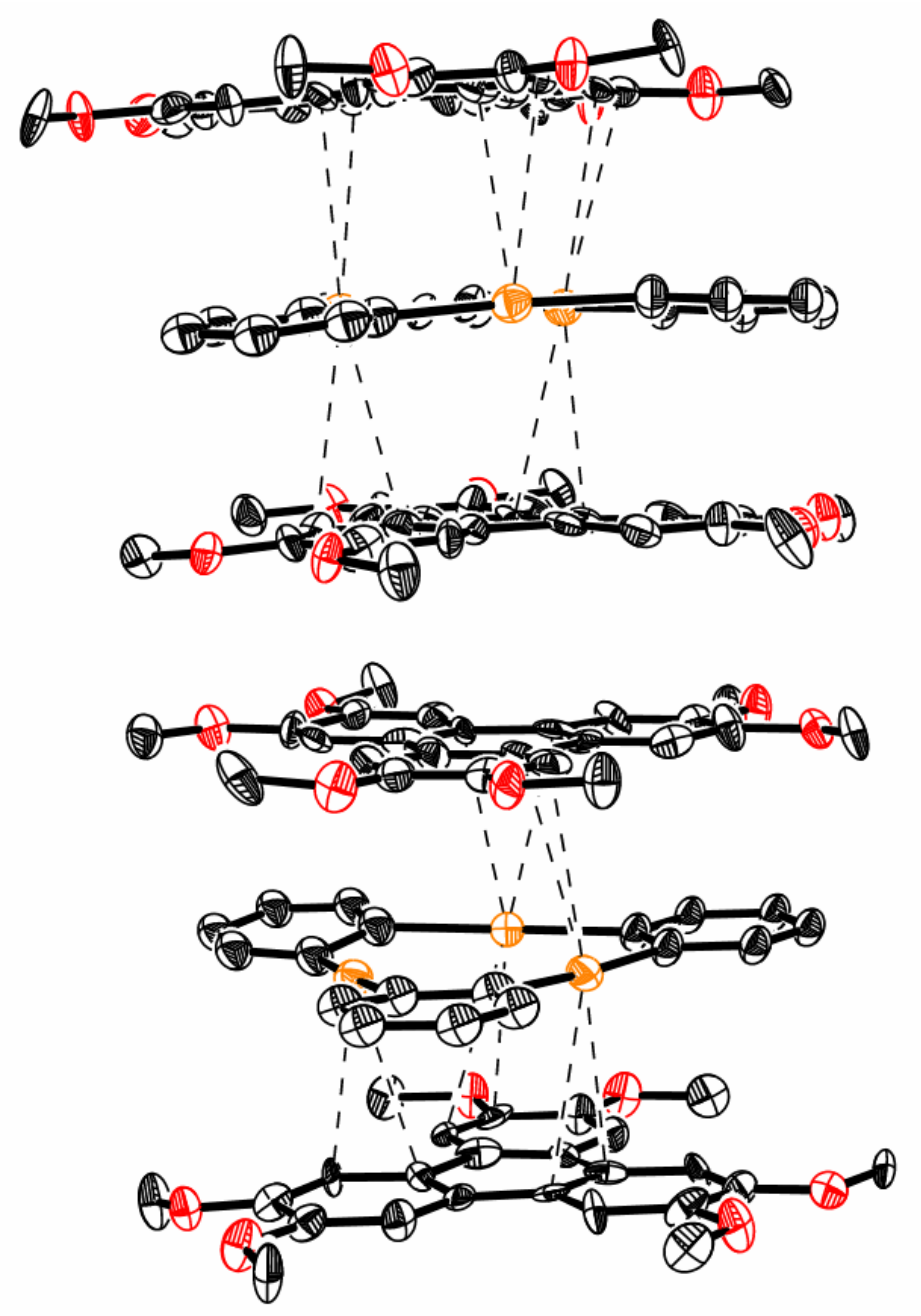

Figure 7.6. Crystal structure of **21a**. Fluorine, hydrogen, and propylene oxide omitted for clarity.

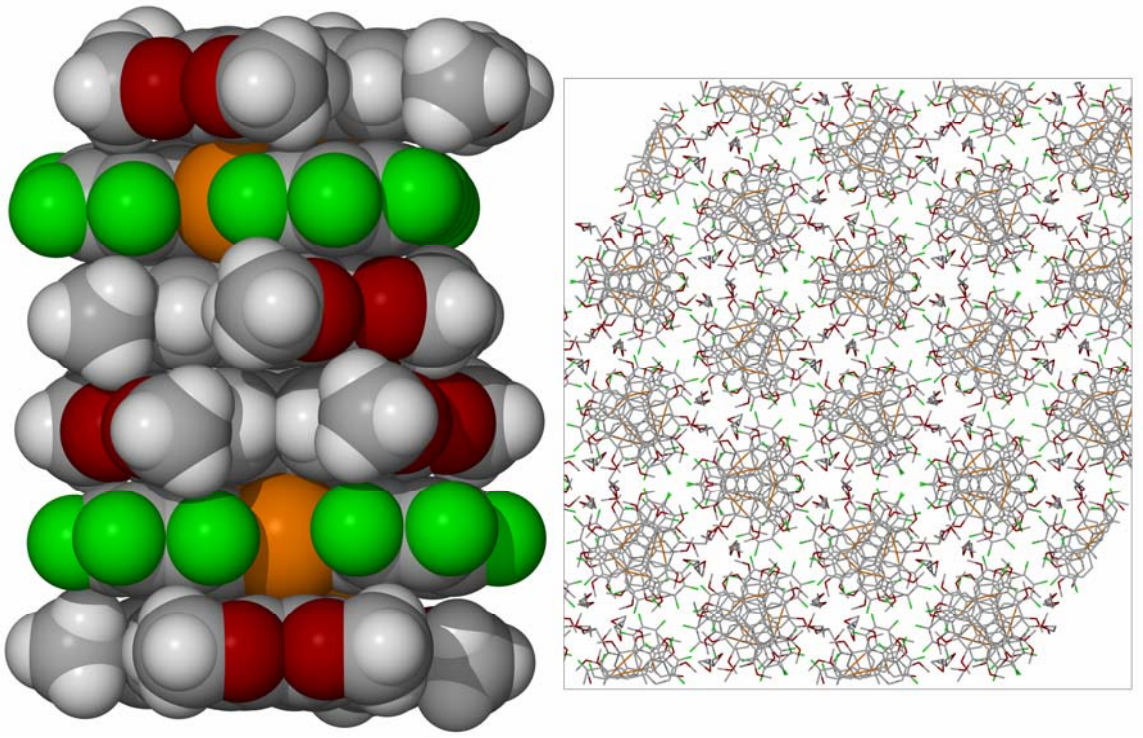

Figure 7.7. Right: Space-filling model of a portion of the stacks formed in **21a**. Propylene oxides omitted for clarity. Left: View along the c-axis in **21a**.

7.5 Powder diffraction of **21-26**

The structures of compounds **21-26** were investigated by X-ray powder diffraction. In all cases, the powder diffraction pattern is dominated by a low angle peak which shifts to lower angle as the length of the alkyl chain increases (Figure 7.8). This diffraction peak can be indexed as the 10 reflection of a two-dimensional hexagonal lattice consisting of a honeycomb array of columnar [**1**•HAT*n*] (Figure 7.9). The presence of a two-dimensional hexagonal array was confirmed by the presence of a peak

at √3 times the initial 2Θ peak which can be indexed as the 11 reflection (Table 7.2). Full powder diffraction patterns for **21**-**26** are shown in Figures 7.10-7.15. On the basis of this indexing, the a parameter of the two dimensional lattice directly corresponds to the inter-column spacing (Table 7.3). In the case of **21** and **22**, the a parameter is close to the van der Waals diameter of the corresponding HAT molecule that can be derived from their crystal structures. For **24** and **25**, the 10 reflection features a shoulder which most probably corresponds to a second hexagonal phase with a slightly different a parameter. This second phase might differ from the main phase by the folding of the aliphatic chains. As expected, the a parameter increases proportionally to the number of carbon in the alklyl chain of the HAT molecule on going from **21** to **26** (Figure 7.15). We also note that the a parameter of compounds **24**-**26** is smaller than that observed in the hexagonal columnar mesophase of the corresponding free HAT*n* molecules.[127] This can be attributed to a greater coiling of the aliphatic chains in the [**1**•HAT*n*] adducts.

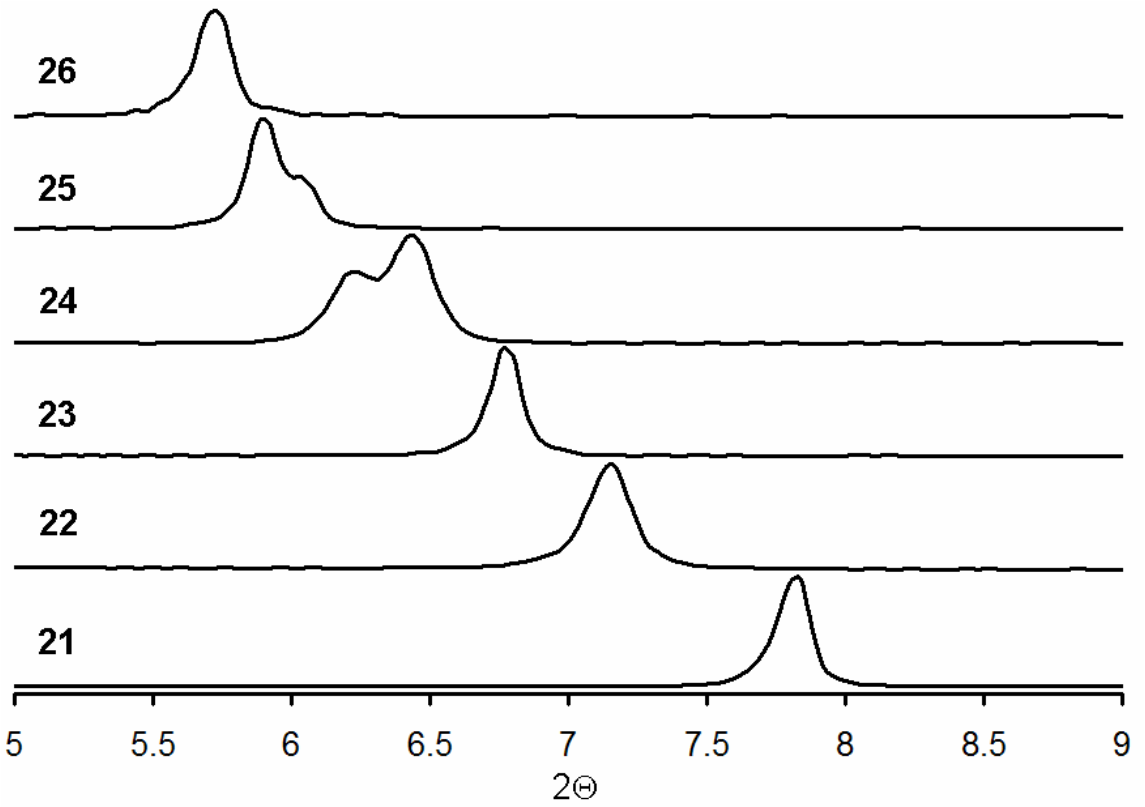

Figure 7.8. Powder diffraction patterns for **21**-**26** featuring the low angle peak.

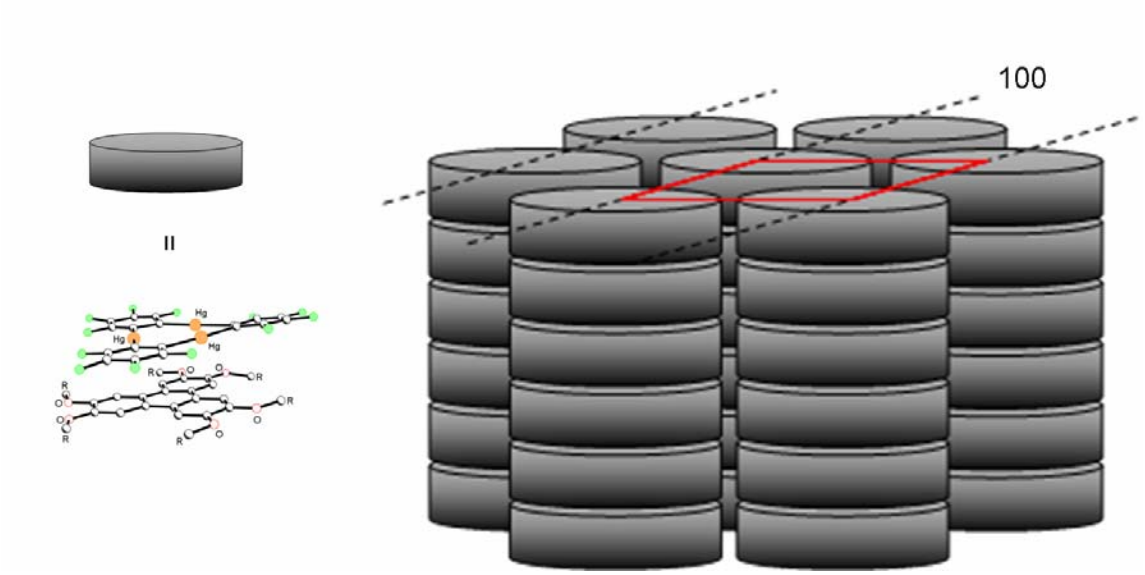

Figure 7.9. Cartoon depicting the proposed simple hexagonal cell used for indexing the powder patterns.

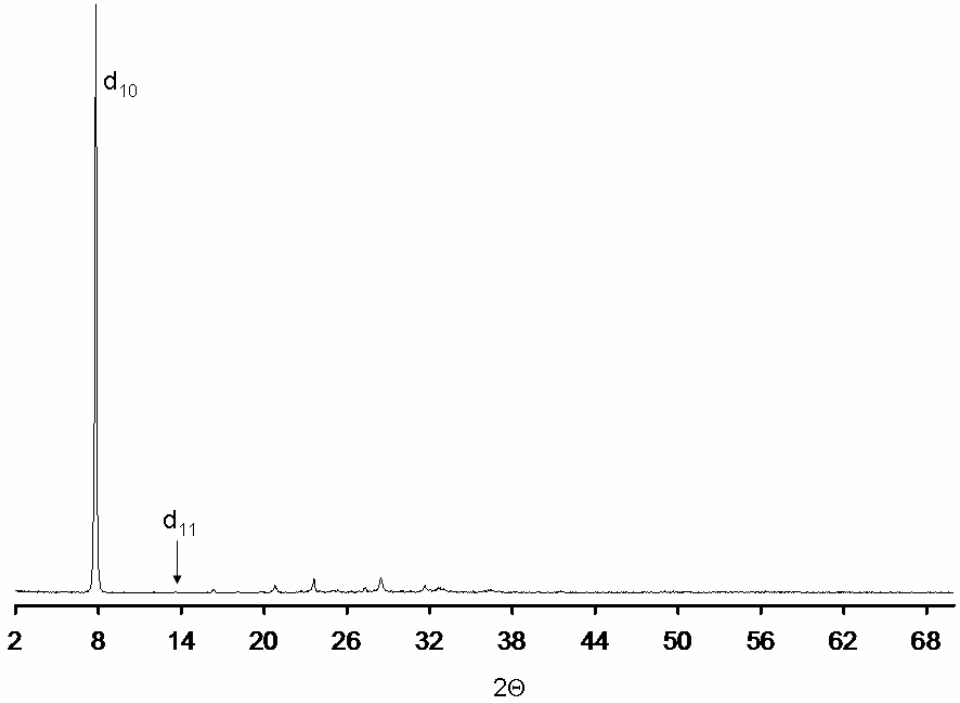

Figure 7.10. Powder diffraction pattern of **21**.

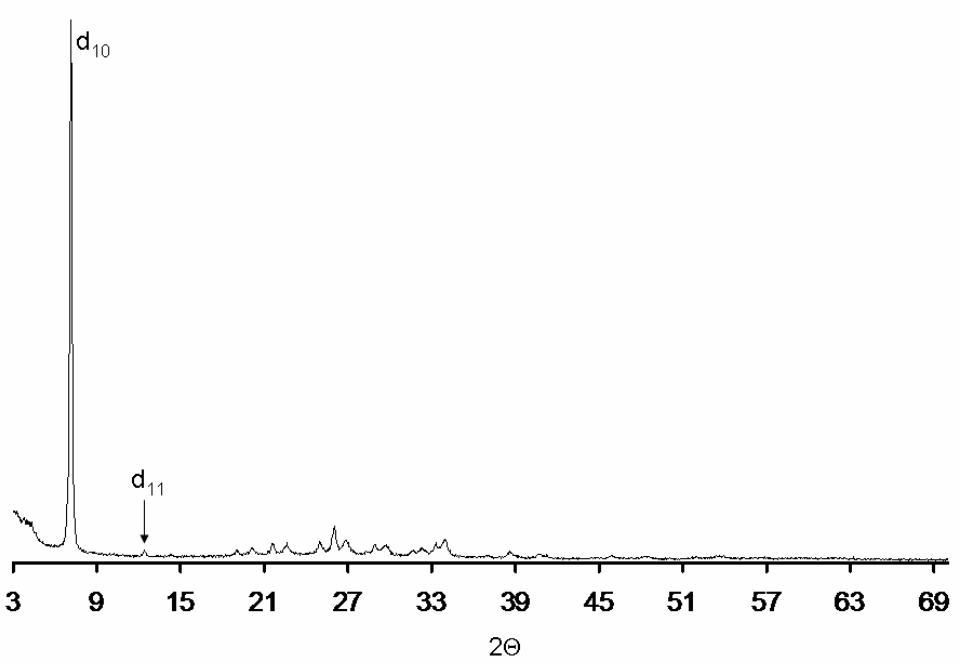

Figure 7.11. Powder diffraction pattern of **22**.

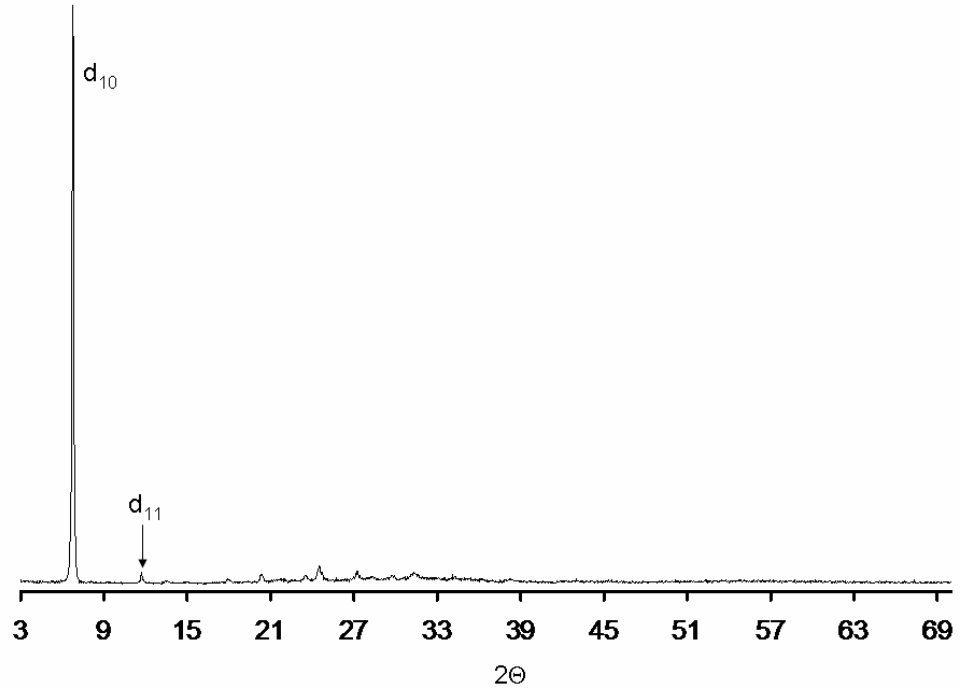

Figure 7.12. Powder diffraction pattern of **23**.

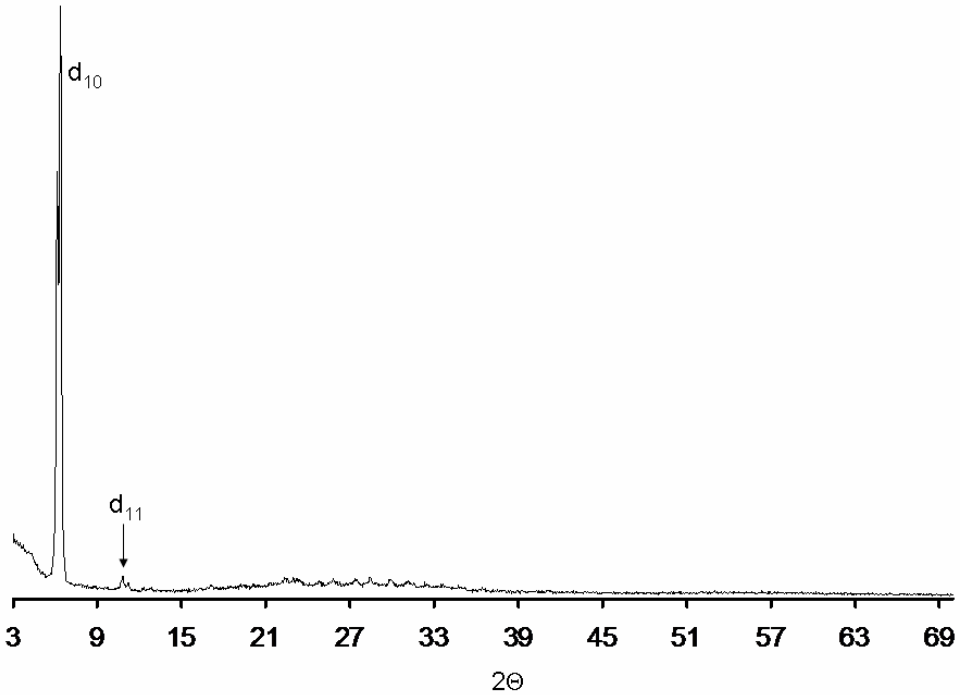

Figure 7.13. Powder diffraction pattern of **24**.

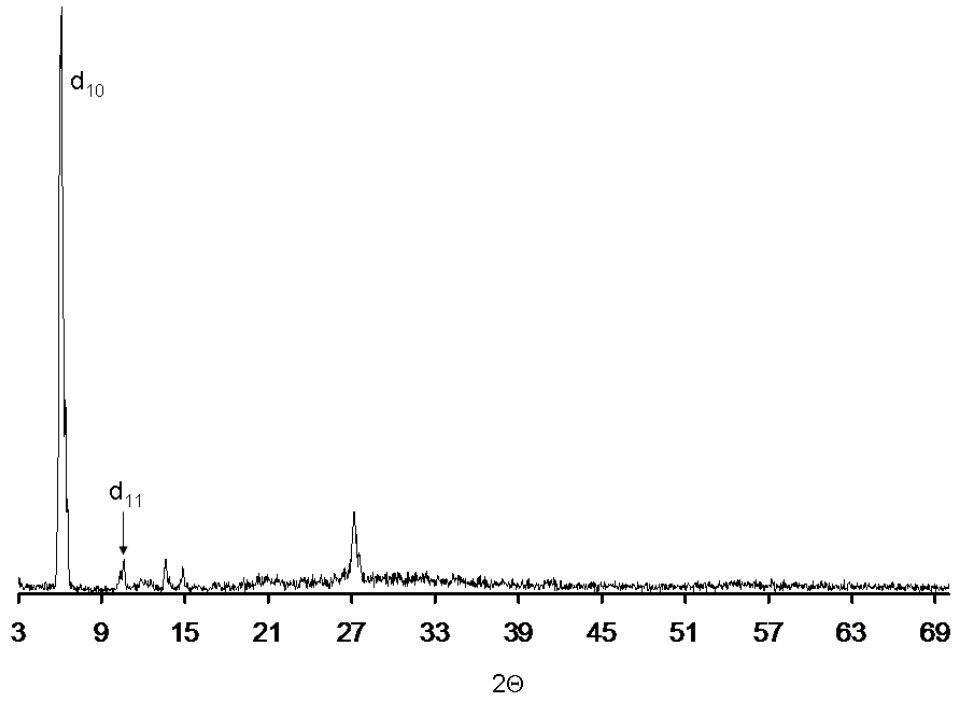

Figure 7.14. Powder diffraction pattern of **25**.

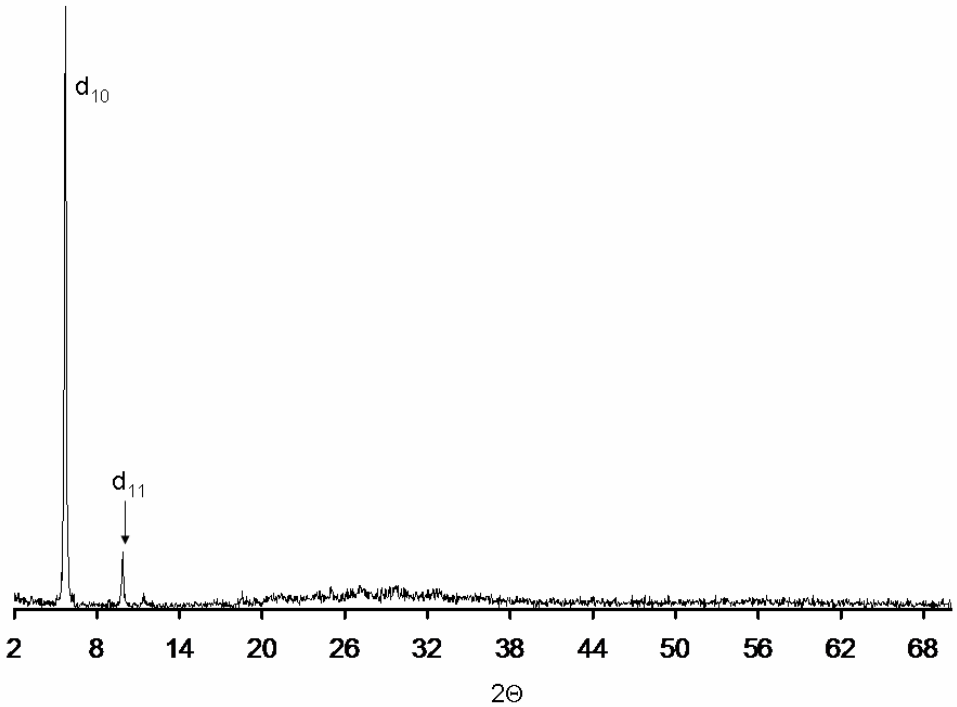

Figure 7.15. Powder diffraction pattern of **26**.

Table 7.2. Values of the d spacing for the 10 and 11 reflections.

	d_{10}	d_{11}
21	11.32	6.50
22	12.33	6.95
23	13.06	7.54
24	13.70, 14.14	7.78, 8.15
25	14.61, 15.01	8.27, 8.50
26	15.43	8.94

Table 7.3. Inter-columnar spacing in Å of **21**-**26** as measured by powder diffraction compared to that of the free HAT*n*.

	with **1**	free
HAT1	13.1	13.12[128]
HAT2	14.2	14.39
HAT3	15.1	
HAT4	15.8, 16.3	18.5[129]
HAT5	16.9, 17.3	18.94[130]
HAT6	17.8	22.4[131]

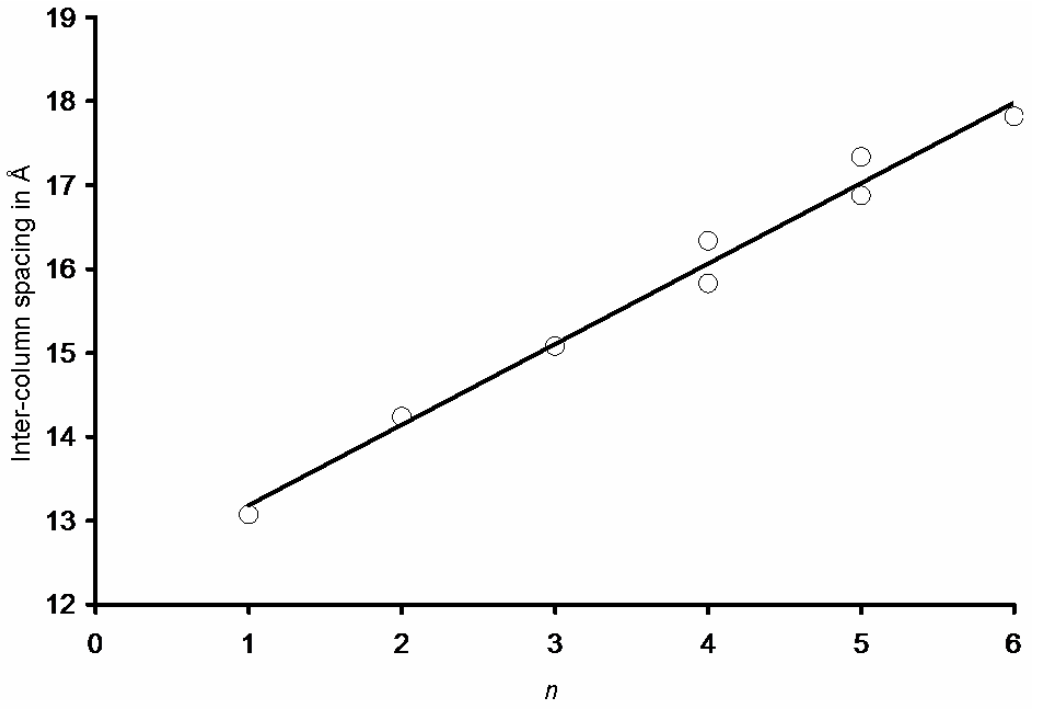

Figure 7.16. Inter-column spacing in Å of **21-26** vs. *n* which is the number of carbon atoms in the aliphatic chains. Two points are present for n = 4 and 5 representing the inter-column spacing for the two different phases.

7.6 Solution stoichiometry of **21-26**

We have performed a titration of HAT1-6 with **1** and monitored the progress by the decrease in the fluorescence emission of HAT1-6. As a solution of **1** in CH_2Cl_2 ($6.95x10^{-3}$ M) is added to a solution of HAT1-6 in CH_2Cl_2 (~$7.1x10^{-5}$ M) a decrease in the fluorescence emission of the HAT*n* molecule is observed. Since no precipitate is observed, quenching of the fluorescence most probably corresponds to formation of a complex between **1** and a HAT*n* molecule in which a mercury heavy atom effect would become operative. At this concentration the formation of higher aggregates is unlikely because of the high dilution.[132] Incremental addition of a solution of **1** ($6.95x10^{-3}$ M) to

a solution of HAT1 (7.45×10^{-5} M) yields the titration curve shown in figure 7.17. Incremental addition of a solution of **1** (6.95×10^{-3} M) to a solution of HAT2 (7.32×10^{-5} M) yields the titration curve shown in figure 7.18. Further addition of **1** to the solutions of HAT1 and HAT2 produced a white precipitate. Incremental addition of a solution of **1** (6.95×10^{-3} M) to a solution of HAT3 (7.18×10^{-5} M), HAT4 (6.85×10^{-5} M), HAT5 (7.05×10^{-5} M) and HAT6 (7.69×10^{-5} M) yields the titration curve shown in figures 7.19-7.22, respectively. The theoretical fit based on a 1:1 stoichiometry yields a stability constant, K, ranging from 5500 to 16400 M^{-1} depending on the nature of the HAT*n* molecules (Table 7.4). These values indicate that the formation of [**1**•HAT*n*] is favored. Furthermore, the K values do not differ greatly for different HAT*n*s; thus, the length of the aliphatic chain does not influence the formation of [**1**•HAT*n*]. In all cases, the 1:1 stoichiometry of the supramolecule has been confirmed by a Jobs analysis also monitored by fluorescence spectroscopy.

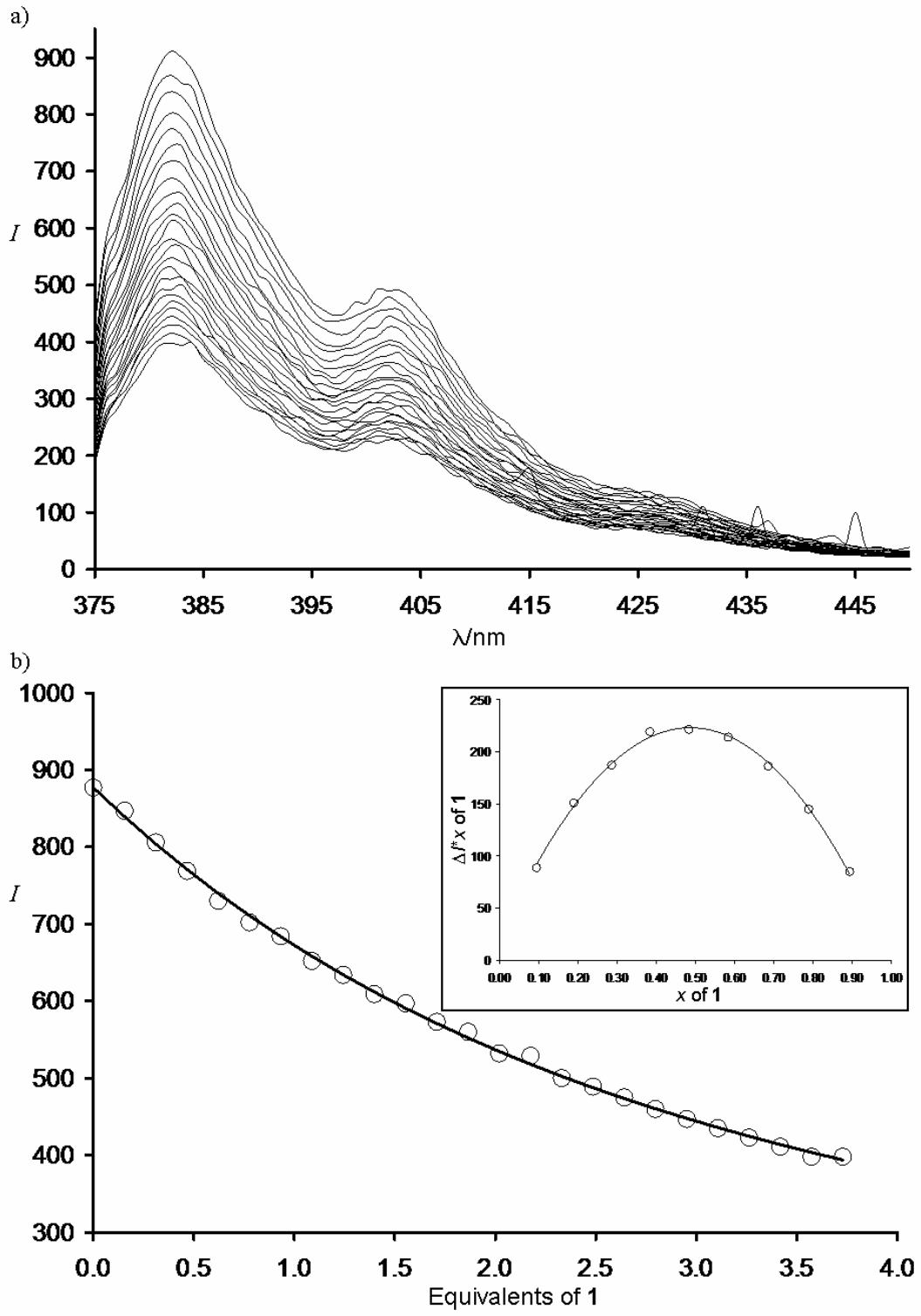

Figure 7.17. a) Luminescence spectra for the titration of HAT1 with **1**. b) Fluorescence intensity at 384 nm vs. equivalents of **1** added. Inset: Job's plot.

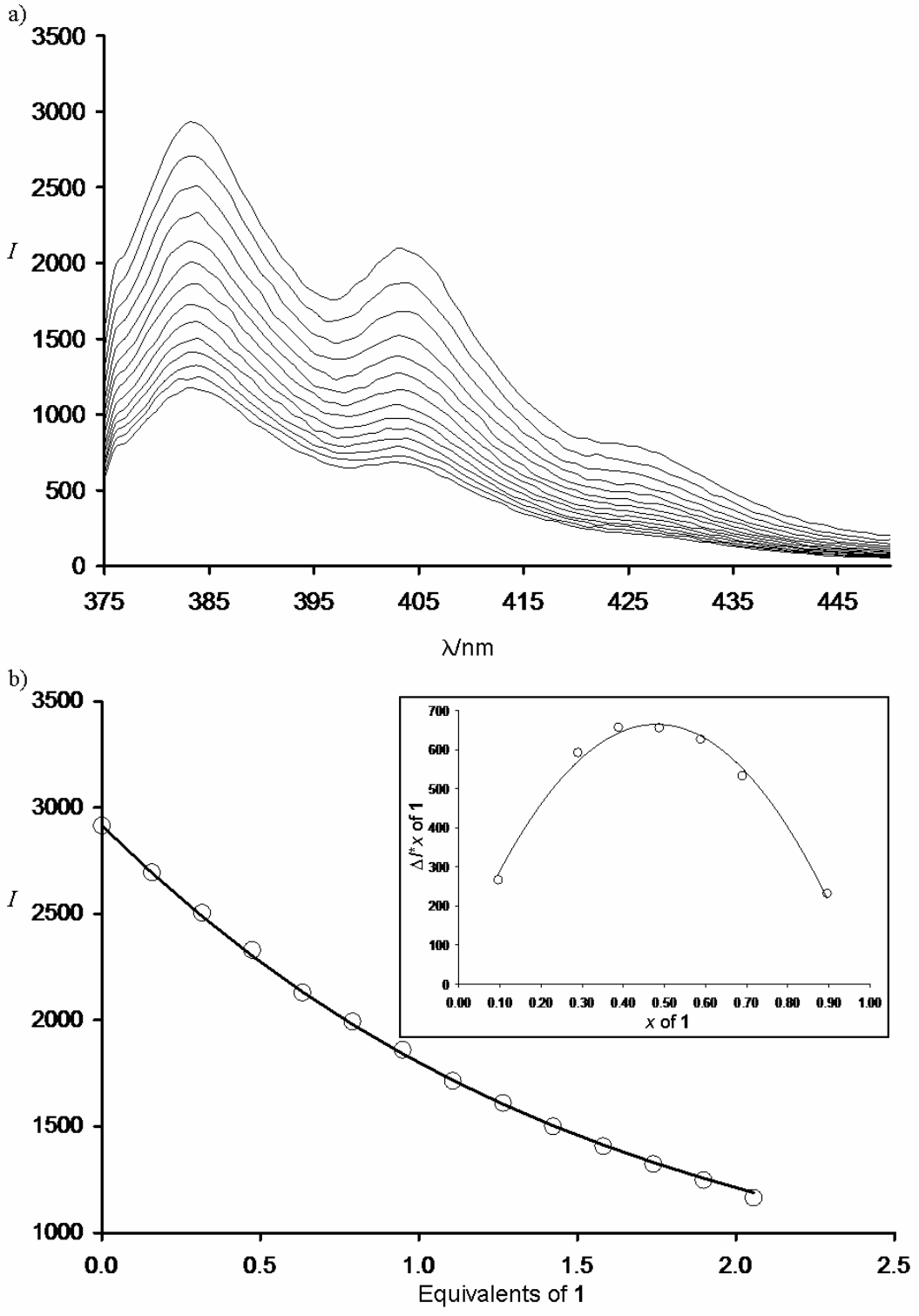

Figure 7.18. a) Luminescence spectra for the titration of HAT2 with **1**. b) Fluorescence intensity at 384 nm vs. equivalents of **1** added. Inset: Job's plot.

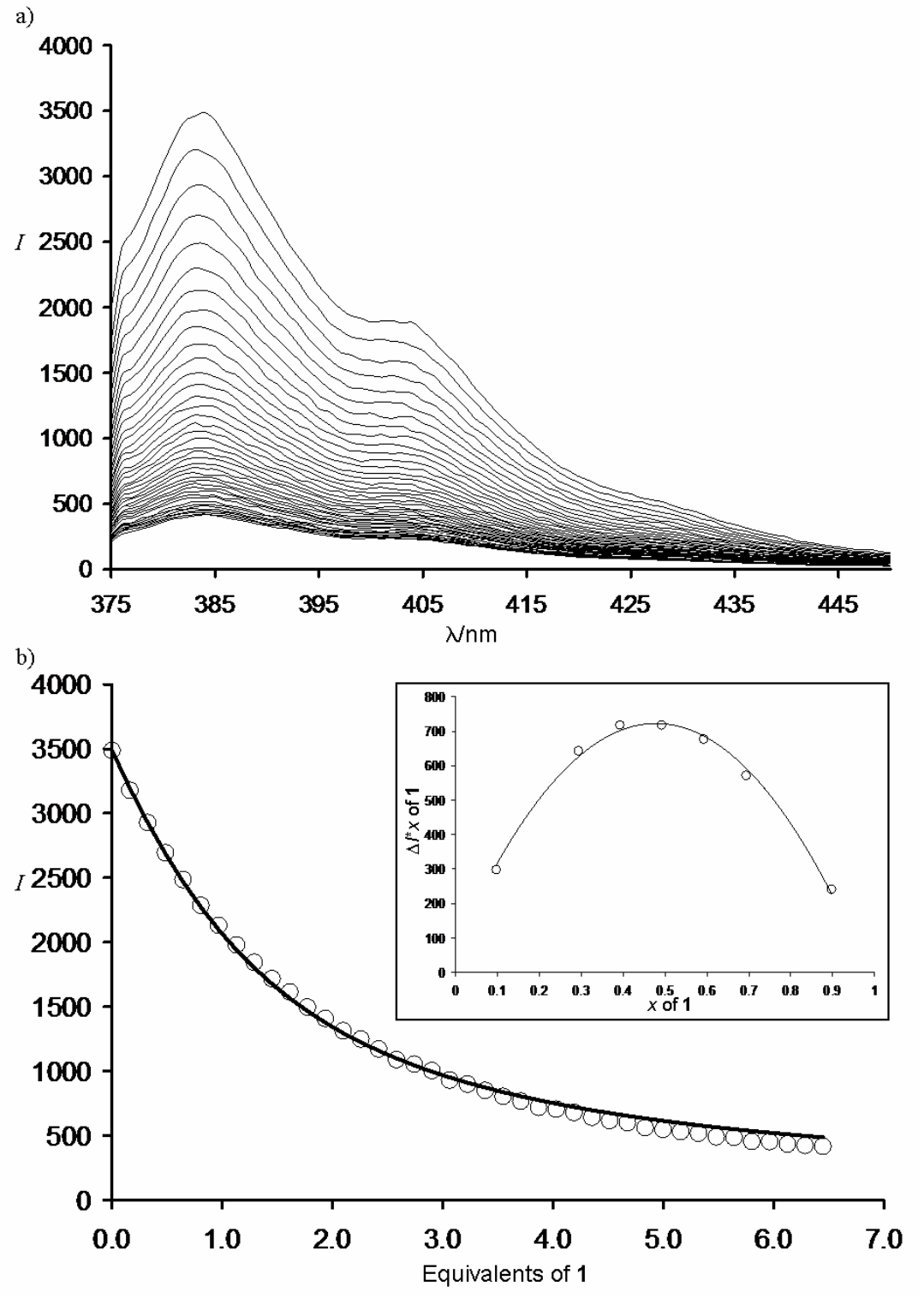

Figure 7.19. a) Luminescence spectra for the titration of HAT3 with **1**. b) Fluorescence intensity at 384 nm vs. equivalents of **1** added. Inset: Job's plot.

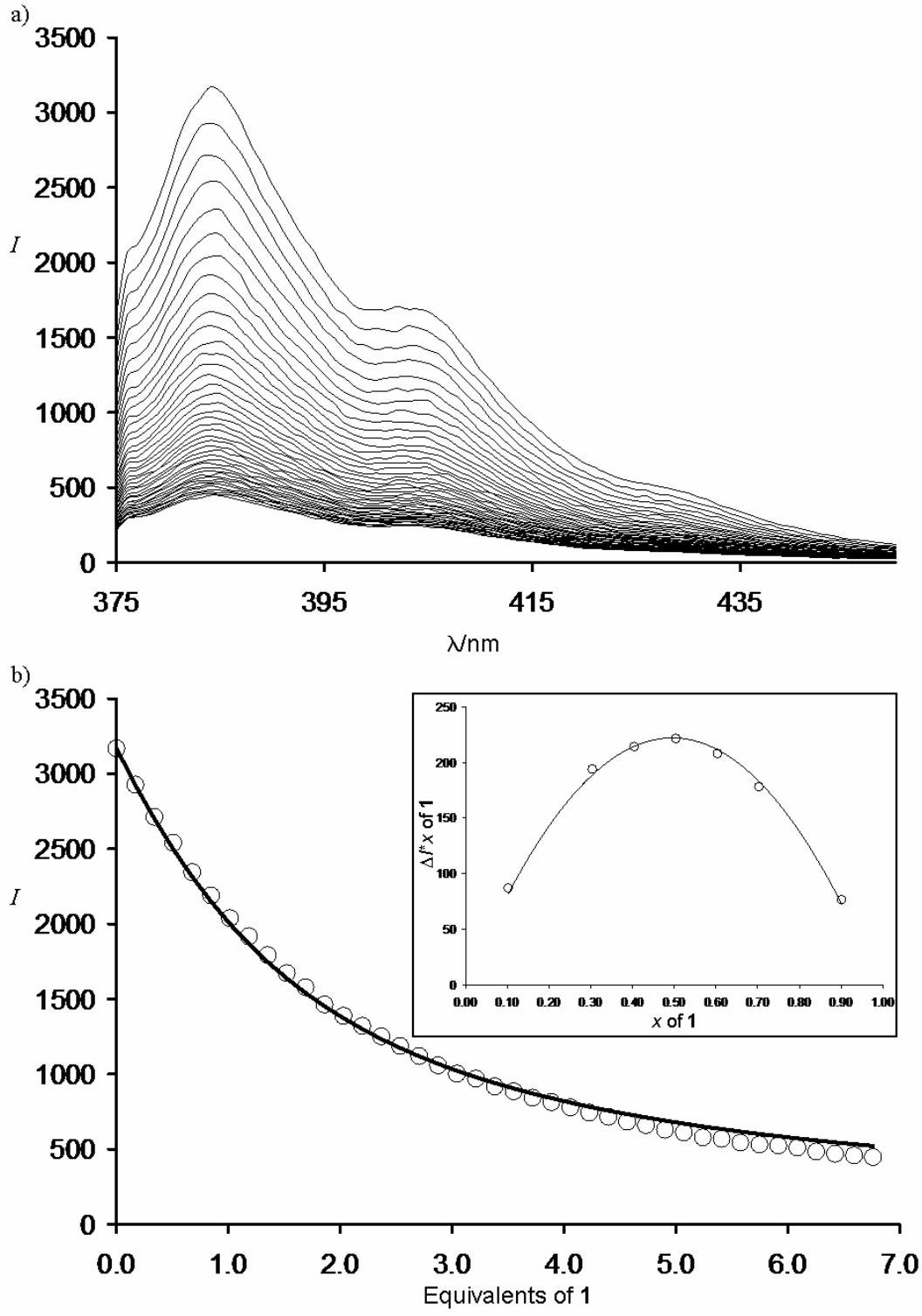

Figure 7.20. a) Luminescence spectra for the titration of HAT4 with **1**. b) Fluorescence intensity at 384 nm vs. equivalents of **1** added. Inset: Job's plot.

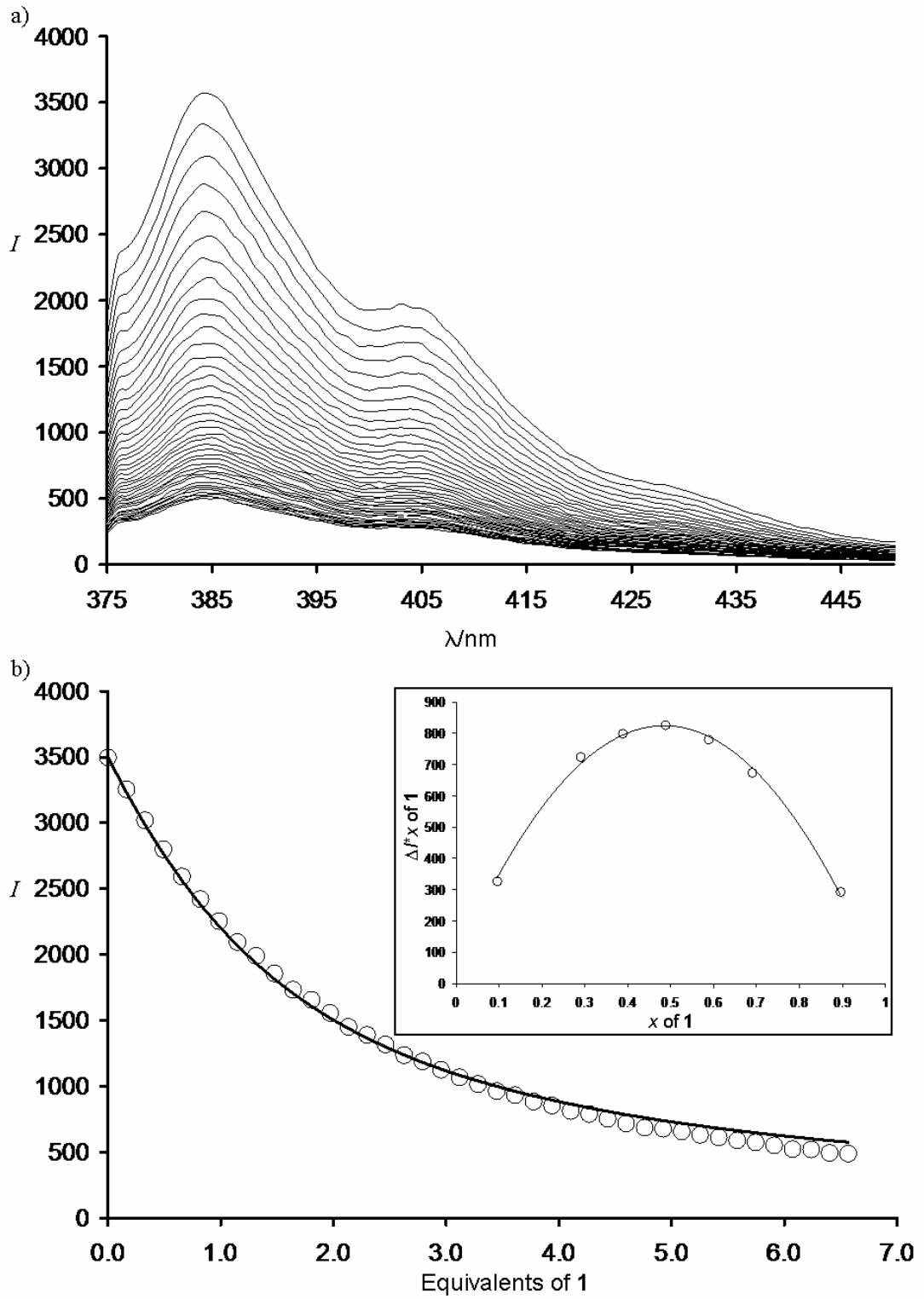

Figure 7.21. a) Luminescence spectra for the titration of HAT5 with **1**. b) Fluorescence intensity at 384 nm vs. equivalents of **1** added. Inset: Job's plot.

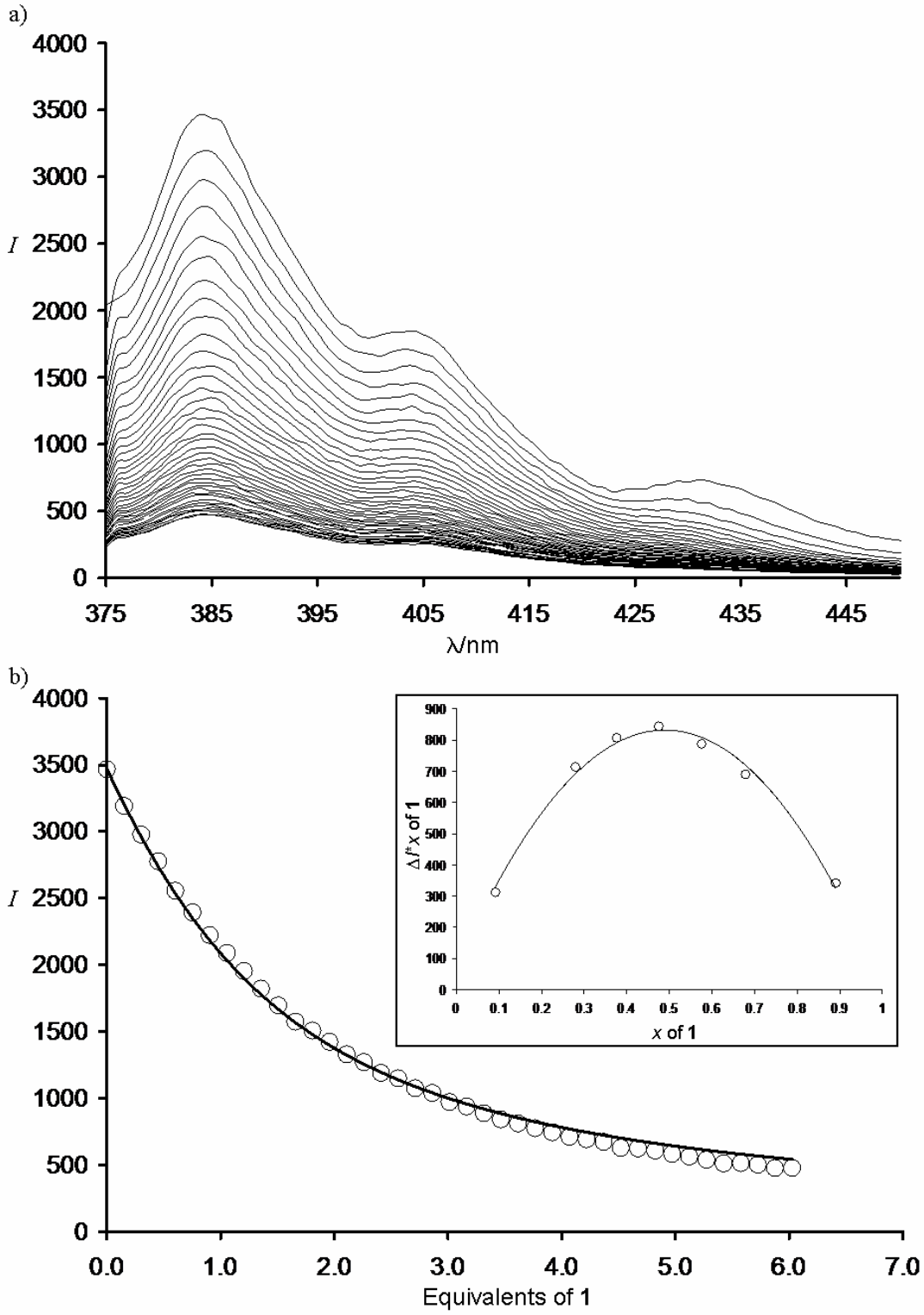

Figure 7.22. a) Luminescence spectra for the titration of HAT6 with **1**. b) Fluorescence intensity at 384 nm vs. equivalents of **1** added. Inset: Job's plot.

Table 7.4. K values in M^{-1} and ΔG in kJ/mol determined by luminescence titrations

	K	ΔG
HAT1	5400	-21.3
HAT2	13800	-23.6
HAT3	16400	-24.0
HAT4	13300	-23.5
HAT5	13400	-23.5
HAT6	14500	-23.7

We have also performed a titration of **1** with HAT5-6 and monitored the progress by ^{199}Hg NMR. To a solution of **1** in CH_2Cl_2 ($7.3x10^{-3}$ M with HAT5, $6.7x10^{-3}$ M with HAT6) μl aliquots of a solution of HAT5 or HAT6 in CH_2Cl_2 (0.34 M HAT5, 0.32 M HAT6) was added and the ^{199}Hg chemical shift was recorded after each addition. The ^{199}Hg chemical shift of **1** in CH_2Cl_2 occurs at -1045.6 ppm relative to $HgMe_2$. Upon addition of the HAT5 or HAT6 solution the ^{199}Hg chemical shift progresses upfield until just over 1 equivalent of HAT5 or HAT6 is reached giving a ^{199}Hg chemical shift of approximately -1091.75 ppm. Further addition of the HAT5 or HAT6 solution yielded very little change in the chemical shift (Figure 7.23). A Jobs analysis was performed on solutions of **1** and HAT5 as well as **1** and HAT6 and confirmed a 1:1 stoichiometry of the complexes in solution. However, due to the ability of **1** to form extended stack structures, we suspected that, at these concentrations, binary stacks of **1** and HAT5 or HAT6 maybe forming in solution. Furthermore, the exact stoichiometry was needed in order to calculate the equilibrium constant, K. Therefore we performed Pulsed-Field Gradient Spin Echo NMR (PGSE) (Figures 7.24 and 7.25) on the samples used in the Job's analysis that had equimolar concentrations of **1** ($3.4x10^{-3}$ M) and the

corresponding HAT*n* ($3.4x10^{-3}$ M HAT5, $3.3x10^{-3}$ M HAT6). This method allows for the determination of the diffusion coefficient, which is inversely proportional to the hydrodynamic radius, of a species.[133] An excellent correlation exists between the hydrodynamic radii derived from the PGSE experiment and the molecular radius derived from a X-ray diffraction experiment. Therefore, to evaluate the radius of HAT5, HAT6, **25** and **26** in solution, we compared their diffusion to that of two standards ETHANOX 330[134] (radius: 6.6 Å) and HAT2[135] (radius: 5.4 Å). ETHANOX 330 was chosen because it has a rather large molecular radius and HAT2 was chosen because it has the same structural motif as HAT5 and HAT6 and the radius is known from the published structure. Several measurements were carried out. In all cases HAT5 and HAT6 diffused at approximately the same rate as ETHANOX 330 while **25** and **26** diffused much slower. HAT2 diffused the fastest in all cases. From this data the radii and volumes listed in Table 7.5 were calculated using the diffusion rate and radius of ETHANOX 330 as standard. Comparing the calculated volumes reveals that **25** and **26** are three times the volume of the sum of the volume of **1** (459.55 $Å^3$)[136] and the volume of the corresponding HAT*n* molecule. Thus stacks consisting of 3 molecules of HAT5 or HAT6 and 3 molecules of **1** are forming in solution at this concentration.

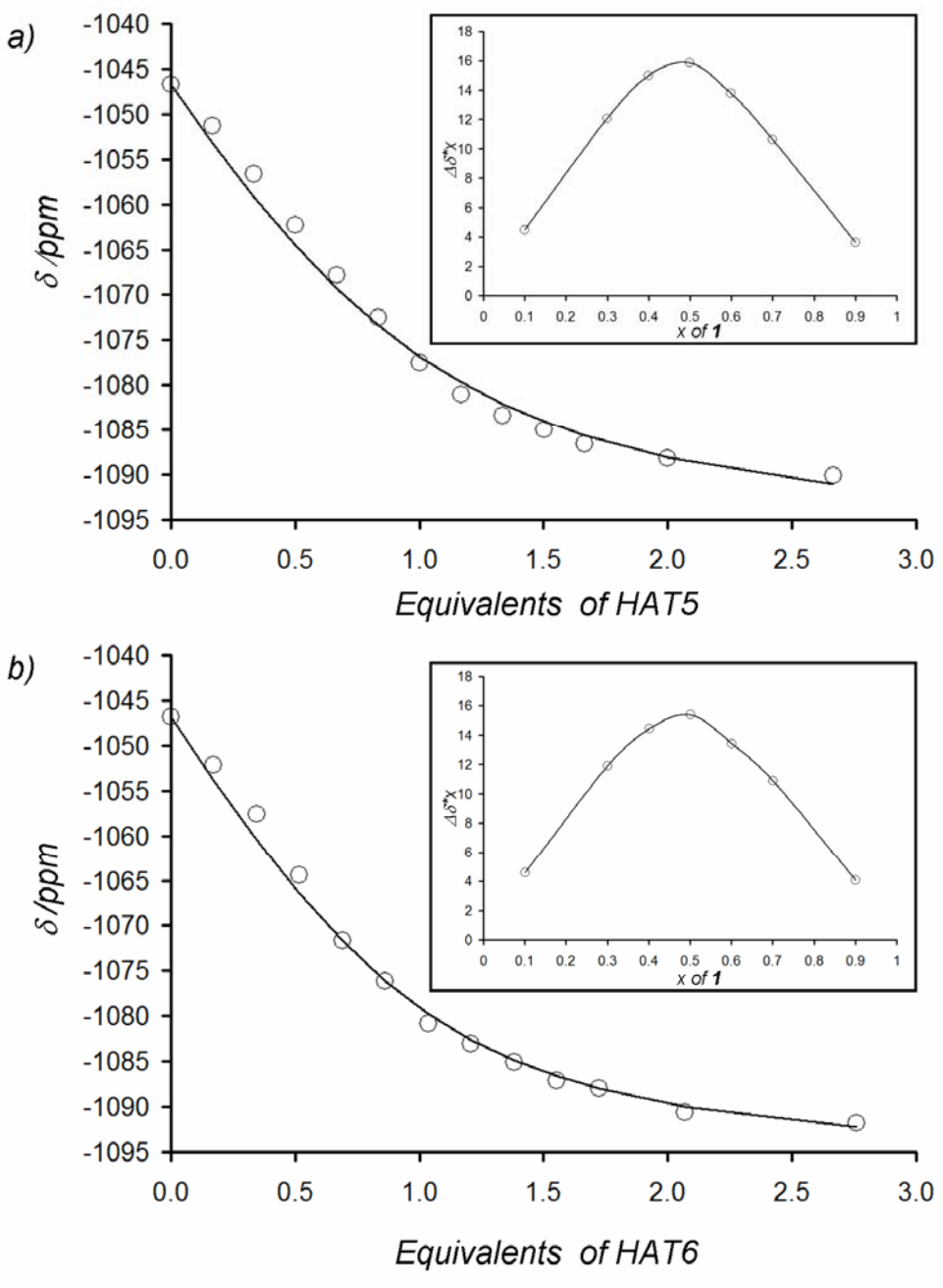

Figure 7.23. ^{199}Hg chemical shift of **1** vs. equivalents of a) HAT5 and b) HAT6. Inset: Job's plot.

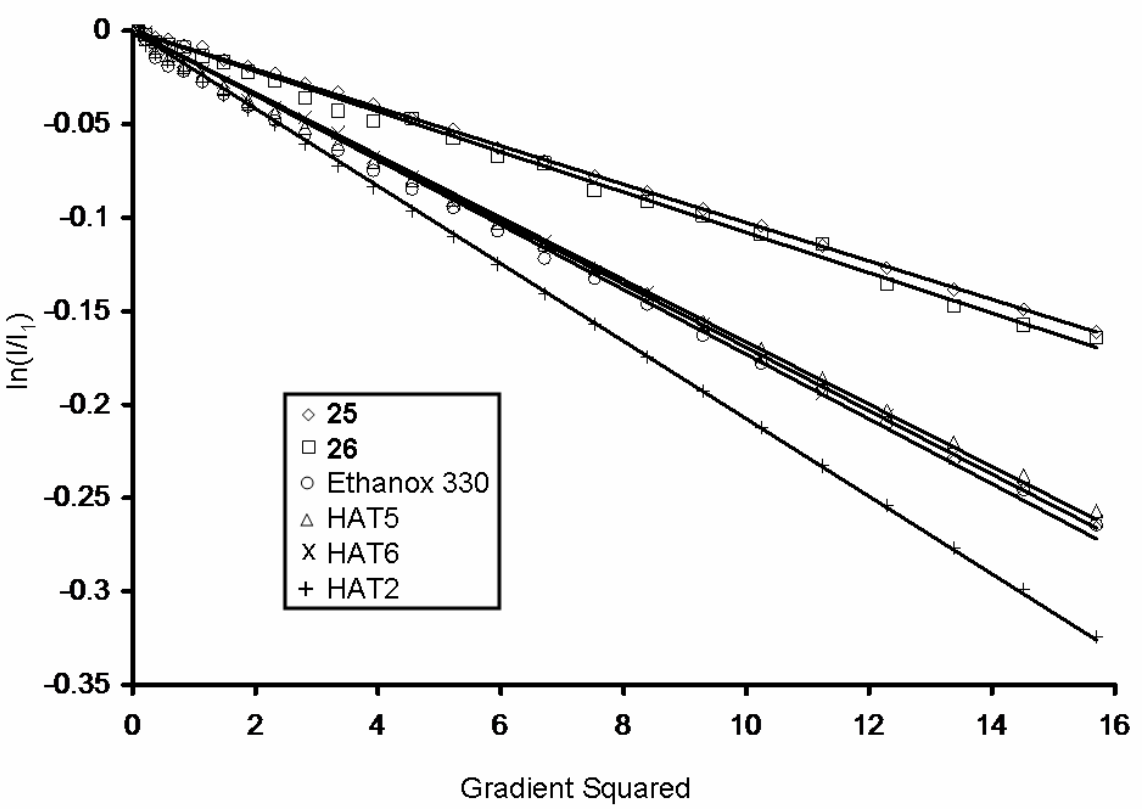

Figure 7.24. Pulse-Gradient Spin Echo NMR (PGSE) results.

Table 7.5. PGSE data. Radii are in Å and Volumes are in Å^3.

	$R_{X\text{-}ray}$	Slope	R_H	Estimated Volume
25	-	-0.0103	11.1	5796
26	-	-0.0107	10.6	4985
Ethanox 330	6.6	-0.0173	-	-
HAT5	-	-0.0166	6.87	1356
HAT6	-	-0.0169	6.75	1288
HAT2	5.4	-0.0207	5.51	700

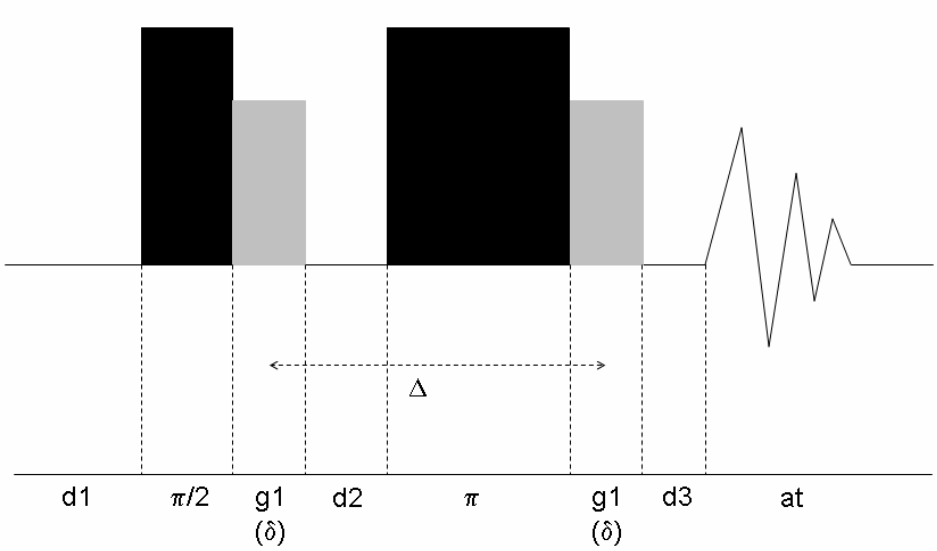

Figure 7.25. Pulse sequence used in PGSE Experiments. d1 = 2 seconds; π = 22 microseconds; d2 = d3 = 60 milliseconds; Δ = 68.2 milliseconds; g1 = 8.2 milliseconds; at = 1.8 seconds.

The results of the PGSE experiment show the propensity of **1** and HAT*n* molecules to aggregate in solution at higher concentrations. The calculated volume most likely correspond to an average volume, thus higher aggregates need to be considered in order to model the equilibrium. These aggregates likely form in a step-wise process with a possible scenario depicted in Scheme 7.2. In this scenario, there are eleven independent equilibrium constants. Since the chemical shifts of the twelve intermediate species as well as the individual 11 equilibrium constants are unknown, it does not appear that such a complex system can be accurately modeled.

$$\mathbf{1} + \mathrm{HAT}n \overset{K_1}{\rightleftharpoons} [\mathbf{1}\bullet\mathrm{HAT}n]$$

$$[\mathbf{1}\bullet\mathrm{HAT}n] + \mathbf{1} \overset{K_2}{\rightleftharpoons} [\mathbf{1}_2\bullet\mathrm{HAT}n]$$

$$[\mathbf{1}_2\bullet\mathrm{HAT}n] + \mathrm{HATn} \overset{K_3}{\rightleftharpoons} [\mathbf{1}_2\bullet\mathrm{HAT}n_2]$$

$$[\mathbf{1}_2\bullet\mathrm{HAT}n_2] + \mathbf{1} \overset{K_4}{\rightleftharpoons} [\mathbf{1}_3\bullet\mathrm{HAT}n_2]$$

$$[\mathbf{1}_3\bullet\mathrm{HAT}n_2] + \mathrm{HAT}n \overset{K_5}{\rightleftharpoons} [\mathbf{1}_3\bullet\mathrm{HAT}n_3]$$

$$[\mathbf{1}_3\bullet\mathrm{HAT}n_3] + \mathbf{1} \overset{K_6}{\rightleftharpoons} [\mathbf{1}_4\bullet\mathrm{HAT}n_3]$$

$$[\mathbf{1}_4\bullet\mathrm{HAT}n_3] + \mathrm{HATn} \overset{K_7}{\rightleftharpoons} [\mathbf{1}_4\bullet\mathrm{HAT}n_4]$$

$$[\mathbf{1}_4\bullet\mathrm{HAT}n_4] + \mathbf{1} \overset{K_8}{\rightleftharpoons} [\mathbf{1}_5\bullet\mathrm{HAT}n_4]$$

$$[\mathbf{1}_5\bullet\mathrm{HAT}n_4] + \mathrm{HATn} \overset{K_9}{\rightleftharpoons} [\mathbf{1}_5\bullet\mathrm{HAT}n_5]$$

$$[\mathbf{1}_5\bullet\mathrm{HAT}n_5] + \mathbf{1} \overset{K_{10}}{\rightleftharpoons} [\mathbf{1}_6\bullet\mathrm{HAT}n_5]$$

$$[\mathbf{1}_6\bullet\mathrm{HAT}n_5] + \mathrm{HATn} \overset{K_{11}}{\rightleftharpoons} [\mathbf{1}_6\bullet\mathrm{HAT}n_6]$$

Scheme 7.2

7.7 Summary

The interaction of HAT1-6 with **1** has been studied in the solid-state and in solution. The crystal structures reveal that **20** and **21a** form supramolecular stacks. Powder diffraction also indicates that **21-26** form supramolecular stacks with inter-columnar distances ranging from 13.2-17.8 Å. The solution studies detailed in this chapter clearly demonstrate that the interaction of **1** with arenes can be observed in solution by fluorescence spectroscopy or ^{199}Hg NMR. At high dilution, titration experiments monitored by fluorescence spectroscopy indicate that **1** complexes HAT*n* molecules with equilibrium constants, K, ranging from 5500-16400, depending on the chain of the alkyl chain. At higher concentration, ^{199}Hg NMR spectroscopy was used to confirm the formation of binary complexes involving **1** and HAT5 or HAT6. At these concentrations, ^{1}H PGSE NMR data was used to study the extent of aggregation and indicated the formation aggregates with an average 3:3 stoichiometry.

7.8 Experimental details

General. Due to the toxicity of the mercury compounds discussed in these studies extra care was taken at all times to avoid contact with solid, solution, and air-borne particulate mercury compounds. The studies herein were carried out in well-aerated fume hood. Atlantic Microlab, Inc., Norcross, GA, and Complete Analysis Laboratories, Inc., Parsippany, NJ, performed the elemental analyses. HAT1 was purchased from TCI America and further purified by column chromatography (silica gel 1:1 CH_2Cl_2:Hexanes). The remainder of commercially available starting materials and

solvents were purchased from Aldrich Chemical and were used as provided. Compound **1** was prepared according to the published procedure outlined by Sartori and Golloch. ^{199}HgNMR measurements were acquired at ambient temperature on an INOVA 400 MHz spectrometer.

General Synthetic Procedure. A solution of compound **1** in CH_2Cl_2 was mixed with a solution of the corresponding HAT in CH_2Cl_2. In the case of HAT1-3, upon mixing immediate precipitation of a white solid occurs to yield [**1**•HAT1] (**21**), [**1**•HAT2] (**22**), [**1**•HAT3] (**23**). Crystals of **21** were obtained by slow diffusion of a solution **1** and a solution of HAT1 in CH_2Cl_2 through pristine CH_2Cl_2. In the case of HAT4 and HAT5, upon slow evaporation of the solvent crystals of [**1**•HAT4] (**24**) and [**1**•HAT5] (**25**) form. In the case of HAT6, upon evaporation of the solvent the waxy solid [**1**•HAT6] (**26**) is obtained.

Compound **20**. Anal. Calc. For $C_{60}H_{60}O_{12}F_{12}Hg_3$: C, 40.0; H, 3.36. Found: C, 34.99; H, 1.89. Decomposes at 285 °C.

Compound **21**. Anal. Calc. For $C_{42}H_{24}O_6F_{12}Hg_3$: C, 34.69; H, 1.66. Found: C, 34.15; H, 1.64. Decomposes at 490 °C.

Compound **22**. Anal. Calc. For $C_{48}H_{36}O_6F_{12}Hg_3$: C, 37.47; H, 2.36. Found: C, 37.56; H, 2.24. Decomposes at 420 °C.

Compound **23**. Anal. Calc. For $C_{54}H_{48}O_6F_{12}Hg_3$: C, 40.00; H, 3.00. Found: C, 39.72; H, 2.66. Decomposes at 420 °C.

Compound **24**. Anal. Calc. For $C_{60}H_{60}O_6F_{12}Hg_3$: C, 42.13; H, 3.54. Found: C, 42.29; H, 3.44. Decomposes at 420 °C.

Compound **25**. Anal. Calc. For $C_{66}H_{72}O_6F_{12}Hg_3$: C, 44.30; H, 4.06. Found: C, 44.01; H, 3.93. Decomposes at 400 °C.

Compound **26**. Anal. Calc. For $C_{72}H_{84}O_6F_{12}Hg_3$: C, 46.11; H, 4.52. Found: C, 46.15; H, 4.46. Decomposes at 400 °C.

Single-Crystal X-ray Analysis. X-ray data for **20**, **21**, **24**, and **25** were collected on a Bruker Smart-CCD diffractometer using graphite-monochromated Mo-Kα radiation (λ = 0.71073 Å). Specimens of suitable size and quality were selected and mounted onto a glass fiber with either Apiezon grease (for low temperature data collections) or epoxy (for room temperature data collections). The structures were solved by direct methods, which successfully located most of the non-hydrogen atoms. Subsequent refinement on F^2 using the SHELXTL/PC package (version 6.1) allowed location of the remaining non-hydrogen atoms.

Pulsed Field Gradient Spin-Echo NMR. All measurements were performed on a Varian Inova 500 MHz spectrometer using Varian's diffusion software package. Spectra were recorded on samples in CD_2Cl_2 at 293 K without spinning. During an experiment, all factors were kept constant while the gradient strength (G) was arrayed between 0 and 7.5 G/cm. The gradient was calibrated using D_2O. Following data collection, the spectra were carefully integrated. The resulting data points were subjected to a linear-least-squares fit which produced, as per $\ln(\frac{I}{I_1}) = -\gamma\delta^2 G^2(\Delta - \frac{\delta}{3})D$, a regression line whose slope is proportional to the diffusion coefficient and inversely proportional to the molecular hydrodynamic radius. One standard Ethanox330 with

crystallographic radius ($R_{X\text{-}ray}$) and therefore hydrodynamic radius (R_H)[137] similar to those expected for HAT5 and HAT6 was selected. The slope obtained for **25** and **26** was compared to those of the standard and those of HAT5 and HAT6.

Powder Diffraction. Powder diffraction patterns were collected on a Bruker-AXS D8 powder high resolution parallel Beam X-Ray diffractometer using germanium incident beam monochromated Cu-Kα radiation (λ = 1.54056 Å). Specimens were mounted glass plates. 2Θ was scanned from 2-70º in continuous mode at 0.04º/sec.

Luminescence Titrations. A 3 ml portion of a solution containing HAT1 ($7.45\text{x}10^{-5}$ M), HAT2 ($7.32\text{x}10^{-5}$ M), HAT3 ($7.18\text{x}10^{-5}$ M), HAT4 ($6.85\text{x}10^{-5}$ M), HAT5 ($7.05\text{x}10^{-5}$ M), or HAT6 ($7.69\text{x}10^{-5}$ M) was added to a quartz cuvette and the emission spectra was collected. To the cuvette a 5 ml aliquot of a solution containing $6.95 \text{ x } 10^{-3}$ M **1** was added and the emission spectra was recollected. This was repeated until the emission did not show any further decrease in intensity or a precipitate began to form.

CHAPTER VIII

COORDINATION OF METALLOCENES TO $[Hg(o\text{-}C_6F_4)]_3$*

8.1 Introduction

As part of our contribution to the supramolecular chemistry of mercury polyfunctional Lewis acids,[2a,5,48] we have been involved in the study of trimeric perfluoro-*ortho*-phenylene mercury ($[o\text{-}C_6F_4Hg]_3$, **1**), a simple tridentate Lewis acid. This derivative, which complexes a number of electron rich species,[3,4a,48] also interacts with arenes including naphthalene, pyrene and triphenylene to afford binary stacks where the arene is π-coordinated to the mercury centers of **1**. This supramolecular complexation mode leads to a perturbation of the photophysical properties of the arene which displays intense room temperature phosphorescence as a result of a mercury heavy atom effect.[38,49] Our continuing interest in the supramolecular chemistry of **1** led us to extend the scope of our studies to metal complexes featuring accessible aromatic ligands. In this chapter, structures and properties of electrophilic double-sandwiches[138] formed by the interaction of **1** with ferrocene and nickelocene is described.

8.2 Synthesis of [**1**•CpFeCp•**1**] (**27**) and [**1**•CpNiCp•**1**] (**28**)

Dark orange crystals of the ferrocene adduct [**1**•CpFeCp•**1**] (**27**) and dark red crystals of the nickelocene adduct [**1**•CpNiCp•**1**] (**28**) were obtained upon evaporation of

---

* Reprinted in part with permission from *Angew. Chem., Int. Ed. Engl,* Haneline, M. R.; Taylor, R. E.; Gabbaï, F. P., "Electrophilic double-sandwiches formed by interaction of Cp_2Fe and Cp_2Ni with the tridentate Lewis acid $[o\text{-}C_6F_4Hg]_3$", *in press*, Copyright 2004 Wiley-VCH Verlag GmbH&Co. KGaA.

CH_2Cl_2 solutions containing **1** and the corresponding metallocene. The 2:1 stoichiometry of these adducts was confirmed by elemental analysis. Both compounds showed no sign of decomposition upon exposure to air for several months thus indicating that **1** stabilizes the usually air-sensitive 20-electron nickelocene complex against aerobic oxidation.[139]

8.3 Crystal structures of **27** and **28**

Compounds **27** and **28** crystallize in the monoclinic space group *C*2/m and are isomorphous (Table 8.1 and Figures 8.1-8.2). With Hg-C distances ranging from 3.20-3.24 Å, the carbon atoms of the Cp rings of the metallocene are in close contact with the mercury centers of **1**. As previously observed in arene adducts of **1**,[38,47,49] these distances are within the sum of the van der Waals radii of mercury (1.7-2.0 Å)[25,24] and carbon (1.7 Å). This structural feature indicates the presence of secondary Hg-π interactions which likely complement attractive electrostatic and dispersion forces present between **1** and the metallocene. The two molecules of **1** are staggered with respect to one another. The bond distances in the metallocene are unchanged compared to those of the pure metallocene.[140] The perfluorophenylene ring containing the C(1) carbon atom and its symmetry equivalent are bent away from the metallocene and form a dihedral angle of 5° for **27** and 4° for **28** with respect to the plane containing the three mercury atoms. Apparently, this deformation allows for a closer approach of the trinuclear mercury core of **1** to the Cp rings of the metallocene. The remaining phenylene ring which contains the C(7) carbon atom is essentially coplanar with the

plane formed by the trinuclear mercury core. While the formation of such electrophilic double sandwiches is unprecedented, we note the existence of a structural parallel with binary compounds such as $[FeCp^*_2]^+[TCNE]^-$ (Cp* = pentamethylcyclopentadienide, TCNE = tetracyanoethylene)[141] and $[Cr(C_6H_6)_2][C_6F_6]$ which feature transition metal complexes sandwiched between π-acidic molecules. In **27** and **28**, the neighboring molecules of [**1**•CpMCp•**1**] (M = Fe (**27**), M = Ni (**28**)) engage in mercurophilic interactions with a Hg-Hg distance of 3.4157(16) Å for **27** and 3.3996(17) Å for **28**. These Hg-Hg distances are within the sum of the van der Waals radius of mercury and are very close to the Hg-Hg distance calculated by Pyykkö for the dimer of dimethyl mercury (3.41 Å).[25,26,54] This aggregation mode is similar to that observed in the structure of [**1**-μ_3-acetone] which forms dimers held by mercurophilic interactions of 3.512 Å. We also note that similar metallophilic interactions are sometimes observed in the structural chemistry of trinuclear coinage metal complexes.[83,142,143]

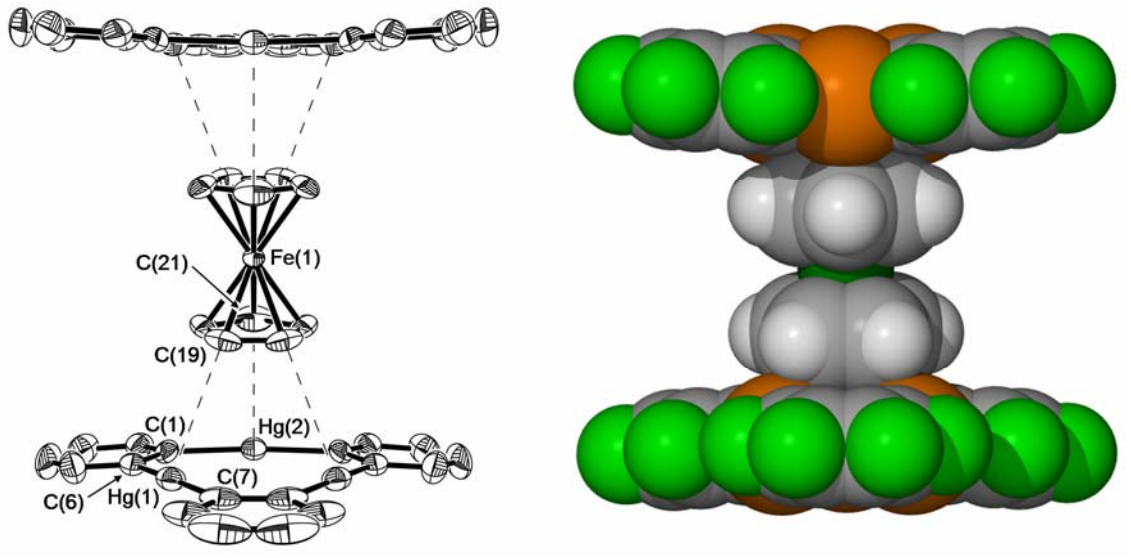

Figure 8.1. Left: ORTEP view of **27** (30% ellipsoid, H and F omitted). Right: Space-filling model of **28**. (C grey, F light green, Hg orange, Ni dark green, and H white). Selected bond lengths [Å] and angles [deg]: **27**: Hg(1)-C(19) 3.217(11), Hg(2)-C(21) 3.222(18), Hg(1)-C(6) 2.055(14), Hg(1)-C(7) 2.086(13), Hg(2)-C(1) 2.039(12), C(6)-Hg(1)-C(7) 174.8(5), C(1)-Hg(2)-C(1A) 176.2(7); **28**: Hg(1)-C(19) 3.204(12), Hg(2)-C(21) 3.237(17), Hg(1)-C(6) 2.089(9), Hg(1)-C(7) 2.102(14), Hg(2)-C(1) 2.048(9), C(6)-Hg(1)-C(7) 175.4(5), C(1)-Hg(2)-C(1A) 176.4(6).

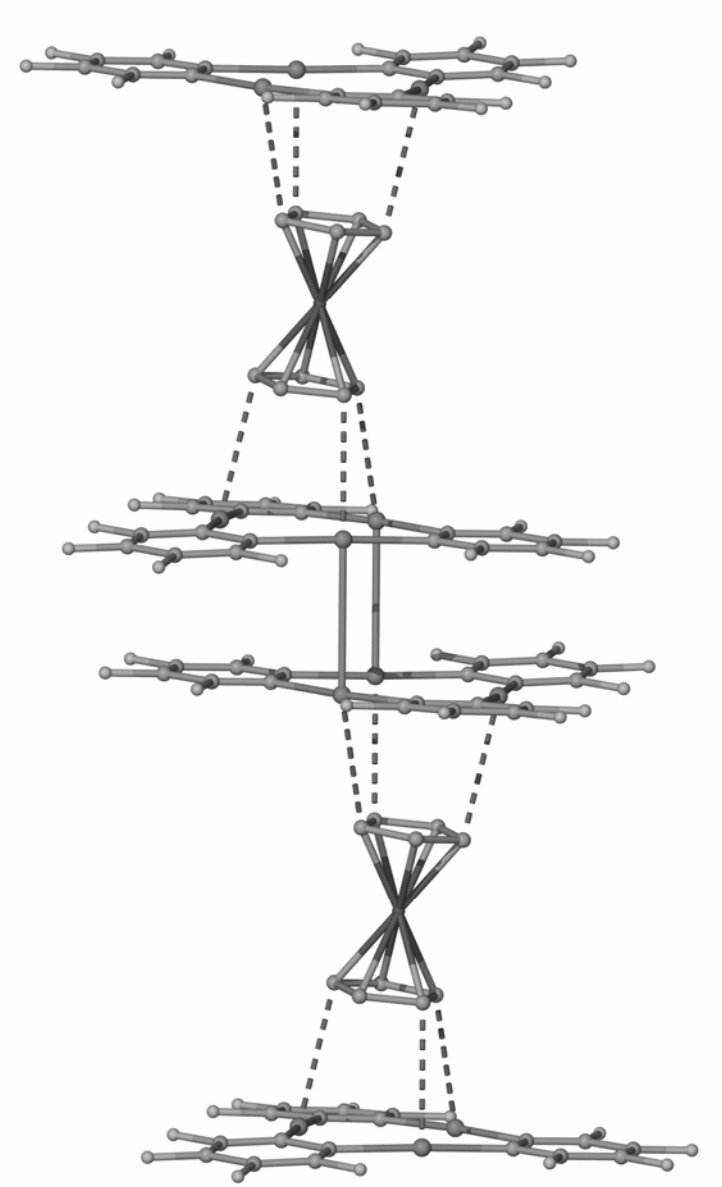

Figure 8.2. Extended structure of compound **28** showing the Hg-Hg interactions. Structure of compound **27** is identical. H omitted.

Table 8.1. Crystal data, data collection, and structure refinement for **27** and **28**.

Crystal data	**27**	**28**
Formula	$C_{46}H_{10}F_{24}Hg_6Fe$	$C_{46}H_{10}F_{24}Hg_6Ni$
M_r	2277.93	2280.79
Crystal size (mm^3)	0.24 x 0.15 x 0.15	0.51 x 0.25 x 0.24
Crystal system	Monoclinic	Monoclinic
Space group	*C*2/m	*C*2/m
a (Å)	10.456(2)	10.554(2)
b (Å)	19.496(4)	19.509(4)
c (Å)	12.312(3)	12.299(3)
β (°)	110.51(3)	109.21(3)
V ($Å^3$)	2350.8(8)	2391.2(8)
Z	2	2
ρ_{calc} (gcm^{-3})	3.218	3.168
μ(Mo K_α)(mm^{-1})	19.947	19.700
F(000) (e)	2016	2020
Data Collection		
T/K	293(2)	293(2)
Scan mode	ω	ω
hkl range	-10→11, -21→21, -13→13	-11→11, -21→21, -13→13
Measured refl.	7384	7493
Unique refl., [R_{int}]	1761 [0.0303]	1781 [0.0483]
Refl. used for refinement	1761	1781
Absorption correction	SADABS	SADABS
T_{min}/T_{max}	0.219215	0.150208
Refinement		
Refined parameters	179	167
R1, wR2 [I>2σ(I)]	0.0295, 0.0866	0.0403, 0.0756
ρ_{fin} (max/min) ($eÅ^{-3}$)	1.017, -1.609	0.889, -1.247

[a] $R1 = \Sigma (F_o - F_c)/ \Sigma F_o$. [b] $wR2 = \{[\Sigma w(F_o^2 - F_c^2)^2]/ [\Sigma w(F_o^2)^2]\}^{1/2}$; $w = 1/[\sigma^2(F_o^2) + (ap)^2 + bp]$; $p = (F_o^2 + 2F_c^2)/3$; a = 0.0747 (**2**), 0.0353 (**3**); b = 14.7461 (**2**), 11.4316 (**3**).

8.4 Diffuse reflectance absorption spectra and solid-state NMR

In an effort to provide a rationale for the dark red color of **28** which does not correspond to that of dark green nickelocene, we have recorded and analyzed the visible diffuse reflectance absorption spectra of **28** and nickelocene. The solution absorption spectrum of nickelocene has been previously reported[144,145] and is dominated by three intense spin-allowed transitions at 426 ($^3A_{2g}\rightarrow{}^3E_{1g}$), 589 ($^3A_{2g}\rightarrow{}^3E_{2g}$) and 695 nm ($^3A_{2g}\rightarrow{}^3E_{1g}$) as well as one weak spin-forbidden transition at 526 nm ($^3A_{2g}\rightarrow{}^1E_{1g}$). The diffuse reflectance spectrum of pristine nickelocene could be satisfactorily modeled on the basis of these four bands, with the spin-forbidden $^3A_{2g}\rightarrow{}^1E_{1g}$ band being the weakest (Figure 8.3 and Table 8.2).[146] In the case of **28**, deconvolution of the diffuse reflectance spectrum indicates that the intensity of the spin-forbidden band at 526 nm is greatly increased. The $^3A_{2g}\rightarrow{}^3E_{1g}$ band also appears to be slightly red-shifted to 715 nm. We have previously shown that aromatic substrates complexed to **1** experience an external mercury heavy atom effect which leads to triplet emission.[47,49] It can therefore be envisaged that the nickelocene molecule in **28** also experiences a heavy atom effect which, because of added spin-orbit coupling, increases the intensity of the formally spin-forbidden $^3A_{2g}\rightarrow{}^1E_{1g}$ transition at 520 nm. The diffuse reflectance spectrum of **27** does not display unusual features and is essentially identical to that of pristine ferrocene (Figure 8.4). As indicated by ^{199}Hg NMR, **1** and ferrocene do not form any detectable adducts in CH_2Cl_2. The solid-state ^{13}C MAS NMR spectrum of **27** (Figure 8.5) exhibits a single resonance for the carbon atoms of the Cp ligand at 72 ppm. Therefore, the Hg-π

interactions observed in the structure of **27** appear to be weak and do not affect the magnetic environment of the Cp carbon atoms which remain equivalent.

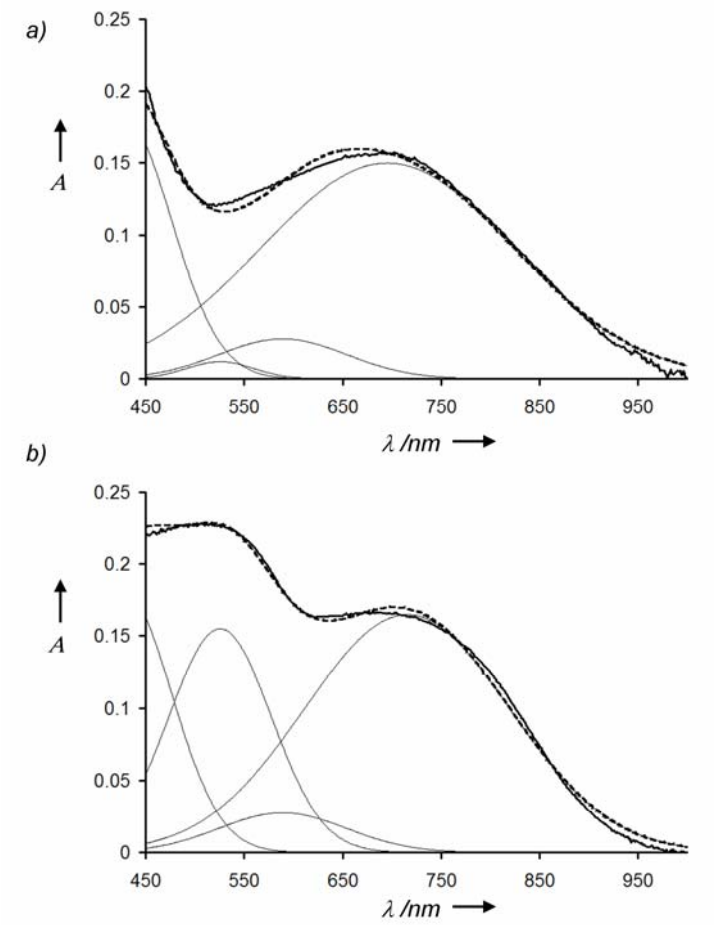

Figure 8.3. Deconvoluted diffuse reflectance absorption spectra of nickelocene (a) and **28** (b).

Table 8.2. Results of the deconvolution.

	Cp_2Ni			**28**		
	□	peak height	fwhm	□	peak height	fwhm
$^3A_{2g} \rightarrow {}^3E_{1g}$:	426 nm	22.8	117	426 nm	22.8	117
$^3A_{2g} \rightarrow {}^3E_{2g}$	589 nm	4.5	152	589 nm	4.5	153
$^3A_{2g} \rightarrow {}^3E_{1g}$	695 nm	48.3	302	715 nm	42.8	244
$^3A_{2g} \rightarrow {}^1E_{1g}$	525 nm	1.0	80	525 nm	20.2	122

fwhm = full width at half maxima; peak height in arbitrary unit

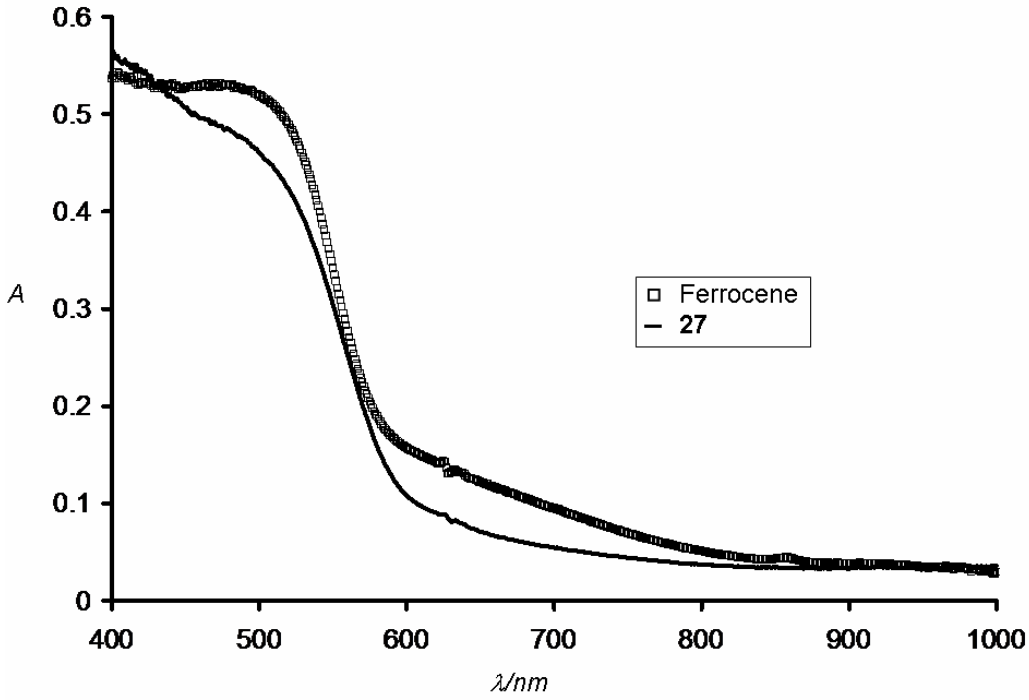

Figure 8.4. Diffuse reflectance absorbance spectra of ferrocene and **27**.

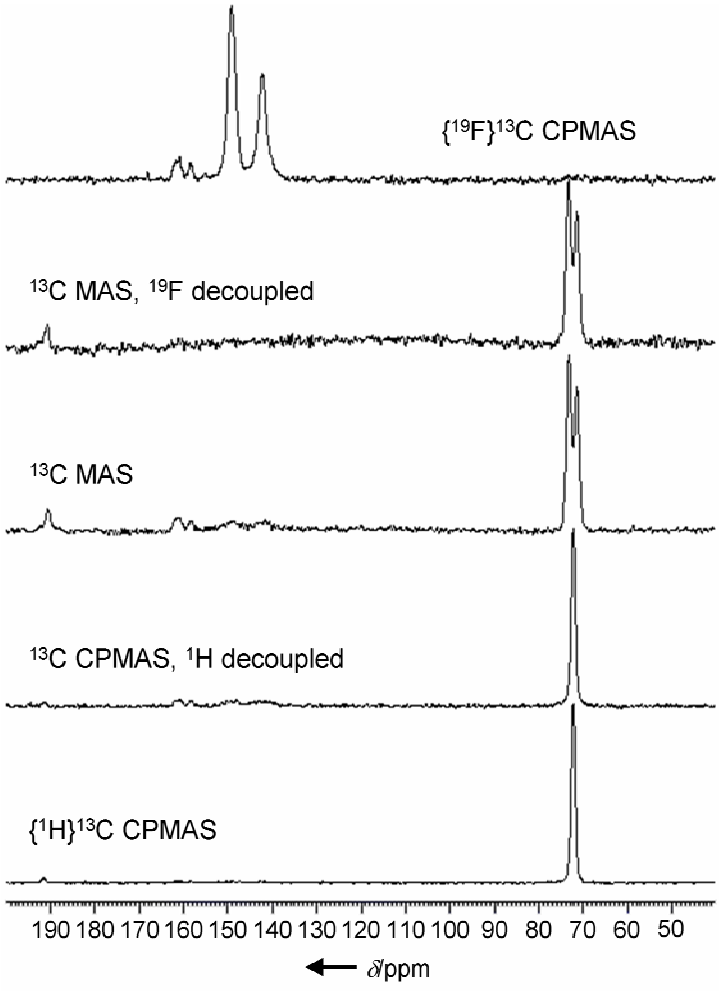

Figure 8.5. Solid-state NMR spectra of compound **27**.

8.5 Magnetic susceptibility measurements

Variable-temperature (2-300 K) magnetic susceptibility data were collected on crushed single crystals of compound **28**. The room temperature X_mT value of 1.1 emu K mol^{-1} is in good agreement with the spin-only value for free nickelocene (S = 1). Below 45 K, however, the value of X_mT decreases sharply (Figure 8.6). This decrease can be attributed to a zero-field splitting effect which arises from spin-orbit coupling.[147] Analysis of the magnetic data on the basis of the equations outlined by Baltzer for an isolated nickelocene[148] afford a zero-field parameter D of 37.65 ± 0.29 cm^{-1} and a g parameter of 2.089 ± 0.003. The zero-field parameter is slightly greater than that estimated for isolated nickelocene (D = 33.76 ± 0.70 cm^{-1}) which might reflect added spin-orbit coupling provided by the six surrounding mercury atoms.[149] We note, however, that weak antiferromagnetic interactions may also stand as a plausible cause for this greater than expected value of the D parameter.[71b,148]

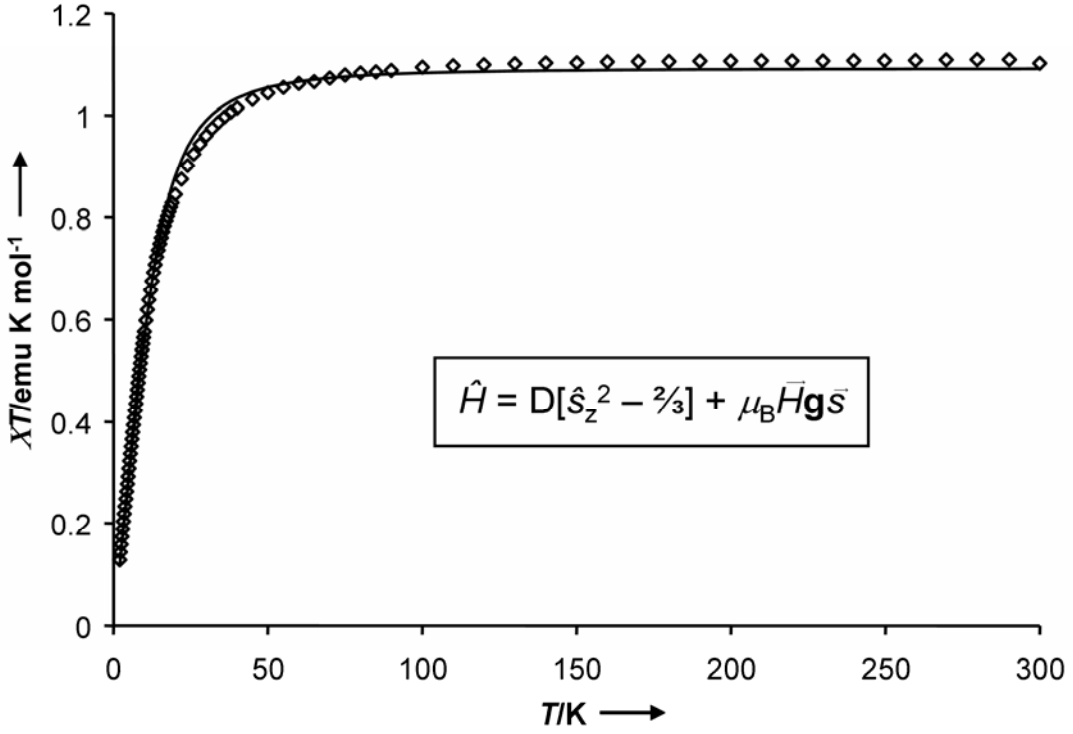

Figure 8.6. Magnetic data for compound **3**. Diamonds represent experimental data points. The black line is the model based on the Hamiltonian in the inset.

8.6 Summary

In summary, we report the synthesis of the 1:2 ferrocene and nickelocene adducts of **1**. In the solid state, these adducts assume an unusual electrophilic double sandwich structure in which a molecule of **1** caps each of the Cp ligands. Adduct **28** is air-stable indicating that the 20-electron nickelocene complex is stabilized toward oxidation. Although electronic effects cannot be ruled out, this stabilization most likely results from the formation of a tight lattice which physically prevents reaction with oxygen. Finally, in the case of **28**, formation of these sandwiches apparently leads to increased spin-orbit

coupling which alters the photophysical and magnetic properties of the nickelocene molecule. Unlike in other donor-acceptor systems involving metallocenes,[141,107] we have found no evidence of charge transfer in **27** and **28**.

8.7 Experimental details

General. Due to the toxicity of the mercury compounds discussed in these studies extra care was taken at all times to avoid contact with solid, solution, and air-borne particulate mercury compounds. The studies herein were carried out in well-aerated fume hood; however, a glovebox was used to manipulate the air sensitive compound nickelocene. Atlantic Microlab, Inc., Norcross, GA, performed the elemental analyses. Nickelocene was purchased from TCI America and used as provided. The remainder of commercially available starting materials and solvents were purchased from Aldrich Chemical and were used as provided. Compound **1** was prepared according to the published procedure outlined by Sartori and Golloch.

General Synthetic Procedure. [**1**•CpFeCp•**1**] (**27**) and [**1**•CpNiCp•**1**] (**28**): A solution of compound **1** (100 mg, 0.096 mmol) in CH_2Cl_2 (15 mL), was mixed with a solution of the metallocene (100 mg, 0.538 mmol for Cp_2Fe and 0.529 mmol for Cp_2Ni) in CH_2Cl_2 (5 mL). Crystals, which formed upon slow evaporation of the solvent, were washed with hexanes to remove excess metallocene. This procedure yielded a quantitative amount of dark orange **27** and dark red **28**, respectively. **27**: Anal. Calc. For $C_{46}H_{10}F_{24}Hg_6Fe$: C, 24.29; H, 0.44. Found: C, 24.32; H, 0.41. Decomposes at 300 °C. **28**: Anal. Calc. For $C_{46}H_{10}F_{24}Hg_6Ni$: C, 24.26; H, 0.44. Found: C, 24.50; H, 0.49.

Decomposes explosively at 275 °C.

^{13}C MAS NMR. ^{13}C MAS NMR spectra were measured with a Bruker 4 mm CPMAS probe at 100.6 MHz and referenced externally to glycine (carbonyl peak at 176.3 ppm). In addition to simple Bloch decay ^{13}C spectra, ^{13}C spectra were measured with ^{19}F decoupling and separately with ^{1}H decoupling. $\{^{1}H\}^{13}C$ and $\{^{19}F\}^{13}C$ CPMAS spectra also were measured.

UV/Vis. Diffuse reflectance visible spectra were recorded on a Labsphere reflectance spectrometer accessory attached to an HP 8453 UV-Vis spectrometer. The diffuse reflectance spectra of **3** and nickelocene were analyzed by deconvolution using the Peakfit program. Both spectra were analyzed on the basis of the four main transitions.

Single-Crystal X-ray Analysis. X-ray data for **2** and **3** were collected on a Bruker Smart-CCD diffractometer using graphite-monochromated Mo-Kα radiation (λ = 0.71073 Å). Specimens of suitable size and quality were selected and mounted onto a glass fiber with superglue and collected at room temperature. The structures were solved by direct methods, which successfully located most of the non-hydrogen atoms. Subsequent refinement on F^2 using the SHELXTL/PC package (version 6.1) allowed location of the remaining non-hydrogen atoms.

Magnetic Analysis. Magnetic susceptibility and magnetization measurements were carried out with a Quantum Design SQUID magnetometer MPMS-XL. DC magnetic measurements were performed with an applied field of 1000 G in the 2-300 K temperature range. Data were corrected for the diamagnetic contributions calculated

from the Pascal constants. The data was satisfactorily modeled based on the equations outlined by Baltzer. The Hamiltonian is $\hat{H} = D[\hat{s}_z^2 - \frac{2}{3}] + \mu_B \cdot \vec{H} \cdot \mathbf{g} \cdot \vec{s}$ where D is the zero-field-splitting parameter and **g** is the g tensor with parallel and perpendicular elements. At low magnetic fields (D > $\mu_B gH$) the magnetic susceptibility elements are $\chi_{\parallel} = \frac{2g_{\parallel}^2 \mu_B^2 N}{kT} \frac{e^{-(D/kT)}}{1+2e^{-(D/kT)}}$ and $\chi_{\perp} = \frac{2g_{\perp}^2 \mu_B^2 N}{D} \frac{1-e^{-(D/kT)}}{1+2e^{-(D/kT)}}$. The approximation $\chi_{iso} = \frac{1}{3}(\chi_{\parallel} + 2\chi_{\perp})$ can be made for isotropic powders. Thus using these equations a D value of 37.651 cm^{-1} and a g of 2.0894 were obtained.

CHAPTER IX

GENERAL CONCLUSIONS

This dissertation has been concerned with an exploration of the potential of trimeric perfluoro-*ortho*-phenylene mercury (**1**) to serve as a building block for supramolecular materials. In the course of these studies, four crystallographic modifications of **1** were discovered and characterized indicating that this compound features a rich polymorphism. In these four modifications, the molecules of **1** tend to aggregate in a cofacial fashion to form extended stacks in which the individual molecules apparently interact via secondary Hg-π or Hg-F interactions. In some cases, these interactions lead to short Hg-Hg contacts, which indicate mercurophilic interactions may also play a role. However, the orientation of the successive molecules appears somewhat random, which probably indicate the preponderance of van der Waals interactions whose magnitude is enhanced by relativistic effects at mercury. DFT calculations performed on **1** reveal that the LUMO is largely comprised of empty mercury 6p orbitals pointing inward toward the center of the molecule (Figure 9.1). As a result, the LUMO has a large lobe in the center of the trinuclear mercury core that extends well above and below the plane formed by the three mercury centers. Based on the location of this large lobe, Lewis basic substrates are likely to interact with **1** at the center of the trinuclear mercury core.

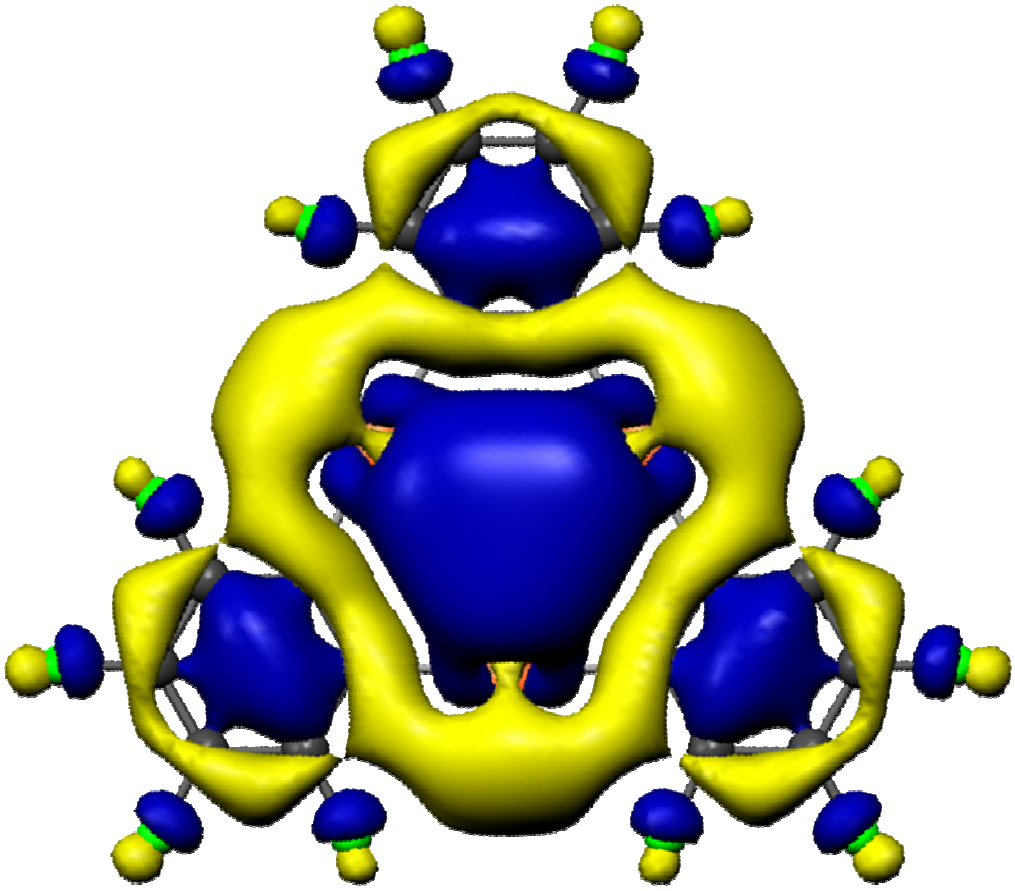

Figure 9.1 Calculated LUMO of **1**.

Further investigation into the electronic properties of **1** were carried out by studying the material formed between **1** and the stable organic radical 2-(phenyl)-4,4,5,5-tetramethylimidazoline-1-oxyl-3-oxide (NIT-Ph). NIT-Ph coordinates to **1** through Hg-O interactions between the electron rich terminus of the N-O moieties on NIT-Ph and the trinuclear mercury core of **1**. These interactions lead to the formation of either discrete NIT-Ph molecules with each oxygen capped by the trinuclear mercury core of **1** ([**1**•μ^3-μ^3-NIT-Ph•**1**], **3**) or binary supramolecular stacks ([**1**•μ^3-NIT-Ph], **4**) (Figure 9.2). Magnetic susceptibility data collected on these compounds indicate that **1**

does not mediate significant coupling of the radical if at all. This point could be clarified if a [radical•**1**•radical] adduct was isolated where the only hope for magnetic interactions would lie in mediation by **1** (Figure 9.3). If such a compound were synthesized the amount of mediation by **1**, if any, could be quantified and could lead to the development of **1** as a building block for supramolecular magnetic materials.

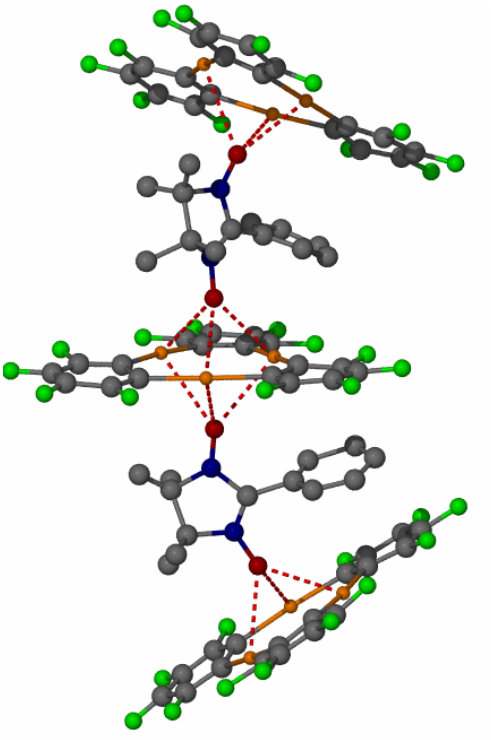

Figure 9.2. Portion of the stack formed in **4**.

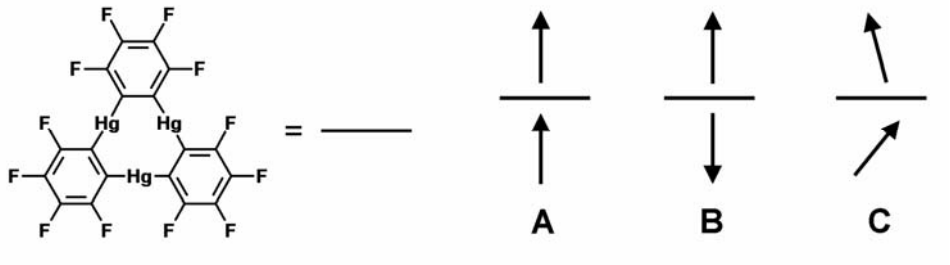

Figure 9.3. Cartoon indicating the three possibilities for magnetic interactions through **1**.

While the interaction of **1** with molecules with organic donors such as nitriles and carbonyls has been extensively studied, the interaction of **1** with molecules with electron rich π-systems remained rather sparse and therefore became an important objective of this dissertation. As part of this work, the interaction of **1** with tetrathiafulvalene (TTF), toluene, *o*-xylene, *m*-xylene, *p*-xylene, mesitylene, biphenyl, naphthalene, acenaphthalene, pyrene, triphenylene, perylene, and coronene have been studied by a combination of solution and solid-state techniques. In the case of TTF, a 2:1 complex containing [**1**•TTF•**1**] was observed (Figure 9.4). In this complex two molecules sandwich a single molecule of TTF and close contacts are observed between the mercury centers of **1** and the sulfur centers of the sandwiched TTF. All other unsaturated systems studied were arenes which form alternating binary supramolecular stacks with **1**. Interestingly, some of these complexes luminesce when irradiated with ultra-violet light. The observed emission for the [**1**•biphenyl], [**1**•naphthalene], [**1**•pyrene] and [**1**•triphenylene], which were studied in detail, corresponds to the phosphorescence of the aromatic (Figure 9.5). This observation reveals that the proximity of the mercury centers induces a heavy atom effect in the arene allowing for

more facile intersystem spin crossing leading to the observed phosphorescence. From a materials standpoint this gives **1** enormous potential for its use in light emitting diodes because the wavelength of the emission can be tuned based on the nature of the arene substrates.

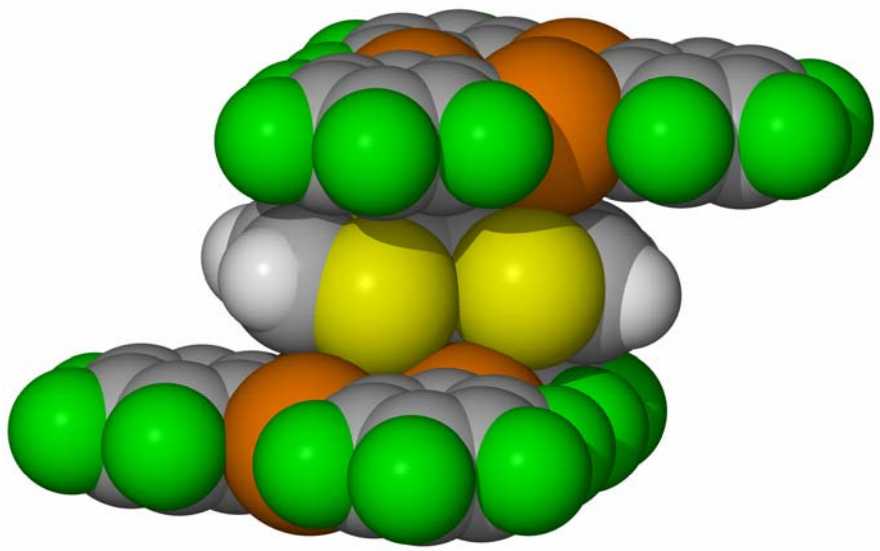

Figure 9.4. Space-filling model of [**1**•TTF•**1**]**.**

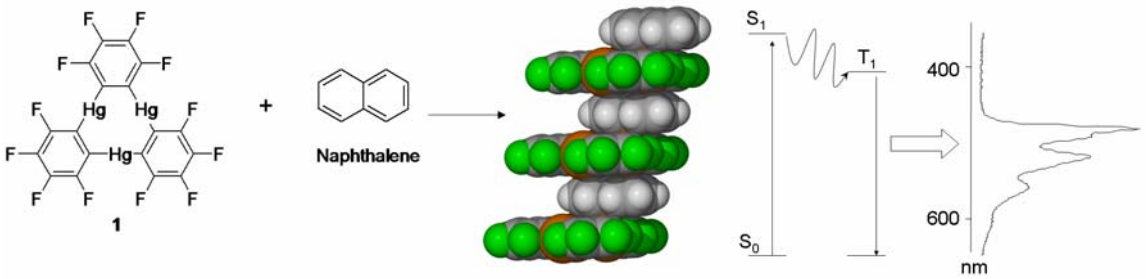

Figure 9.5. Depiction of the reaction of naphthalene with **1** which yields a supramolecular stack. **1** induces a heavy atom effect producing the phosphorescence of naphthalene.

In an effort to study the complexation in solution, the interactions of **1** with highly soluble hexaalkoxytriphenylenes (HAT*n*, *n* = number of carbon atoms in the alkyl chain) was investigated. Reaction of **1** with HAT0 and HAT1 yielded crystals containing extended supramolecular stacks of **1** and HAT*n*. Powder diffraction confirmed a hexagonal close-packed arrangement of columns for the [**1**•HAT1-6] adducts of **1** (Figure 9.6). Interestingly, when a solution of **1** is added to a solution of HAT*n* a decrease in the fluorescence intensity is observed. A rigorous titration using this detection method yields equilibrium constants ranging from 5400 to 16400 M^{-1} for HAT1-6. A Job's analysis confirmed that **1** and HAT*n* interact in a 1:1 ratio. The equilibrium constants indicate the formation of a 1:1 adduct [**1**•HAT*n*] is favored and the narrow range of equilibrium constants indicates that the length of the aliphatic chain has very little effect on adduct formation. The interaction between HAT5 or HAT6 and **1** can also be observed by ^{199}Hg NMR spectroscopy; however solutions used in this measurement are at a much higher concentration than the fluorescence measurements. PGSE NMR experiments on samples of higher concentration reveal the formation of aggregates in solution. Based on this the calculation of an equilibrium constant from NMR data proves to be unfeasible.

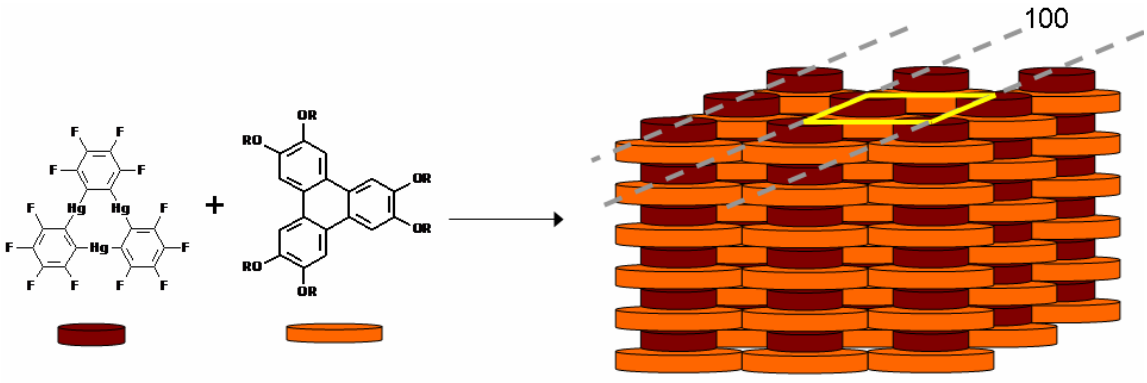

Figure 9.6. Cartoon depicting the general packing of **1** and HAT*n* into hexagonal columnar arrays.

This work was also extended to include organometallic substrates with accessible aromatic groups. For this investigation two metallocenes, namely ferrocene and nickelocene, were chosen based on their availability as well as the exposed nature of the cyclopentadiene (Cp) ligands. Interaction of **1** with MCp_2 (M = Fe or Ni) yields crystals in which the metallocene is sandwiched by two molecules of **1** thus forming an electrophilic double sandwich structure of the type [**1**•MCp_2•**1**] (M = Fe (**27**) or Ni (**28**)) (Figure 9.7). The structure of **27** is isomorphous with **28**. Interestingly, **28** is air stable which indicates coordination to **1** stabilizes the 20 electron species towards oxidation. Furthermore, **28** is dark red while pristine nickelocene is dark green. This led to an investigation of the solid-state absorption spectra of **28**. Comparison of the spectra of **28** to that of pristine nickelocene revealed an intense absorption band for **28** at 526 nm. Deconvolution of the spectra revealed that this band is the spin-forbidden transition $^3A_{2g} \rightarrow {}^1E_{1g}$. As demonstrated previously the proximity of the trinuclear mercury core can lead to a heavy atom effect on an aromatic substrate. It can therefore be envisaged

that the nickelocene molecule in **28** also experiences a heavy atom effect which, because of added spin-orbit coupling, increases the intensity of the formally spin-forbidden $^3A_{2g} \rightarrow {}^1E_{1g}$ transition. On a final note, close Hg-Hg interactions are observed between the neighboring electrophilic double sandwiches in crystals of **27** and **28**. These interactions have a distance of 3.4 Å, which is comparable to the distance calculated for Hg-Hg interactions.

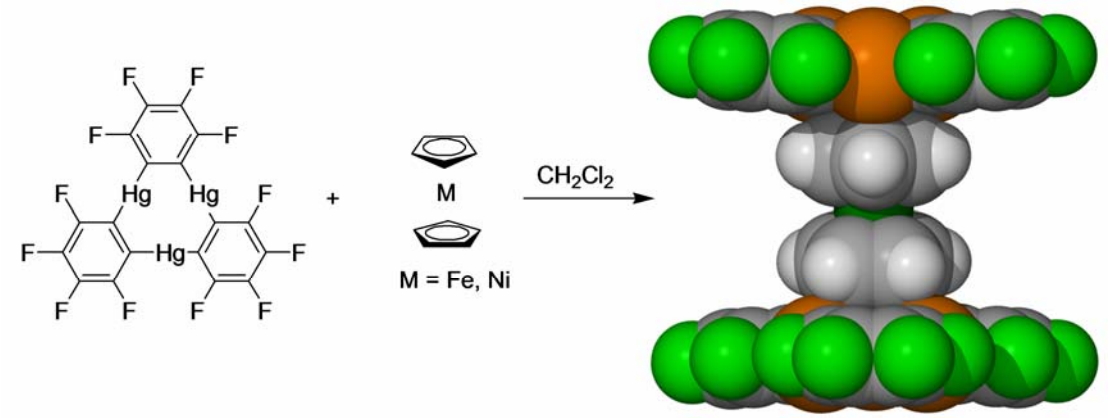

Figure 9.7. Reaction of **1** with metallocenes.

In all of the above cases, the mercury centers of **1** form close contacts with the carbon atoms of the aromatic substrates. These contacts which typically range from 3.20-3.55 Å likely reflect the presence of secondary mercury-π interactions. However, the involvement of electrostatic and van der Waals forces can not be ruled out. Calculations of the electrostatic potential surface of these substrates could help to support the involvement of electrostatic forces in the cohesion of these supramolecular stacks.

Overall these results show that **1** can engage in a variety of interactions with a host of neutral donors. Magnetic studies reveal that **1** likely does not mediate magnetic interactions. When used as a supramolecular building block, **1** generally forms stacked structures which alternate molecules of **1** and substrate within the stack. Furthermore, **1** displays a propensity to induce a heavy atom effect on substrates which is evident in the absorption and emission spectra of the adducts.

REFERENCES

1 a) Schmidtchen, F. P.; Berger, M. *Chem. Rev.* **1997**, *97*, 1609-1646; b) Piers, W. E.; Irvine, G. J.; Williams, V. C. *Eur. J. Inorg. Chem.* **2000**, *10*, 2131-2142; c) Hoefelmeyer, J. D.; Schulte, M.; Tschinkl, M.; Gabbaï, F. P. *Coord. Chem. Rev.* **2002**, *235*, 93-103.

2 a) Hawthorne, M. F.; Zheng, Z. *Acc. Chem. Res.* **1997**, *30*, 267-276; b) Hawthorne, M. F.; Yang, X.; Zheng, Z. *Pure Appl. Chem.* **1994**, *66*, 245-254.

3 Shubina, E. S.; Tikhonova, I. A.; Bakhmutova, E. V.; Dolgushin, F. M.; Antipin, M. Y. V.; Bakhmutov, I.; Sivaev, I. B.; Teplitskaya, L. N.; Chizhevsky, I. T.; Pisareva, I. V.; Bregadze, V. I.; Epstein, L. M.; Shur, V. B. *Chem. Eur. J.* **2001**, *7*, 3783-3790.

4 a) Chistyakov, A. L.; Stankevich, I. V.; Gambaryan, N. P.; Struchkov, Yu. T.; Yanovsky, A. I.; Tikhonova, I. A.; Shur, V. B. *J. Organomet. Chem.* **1997**, *536*, 413-424; b) Shur, V. B.; Tikhonova, I. A.; Dolgushin, F. M.; Yanovsky, A. I.; Struchkov, Yu. T.; Volkonsky, A.Yu.; Solodova, E. V.; Panov, S. Yu.; Petrovskii, P. V.; Vol'pin., M. E. *J. Organomet. Chem.* **1993**, *443*, C19-C21.

5 Wuest, J. D. *Acc. Chem. Res.* **1999**, *32*, 81-89.

6 King, J. B.; Gabbaï, F. P. *Organometallics* **2003**, *22*, 1275-1280.

7 Wuest, J. D.; Zacharie, B. *J. Am. Chem. Soc.* **1985**, *107*, 6121-6123.

8 Lee, H.; Diaz, M.; Hawthorne, M. F.; *Tetrahedron Lett.* **1999**, *40*, 7651-7655.

9 Sartori, P.; Golloch, A. *Chem. Ber.* **1968**, *101*, 2004-2009.

10 Tikhonova, I. A.; Dolgushin, F. M.; Tugashov, K. I.; Petrovskii, P. V.; Furin, G. G.; Shur, V. B. *J. Organomet. Chem*. **2002**, *654*, 123-131.

11 a) Viets, D.; Lork, E.; Watson, P. G.; Mews, R. *Angew. Chem.* **1997**, *109*, 655-656; b) Viets, D.; Lork, E.; Watson, P. G.; Mews, R. *Angew. Chem. Int. Ed. Engl.* **1997**, *36*, 623-624.

12 Wittig, G.; Bickelhaupt, F. *Chem. Ber.* **1958**, *91*, 883-894.

13 Shur, V. B.; Tikhonova, I. A.; Yanovskii, A. I.; Struchkov, Yu. T.; Petrovskii, P. V.; Panov, S. Yu.; Furin, G. G.; Vol'pin, M. E. *J. Organomet. Chem.* **1991**, *418*, C29-C32.

14 Shur, V. B.; Tikhonova, I. A.; Yanovskii, A. I.; Struchkov, Yu. T.; Petrovskii, P. V.; Panov, S. Yu.; Furin, G. G.; Vol'pin, M. E. *Dokl. Akad. Nauk SSSR* **1991**, *321*, 1002-1004.

15 Tikhonova, I. A.; Dolgushin, F. M.; Yanovsky, A. I.; Struchkov, Yu. T.; Gavrilova, A. N.; Saitkulova, L. N.; Shubina, E. S.; Epstein, L. M.; Furin, G. G.; Shur, V. B. *J. Organomet. Chem.* **1996**, *508*, 271-273.

16 Koomen, J. M.; Lucas, J. E.; Haneline, M. R.; Beckwith King, J. D.; Gabbaï, F. P.; Russell, D. H. *Int. J. Mass Spectrom.* **2003**, *225*, 225-231.

17 a) Lee, H.; Knobler, C. B.; Hawthorne, M. F. *J. Am. Chem. Soc.* **2001**, *123*, 8543-8549; b) Lee, H.; Diaz, M.; Knobler, C. B.; Hawthorne, M. F. *Angew. Chem.* **2000**, *112*, 792-794; c) Lee, H.; Diaz, M.; Knobler, C. B.; Hawthorne, M. F. *Angew. Chem. Int. Ed.* **2000**, *39*, 776-778.

18 Ball, M. C.; Brown, D. S.; Massey, A. G.; Wickens, D. A. *J. Organomet. Chem.* **1981**, *206*, 265-277.

19 Baldamus, J.; Deacon, G. B.; Hey-Hawkins, E.; Junk, P. C.; Martin, C. *Aust. J. Chem.* **2002**, *55*, 195-198.

20 Tikhonova, I. A.; Dolgushin, F. M.; Yanovsky, A. I.; Starikova, Z. A.; Petrovskii, P. V.; Furin, G. G.; Shur, V. B. *J. Organomet. Chem.* **2000**, *613*, 60-67.

21 Lamsabhi, A. M.; Bouab, W.; Esseffar, M.; Alcami, M.; Yanez, M.; Abboud, J. M. *New J. Chem.* **2001**, *25*, 509-517.

22 Beckwith King, J. D.; Tsunoda, M.; Gabbaï F. P. *Organometallics* **2002**, *21*, 4201-4205.

23 Nyburg, S. C.; Faerman, C. H. *Acta Crystallogr. Sect. B* **1985**, *41*, 274-279.

24 Canty, A. J.; Deacon, G. B. *Inorg. Chim. Acta* **1980**, *45*, L225-L227.

25 Pyykkö, P.; Straka, M. *Phys. Chem. Chem. Phys.* **2000**, *2*, 2489-2493.

26 Beckwith King, J. D.; Haneline, M. R.; Tsunoda, M.; Gabbaï, F. P. *J. Am. Chem. Soc.* **2002**, *124*, 9350-9351.

27 Pyykkö, P.; Runeberg, N.; Mendizabal, F. *Chem. Eur. J.* **1997**, *3*, 1451-1457.

28 Pyykkö, P. *Chem. Rev.* **1997**, *97*, 597-636.

29 Burini, A.; Fackler, Jr., J. P.; Galassi, R.; Grant, T. A.; Omary, M. A.; Rawashdeh-Omary, M. A.; Pietroni, B. R.; Staples, R. J. *J. Am. Chem. Soc.* **2000**, *122*, 11264-11265.

30 a) Frank, W.; Dincher, B. *Z. Naturforschung Teil B* **1987**, *42*, 828-834; b) Ulvenlund, S.; Rosdahl, J.; Fischer, A.; Schwerdtfeger, P.; Kloo, L. *Eur. J. Inorg. Chem.* **1999**, 633-642.

31 Olah, G. A.; Yu, S. H.; Parker, D. G. *J. Org. Chem.* **1976**, *41*, 1983-1986.

32 a) Damude, L. C.; Dean, P. A. W. *J. Organomet. Chem.* **1979**, *181*, 1-15. b) Damude, L. C.; Dean, P. A. W.; Sefcik, M. D.; Schaefer, J. *J. Organomet. Chem.* **1982**, *226*, 105-114.

33 Lau, W.; Huffman, J. C.; Kochi, J. K. *J. Am. Chem. Soc.* **1982**, *104*, 5515-5517.

34 a) Borovik, A. S.; Bott, S. G.; Barron, A. R. *Angew. Chem.* **2000**, *112*, 4283-4284; b) Borovik, A. S.; Bott, S. G.; Barron, A. R. *Angew. Chem. Int. Ed.* **2000**, *39*, 4117-4118.

35 a) Kiefer, E. F.; Waters, W. L.; Carlson, D. A. *J. Am. Chem. Soc*. **1968**, *90*, 5127-5131; b) Kitching, W.; Drew, G. M.; Alberts, V. *Organometallics* **1982**, *1*, 331-335.

36 Kuz'mina, L. G.; Struchkov, Yu. T. *Croat. Chem. Acta* **1984**, *57*, 701-724, and references therein.

37 Gardinier, J. R.; Gabbaï, F. P. *J. Chem. Soc. Dalton Trans.* **2000**, 2861-2865.

38 Tsunoda, M.; Gabbaï, F. P. *J. Am. Chem. Soc.* **2000**, *122*, 8335-8336.

39 Caillet, J.; Claverie, P. *Acta Crystallogr. Sect. A* **1975**, *31*, 448-461.

40 Vecchiotti, L. *Chem. Ber.* **1930**, *63*, 2275-2276.

41 Wittig, G.; Bickelhaupt, F. *Chem. Ber.* **1958**, *91*, 883-894.

42 Al-Jabar, N. A. A.; Massey, A. G. *J. Organomet. Chem.* **1984**, *275*, 9-18.

43. Tinga, M. A. G. M.; Schat, G.; Akkerman, O. S.; Bickelhaupt, F.; Horn, E.; Kooijman, H.; Smeets, W. J. J.; Spek, A. L. *J. Am. Chem. Soc.* **1993**, *115*, 2808-2817.

44 Goedheijt, M. S.; Nijbacker, T.; Akkerman, O. S.; Bickelhaupt, F.; Veldman, N.; Spek, A. L. *Angew. Chem. Int. Ed. Engl.* **1996**, *35*, 1550-1552.

45 Gabbaï, F. P.; Schier, A.; Riede, J.; Schichl, D. *Organometallics* **1996**, *15*, 4119-4121.

46 Williams, V. C.; Piers, W. E.; Clegg, W.; Elsegood, M. R. J.; Collins, S.; Marder, T. B. *J. Am. Chem. Soc.* **1999**, *121*, 3244-3245.

47 Haneline, M. R.; Taylor, R.; Gabbaï, F. P. *Chem. Eur. J.* **2003**, *9(21)*, 5188-5193. and references cited therein.

48 Shur, V. B.; Tikhonova, I. A.; *Russ. Chem. Bull.* **2003**, *52*, 2539-2554 and references cited therein.

49 Haneline, M. R.; Tsunoda, M.; Gabbaï, F. P. *J. Am. Chem. Soc.* **2002**, *124*, 3737-3742.

50 Grdenic, D. *Chem. Ber.* **1959**, *92*, 231-234.

51 Brown, D. S.; Massey, A. G.; Wickens, D. A. *Acta Cryst.* **1978**, *B34*, 1695-1697.

52 Brown, D. S.; Massey, A. G.; Wickens, D. A. *Inorg. Chim. Acta* **1980**, *44*, L193-L194.

53 Zamora, F.; Sabat, M.; Janik, M.; Siethoff, C.; Lippert, B. *J. Chem. Soc., Chem. Commun.* **1997**, 485-486.

54 For other example of short Hg(II)-Hg(II) interactions see: Pickett, N. L.; Just, O.; VanDerveer, D. G.; Rees, J. S. *Acta Crystallogr., Sect. C: Cryst. Struct. Commun.*, **2000**, *C56*, 412-413.

55 Munoz, J. J.; Morales, R.; Martinez, J. L.; Joens, J. A. *J. Org. Chem.* **1990**,*55*, 1122-1125.

56 Yam, V. W. W.; Lo, K. K. W. *Chem. Soc. Rev*. **1999**, *28*, 323-334.

57 (a) Schmidbaur, H., Ed. *Gold: Progress in Chemistry, Biochemistry, and Technology*; J. Wiley & Sons: Chichester, 1999. (b) Schmidbaur, H. *Gold Bull.* **2000**, *33*, 3-10. (c) Schmidbaur, H. *Chem. Soc. Rev.* **1995**, *24*, 391-400.

58 Castro, E. A. *Molecules* **2003**, *8*, 418-429.

59 Saitkulova, L. N.; Bakhmutova, E. V.; Shubina, E. S.; Tikhonova, I. A.; Furin, G. G.; Bakhmutov, V. I.; Gambaryan, N. P.; Chistyakov, A. L.; Stankevich, I. V.; Shur, V. B.; Epstein, L. M. *J. Organomet. Chem.* **1999**, *585*, 201-210.

60 Castro, E. A. *J. Molecular Struct. (Theochem)* **2002**, *619*, 45–50.

61 ADF2003.01. SCM, Theoretical Chemistry, Vrije Universiteit, Amsterdam, The Netherlands.

62 Guerra, C. F.; Snijders, J. G.; Te Velde, G.; Baerends, E. *J. Theor. Chem. Acc.* **1998**, *99*, 391-403.

63 Te Velde, G.; Bickelhaupt, F. M.; Baerends, E. J.; Fonseca Guerra, C.; Van Gisbergen, S. J. A.; Snijders, J. G.; Ziegler, T. *J. Comput. Chem.* **2001**, *22*, 931-967.

64 Becke, A. D. *Phys. Rev. A: At., Mol., Opt. Phys.* **1988**, *38*, 3098-3100.

65 Lee, C.; Yang, W.; Parr, R. G. *Phys. Rev. B: Condens. Matter* **1988**, *37*, 785-789.

66 Schmidbaur, H.; Öller, H.-J.; Wilkinson, D. L.; Huber, B. *Chem. Ber.* **1989**, *122*, 31-36.

67 a) Beauchamp, A. L.; Olivier, M. J.; Wuest, J. D.; Zacharie, B. *Organometallics* **1987**, *6,* 153-156. b) Tschinkl, M.; Schier, A.; Riede, J.; Gabbaï, F. P. *Organometallics* **1999**, *18*, 1747-1753. c) Vaugeois, J.; Wuest, J. D. *J. Am. Chem. Soc.* **1998**, *120*, 13016-13022. d) Vaugeois, J.; Simard, M.; Wuest, J. D. *Organometallics* **1998**, *17*, 1215-1219. e) Simard, M.; Vaugeois, J.; Wuest, J. D. *J. Am. Chem. Soc.* **1993**, *115*, 370-372. f) Wuest, J. D.; Zacharie, B. *J. Am. Chem. Soc.* **1987**, *109*, 4714-4715. g) Beauchamp, A. L.; Olivier, M. J.; Wuest, J. D.; Zacharie, B. *J. Am. Chem. Soc.* **1986**, *108*, 73-77. h) Wuest, J. D.; Zacharie, B. *Organometallics* **1985**, *4*, 410-411.

68 Wedge, T. J.; Hawthorne, M. F. *Coord. Chem. Rev.* **2003**, *240(1-2)*, 111-128.

69 Tsunoda, M.; Gabbaï, F. P. *J. Am. Chem. Soc.* **2003**, *125*, 10492-10493.

70 Ball, M. C.; Brown, D. S.; Massey, A. G. *J. Organomet. Chem.* **1981**, *206*, 265-277.

71 a) Tikhonova, I. A.; Dolgushin, F. M.; Tugashov, K. I.; Furin, G. G.; Petrovskii, P. V.; Shur, V. B. *Russ. Chem. Bull.* **2001**, *50(9)*, 1673-1678. b) Tikhonova, I. A.; Dolgushin, F. M.; Tugashov, K. I.; Ellert, O. G.; Novotortsev, V. M.; Furin, G. G.; Antipin, M. Yu.; Shur, V. B. *J. of Organomet. Chem.* **2004**, *689(1)*, 82-87.

72 a) Haneline, M. R.; King, J. B.; Gabbai, F. P. *J. Chem. Soc. Dalton Trans.* **2003**, *13*, 2686-2690. b) Omary, M. A.; Kassab, R. M.; Haneline M. R.; Elbjeirami, O.; Gabbaï, F. P. *Inorg. Chem.* **2003**, *42*, 2176-2178.

73 Volodarsky, L. B.; Reznikov, V. A.; Ovcharenko, V. I. *Synthetic Chemistry of Stable Nitroxides*; CRC Press: Boca Raton, 1994.

74 Zheludev, A.; Barone, V.; Bonnet, M.; Delley, B.; Grand, A.; Ressouche, E.; Rey, P.; Subra, R.; Schweizer, J. *J. Am. Chem. Soc.* **1994**, *116*, 2019-2027.

75 Ullman, E. F.; Osiecki, J. H.; Boocock, D. G. B.; Darcy, R. *J. Am. Chem. Soc.* **1972**, *94*, 7049-7059.

76 Osiecki, J. H.; Ullman, E. F. *J. Am. Chem. Soc.* **1968**, *90*, 1078-1079.

77 Carlin, R. L. *Magnetochemistry*; Springer-Verlag: Berlin, 1986.

78 Wang, L.; Zhang, C.; Liao, D.; Jiang, Z.; Yan, S. *J. Molecular Struct.*, **2003**, *657*, 1-6.

79 Stroh, C.; Belorizky, E.; Turek, P.; Bolvin, H.; Ziessel, R. *Inorg. Chem.* **2003**, *42*, 2938-2949.

80 Fegy, K.; Sanz, N.; Luneau, D.; Belorizky, E.; Rey, P. *Inorg. Chem.* **1998,** *37*, 4518-4523.

81 Wei, H.; Wong, H.; Lee, G.; Wang, Y. *J. Chin. Chem. Soc.*, (**1996**), *43(3)*, 253-259.

82 *Theory and Applications of Molecular Paramagnetism*; Boudreaux, E. A.; Mulay, L. N., Eds; John Wiley & Sons: New York, 1976.

83 Rawashdeh-Omary, M. A.; Omary, M. A.; Fackler, J. P., Jr.; Galassi, R.; Pietroni, B. R.; Burini, A. *J. Am. Chem. Soc.* **2001**, *123*, 9689-9691.

84 Olmstead, M. M.; Jiang, F.; Attar, S.; Balch, A. L. *J. Am. Chem. Soc.* **2001**, *123*, 3260-3267.

85 The structure of [tht•$HgCl_2$] features short intramolecular primary Hg-S bonds and long intermolecular secondary Hg-S interactions: see Branden, C. I.; *Ark. Kemi. Sverige* **1964**, *22*, 495-500.

86 Borovik, A. S.; Bott, S. G.; Barron, A. R. *J. Am. Chem. Soc.* **2001**, *123*(45), 11219-11228.

87 a) Branch, C. S.; Barron, A. R. *J. Am. Chem. Soc.* **2002**; *124*(47), 14156-14161. b) Borovik, A. S.; Barron, A. R. *J. Am. Chem. Soc.* **2002**, *124*(14), 3743-3748.

88 a) Alcock, N. W.; Lampe, P. A.; Moore, P. *Dalton Trans.* **1978**, 1324-1328. b) Lampe, P. A.; Moore, P. *Inorg. Chim. Acta* **1979**, *36*, 27-30. c) Cathy, A. J.; Chaichit, N.; Gatehouse, B. M. *Acta Crystallogr., Sect. B* **1980**, *36*, 786-789. d) Furmanova, N. G.; Struchkov, Yu. T.; Kalinin, V. N.; Finkel'shtein, B. Ya.; Zakharkin, L. I. *Zh. Strukt. Khim.* **1980**, *21*, 96-100. e) Hosseini, M. W. *Chem.*

Commun. **1995**, 609-610. f) Tschinkl, M.; Bachman, R. E.; Gabbai, F. P. *J. Organomet. Chem.* **1999**, *582*, 40-44.

89 Vaugeois, J.; Simard, M.; Wuest, J. D. *Coord. Chem. Rev.* **1995**, *145*, 55-73.

90 a) Dahl, T. *Acta Chem. Scand.* **1998**, *52*, 1006–1009. b) Dahl, T. *Acta Chem. Scand.* **1994**, *48*, 95–106. c) Dahl, T. *Acta Chem. Scand. Ser. A* **1975**, *A29*, 170–174. d) Dahl, T. *Acta Chem. Scand., Ser. A* **1971**, *25*, 1031–1039. e) Britton, D. *J. Chem. Crystallogr.* **1997**, *27*, 405–412. f) Swift, J. A.; Reynolds, A. M.; Ward, M. D. *Chem. Mater.* **1998**, *10*, 4159–4168.

91 For general references on arene–fluoroarene interactions, see: a) Weck, M.; Dunn, A. R.; Matsumoto, K.; Coates, G. W.; Lobkovsky, E. B.; Grubbs, R. H. *Angew. Chem., Int. Ed.* **1999**, *38*, 2741–2745. b) Bartholomew, G. P.; Bu, X.; Bazan, G. C. *Chem. Mater.* **2000**, *12*, 2311–2318. c) Collings, J. C.; Roscoe, K. P.; Thomas, R. L.; Batsanov, A. S.; Stimson, L. M.; Howard, J. A. K.; Marder, T. B. *New J. Chem.* **2001**, *25*, 1410–1417.

92 Ma, J. C.; Dougherty, D. A. *Chem. Rev.* **1997**, *97*, 1303–1324.

93 Weber, T.; Riedle, E.; Neusser, H. J.; Schlag, E. W. *Chem. Phys. Lett.* **1991**, *183*, 77–83.

94 For a series of general reviews on this topic see: (a) Kaufmann, D. E.; Otten, A. *Angew. Chem., Int. Ed. Engl.* **1994**, *33*, 1832-1834. (b) Dietrich, B. *Pure Appl. Chem.* **1993**, 65, 1457-1464.

95 See for example: a) Lopez, P.; Oh, T. *Tetrahedron Lett.* **2000**, *41*, 2313-2317. b) Ooi, T.; Takahashi, M.; Maruoka, K. *J. Am. Chem. Soc.* **1996**, *118*, 11307-11308.

96 a) Shriver, D. F.; Biallas, M. J. *J. Am. Chem. Soc.* **1967**, *89*, 1078-1081. b) Katz, H. E. *J. Org. Chem.* **1985**, *50*, 5027-5032. c) Horner, J. H.; Squatritto, P. J.; McGuire, N.; Riebenspies, J. P.; Newcomb, M. *Organometallics* **1991**, *10*, 1741-1750. d) Tschinkl, M.; Schier, A.; Riede, J.; Gabbaï, F. P. *Inorg. Chem.* **1997**, *36*, 5706-5711. e) Altmann, R.; Jurkschat, K.; Schuermann, M.; Dakternieks, D.; Duthie, A. *Organometallics* **1998**, *17*, 5858-5866. f) Uhl, W.; Hannemann, F. *J. Organomet. Chem.* **1999**, *579*, 18-23.

97 a) Katz, H. E. *J. Org. Chem.* **1989**, *54*, 2179-2183. b) Nozaki, K.; Yoshida, M.; Takaya, H. *Bull. Chem. Soc. Jpn*. **1996**, *69*, 2043-2052. c) Saied, O.; Simard, M.; Wuest, J. D. *Organometallics* **1998**, *17*, 1128-1133. d) Gabbaï, F. P.; Schier, A.; Riede, J.; Hynes, M. J. *Chem. Commun.* **1998**, *8*, 897-898.

98 Lee, H.; Knobler, C. B.; Hawthorne, M. F. Angew. Chem., Int. Ed. **2001**, 40, 2124-2126.

99 Tschinkl, M.; Schier, A.; Riede, J.; Gabbaï, F. P. *Angew. Chem., Int. Ed.* **1999**, *38*, 3547-3549.

100 a) Yang, X.; Zheng, Z.; Knobler, C. B.; Hawthorne, M. F. *J. Am. Chem. Soc.* **1993**, *115*, 193-195. b) Beckwith, J. D.; Tschinkl, M.; Picot, A.; Tsunoda, M.; Bachman, R.; Gabbaï, F. P. *Organometallics* **2001**, *20*, 3169-3174.

101 Fowley, L. A.; Lee, J. C.; Crabtree, R. H.; Siegbahn, P. E. M. *Organometallics* **1996**, *15*, 1157-1165 and references therein.

102 a) Brouwer, E. B.; Enright, G. D.; Ratcliffe, C. I.; Facey, G. A.; Ripmeester J. A. *J. Phys. Chem. B,* **1999**, *103*, 10604 –10616. b) Ok, J. H.; Vold, R. R.; Vold, R. L. *J. Phys. Chem.* **1989**, *93*, 7618-7624. c) Nishikiori, S.; Ratcliffe, C. I.; Ripmeester, J. A. *J. Phys. Chem.* **1991**, *95*, 1589-1596. d) Chopra, N.; Chapman, R. G.; Chuang, Y.-F.; Sherman, J. C.; Burnell, E. E.; Polson, J. M. *J. Chem. Soc.; Faraday Trans.* **1995**, *91*, 4127-4131.

103 Ripmeester, J. A.; Wright, D. A.; Fyfe, C. A.; Boyd, R. K. *J. Chem. Soc.; Faraday Trans.* **1978**, *74*, 1164-1178.

104 Aliev, A. E.; Harris, K. D. M.; Guillaume, F. *J. Phys. Chem.* **1995**, *99*, 1156-1165.

105 (a) Coates, G. W.; Dunn, A. R.; Henling, L. M.; Dougherty, D. A.; Grubbs, R. H. *Angew. Chem., Int. Ed. Engl.* **1997**, *36*, 248-251. (b) Coates, G. W.; Dunn, A. R.; Henling, L. M.; Ziller, J. W.; Lobkovsky, E. B.; Grubbs, R. H. *J. Am. Chem. Soc.* **1998**, *120*, 3641-3649.

106 (a) Renak, M. L.; Bartholomew, G. P.; Wang, S.; Ricatto, P. J.; Lachicotte, R. J.; Bazan, G. C. *J. Am. Chem. Soc.* **1999**, *121*, 7787-7799. (b) Bartholomew, G. P.; Bazan, G. C.; Bu, X.; Lachicotte, R. J. *Chem. Mater*. **2000**, *12*, 1422-1430.

107 Aspley, C. J.; Boxwell, C.; Buil, M. L.; Higgitt, C. L.; Long, C.; Perutz, R. N. *Chem. Commun.* **1999**, 1027-1028.

108 a) Collings, J. C.; Batsanov, A. S.; Howard, J. A. K.; Marder, T. B. *Acta Crystallogr., Sect. C* **2001**, *57*, 870-872. b) Dai, C.; Nguyen, P.; Marder, T. B.; Scott, A. J.; Clegg, W.; Viney, C. *Chem. Commun.* **1999**, 2493-2494.

109 Williams, J. H. *Acc. Chem. Res.* **1993**, *26*, 593-598.

110 Lorenzo, S.; Lewis, G. R.; Dance, I. *New J. Chem.* **2000**, *24*, 295-304.

111 Parks, D. J.; Piers, W. E.; Parvez, M.; Atencio, R.; Zaworotko, M. J. *Organometallics* **1998**, *17*, 1369-1377.

112 Tinland, B. *Acta Phys. Acad. Sci. Hung.* **1968**, *25*, 111-114.

113 (a) Bock, H.; Nick, S.; Na¨ther, C.; Bensch, W. *Chem.-Eur. J.* **1995**, *1*, 557-563. (b) Eaton, V. J.; Steele, D. *J. Chem. Soc., Faraday Trans. 2* **1973**, *69(11)*, 1601-1608. (c) Unanue, A.; Bothorel, P. *Bull. Soc. Chim. Fr.* **1966**, *5*, 1640-1643. (d) Chau, J. Y. H.; Le´Fevre, C. G.; Le´Fevre, R. J. W. *J. Chem. Soc.* **1959**, 2666-2669. (e) Cheng, C. L.; Murthy, D. S. N.; Richtie, G. L. D. *J. Chem. Soc., Faraday Trans. 2* **1972**, *68*, 1679-1690.

114 Rouille, G.; Krasnokutski, S.; Huisken, F.; Henning, T.; Sukhorukov, O.; Staicu, A. *J. Chem. Phys.* **2004**, *120*, 6028-6034.

115 Clar, E. *Spectrochim. Acta* **1950**, *4*, 116-121.

116 For biphenyl, see: (a) Suzuki, T.; Kudo, G.; Nukui, K.; Mizuno, M.; Abe, K.; Shigenari, T. J. *Luminescence* **2000**, *87-89*, 623-625. (b) Makoto, S. *J. Phys. Soc. Jpn.* **1974**, *36*, 1636-1642.

117 For naphthalene, see: Craig, D. P.; Wolf, H. C. *J. Chem. Phys.* **1964**, *40*, 2057-2059.

118 For triphenlylene, see: Chojnacki, H.; Laskowski, Z.; Lewanowicz, A.; Ruziewick, Z.; Wandas, R. *Chem. Phys. Lett.* **1986**, *124*, 478-482.

119 Gustav, K.; Seydenschwanz, C. *Chem. Phys. Lett.* **1984**, *109*, 156-159.

120 Ramamurthy, V.; Eaton, D. F.; Caspar, J. V. *Acc. Chem. Res.* **1992**, *25*, 299-307.

121 Hochstrasser, R. M.; Lower, S. K. *J. Chem. Phys.* **1964**, 40, 1041-1046.

122 McGlynn, S. P.; Azumi, T.; Kinoshita, M. *Molecular Spectroscopy of the Triplet State*; Prentice Hall: Englewood Cliffs, NJ, 1969.

123 Fujii, T.; Suzuki, S.; Komatsu, S. *Chem. Phys. Lett.* **1978**, *57*, 175-178.

124 The spin-orbit coupling constant (ξ) for the 5d orbital is ~5100 cm^{-1} in species with a $5d_{10}$ configuration: Griffith, J. S. *Theory of Transition Metal Ions*; Cambridge University Press: Cambridge, 1964.

125 a) Sasson, R.; Braitbart, O.; Weinreb, A. *J. Lumin.* **1988**, *39*, 223-225. b) Bello, J. M.; Hurtubise, R. J. *Anal. Chem.* **1988**, *60*, 1285-1290. c) Wang, J.; Hurtubise, R. J. *Anal. Chim. Acta* **1996**, *332*, 299-305.

126 Simmerer, J.; Glüsen, B.; Paulus, W.; Kettner, A.; Schuhmacher, P.; Adam, D.; Etzbach, K.-H.; Siemensmeyer, K.; Wendorff, J. H.; Ringsdorf, H.; Haarer, D. *Adv. Mater.* **1996**, *8*, 815-819.

127 a) Andresen, T. L.; Krebs, F. C.; Thorup, N.; Bechgaard K. *Chem. Mater.* **2000,** *12,* 2428-2433. b) Allen, M. T.; Harris, K. D. M.; Kariuki, B. M.; Kumari, N.;

Preece, J. A. *Liq. Cryst.* **2000**, *27*, 689-692. c) Braitbart, O.; Sasson, R.; Weinreb, A. *Mol. Cryst. Liq. Cryst.* **1988**, *159*, 233-242. d) Calucci, L.; Zimmermann, H.; Wachtel, E. J.; Poupko, R.; Luz, *Z. Liq. Cryst.* **1997**, *22*, 621-630.

128 Andresen, T. L.; Krebs, F. C.; Thorup, N.; Bechgaard K. *Chem. Mater.* **2000,** *12,* 2428-2433.

129 Allen, M. T.; Harris, K. D. M.; Kariuki, B. M.; Kumari, N.; Preece, J. A. *Liq. Cryst.* **2000**, *27*, 689-692.

130 Braitbart, O.; Sasson, R.; Weinreb, A. *Mol. Cryst. Liq. Cryst.* **1988**, *159*, 233-242.

131 Calucci, L.; Zimmermann, H.; Wachtel, E. J.; Poupko, R.; Luz, Z. *Liq. Cryst.* **1997**, *22*, 621-630.

132 Markovitsi, D.; Rigaut, F.; Mouallem, M. *Chem. Phys. Lett.* **1987**, *135*, 236-242.

133 Valentini, M.; Pregosin, P. S.; Ruegger, H. *Dalton Trans.* **2000**, *24*, 4507-4510.

134 ETHANOX 330 = 1,3,5-trimethyl-2,4,6-tris(3,5-di-*tert*-butyl-4-hydroxybenzyl)benzene. Chetkina, L. A.; Zavodnik, V. E.; Sobolev, A. N.; Bel'skii, V. K *Kristallografiya* **1984**, *29*, 389-391.

135 Andresen, T. L.; Krebs, F. C.; Thorup, N.; Bechgaard K. *Chem. Mater.* **2000,** *12,* 2428-2433.

136 Volume determined from the crystal structures of **1** discussed in Chapter II.

137 Valentini, M.; Pregosin, P. S.; Ruegger, H. *Organometallics* **2000**, *19*, 2551-2555.

138 "Electrophilic sandwich" is a term first proposed by Hawthorne and coworkers to describe supramolecules in which an anion is sandwiched by two electrophilic hosts. See: 17b

139 a) Fischer, E. O.; Jira, R. *Z. Naturforsch.* **1953**, *8b*, 217-219. b) Wilkinson, G.; Pauson, P. L.; Cotton, F. A. *J. Am. Chem. Soc.* **1954**, *76*, 1970-1974.

140 a) Dunitz, J. D.; Orgel, L. E.; Rich, A.*Acta Crystallogr.* **1956**, *9*, 373-375. b) Seiler, P.; Dunitz, J. D. *Acta Crystallogr., Sect. B: Struct. Sci.* **1980**, *36*, 2255-2260.

141 For recent reviews see: a) Miller, J. S.; Epstein, A. J. *Coord. Chem. Rev.* **2000**, *206-207*, 651-660; b) Miller, J. S. *Inorg. Chem.* **2000**, *39*, 4392-4408.

142 Singh, K.; Long, J. R.; Stavropoulos, P. *J. Am. Chem. Soc.* **1997**, *119*, 2942-2943.

143 Hayashi, A.; Olmstead, M. M.; Attar, S.; Balch, A. L. *J. Am. Chem. Soc.* **2002**, *124*, 5791-5795.

144 Warren, K. D. *J. Chem. Phys.* **1973**, *77*, 1681-1686.

145 In earlier work the spin-forbidden band at 526 nm has been assigned to the $^3A_{2g} \rightarrow {}^1A_{1g}$ transition, see: Pavlik, I.; Cerny, V.; Maxova, E. *Collect. Czech. Chem. Commun.* **1970**, *3*, 3045-3063.

146 The diffuse reflectance spectra of **28** and nickelocene were deconvoluted using the Peakfit program. Both spectra were analyzed on the basis of the four main transitions.

147 Figgis, B. N.; Hitchman, M. A. *Ligand Field Theory and Its Applications*; John Wiley & Sons: New York, 2000.

148 Baltzer, P.; Furrer, A.; Hulliger, J.; Stebler, A. *Inorg. Chem.* **1988**, *27*, 1543-1548.

149 Heavy atom ligands have been shown to increase the zero-field splitting parameter of transition metal complexes by added spin-orbit coupling. See for example: a) Krzystek, J.; Park, J.-H.; Meisel, M. W.; Hitchman, M. A.; Stratemeier, H.; Brunel, L.-C.; Telser, J. *Inorg. Chem.* **2002**, *41*, 4478-4487; b) Chen, J.-J.; Du, M.-L.; Li, Z.-M. *Z. Naturforsch., A: Phys. Sci.* **1994**, *49*, 1013-1015.

VITA

MASON REAMES HANELINE

416 Williford Rd
Ball, LA 71405
drmisterh@gmail.com

Education:

Ph.D. in Inorganic Chemistry from Texas A&M University
Graduated: December 2004

B.S. in Chemistry from Virginia Polytechnic Institute and State University
Graduated: May 2000 Cum Laude

Publications:

Haneline, M. R.; Gabbaï, F. P. *Angew. Chem., Int. Ed.* **2004** *in press.*

Haneline, M. R.; Gabbaï, F. P. *C. R. Chimie* **2004**, *7*, 871-876.

Haneline, M. R.; Taylor, R.; Gabbaï, F. P. *Chem. Eur. J.* **2003**, *9(21)*, 5188-5193.

Haneline, M. R.; King, J. B.; Gabbaï, F. P. *Dalton Trans.* **2003**, *13*, 2686-2690.

Omary, M. A.; Kassab, R. M.; Haneline, M. R.; Bjeirami, O. El; Gabbaï, F. P. *Inorg. Chem.* **2003**, *42(7)*, 2176-2178.

Koomen, J. M.; Lucas, J. E.; Haneline, M.; King, J. B.; Gabbaï, F. P.; Russell, D. H. *Int. J. Mass Spectrom.* **2003**, *225(3)*, 225-231.

King, J. B.; Haneline, M. R.; Tsunoda, M.; Gabbaï, F. P. *J. Am. Chem. Soc.* **2002**, *124*, 9350-9351.

Haneline, M. R.; Tsunoda, M.; Gabbaï, F. P. *J. Am. Chem. Soc.* **2002**, *124*, 3737-3742.

Awards:

Procter & Gamble Fellowship
Martell Travel Award
Deans Fellowship from Texas A&M University